OBSERVATIONAL ASPECTS OF CORE COLLAPSE SUPERNOVAE

A THESIS

SUBMITTED FOR THE DEGREE OF

DOCTOR OF PHILOSOPHY

IN

THE FACULTY OF SCIENCE

INDIAN INSTITUTE OF SCIENCE

BY

UDAY KUMAR GURUGUBELLI

DEPARTMENT OF PHYSICS
INDIAN INSTITUTE OF SCIENCE
BANGALORE - 560 012, INDIA

NOVEMBER 2010

To
Jagadguru Shri Adi Shankaracharya
and
my parents...

“Om Poornamadah Poornamidam
Poornat Poornamudachyate,
Poornasya Poornamaadaya
Poornamevavashishyate,
Om Shantih, Shantih, Shantih”

– Brihadaranyaka Upanishad.

DECLARATION

I hereby declare that the matter contained in the thesis entitled **"Observational aspects of Core Collapse Supernovae"** is the result of investigations carried out by me at the Indian Institute of Astrophysics under the supervision of Dr. G. C. Anupama. This thesis has not been previously submitted for the award of any degree, diploma, associateship, fellowship etc. at any University or Institute.

Uday Kumar G.
(Candidate)

Indian Institute of Astrophysics
Bangalore-560034, India.
and
Joint Astronomy Program
Department of Physics
Indian Institute of Science
Bangalore-560012, India.

CERTIFICATE

This is to certify that the matter contained in the thesis entitled "**Observational aspects of Core Collapse Supernovae**" submitted to Indian Institute of Science by **Mr. Uday Kumar Gurugubelli** for the award of the degree of Doctor of Philosophy in the Faculty of Science is based on the results of investigations carried out by him under my supervision and guidance at the Indian Institute of Astrophysics. This thesis has not been previously submitted for the award of any degree, diploma, associateship, fellowship etc. at any University or Institute.

Dr. G. C. Anupama
(Supervisor)

Indian Institute of Astrophysics
Bangalore-560034, India

ACKNOWLEDGEMENTS

He who thanks but with the lips
Thanks but in part;
The full, the true Thanksgiving
Comes from the heart.
−− J.A. Shedd

It would not have been possible to write this doctoral thesis without the help and support of the kind people around me, to only some of whom it is possible to give particular mention here.

First and foremost, I would like to thank my thesis supervisor Prof. G C Anupama, for her continuous support on my Ph.D study and research. She has provided me with many helpful suggestions, important advice and immense knowledge during the course of this work. It has been an honor to be her first Ph.D. student. My sincere thanks also goes to Prof. Arnab Rai Choudary, Indian Institute of Science, who made many valuable suggestions and gave constructive advice. The good advice, support and friendship of Prof. D K Sahu has been invaluable on both academic and personal level, for which I am extremely grateful.

I would like to acknowledge the Director of Indian Institute of Science, Prof. P Balaram for supporting me to complete this work through Joint Astronomy Programme. I wish to express my cordial appreciation to all the faculty members and students of Department of Physics, Indian Institute of Science for their support and encouragement. I sincerely thank the administrative staff of the institute for helping me during registration.

I would like to take this opportunity to thank the Director of Indian Institute of Astrophysics, Prof. Siraj Hassan for giving me the opportunity to work in this institute and providing all the facilities required for research work. I would like to thank Prof. H C Bhat, Prof. S K Saha, Prof. Annapurni Subramaniam, Prof. R. Ramesh and all members of Board of Graduate Studies for the help and support provided throughout the course of my work. I thank all the faculty of IIA for the fruitful discussions I had with them and providing a research environment. I thank Prof. N. G. Kantharia, Prof. A. P. Rao, Dr, Eswar, Dr. Sabyasachi and all the faculty of NCRA-TIFR for their guidance and support during my GMRT observations. I specially thank Prof. N. G. Kantharia for her support and guidance in radio reductions and analysis.

I would like to thank the faculty and present/former staff of CREST, Dr. B. C.Bhatt, Dr. P. Parihar, Dr. Muneer, Dr. Shantikumar, Ms. Bama, Nandkumar, Vanni, Srividya,

Ravi, Sasikumar, Aman, Ritu, Pepsi and Sonam for the help and guidance they provided for observations throughout the research period. I thank all the instructors who ignited the passion for astronomy during course work. I am grateful to the librarians and staff of library and computer center of both institutes for helping and assisting me in many different ways.

My stay in IIA was made enjoyable in large part due to the many friends and groups that became a part of my life. I am grateful for the time spent with roommates and friends and our memorable trips. I thank all my seniors from whom I learned lots of things. I extend my heartfelt thanks to my friends Nagaraj, Malay, Blesson, Vigeesh, Nataraj, Bharat, Ramya, Rumpa, Tapan, Girijesh, Veeru, Chandu, Krishna, Amit, Pradeep, Abhay, Sreeja, Manju, Suresh, Smitha, Drisya, Anant, Madhu, Indu, Ramya, Ratna, Prasanth, Dinesh, Arya, Sinduja, Hema, Sudhakar, Int.PhD & Int.M-Tech buddies for the support and encouragement throughout my stay in IIA. I would also thank my dear friends Phani and Mallesh for their warm affection and encouragement.

I wish to thank my entire extended family for providing a loving environment for me. I am very grateful to my sister, brother and brother-in-law for their kindness and affection, and for never letting me feel that I am away from them. Finally I would like to express my heartiest thanks to my parents who kept me away from social obligations and encouraged me to concentrate on my studies.

TABLE OF CONTENTS

Abstract

The discovery of several bright supernovae (SNe) in recent years has evoked a great deal of interest in these objects. The study of these objects are of importance not only as probes to the end stages of stellar evolution, but also as probes for cosmology. Though the basic classification of supernovae was restricted to type I and type II, pecularities became apparent over the last two decades that have been confirmed into new classes, currently designated as types Ia, Ib, Ic, IIL, IIP, IIn and IIb. Diversity in the behaviour of supernovae within a class has also become apparent, such as photometric and spectroscopic sequence in type Ia, and the existence of the super-luminous hypernovae, which, at times are found to be associated with GRB events. Core collapse supernovae are the end stages of most stars, more massive than ~ 8 $M_{\odot}$. As such, they provide a key test of stellar evolution. Further, they play a major role in driving the chemical and dynamical evolution of galaxies, and have also been proposed to be major contibutors to dust epochs when the Universe was still young. SNe explosions provide unique natural laboratories for studying, in real time, the physics of a variety of combustion, hydrodynamic, nuclear and atomic processes. All subclasses of SNe, except for type Ia, are core collapse events. The differences in the observed properties of the various subclasses, and even within a single subclass, may be attributed to the progenitor mass, metallicity and environment. The light curve and the spectral development would enable obtaining certain critical parameters related to the progenitor. It is hence important to study individual SNe events. The aim of this work is to (a) study the individual objects in detail and obtain critical parameters such as the radioactive Nickel mass ejected during the explosion, the mass of the ejected material, velocity with which the material has been ejected, the explosion energy and the distance to the supernova; (b) estimate progenitor mass and radius; (c) group the individual events according to certain common properties and inter-compare the properties of the various groups to arrive at a possible evolutionary sequence of the progenitors.

This thesis consists of 6 chapters.

Chapter 1 gives a general introduction to the evolution of massive stars and supernovae.

Chapter 2 describes the telescope and instrument, observations and reduction procedures. All data were obtained using the 2m Himalayan Chandra Telescope (HCT), Hanle, India. The technical details of telescope and instrument are given in the chapter. This chapter also discusses in detail the various techniques used in photometric and spectro-

scopic data reductions.

Chapter 3 discusses the properties of Type IIP supernovae with a detailed study of SN 2004A and SN 2008in. The distances to the supernovae are estimated using the Standard Candle Method (SCM) (Hamuy & Pinto, 2002) and the Expanding Photosphere Method (EPM)(Krishner & Kwan, 1974, 1975, Hamuy et al. 2001) . In addition, the explosion energy, radius of progenitor, the nickel mass and the mass ejected during the explosion are estimated using the observed light curves and the spectra (Hamuy 2003, Elmahamdi 2003, Litvinova & Nadyozhin 1985). The progenitor mass is also estimated based on the estimate of the ejected mass.

Chapter 4 describes the evolution of the Type IIn supernova SN2005kd, which is characterized by narrow emission lines in the early spectra. Some Type IIn supernovae show a plateau phase in the light curve, and SN 2005kd is of this kind. The narrow emission lines in the spectra show that the SN ejecta interacted with the pre-supernova circumstellar material that is a result of mass loss from the progenitor during its evolution.

Chapter 5 discusses the properties of stripped envelope core collapse supernovae using the observations of type Ib/c supernovae SN 2006jc, SN 2007ru, and SN 2009jf. SN 2006jc was found to be peculiar, with narrow He I emission lines arising due to the SN ejecta interaction with a helium enriched pre-supernova circumstellar material. SN 2007ru shows very broad lines in the spectra indicating a velocity of 20,000 kms^{-1}. The light curve evolution of SN 2007ru indicates a fast rise time and post-maximum decline more rapid than other broad-line Ic supernovae. The light curves of SN 2009jf are broad, with slow decline, indicating the presence of massive ejecta. He I line is identified with velocity of 16,000 km^{-1}.

The photometric and spectroscopic evolution of all the above SNe are described in detail and compared with other similar supernovae. The various physical parameters related to the explosion and progenitors of SNe are also estimated.

Chapter 6 is devoted to conclusions and future plans for the work in this thesis.

PhD thesis is based on the following publications

1) *Photometric and spectroscopic evolution of type II-P supernova SN 2004A*, **Gurugubelli U. K.**, Sahu D. K., Anupama G. C., Chakradhari N. K., 2008, BASI, 36, 79G

2) *Optical photometry and spectroscopy of the Type Ibn supernova SN 2006jc until the onset of dust formation*, Anupama G. C., Sahu D. K., **Gurugubelli U. K.**, Prabhu T. P., Tominaga N., Tanaka M., and Nomoto K. 2009, MNRAS, 392, 894A

3) *The Peculiar Type Ib Supernova 2006jc: A WCO Wolf-Rayet Star Explosion*, Tominaga N., Limongi M., Suzuki T., Tanaka M., Nomoto K., Maeda K., Chieffi A., Tornambe A., Minezaki T., Yoshii Y., Sakon I., Wada T., Ohyama Y., Tanabe T., Kaneda H., Onaka T., Nozawa T., Kozasa T., Kawabata K. S., Anupama G. C., Sahu D. K., **Gurugubelli U. K.**, Prabhu T. P., and Deng J., 2008, ApJ, 687, 1208.

4) *The Broad-Line Type Ic Supernova SN 2007ru: Adding to the Diversity of Type Ic Supernovae*, Sahu D. K., Tanaka M., Anupama G. C., **Gurugubelli U. K.**, and Nomoto K. 2009, ApJ, 697, 676S

5) *Optical Studies of the type Ib supernova SN 2009jf*, Sahu D. K., **Gurugubelli U. K.**, Anupama G. C., and Nomoto K., 2010 MNRAS. Submitted.

6) *Optical and radio studies of type IIn supernova SN 2005kd*, **Gurugubelli U.K.**, Anupama G. C., Kantharia N.G., and Sahu D. K. (in preparation)

7) *Photometric and spectroscopic studies of type II-P supernova SN 2008in*, **Gurugubelli U.K.**, Anupama, G.C., Sahu, D.K. (in preparation).

IAU Circulars & ATEL

1) **Gurugubelli U. K.**, Sahu, D.K., Anupama, G.C., Anto, P. 2010, CBET, 2222.

2) **Gurugubelli U. K.**, Anupama, G.C., Sahu, D.K., Sonam, S., Anto, P. 2010, CBET, 2197.

3) **Gurugubelli, U. K.**, Anupama, G. C., Sahu, D. K., Kaur, A., 2009, CBET, 1687.

4) **Gurugubelli, U. K.**, Anupama, G. C., Sahu, D. K., 2006, CBET, 790.

5) **Gurugubelli, U. K.**, Anupama, G. C., Sahu, D. K., CBET, 789.

6) Anupama, G. C., **Gurugubelli, U. K.**, Sahu, D. K, GCN, 9576.

7) Sahu, D. K., Anupama, G. C., **Gurugubelli, U. K.**, 2009, CBET, 1955.

8) Sahu, D. K., Anupama, G. C., **Gurugubelli, U.K.**, 2009, CBET, 1917.

9) Ramya, S. **Gurgubelli, U. K.** Kantharia, N. G.; Anupama, G. C. Prabhu, T. P., 2009, ATel, 2227.

10) Poster presented on SN2004A during the Astronomical Society of India - 2007.

11) Poster presented on SN2005kd during the Astronomical Society of India - 2009.

LIST OF FIGURES

LIST OF TABLES

CHAPTER 1

INTRODUCTION

1.1 Supernovae classification and Optical properties

A star that at the end stages of its evolution explodes and becomes extremely luminous, outshining its host galaxy luminosity, is called a supernova (SN). The release of energy in this explosion is of the order of $\sim 10^{50} - 10^{52}$ erg s^{-1}. SNe were classified spectroscopically by Minkowski (1941) into two different kinds, Type I and II. Type I SNe are defined by the absence of hydrogen in their spectra and Type II prominently exhibit hydrogen in their spectra. There are further diversities in the supernovae classification. SNe I are further classified spectroscopically into subclasses Ia, Ib, and Ic based on the presence/absence of Si, He lines. SNe Ia are characterized by a deep absorption trough around 6150 Å produced by blueshifted Si II $\lambda\lambda$ 6347, 6371 Å (collectively called λ 6355 Å). Objects which belong to Ib and Ic subclasses do not show this line. The presence of moderately strong optical HeI lines, especially He I λ 5876 Å, distinguishes SNe Ib from SNe Ic (Wheeler & Harkness 1986; Harkness & Wheeler 1990). The taxonomy of supernovae based on spectroscopy is shown in Figure 1.1. Type Ia supernovae are a result of thermonuclear explosions due to carbon detonation or deflagration of an accreting white dwarf that exceeds the Chandrashekar limit. All other types of supernovae are due to the collapse of the iron core of a massive star and are collectively called Core Collapse Supernovae (CCSNe). Excellent reviews on supernovae and their properties may be found in Trimble (1982), Trimble (1983), Woosley & Weaver (1986) and Filippenko (1997).

The late time (t $\gtrsim$ 4 months) optical spectra of SNe provide additional constraints on the classification scheme. SN Ia show blends of dozens of Fe emission lines, mixed with some Co lines. SNe Ib and Ic, on the other hand, have relatively unblended emission lines of intermediate mass elements such as O and Ca. At this phase, SNe II are dominated by

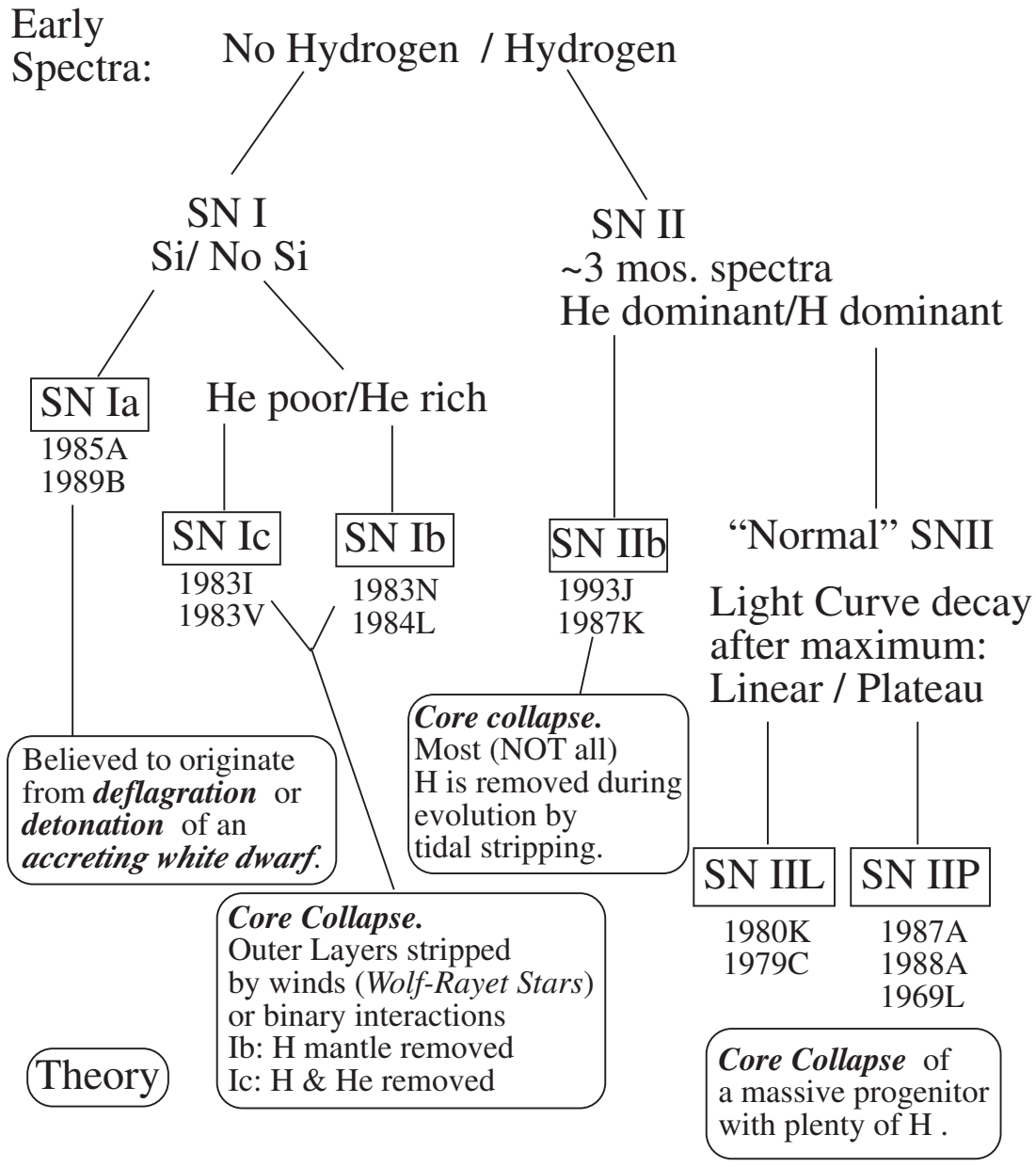

Figure 1.1: Taxonomy of supernovae classification based on spectroscopy. This figure is obtained from `http://rsd-www.nrl.navy.mil/7212/montes/snetax.html`.

the strong Hα emission line; in other aspects, most of them spectroscopically resemble SNe Ib and Ic, but the emission lines are even narrower and weaker.

A supernova spectrum near maximum consists of a broad emission and absorption on top of the continuum which carries much of the energy for the first month (Type I) to year (Type II). Many of the narrow absorption lines, particularly in the ultraviolet, are interstellar. A comparison of spectra of different types of supernova near maximum is shown in the Figure 1.2. The spectral lines are very broad and blended with each other at the early phase indicating ejecta velocities of $\sim$ 15,000 km s^{-1}, that decrease to $\sim$ 3,000 kms^{-1} at the later phases. This decrease does not represent a real deceleration of the gas. Rather, our line of sight is penetrating to deeper layers as the gas expands, layers that move slower than the outer ones. As the supernova evolves in time, the lines become visible and narrower. A late phase comparison spectra is shown in Figure 1.2. Lines that have been identified in both types include H, K, Ca II, the infrared Ca II triplet, the Mg Ib, and Na ID. The photosphere temperature, obtained by fitting a blackbody to the continuum, gradually declines from ~12,000 - 15,000 K at maximum light to $\sim$ 5000 - 6000 K a few weeks after. The photosphere grows linearly for first few weeks and then moves very slowly. The typical values for photospheric radius are $\sim$ 1 - 5 $\times$ 10^{15} cm.

The light curves of SNe Ia are broadly similar, where as those of SNe II exhibit much dispersion (Minkowski 1964). Despite their varieties, the majority of early-time light curves of SNe II (t$\lesssim$ 100 days) can be usefully subdivided into two relatively distinct subclasses. The light curves of SNe II-L ("linear") generally resemble those of SNe I, where as SNe II-P ("plateau") remain with in $\sim$ 1 mag of maximum brightness for an extended period. The comparison of different types of light curves of supernovae is shown in Figure 1.3. As it is shown in Figure 1.3, all Type I (Ia, Ib and Ic) supernovae light curve evolution is somewhat similar where as it differs in the case of Type II.

The Type II-P light curves are heterogeneous. The peak absolute magnitudes of SNe II-P show a very wide dispersion $\sim$ 2 orders of mag, almost certainly due to differences in the radii of the progenitor stars. The plateau ranges from $\sim$ 70 to 120 days. Most SNe II-L, on the other hand, have a nearly uniform peak absolute magnitude $\sim$ 2.5 mag fainter than SNe Ia, although a few exceptionally luminous SNe II-L (SN 1979C) are known. At late time (t $\gtrsim$ 150 days), the light curves of most SNe II resemble each other, both in shape and absolute flux. The decline rate is close to that expected from the decay of ^{56}Co to ^{56}Fe (0.98 mag/100 days), especially in V. The size and mass of the envelope vary according to type, i.e Type II-L supernovae have lower values of envelope mass ($\sim$ 1 - 2 $M_{\odot}$) where as Type II-P have higher values of envelope mass. At the later stages of its

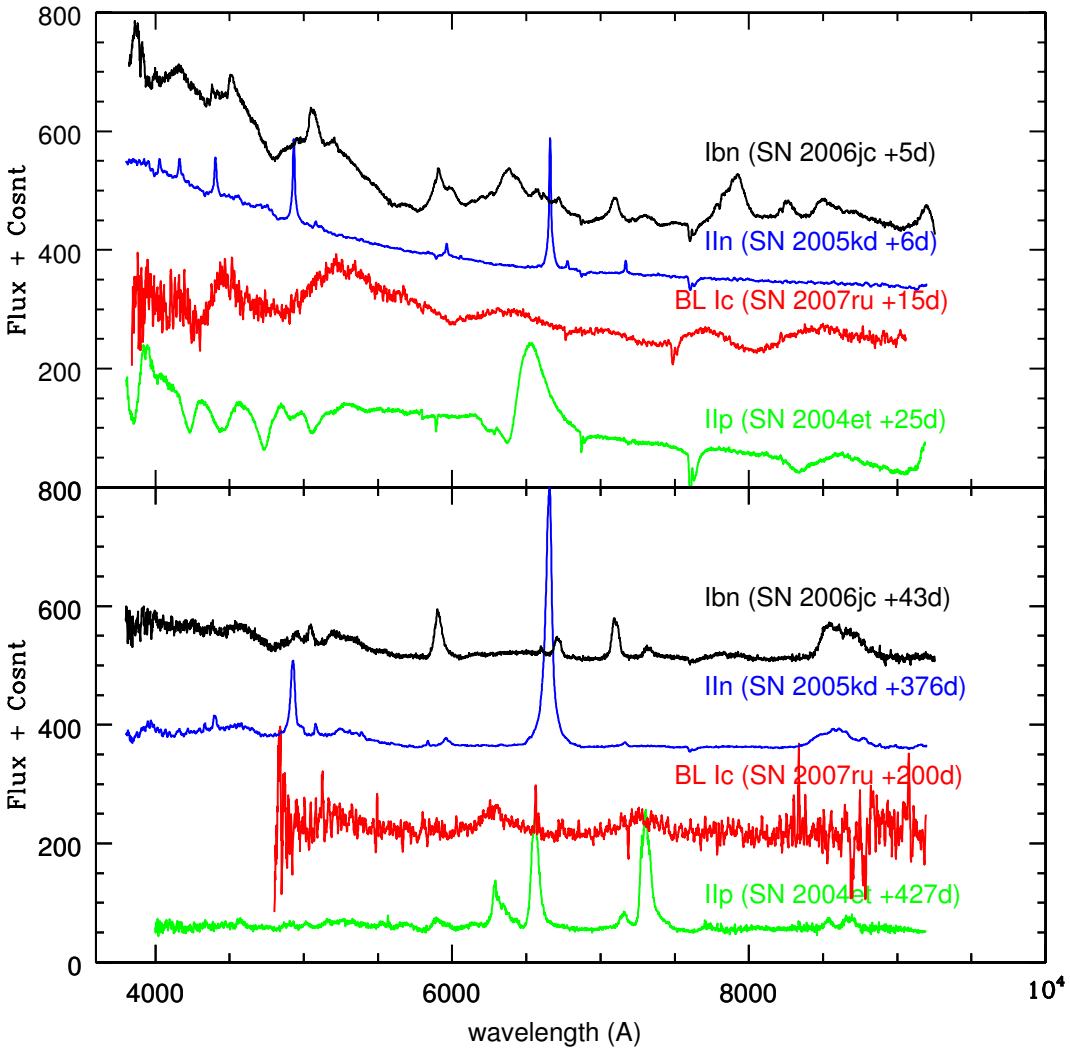

Figure 1.2: Spectral comparision of different kinds of supernovae at two different epochs.

evolution, though the light curve is powered by radioactive decay of ^{56}Co to ^{56}Fe, there is a considerable difference in the slopes of the light curves, depending on the efficiency with which γ-rays are trapped in the expanding ejecta.

Supernovae colors change in a fairly regular way as the objects fade. The $B-V$ color index reddens gradually from ~ 0.0, a maximum light, to $\sim +1.0$ a month or so later, then flattens out (Type II) or turns over (Type I). $U-B$ also reddens monotonically by about a magnitude (-1 to 0 in Type II; 0 to +1 in Type I) in the same period, then changes more slowly (Type II) or flattens out (Type I).

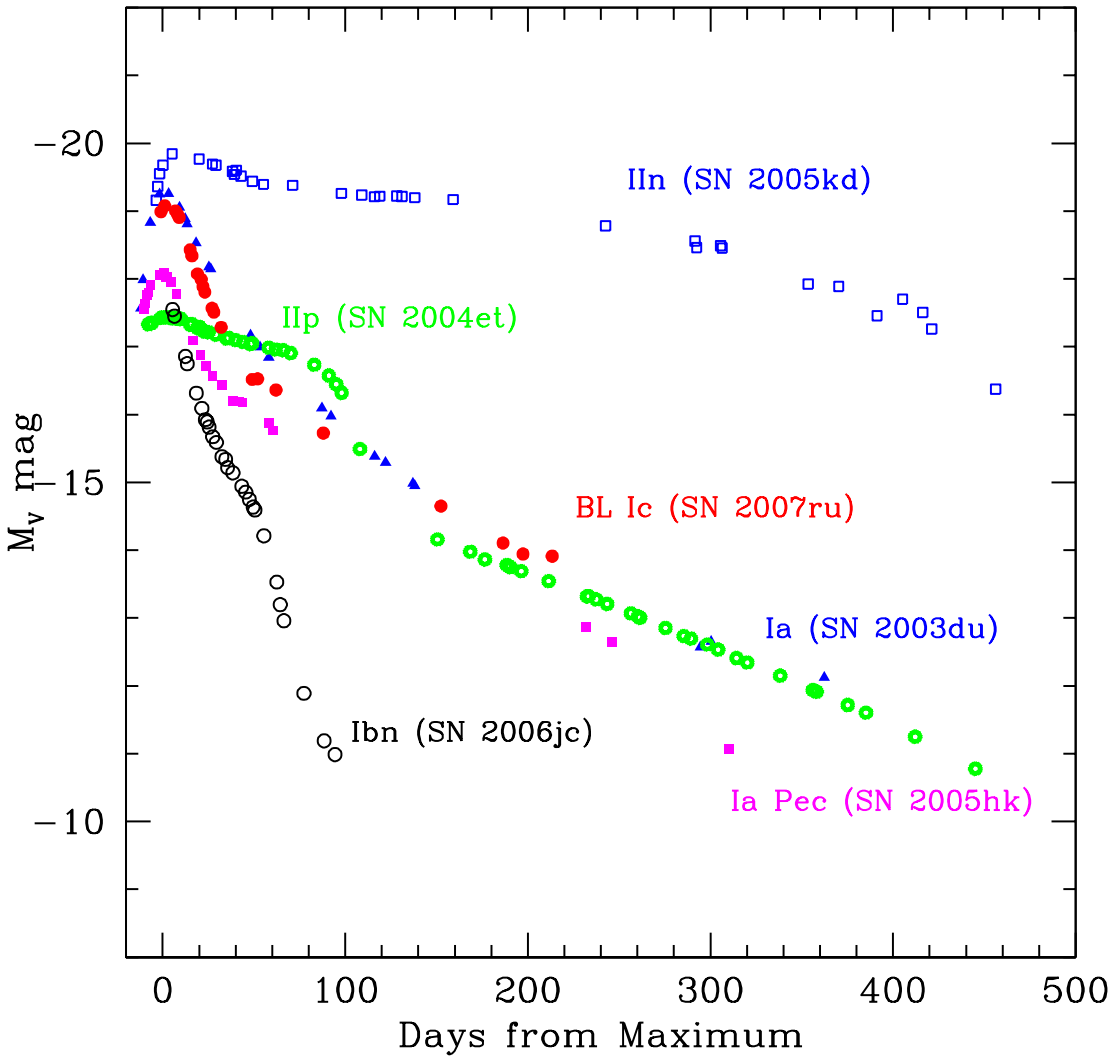

Figure 1.3: Light curve comparision of different kinds of supernovae.

Core collapse supernovae arise within Population I stars. The evidence is that a) they occur only in Hubble types with dominant young components, at a frequency that increases with blueness of the galaxy; b) within these galaxies, they happen mostly in the spiral arms and c) their distribution in galaxies in generally is like that of the neutral hydrogen. The restriction to spiral arms requires an association with the most massive, short lived stars. The implied lower mass limit depends on details of gas speed and pattern speed that must vary considerably from one galaxy to another, but is surely $\gtrsim 4$ $M_\odot$. Smartt (2009) has recently provided a detailed review on the progenitors of CCSNe

based on direct identification of the progenitors, detailed studies of the local population and several other observational constraints. From these studies, it is apparent that the minimum progenitor mass for SNe is 8 $M_{\odot}$.

The frequency of occurrence of supernovae, and how this depends on galaxy type, mass, luminosity, composition etc., matters both for constraining parent populations and for deciding how much each event must contribute toward nucleosynthesis, cosmic rays and pulsar production. One important constraint on the masses of the CCSNe progenitors come from the Initial Mass Function (IMF), the number of stars born per unit time and unit mass interval, though SNe rate comes from the external galaxies. If CCSNe arise from stars with masses greater than $\sim 8M_{\odot}$, then the IMF necessitates that stars in the 8 - 15 $M_{\odot}$ mass range should dominate the rate of explosions.

1.2 Evolution of the Massive stars and the Supernova Explosion

A star, gravitationally bounded blob of hydrogen gas, would proceed through well defined series of nuclear reactions as the gas at its center gets hotter and denser under the continued action of gravitation. Each reaction ignites near the center of the star and feeds on the ashes of its predecessors, which continue to occur further out.

The different stages of ignition and burning of a particular element and the fate of the star depends on the following: 1) the gravitational potential energy which scales as M^2. The more massive a star is, the more energy per gram available as it contracts, and therefore, the lower the central density at which it achieves a given central temperature; 2) the burning of the degenerate fuel is likely to be explosive because its pressure does not immediately respond to the increase in its temperature as energy released.

Pre-main-sequence low mass stars whose core hydrogen exhaust, having inert helium core evolve towards red-gaint phase, provided, it still has enough hydrogen envelope. For the stars having mass $\lesssim 0.35M_{\odot}$, helium becomes degenerate before getting hot enough to burn. These stars end up as helium white-dwarfs if they do not have a binary companion. The non-degenerate helium ignites if the mass of the star is $\gtrsim 2M_{\odot}$ and the star proceeds to next level in their nuclear sequence. For the intermediate stars $\sim$ 0.35 - 2 $M_{\odot}$, helium ignites, partially degenerate, explosively, and is called "helium flash".

At the next stage of evolution, stars in the 0.35 - 2 $M_{\odot}$ mass range exhaust core helium, too cool to ignite their degenerate cores with helium burning products (carbon and oxygen), end up as carbon-oxygen white dwarfs. Stars with initial masses $\gtrsim 2M_{\odot}$ can also

end up with carbon-oxygen white dwarfs if mass loss strips down far enough to turn off helium shell burning before the carbon-oxygen core is sufficiently dense, hot and massive enough ($\gtrsim 1.4\ M_\odot$) to ignite. Stars having the mass range of 6 - 8 $M_\odot$, will give rise to carbon detonation or deflagration Type Ia supernovae, the details of which are not discussed here.

Single stars in excess of 8 $M_\odot$ eventually develop non-degenerate carbon-oxygen cores larger than the Chandrashekar mass, as do binary components with main sequence masses $\gtrsim 15\ M_\odot$. Nuclear burning proceeds in them until the core evolves a Chandrashekar mass of degenerate iron. At this point, the photon temperature is $\sim 8 \times 10^9$ K and the degeneracy energy of the electrons is comparable with the neutron-proton mass difference, permitting photo-disintegration of the iron and electron captures to take place. These erode pressure support within the core, which begins a rapid collapse to neutron star densities (or beyond), releasing $\gtrsim 10$ % of mc^2.

Very massive stars ranging from 15 - 100 $M_\odot$, in the absence of major mass loss, carry out the natural sequence of nuclear reactions, without any interruption, until a sort of onion structure has been built up around a core of iron-peak elements. Quasihydrostatic evolution continues until the iron core mass approaches the Chandrasekhar limit. Nuclear binding is at a maximum near ^{56}Fe, thus these cores are not capable of further exoergic reactions, and some form of collapse is unavoidable. Whether they end up as black holes or as neutron stars, eventually they must become neutronized by inverse beta decays ($e + p \rightarrow n + \nu_e$). Indeed some neutronization occurs, so that the dominant species near the center are ^{48}Ca, ^{56}Ni, ^{54}Cr and ^{50}Ti, but the electron capture is not cause of the initial collapse. Rather, as the central temperature rises above 3×10^9 K, the photons begin to break up the nuceli into alpha particles and free n's and p's. The resultant cooling removes pressure support at the center, and the core begins to collapse.

Once the collapse starts, it goes much faster than either of the processes that triggered it, photo-disintegration being inhibited by the populating of excited states of the nuclei and electron capture by neutrino trapping and neutron shell blocking. The details of these complex processes do not matter much for the hydrodynamics of the core collapse, which is essentially homologous. But in order for the collapse to make, for example Type II supernova, about 1% of available energy must be deposited at the base of an extended, hydrogen-rich (supergiant) envelope. This in turn requires two things- the existence of an appropriate envelope and a suitable energy transport mechanism. Most massive single stars probably still have such an envelope when their cores become unstable, even after extensive mass loss during hydrogen and helium burning.

Two kinds of transport mechanisms have been proposed though neither of them proven satisfactory. Colgate et al. 1961 suggested that the collapsing core would bounce at high density (due to adiabatic compression and hardening of the equation of state at nuclear densities), generating an outgoing shock wave capable of ejecting the envelope. Shortly after, Colgate & White (1966) and Colgate (1968) proposed alternatively that neutrinos made by electron capture would deposit much of their energy and momentum at the base of the envelope, thus ejecting it.

1.3 Dust Formation and Evolution in Supernovae

CCSNe have been considered to be one of the sources of dust in the universe. What kind and how much mass of dust are formed in the ejecta and are injected into the interstellar medium (ISM) depend on the type of CCSNe, through the difference in the thickness (mass) of outer envelope. Dust formation in the ejecta of SNe had been directly observed for the first time in SN 1987A (see McCray (1993) for a review), after then the same was reported in a handful of CCSNe. Based on the observations of nearby SNe, the mass of dust formed in the ejecta has been considered to be less than $10^{-3} M_{\odot}$ per SN, which is more than two to three orders of magnitude smaller than the dust mass predicted by theoretical investigations (Kozasa et al. 1989, Kozasa et al. 1991; Todini & Ferrara 2001; Nozawa et al. 2003). Furthermore, the observed dust mass is too small to explain the amount of dust observed in the host galaxies of quasars at redshift of $z \gtrsim 5$ (e.g. Bertoldi et al. 2003) where CCSNe are considered to be a major source of dust because the cosmic age is too young for AGB stars to supply the dust. So, how much mass of dust forms in the ejecta has been still controversial.

The amount of mass and the kind of dust that are injected from a SN into ISM depend not only on the formation in the ejecta but also on the destruction in the supernova remnant (SNR) where dust grains are injected into and eroded by sputtering in the hot gas swept up by the reverse and forward shocks produced by the interaction of ejecta with interstellar/circumstellar medium. Both processes depend on the type of SNe through the thickness (mass) of outer envelope i.e. with the same kinetic energy of explosion, the thicker outer envelope makes the expansion velocity slower and results in the gas density within He core being high enough to form large sized dust. Furthermore, the lower gas density in the shocked region caused by the delayed arrival of the reverse shock at the dust forming region decreases the erosion rate of dust by sputtering.

At present, observations claim that the mass of dust formed in the ejecta to be less

than $10^{-3} M_{\odot}$ and to be too small to contribute to the inventory of dust in our Galaxy. However, the conclusion is not necessarily definite, based on the limited number of the observations and the assumption that thermal radiation from dust is optically thin in some cases; as pointed out by Meikle et al. (2007), the dust may reside in optically thick clumps in the ejecta. Also, the NIR and MIR observations could miss the cool dust, since dust grains might cool down quickly after the formation as is demonstrated by Nozawa et al. (2008a). A discussion on dust formation and evolution can be found in Kozasa et al. (2009).

1.4 Radio Emission from Supernovae

Emission in the radio regions has been observed in several supernovae; measurements of the multi-frequency radio light curves and their evolution with time show the density and structure of the circumstellar medium (CSM), evidence for possible binary companions, clumpiness or filamentation in the presupernova wind, mass-loss rates and changes therein for the presupernova stellar system and, through stellar evolution models, estimates of the zero age main sequence presupernova stellar mass and the stages through which the star passed on its way to explosion.

In the extensive study of the radio emission from SNe, the following effects have been noted (Weiler et al. 2005):
1) type Ia SNe are not radio emitters to the possible detection limit,
2) type Ib/c SNe are radio luminous with steep spectral indices (generally $\alpha < -1$; S $\propto \nu^{+\alpha}$) and have a fast turn-on/turn-off, usually peaking at 6 cm near or before optical maximum,
3) type II SNe show a range of radio luminosities with flatter spectral indices (generally $\alpha > -1$) and a relatively slow turn-on/turn-off, usually peaking at 6 cm significantly after optical maximum.

All known radio supernovae appear to share common properties of:
1) Nonthermal synchrotron emission with high brightness temperature,
2) A decrease in absorption with time, resulting in a smooth, rapid turn-on first at shorter wavelengths and later at longer wavelengths,
3) A power-law decline of the flux density with time at each wavelength after maximum flux density (optical depth ~ 1) is reached at that wavelength.

The characteristic radio light curves arise from the competing effects of slowly de-

clining non-thermal radio emission and more rapidly declining thermal or non-thermal absorption yielding a rapid turn-on and slower turn-off of the radio emission at any single frequency. Since absorption processes are greater at lower frequencies, transition from optically thick to optically thin (turn-on) occurs first at higher frequencies and later at lower frequencies.

Chevalier (1982a, b) proposed that the relativistic electrons and enhanced magnetic field necessary for synchrotron emission arise from the SN blastwave interacting with a relatively high density circumstellar material which has been ionized and heated by the initial UV/X-ray flash. This CSM density (ρ), which decreases as an inverse power, s, of the radius, r, from the star, is presumed to have been established by a presupernova stellar wind with mass-loss rate, $\dot{M}$, and velocity, ω_{wind}, ($i.e., \rho \propto \frac{\dot{M}}{\omega_{wind} r^s}$) from a massive stellar progenitor or companion. For a constant mass-loss rate and constant wind velocity $s = 2$. This ionized CSM is the source of some or all of the initial thermal gas absorption. Additionally, Chevalier (1998) has proposed that synchrotron self-absorption (SSA) may play a role in some objects. A rapid rise in the observed radio flux density results from a decrease in these absorption processes as the radio emitting region expands and the absorption processes, either internal or along the line-of-sight, decrease. Weiler et al. (1990) have suggested that this CSM can be "clumpy" or "filamentary," leading to a slower radio turn-on, and Montes et al. (1997) have proposed the possible presence of a distant ionized medium along the line-of-sight that is sufficiently distant from the explosion. hence, it is unaffected by the blastwave and can cause a spectral turn-over at low radio frequencies. In addition to clumps or filaments, the CSM may be radially structured with significant density irregularities such as rings, disks, shells, or gradients.

SNe IIn have the spectroscopic feature of narrow emission lines (Schlegel 1990), typically hydrogen, which indicates that circumstellar interaction plays a role in the emission from early times.

The H emission from circumstellar interaction implies strong mass loss before the supernova, so the H envelope is likely to be depleted at the time of the supernova. The sequence of massive star supernova types II-P (plateau light curve), II-L (linear light curve), IIb, IIn (narrow line), Ib, and Ic roughly represents a sequence of increasing mass loss during the stellar evolution. The mass loss affects the velocity distribution of the ejecta composition; in particular, only the II-Ps typically end up with H moving at low velocity. Radio and Xray observations of extragalactic supernovae show varying mass loss properties that are in line with expectations for the progenitor stars. For young supernova remnants, pulsar wind nebulae and circumstellar interaction provide probes of the

inner ejecta and higher velocity ejecta, respectively.

The early interaction in extragalactic supernovae can be observed in a number of ways: radio emission from shock accelerated electrons, X-ray emission from hot gas and nonthermal processes, optical emission from cooling shock waves and radiatively heated gas, and infrared emission from radiatively or shock heated dust grains. Radio is the best marker of interaction because it has been observed from all the types of massive star supernovae (Weiler et al. 2005). On the other hand, radio emission has never been detected from SNe Ia.

The SNe Ib/c probably are dominated by synchrotron self-absorption and their typical velocities are 30000 km s^{-1}. There are three reasons for the higher velocities in the SNe Ib/c vs. SNe Type II: shock acceleration during the supernova continues to higher velocities in the SNe Ib/c because of the more compact progenitors, the lower circumstellar densities around the SNe Ib/c give less deceleration of the interaction region, and the SNe Ib/c typically have lower ejecta masses than, but similar energies to, the SNe Type II so the ejecta have higher mean velocities.

Among the SNe Type II, the range in radio luminosity is probably due to a range in mass loss density. At the low luminosity end are the SNe Type II-P, which have been detected only in recent years. The mass loss rates that are implied by the radio (and X-ray) observations are consistent with those suggested by stellar evolution calculations, which are deduced from observations of Galactic stars (Chevalier et al. 2006). Even over the mass range 10 - 20 $M_{\odot}$, there is a considerable range of mass loss rate. The existing data are consistent with the expected correlation between mass loss rate and progenitor mass determined from direct observations, although there are not yet enough data to provide a good test.

The SNe II-L have a higher mass loss rate, as expected if they came from single stars. If binaries play a role, the expected mass loss rates are not so clear. At the high radio luminosity end of the SNe II are the SNe IIn, which appear to have massive, clumpy circumstellar media. In order to obtain the high radio, X-ray, and optical luminosities, the progenitor star must have lost several $M_{\odot}$ within $\sim 10^3$ years of the supernova.

For the SNe II (except for SN 1987A), free-free absorption is the likely absorption process, so there is a fairly direct estimate of the circumstellar density, although uncertainties arise because of the dependence of the absorption on the circumstellar temperature.

In the case of SN 1987A, the initial rise of the radio emission was likely due to synchrotron self-absorption, so estimates of mass loss density are uncertain, but, if the efficiency of synchrotron production is similar to that for the SNe Type Ib/c, the density is

remarkably low. This low density is supported by the rapid expansion that the supernova shock wave made to the time that the first radio imaging observations were carried out.

Since 1990, the radio flux from SN 1987A has been rising because of its interaction with mass lost during a previous red supergiant stage. This increase was anticipated by the observation of dense gas that had been radiatively illuminated and the ensuing interaction has been observed over a broad wavelength range (McCray 2005). The transition from red supergiant to blue supergiant explosion took $\sim 10^4$ years. The radio light curve of SN 1987A is unusual because of its previous red supergiant phase, although few radio supernovae are followed past an age of three years. Another object that seems to have made a transition to dense gas interaction is SN 2001em, which was initially observed as a SN Type Ib/c and within three years made a transition to SN Type IIn, at which time it was a luminous radio and X-ray source (Chugai & Chevalier 2006 and references therein). In this case, there was apparently a phase of dense mass loss within $\sim 10^3$ years of the supernova explosion which ended before the supernova occurred.

Like the SNe Type II, the SNe Type Ib/c also have a considerable range in peak radio luminosity. The observed range in luminosity is roughly consistent with the observed range of mass loss densities for Galactic Wolf-Rayet stars if the efficiency factors (fractions of postshock energy density in magnetic fields and relativistic electrons) do not vary greatly between objects and are ~0.1. SN 2002ap and SN 2003L roughly represent the low and high extremes for the radio luminosities expected for SNe Type Ib/c.

In addition to radio emission, X-ray emission has been detected from essentially all types of massive star supernovae. However, there is typically only a small amount of data for any particular supernova, so that the X-ray data can provide a consistency check on deductions from the radio emission, but do not yield much additional information on the mass loss properties of the progenitors. In the case of SNe Type II, the X-ray emission is likely to be thermal emission from the shocked ejecta gas. The interpretation of the emission generally depends on the density structure of the supernova. In the case of SNe Type Ib/c, the thermal interpretation generally does not produce sufficient luminosity, so non-thermal mechanisms are indicated (Chevalier & Fransson 2006). Near maximum optical light, inverse Compton emission can be important, but it cannot explain later emission. Chevalier & Fransson (2006) suggested that the late emission can be explained by synchrotron radiation in a scenario where the forward shock wave is cosmic ray dominated so that the electron energy spectrum flattens at high energy.

Optical emission from circumstellar interaction occurs if the interaction is sufficiently dense to produce a radiatively cooling reverse shock wave. It is in this case that a signif-

icant fraction of the interaction power can appear at optical wavelengths. Thus, optical emission from interaction is detected from types IIn, II-L, and IIb supernovae, but not from Type II-P or Type Ib/c supernovae. The H line profiles observed for Type II-L and Type IIb supernovae typically have the boxy shape that is expected for emission from a fairly narrow region near the reverse shock front. The SNe Type IIn have narrow centrally peaked H emission that is likely to be from slow shock waves driven into circumstellar clumps, although a detailed theory for the formation of such lines is not yet available.

Overall, there is reasonable agreement between the circumstellar media inferred from supernova observations and what is expected around the progenitor. One area of uncertainty is still what are the expectations where binary interaction has been important for the progenitor. In addition, the supernova observations are sensitive to clumping in the circumstellar wind and may provide a method to investigate clumping in winds from late type stars (e.g., Weiler et al. 2005).

CHAPTER 2

INSTRUMENT, OBSERVATIONS AND REDUCTIONS

2.1 Optical Observations

The observational data required for the present work were obtained with the 2m Himalayan Chandra Telescope (HCT), of Indian Astronomical Observatory (IAO), located at Hanle, India, and is operated remotely from Centre for Research & Education in Science &Technology (CREST), Hosakote, via a dedicated satellite link, by the Indian Institute of Astrophysics. The telescope was manufactured by the EOS Technologies Inc., Tuscon, Arizona, USA and is equipped with three science instruments which are mounted on an instrument mount cube at the Cassegrain focus with F-ratio of 9. The mounted instruments are the Himalaya Faint Object Spectrograph and Camera (HFOSC), the near-IR imager and the Optical CCD imager. All the optical data used in this work were acquired with the HFOSC.

2.2 Overview of the Optical Telescope

The Himalaya Faint Object Spectrograph and Camera is an optical imager cum spectrograph was built at the Copenhagen University Observatory. The instrument is a focal reducer type of instrument i.e by using a collimator with the same F-ratio as the telescope and the camera, the effective focal length of the telescope is reduced. This allows a larger field coverage for a given detector, and also low-resolution spectroscopy, with the insertion of dispersive elements between the collimator and camera.

HFOSC is mounted on an optical bench, on which the collimator and camera are

placed. There are three wheels in the HFOSC: an aperture/slit wheel in front of the collimator at the telescope focal plane, a filter wheel and a grism wheel, both between the collimator and the camera. Between these two latter wheels, there is a rotational shutter wheel.

The converging light beam from the telescope primary mirror passes through an interface unit, the Filter and Spectral lamp Unit (FASU), which is mounted between the instrument mount cube and the main HFOSC instrument. The main instrument is mounted into the interface unit. The FASU, which houses the narrow band filters and spectral lamps for wavelength calibration, has two filter wheels, three wavelength calibration lamps and one flat-field lamp.

The beam from the telescope, passing through FASU, comes to focus at the main instrument. The parallel beam is focused by the camera on to the detector. As mentioned above, the filter and grism wheels are placed in the parallel beam, in between the collimator and the camera. The instrument is mounted in the on-axis port of the instrument mount cube of the 2-m HCT telescope.

2.2.1 Detector

The detector used with the HFOSC is a thinned and backside illuminated SITE ST-002 Charge Coupled Device (CCD) chip. It has an imaging area of 2048×4096 pixels of size $15\mu \times 15\mu$ each. The central unvignetted 2048×2048 chip area is used in the imaging mode, where as 500×3500 chip area is used in the spectroscopic mode. The detector has two output amplifiers, A & B which can be operated in both high and low gain modes. Though both amplifiers can be used simultaneously, reading out through a single amplifier is usually prefered for simplicity of reduction. The amplifier A is recommended due to its slightly lower Read Out Noise (RON). The basic characterstics of the HFOSC are given in Table 2.1. Gain and readnoise values of the CCD obtained during laboratory tests are given in Table 2.2. The sensitivity of the detector varies from 20% near *U* & *I* band to 70% in *V* & *R* bands. The dark counts are found to be 0.3 e/h and 2.0 e/h in MPP and non MPP modes respectively. The full well capacity in MPP is found to be 51K ADU and hence counts above 51K suffer from severe nonlinearity in the gain.

By default, amplifier A in the MPP and high gain mode is used. The CCD controller takes nearly 20 seconds to clear the detector from residual as well as charges accumulated due to dark current. This overhead is due to the special architecture of the SITE CCD being used. The entire 2K $\times$ 4K chip is read out in 165 seconds where as central 2K $\times$ 2K region, used in imaging mode takes only 83 seconds and 125 seconds in spectroscopy

mode.

Table 2.1: Basic characteristics of HFOSC system

Wavelength coverage	350-900 nm
Detector	2048 × 4096 pixels CCD with pixel size $15\mu \times 15\mu$
CCD Pixel Scale	$0.296''$/pixel
Collimeter focal length	252 nm
Camera focal length	147 mm
Reduction factor	0.58
Spectral resolutions	R∼150 to R∼4500 using a set of 11 grisms
Field of View	10×10 arcmin (unvignetted)
Filters	Bessell $UBVRI$ and 372.7(10), 486.1(10), 5000.7(10),656.3(10),672.4(10) narrow bands

Table 2.2: Gain and Readnoise of the HFOSC CCD

	Amplifier A		Amplifier B	
	High gain	Low gain	High gain	Low gain
RON e^-/ADU	4.8	8.0	5.1	8.0
Gain e^-/ADU	1.22	5.6	1.21	5.6

2.2.2 Introduction to Charge-Coupled Devices

CCD is a light detector and can be used as memory device due to their light gathering capability. The fundamental principle behind its operation is photoelectric effect. When the incident photon is absorbed in silicon, an electron-hole pair is created, stored and collected through gates. An electrical potential is maintained within the device to prevent the electron-hole pair recombination. The resulting signal is amplified and digitized for further processing.

CCD theory and Operation

CCD must perform four tasks in generating an image. They are:-

(1) Charge generation:- The incident photon can interact with the silicon atoms and excite valance electrons into conduction band creating electron-hole pairs. The electron-hole pairs are free to move and diffuse in the silicon lattice structure and finally recombine

after their average lifetime. An electrical potential will be maintained to prevent the electron-hole recombination. Silicon has a band gap of 1.14 eV, so photons with energy above 1.14 eV generate single electron-hole pairs whereas photons with energy above 1.14 eV produce multiple electron-hole pairs. For photons with energies below 1.14 eV, the photon does not have sufficient energy to elevate a valance band electron to conduction band. For energies above 10keV, the probability of interaction is small. Thus silicon atom is transparent to such photons.

(2) Charge Collection:- Once electrons have been freed to the conduction band of the silicon, they must be collected and held in place until the readout. Each pixel has a conductive sub pixel sized electrodes called gates. These gate structures provide each pixel with the ability to collect the free electrons and hold them in a potential well until the end of the exposure.

(3) Charge Transfer:- When an exposure ends, the clock voltages are manipulated such that the electrons that have been collected and held +10 volt potential well, can now move down the vertical registers from one pixel to next. The electrons created anywhere within the pixel during the exposure will be forced to migrate toward the deepest potential well.

When the exposure is terminated and CCD readout begins, the voltages applied to each gate are cycled such that the charge stored within each pixel during the integration is electronically shifted This process is called clocking the device. A simple change in the voltage potentials allows the charge to be shifted in a serial fashion along columns from one CCD pixel to another throughout out the array. Each charge transfer is associated with an efficiency factor which is the ratio of the charge transferred to the charge actually collected called charge transfer efficiency. The columns of the array are connected in parallel and thus each pixel shift is mimicked throughout the entire array simultaneously. One clock cycle moves each row of pixels up one column, with the top row being shifted to output shift register or horizontal shift register.

(4) Charge Detection:- Each pixel in the output register is shifted out one at a time into the output electronics. Each pixel's collected charge is sensed and amplified by an output amplifier. Here the charge collected within each pixel is measured as a voltage and converted into an output digital number (DN) and is typically referred as either counts or ADUs. The amount of voltage needed (i.e. the number of collected electrons or received photons) to produce 1 ADU is termed the gain of the device.

The process of shifting each entire CCD row into the output register, shifting each pixel along this register horizontally, and finally performing the voltage conversion of

each pixel's stored charge by the A/D to produce a DN value is continued until the entire array of pixels has been read out.

Gain of the CCD and Signal to Noise Ratio (SNR)

CCD data values are initially in the digital numbers (DN) equal to the number of electrons divided by number of electrons per ADU. Thus, DN is considered either as counts or ADUs. The amount of voltage needed, or the number of collected electrons needed to produce 1 ADU is the gain of the device.

Poisson (photon) statistics are usually invoked when dealing with photon-counting devices, with the SNR being given by $\sqrt{N}$, where N is the total photon count from the source, for cases where the system and background noise contributions are negligible. If other noise sources are significant, then the SNR is given by the well-known "CCD equation"

$$S/N = N_*/\sqrt{N_* + n_{pix}(N_s + N_d + N_r^2)}, \tag{2.1}$$

where N_*= the total number of the photons from the source. n_{pix}=the number of pixels contained within the software aperture. N_s=the total number of sky photons per pixel. N_d=the dark current in photons per pixel. N_r^2=the read noise in electrons per pixel.

Noise sources in CCDs

A noise source is anything that contributes to uncertainty or errors in estimation of some quantity of astronomical interest. Different noise sources of CCD are:-

(1) Readout Noise:- Readout noise is usually quoted for a CCD in terms of the number of electrons introduced per pixel into the final signal upon readout of the device. Read noise consists of two inseparable components. First is the error induced while converting from an analog signal to digital number, which is not perfectly repeatable. Second, the electronics themselves will introduce spurious electrons into entire process, yielding unwanted random fluctuations in the output. These two effects combine to produce an additive uncertainty in the final output value for each pixel. The average (1 σ) level of this uncertainty is the read noise and is limited by the electronic properties of the on-chip output amplifier and the output electronics. In the output CCD image, read noise is added into every pixel every time the array is read out.

(2) Dark Current:- Dark current is the electrons generated due to the thermal agitation which will add to the electrons that are created by the incident photons. Dark

current for a CCD is usually specified as the number of thermal electrons generated per second per pixel or as the actual current generated per area of the device which obeys Poisson statistics. To keep this dark current low, different cooling mechanisms will be accomplished, for example cooling by liquid nitrogen. The liquid nitrogen is placed in the dewar, though not in direct physical contact with the CCD, cools the device to temperatures near to -100° C.

(3) Bias:- Bias or Zero images allow one to measure the zero noise level of the CCD. To avoid negative numbers in the output image, CCD electronics are set up to provide a positive offset value for each accumulated image. This offset value, the mean "zero level", is called the bias level. To evaluate the bias or zero noise level and its associated uncertainty, specific calibration processes are used. The two most common ones are (1) overscan regions produced with every object frame or (2) usage of bias frames. Bias frames are taken with shutter closed, for a integration time 0.0 seconds. This type of image is simply a readout of the unexposed CCD pixels through the on-chip electronics, through the A/D converter, and then out to the computer producing a two-dimensional bias or zero image. Overscan strips are a number of rows or columns (usually 32) or both that are added to and stored with each image frame. These overscan regions are not physical rows and columns on the CCD device itself but additional pseudo-pixels generated by sending additional clock cycles to the CCD output electronics.

2.2.3 CCD data reduction processes

Reduction processes are steps taken to minimize the influence of data acquisition imperfections on the estimation of the desired astronomical quantity. To obtain optimal results, it is essential to know the sources of noise that may affect the results and to consider these within the context of the astronomy. First, a median combined bias frame is subtracted from the object frame. The resultant image is n divided by a bias subtracted master flat field image. These two steps have corrected the object frame for bias level, dark current and non-uniformity within each image pixel. Thus, the basic reduction processes are bias subtraction and flat fielding.

Bias subtraction:- Firstly, bias combining has to be done as the random noise will be reduced when the average of several bias frames (mean, median or mode) is taken. Then the combined bias frame is subtracted from the object frame. There are two types of subtraction: Pixel by Pixel subtraction in which all bias frames in each pixel are averaged and then subtracted from the object frame or constant subtraction in which the bias frames of all pixels are averaged and that constant value is subtracted from the object frame.

Flat fielding:- Within the CCD, each pixel has a slightly different gain or QE value when compared with its neighbors. In-order to flatten the relative response for each pixel to the incoming radiation, a flat field image is obtained and used to perform this calibration. Ideally a flat field image would consist of uniform illumination of every pixel by a light source of identical spectral response to that of the object frames. That is, the flat field image should be spectrally and spatially flat. Once a flat field image is obtained, one then simple divides each object frames by it which results in the instant removal of pixel-to-pixel variations.

For imaging applications, a very common procedure to obtain a flat field image is to illuminate the dome screen with a bright source inside the telescope dome, and take a number of relatively short exposure so as to not saturate the CCD. Since the pixels within the array have different responses to different colours of light, flat field images need to be obtained in each filter that is to be used for the target observations. As with bias frames, the flats exposed in each filter are combined and averaged together to form a master flat field, which can be used for calibration of the CCD. Other methods of obtaining a CCD flat field image include taking CCD exposure of the dawn or dusk sky or obtaining spatially offset images of the dark night sky; these can then be median combined to remove any stars that may be present. Flat fields obtained by observation of an illuminated dome or dome screen are referred to as dome flats, while observations of the twilight or night sky are called sky flats. CCD imaging and photometric applications use dome or sky flats to remove the variations. Twilight flats have been used in this work.

Normalization of the flat fielded frame has to be done by dividing the bias subtracted flat field frame by the mean number of counts of the same. The bias-subtracted object frame is then devided by this normalized, bias subtracted flat frame. A good flat field allows a measurement to be transformed from its instrumental values into numeric results in a standard system that results in an answer that agrees with other measurements made by other observers. The steps above correct the object frame for bias level, dark current and non-uniformity within each image pixel.

2.2.4 Reduction Procedures

Photometry

Photometry is a part of observational astronomy that deals with measurement of the intensity of radiation from celestial objects. It determines the amount and temporal nature of flux emitted by an object as a function of wavelength.

The basic photometric toolbox must contain methods that perform the following primary tasks, (1) estimation of the background (sky) level and (2) calculation of the flux contained within the object of interest. To a good approximation, the stellar images are represented by a Point Spread Function (PSF) of more or less Gaussian shape.

Photometric Systems

The magnitude of a star depends on the system with which one is measuring it. Astronomers have settled on a number of different photometric systems, each one based on a particular passband. A telescope, a set of filters, light detector, and a method for correcting the atmospheric extinction form a natural photometric system. The standard system is defined by a list of magnitudes and colours measured for a set of typical standard stars.

Photometric systems can be classified into three categories based on the wavelength intervals transmitted by their filters:- Broad band systems with filter widths 1000 Å, intermediate band system with filter widths 200 Å, narrow band systems with filter widths 30 Å.

Different types of photometry

The basic photometric toolbox must contain methods that perform the following primary tasks:- (1) Determination of the centre of an image: Firstly, a subarray centered on an initial guess for the centre of the star is extract from the CCD frame. The size of subarray should have enough number of pixels, to allow an estimation of the sky background. The size of subarray must contain not only the star but also enough pixels to allow an estimation of the sky background. From this subarray, the x and y marginal sums $P(x_i)$ and $P(y_i)$ are formed by summing the pixel intensities down the columns and across the rows. If $I(ij)$ is the intensity at the pixel,

$$P(x_i) = \Sigma I_j(ij) \qquad P(y_j) = \Sigma_i I(ij) \tag{2.2}$$

By fitting one dimensional function (Gaussian) to these marginal sums, we can estimate the image center in both co-ordinates.

(2) Estimation of the background (sky) level: The importance of properly estimating the background level on a CCD resides in the fact that the same pixels that collect photons of interest from an astronomical source also collect photons from the "sky" or background source, which are of no interest. In order to determine this background level, a common technique is to place a software annulus around the source of interest and then use statisti-

cal analysis to estimate its mean level on per pixel basis. The background or sky annulus is defined by an inner and outer radius or by inner radius and width. The inner radius of the annulus should be far from the center of the star (several times of FWHM) so that its contribution to the signal in the background annulus is negligible. Another way by which the estimation of the background level can be made is to simply extract the values of all the pixels within the annulus, sum them, and divide by the total number of pixels within the annulus. This gives the average value per pixel for the background level of CCD image.

(3) Calculation of the flux contained within the object of interest. The total signal from the star inside an aperture of radius R in magnitudes,

$$m = -2.5logI, \tag{2.3}$$

where $I = \Sigma I_{ij} - n_{pix} i_{sky}$
n_{pix} = no. of pixels in the aperture.
i_{sky} = background sky value per pixel.

There are two ways to estimate the integrated flux of the object of interest.

Aperture Photometry

Aperture photometry is a straightforward procedure to measure the flux of the source object without including possible contributions from the contaminating sources such as bias levels, sky counts and defects of the CCD. It suits best for isolated stars on flat backgrounds where the intensity of the object is calculated by summing all the pixel values within the specified aperture and subtract the sky counts within that area. The aperture used may be circular, square or any shape deemed useful. Now, the difficult task here is to determine the size or radius of the aperture. The aperture radius should be in such a way that it should include most of the light of the object and a little from the sky so that the error will be low. The sky background is usually estimated by taking an annulus around the object. This aperture is known as a optimal aperture which is a few times the FWHM of the object. Thus, the optimal aperture is the one which is large enough to enclose most of the flux, but otherwise small enough to reduce the error.

Point Spread Function photometry (PSF)

In many images, many stars are faint and overlap due to the crowding in the image. Another problem is that the signal to noise ratio is often low for faint stars. Also, when the measured star is located on luminous uneven background consisting of nebulae or faint stars in galaxies, it is difficult to obtain a good background level for aperture photometry. Provided that a good PSF, a good model for the uneven background can be obtained. PSF fitting usually performs better. The point spread function(PSF) is the image of a star (a point light source) on the detector. The PSF is a two dimensional analytical approximation by which profiles of an astronomical point sources are fitted. The PSF is derived from the stars in the image, either as an empirical image or by fitting an analytical function to the stellar images. PSF fitting means that the normalized PSF is fitted to a star in the image to obtain intensity and magnitude. The background level is estimated simultaneously with the PSF fit from surrounding area of the stars.

Profile fitting techniques work by matching the implied PSF to the actual digital data in a 2D fashion and within some radius called the fitting radius. An attempt is then made to maximize some goodness of fit criteria between the assumed PSF and the observed one. PSF fitting can be further optimized by fitting N point sources within the image simultaneously and using some combination of statistically weighted mean values for the final fitting parameteres. This photometry is the only method applicable to crowded fields.

Magnitude estimation of the supernovae

The magnitude of the supernova can be estimated using photometric techniques such as aperture photometry, weighted aperture photometry and PSF fitting photometry. Since supernovae are always associated with galaxies, where the background from the galaxy is quite high and also non-uniform, though the supernova is not in a crowded field, it is good to opt for PSF photometry than aperture photometry. The frames have to be corrected for atmospheric extinctions and airmass before estimating the magnitude. Then supernova magnitudes are obtained using transformation equations determined for the instrumental setup.

Atmospheric Extinction Corrections and Air Mass Calculations

Even on the clearest of nights, the stars are dimmed significantly by absorption and scattering of light by the earth's atmosphere. The amount of light loss depends on the height of the star above the horizon, the wavelength of observation and the current atmospheric

conditions. Because of this complex behaviour, the measured magnitudes and colour indices are corrected for "above the earth's atmosphere"

At altitudes more than 30° (zenith distance of 60°) above the horizon, the simple plane-parallel approximation model of the atmosphere between an observer and a star is accurate to within 0.2 %. This approximation gives the airmass, the mass of the air traversed by the starlight X as

$$X = \sec(z), \tag{2.4}$$

where

$$\sec(z) = (\sin\phi \times \sin\delta + \cos\phi \times \cos\delta \times \cos H)^{-1}\,, \tag{2.5}$$

where ϕ is the observer's latitude, δ is the declination of the star and H is the hour angle in degrees. For zenith distances greater than 60°, the plane parallel approximation fails. A measured magnitude m_λ, is corrected to the magnitude that would be measured above the earth's atmosphere, m_{λ_0}, by the following equation

$$m_{\lambda_0} = m_\lambda - (K_\lambda^{'} + K_\lambda^{"}c)X, \tag{2.6}$$

where $K_\lambda^{'}$ is called the principal extinction coefficient and $K_\lambda^{"}$ is the second order extinction coefficient. Here 'c' is the observed colour index. The second order term can be neglected. Thus the equation becomes

$$m_{\lambda_0} = m_\lambda - (K_\lambda^{'}X), \tag{2.7}$$

where K_λ is extinction. The average extinction values (Stalin et. al 2008) determined for the IAO site in *UBVRI* bands, namely 0.3365, 0.2099, 0.1255, 0.0925 and 0.0726 are used in this work.

Transforming to a Standard System

A system of magnitudes and colours, such as the *UBVRI* system, is defined by a set of standard stars measured by a particular detector and filter set. In order to compare the observations at different observatories, the observations must be transformed from the instrumental systems to a standard system. Once the observed magnitude has been corrected for atmospheric extinction, it can be transformed to a standardized magnitude. The basic equation is

$$M_{\lambda_1} - M_{\lambda_2} = \alpha(m_{\lambda_1} - m_{\lambda_2}) + \beta, \tag{2.8}$$

where α and β are the colour coefficient and zero-point constant, respectively, of the instrument. These coefficients and zero-point constants are determined from the observations of standard stars.

Spectroscopy

The spectroscopic data are obtained through grisms 7 & 8, which cover the wavelength range 3800 - 6840Å and 5800 - 8350Å with resolutions of $R \sim 1330$ and 2190 respectively. Spectra are obtained using the 167l (long) slit for supernova and with 1340l (long) slit for spectroscopic standards. The data reductions are carried out in the following way 1) all the observed object, standard and comparison frames are bias corrected and flat-fielded; 2) extract one dimensional spectra of the object, standard and comparison frames using optimal extraction method; 3) perform wavelength calibration and rebinning onto a linear wavelength scale; 4) correct for the site extinction and derive instrumental response or sensitivity function for each grism; 5) and then apply the sensitivity function on the object spectrum. This process is known as flux calibration.

As the first step bias needs to be subtracted from the comparison, object and standard spectra to eliminate signal registered by the detector in the absence of the exposure light. Pixel-to-pixel variation are eliminated by the dividing the frame with bias corrected master flat. Then one dimensional spectra is extracted from the object frame, by summing the contributions of each pixel over a range of spatial pixels. The spectra are extracted by optimal or weighted variance extraction, there by achieving better signal-to-noise ratio. The background level is estimated by specifying two regions on the either side of the profile, in which a low order polynomial is fitted and then subtracted from the object frame.

The transformation of the pixel value to wavelength along the dispersion direction is called wavelength calibration. The wavelengths of the known spectral lines in the comparison spectra are used to determine a function that relates pixel number to wavelength, and is then applied it to the one dimensional extracted spectra. Then the spectra should be corrected for extinction. A standard star for which spectral energy distribution is accurately known is used to produce the instrumental response curve. The object wavelength, extinction corrected spectra will be divided by this response curve which gives the final flux calibrated spectra of the object. But the fluxes are not absolute. To get the absolute fluxes, the magnitudes at the effective wavelength of *UBVRI* bands are obtained from the flux calibrated spectra. Then a correction curve is obtained comparing the spectroscopic magnitudes with the photometric magnitudes at those wavelengths and that correction is applied to the observed spectra. All spectra in this thesis are reduced in the same way as

explained above.

2.3 Radio Observations

Low frequency radio observations in 1280 MHz and 610 MHz bands were done using The Giant Meter Wave Radio Telescope (GMRT), operated by the National Center for Radio Astrophysics (NCRA), TIFR, Pune. GMRT consists of 30 fully steerable parabolic dishes, of 45 m diameter each. Twelve antennas form a random array in a central 1 km $\times$ 1 km area and the remaining 18 are equally distributed along the 3 arms of an approximate 'Y' configuration resulting in a maximum baseline separation of about 25 km. GMRT operates at six frequency bands around 50, 150, 233, 327, 610 and 1420 MHz. Readers are requested to refer to the GMRT webpage `http://www.ncra.tifr.res.in` for more technical details.

The data ware reduced in the standard manner using NRAO "AIPS" package. The bad data points were removed and calibrated using flux and phase calibrators. Bandpass calibration was done using the flux calibrator and applied to the target source to improve the signal to noise ratio. Then, the data was used to make an image of the target source. Self calibration was run on the target source to remove artifacts and to improve the dynamic range. The supernova flux was then measured by fitting a gaussian model.

CHAPTER 3

TYPE II-P SUPERNOVA

3.1 Introduction

The Type II-P supernovae are hydrogen rich explosions that exhibit a distinct plateau phase in their light curve almost immediately after maximum, lasting for nearly 80 - 100 days. A majority of the Type II-P supernovae have typical mid-plateau magnitudes of $M_v \sim$ -17 mag (Richardson et al. 2002). This class of SNe are however heterogeneous and span a factor of 100 (i.e ratio of maximum to minimum) in both luminosity and in mass of ^{56}Ni synthesized during the explosion. The spectra of Type II-P supernova, at early stages is nearly featureless and quite blue, indicating high color temperature ($\gtrsim$ 10,000 K). Sometimes hydrogen Balmer lines and He I λ 5876 Å are visible. Initially, the widths of the Balmer lines and the blue shifts of their P-Cygni absorption minima decrease as the photosphere quickly recedes to the inner, more slowly moving layers of the ejecta. The temperature rapidly decreases with time, reaching $\sim$ 5000 K with in a few weeks, as expected from the adiabatic expansion and associated cooling of the ejecta. It remains roughly constant at this value during the plateau, while the hydrogen recombination wave moves through the massive hydrogen ejecta and releases the energy deposited by the shock. At this stage strong Balmer lines and Ca II, H & K with well developed P-Cygni profiles appear, as do weaker lines of Fe II, Sc II and other iron-group elements. Subsequently as the light curve drops to the late-time tail, the spectrum gradually takes on a nebular appearance; the continuum fades, but $H\alpha$ becomes strong and prominent emission lines of [O II], [Ca II] and Ca II also appear.

The progenitor stars of several of the nearest SNe Type II-P have been discovered (Smartt 2009) and are found to be red supergaints (RSG) as predicted by both stellar evolutionary theory and light curve modeling. The key physical parameters that largely

determine the observable display are (a) the total energy deposited by core processes in the overlaying mantle, (b) the density distribution and composition of the pre-supernova star (including any previously ejected circumstellar material) and (c) the energy input from radioactive material produced and ejected in the explosion. The simplified models of the envelope of red giants, to a central point explosion yields an optical display in reasonable agreement with many features of observed Type II supernovae light curves, particularly those of Type II-P, provided that the envelope is sufficiently extended and the total energy of the explosion is of the order of 10^{51} erg. Stellar evolution calculations that neglect mass loss have shown that 15 $M_{\odot}$ and 25 $M_{\odot}$ population I stars should have such extended envelope at the time of collapse of their iron core. Weaver & Woosley (1980) extended these calculations and found that the light curves as well as the photospheric temperatures, radii, and velocities resulting from the ensuing explosions were in excellent quantitative agreement with those of Type II-P supernovae.

Taking the case of the 15 $M_{\odot}$ star as representative example, Woosely & Weaver found that theoretical models indicate that the observable supernova event begins when the shock initiated in the core and reaches the star's surface, which causes a soft X-ray pulse about 30 min long. The supernova's luminosity then falls rapidly as its surface is cooled by expansion and radiative emission. Meanwhile, the rest of the star's material is cooled and accelerated by adiabatic expansion. The bulk of the star remains sufficiently optically thick during this acceleration that 99% of the total supernova energy is converted to kinetic energy in the expanding debris. Only 1% (typically about 10^{49} erg) thus remains to be radiated when the star finally starts to become optically thin after expanding to about 10^{15} cm, or about 30 times its initial radius.

A two-to three-month-long plateau in emission then follows as a cooling wave associated with the transparency induced by hydrogen recombination propagates through the star's exploding envelope. During this period, the photospheric temperature is observed to remain roughly fixed at $\sim$ 6000 K, the temperature at which hydrogen recombines at the typical envelope densities of 10 - 13 g cm^{-1}. The absolute size of the photosphere remains approximately fixed at about 1.5×10^{15} cm as a result of the near-cancellation of the expansion of the envelope and the inward motion of the photosphere relative to the envelope material as it follows the recombination wave. The resulting nearly constant luminosity phase persists until the recombination wave reaches the slowly moving ($\sim$1000 km s^{-1}) mantle, which is relatively dense and very optically thick.

At later times, the luminosity of the 15 $M_{\odot}$ supernova results from the diffusion out of the mantle of thermalized radiation from the decay of explosively generated ^{56}Ni and

its daughter ^{56}Co. Models in which ^{56}Ni decay is turned off display a much more sharply falling luminosity tail, since the residual thermal energy in the mantle diffuses out over a characteristic time of only one to two months. In the models containing energy input from radioactivity, temporary trapping of the decay energy in the optically thick mantle produces a luminosity decline somewhat slower than the 78-day half-life of ^{56}Co.

3.2 Physical parameters of the Type IIP supernovae

The key physical parameters that determine the supernova explosion and its evolution, such as the energy of the explosion, the amount of radioactive nickel synthesized during the explosion and the total mass ejected during the explosion can be estimated based on observables. Litvinova & Nadezhin (1983) have computed a series of hydrodynamical models of Type-II supernova outbursts and derived approximate relations connecting total energy (E), the mass of the envelope ejected (M), and the pre-supernova radius (R), with observables such as the duration of the plateau in the light curve (Δt), and mid-plateau absolute magnitude in the wavelength band (V) and photospheric velocity (u_{ph}) observed near the middle of the plateau. The relations (Litvinova & Nadezhin 1985) are:

$$\log E = 0.135V + 2.34 \log \Delta t + 3.13 \log u_{ph} - 3.205, \tag{3.1}$$

$$\log M = 0.234V + 2.91 \log \Delta t + 1.96 \log u_{ph} - 1.829, \tag{3.2}$$

$$\log R = -0.572V - 1.07 \log \Delta t - 2.74 \log u_{ph} - 3.350. \tag{3.3}$$

These equations provide a simple and quick method to derive E, M and R from observations without detailed specific models for each SN. It should, however be noted here that these estimates are indicative, since the formulae are obtained from models with ejected masses and explosion energies $M = 1 - 16\ M_{\odot}, E = 1.82 - 29.1 \times 10^{50}$ erg, while quite a few SNe II-P have been observed to have values beyond these limits (Hamuy 2003).

3.2.1 Estimation of ^{56}Ni mass

Nickel mass from bolometric luminosity of exponential tail

The lightcurve of supernovae in the nebular phase is powered by the radioactive decay of ^{56}Co to ^{56}Fe, which is a daughter nuclei of ^{56}Ni. Thus, the bolometric luminosity in the nebular phase of Type II-P supernovae can be used to estimate the amount of ^{56}Ni mass

freshly synthesized during the explosion by assuming that all of the γ-rays resulting from the ^{56}Co $\rightarrow$^{56}Fe decay are fully thermalised. Following Hamuy (2003), the first step is to convert the V band tail magnitudes to bolometric luminosity using the following relation,

$$\log L_t = -0.4([V_t - A_{Gal}(V) - A_{host}(V) + BC] + 5\log D - 8.14), \tag{3.4}$$

where L_t is the tail luminosity in erg s^{-1}, D is the distance in cm, BC is bolometric correction that permits one to transform V magnitudes into bolometric magnitudes, and the additive constant provides the conversion from Vega magnitudes into cgs units. Hamuy (2003) estimated the value of BC to be 0.26 $\pm$ 0.06 during the nebular phase from SN 1987A and SN 1999em. Using the tail luminosity, nickel mass can then be found by using the following relation,

$$M_{Ni} = 7.866 \times 10^{-44}\ L_t \exp\left[\frac{(t - t_o)/(1 + z) - 6.1}{111.26}\right] M_\odot, \tag{3.5}$$

where 6.1 is the half-life (in days) of ^{56}Ni and 111.26 is the e-folding time (in days) of the ^{56}Co decay, each of which releases 3.57 MeV in the form of γ-rays (Woosely, Pinto & Hartmann 1989).

Nickel mass from the "Steepness of Decline" correlation

An alternative way of estimating ^{56}Ni mass was suggested by Elmhamdi et al. (2003) to improve the accuracy of Hamuy (2003) method, by defining inflection time during transition from plateau to the radioactive tail as a zeropoint. The inflection time is defined as the moment when the first derivative at the transition phase, $S = -dM_V/dt$ called as steepness of decline, is maximal. The linear correlation between photometric ^{56}Ni and the absolute magnitude $M_V(t_i - 35)$ in the case of SN 1997D is given by the following equation:

$$\log M(^{56}Ni) = -0.438\ M_V(t_i - 35) - 8.46. \tag{3.6}$$

Elmhamdi et al. (2003) also found that the steepness (S) anticorrelates with ^{56}Ni mass, i.e, the lower the ^{56}Ni mass the larger S. However, an accurate determination of S necessitates a V light curve with a reasonably high density of observational points at the end of the plateau phase and the beginning of the radioactive tail. The correlation yields the following relation:

$$\log M(^{56}Ni) = -6.2295\ S\ - 0.8147. \tag{3.7}$$

Hendry et al. (2006) reexamined the results of Elmhamdi et al. (2003) and derived the following relationship to get more accurate value of ^{56}Ni mass:

$$\log M(^{56}Ni) = -6.9935(\pm 0.3791)\ S\ -\ 0.7383(\pm 0.0355). \tag{3.8}$$

3.3 Distance Estimation

3.3.1 Expanding Photosphere Method

The Expanding Photosphere Method (EPM) is basically a geometric technique used to determine the distance to variable stars (Baade 1926), by comparing the linear radius of the expanding photosphere with the angular size (θ) to derive the distance (D) by assuming that the geometry is spherical and the radius of the progenitor is small compared with the size of the photosphere. An interesting feature of this method is that if the date of explosion is known, then each measurement of θ/v_{phot} provides an independent estimate for D. If we assume that the spherically symmetric SN photosphere radiates isotropically as a black body, conservation of flux demands

$$4\pi R^2 \pi B_\nu(T_c) = 4\pi D^2 f_\nu, \tag{3.9}$$

where B is the Planck function at color temperature T_c and f_ν is the flux received at Earth. The observable parameter that goes inside EPM are v_{phot}, that is the photosphere velocity derived from the P Cygni absorption troughs of the spectra, typically from Fe II $\lambda\lambda$ 4924, 5018, 5169 Å and occasionally Sc II λ 5527 Å and Sc II λ 5658 Å, f_ν and T_c. The consistency of this technique depends mainly on three assumptions: 1) the photosphere radiates as a blackbody; 2) the photosphere is spherically symmetric and 3) the photospheric velocity is accurately determined by measuring the blue shift of weak P-Cygni absorption lines.

At first, by assuming that the photosphere radiates as a black body, Baade (1926) measured the distance to variable stars. Kirshner & Kwan (1974) applied the basic idea of EPM to SNe II-P and demonstrated that a Type II-P SNe photosphere radiates as a dilute blackbody because of the dominance of electron scattering over absorption processes. That is, the continuum spectrum that is ultimately released from the electron-scattering photosphere (defined as the surface of last scattering, τ=2/3) is produced in the deeper layer at which the radiation field thermalizes to the local gas temperature, known as the thermalization depth. This smaller radius is the location of the last true absorption and

re-emission of the photons that make up the thermal continuum. The blackbody spectrum ultimately released by the electron-scattering photsphere thus possess a luminosity appropriate for a smaller radiating surface. The amount by which the flux diluted is parameterized by the relation $\zeta = R_{therm}/R_{phot}$, where R_{therm} is the radius at the thermalization depth, R_{phot} is the photosphere's radius (i.e radius of the surface of last scattering) and ζ is called the distance correction factor since its inclusion in above equation corrects the derived distance, such that distances derived without the flux dilution, will be overestimated by a factor ζ.

In principle, ζ could depend on many things, including the chemical composition and density structure of the progenitor star and the expansion rate and luminosity of the SN explosion. Studies of theoretical models of realistic SN atmospheres with a wide range of properties, however, have demonstrated that ζ is in fact a nearly one-dimensional function of color temperature (T_c), with only a small density dependence at shorter wavelengths.

Eastman et al. (1996) studied 63 model atmospheres, and provided convenient analytic approximations for ζ as a function of color temperature for an SNe II-P, determined for four broadband filter combinations, BV, BVI, VI, and JHK (the R band is generally not used, since it is dominated by the Hα line, which can vary significantly among SNe II-P). The variation of ζ with temperature is well fit by the following polynomial form,

$$\zeta_\nu(T) = \Sigma_i a_i(\nu)\left(\frac{10^4\ K}{T}\right)^i \tag{3.10}$$

and the coefficients are taken from Hamuy et al. (2001).

If we rewrite the above equation after including the extinction and flux dilution then,

$$f_\nu = \zeta^2\theta^2\pi B_\nu(T_c)10^{-0.4A_\nu}. \tag{3.11}$$

If we replace f_ν with the observed broadband magnitude, then the equation becomes,

$$m_{BVI} = -5\log\theta - 5\log[\zeta(T_c)] + b_{BVI} + A_{BVI}, \tag{3.12}$$

where b_{BVI} is the broad band magnitude of the Planck function integrated over the transmission function for the B,V or I bandpass (plus an arbitrary constant). The dependence of b_{BVI} on temperature is very well fit by the following polynomial form,

$$b_\nu(T) = \Sigma_i c_i(\nu)\left(\frac{10^4\ K}{T}\right)^i, \tag{3.13}$$

and the coefficients are taken from Hamuy et al. (2001).

With the estimated magnitudes and velocities in hand, we solve for θ and T_c by minimizing the quantity,

$$\epsilon = \sum_{BVI} \Big\{ m_{BVI} - A_{BVI} + 5\log\theta + 5\log[\zeta(T_c)] - b_{BVI}(T_c) \Big\}^2, \tag{3.14}$$

by fitting through the method of least squares or a more robust method such as minimum absolute deviations method.

3.3.2 Standard Candle Method (SCM)

Hamuy & Pinto (2002) showed that Type II-P supernovae can be used as standard candle. The correlation between expansion velocities of the ejecta of Type II plateau supernovae and their bolometric luminosities during the plateau phase permits one to standardize the candles and decrease the scatter in the Hubble diagram from $\sim$ 1 mag to levels of 0.4 and 0.3 mag in V and I bands respectively. By using the V and I magnitudes measured in day 50 (corrected for dust extinction) and expansion velocities derived at the same epoch from the spectra, and using 17 Type II-P SNe that had precise optical photometry uncontaminated by host galaxy light and optical spectroscopy, Hamuy & Pinto (2002) found the following correlation,

$$V_P - A_V + 6.504(\pm 0.995)\log(v_p/5000) = 5\log(cz) - 1.294(\pm 0.131), \tag{3.15}$$

$$I_P - A_I + 5.820(\pm 0.764)\log(v_p/5000) = 5\log(cz) - 1.797(\pm 0.103). \tag{3.16}$$

Hamuy (2004) refined this method by taking a larger sample of 24 objects and measured the velocities from the Fe II λ 5169 Å lines to the following relation for V and I magnitudes respectively,

$$V_{50} - A_V + 6.564(\pm 0.88)\log(v_{50}/5000) = 5\log(cz) - 1.478(\pm 0.11), \tag{3.17}$$

$$I_{50} - A_I + 5.869(\pm 0.68)\log(v_{50}/5000) = 5\log(cz) - 1.926(\pm 0.009). \tag{3.18}$$

Nugent et al. (2006) proposed another refinement to this method by using the $(V - I)$ color during the plateau phase and fit the following relation,

$$M_I = -\alpha\log(V_{FeII}/5000) - 1.36[(V - I) - (V - I)_0] + M_{I_0}, \tag{3.19}$$

Table 3.1: List of Landolt standard stars used for calibration.

Date	Standards				
2004 Mar 10	PG0918	PG0942	PG1047	PG1323	PG1530
2004 May 11	PG1633	PG1657	SA113	SA107	
2004 May 13	PG1530	PG1525	PG1407	PG1528	PG1633

where α = 6.69±0.5 and M_{I_0} = -17.49±0.08 (H_0=70 km s^{-1} Mpc^{-1}) for a $(V-I)_0 = 0.53$.

The Standardized Candle Method (SCM) is found to provide distance estimates with a lower scatter in the Hubble diagram. This method appears to be better than the EPM as it is based on observables and one does not require atmosphere models, and a detailed coverage during the plateau phase.

3.4 SN 2004A

3.4.1 Introduction

SN 2004A was discovered on 2004 January 9.84 UT and later confirmed on January 10.75 UT by K. Itagaki, around 22″ west and 17″ north of the center of a nearby spiral galaxy NGC 6207. Optical spectra taken on January 11.8 and 11.9 UT showed blue continuum and hydrogen Balmer lines with P-Cygni profiles, consistent with a Type II SN (Kawakita et al. 2004). The observed blue continuum and weak emission features suggested that the SN was discovered young. The expansion velocity, measured from the minima of the Balmer lines, was around 12000 km s^{-1}. Our photometric monitoring of SN 2004A began on 2004 January 27 and continued until 2004 September 06. Photometric standard star fields listed in the Table 3.1 from Landolt (1992) were observed during photometric nights to calibrate a sequence of secondary standards in the supernova field. Figure 3.1 shows the field of SN 2004A with the secondary standards marked. The calibrated magnitudes of the secondary standards are given in Table 3.2, while the journal of SN 2004A photometry and the calibrated magnitudes are given in Table 3.3.

The journal of spectroscopic observations of SN 2004A is given in Table 3.4. The spectroscopic observations started on 2004 February 28 and continued until 2004 June 30.

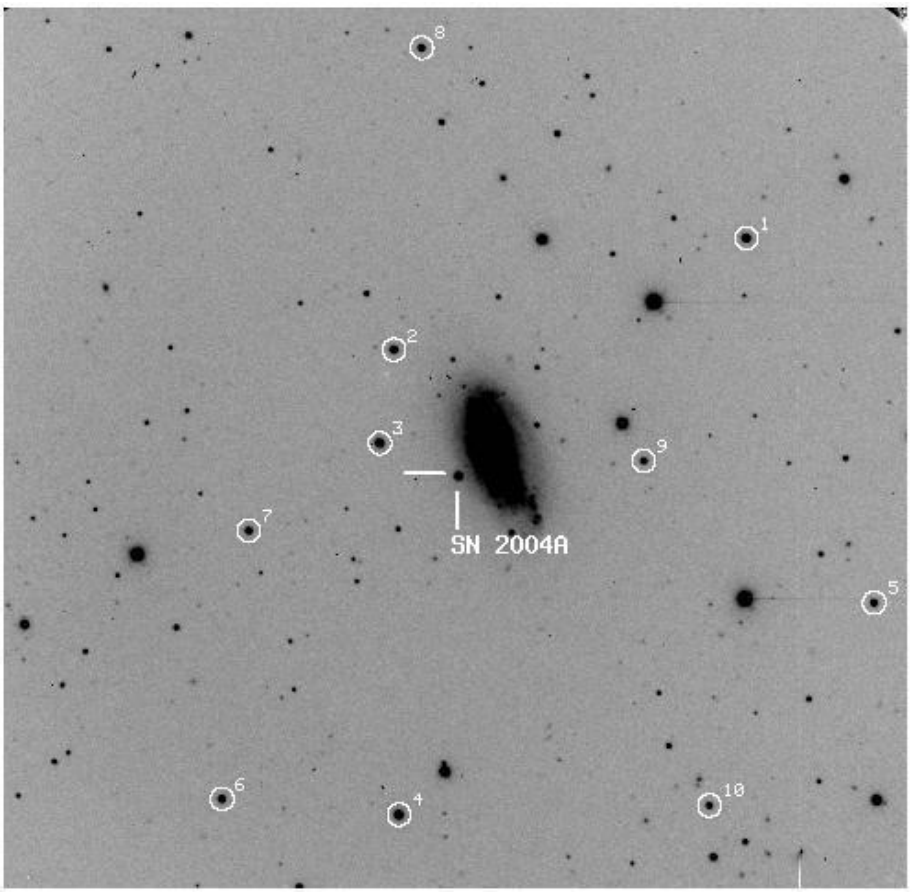

Figure 3.1: Finder chart for SN 2004A. The stars those labeled by numbers are used as local standards to calibrate the supernova.

Table 3.2: Photometry of the stars in the field of SN 2004A.

Star ID	*B*	*V*	*R*	*I*
1	15.85(0.004)	15.24(0.019)	14.88(0.005)	14.49(0.03)
2	16.45(0.006)	15.66(0.028)	15.28(0.002)	14.88(0.02)
3	16.08(0.002)	15.24(0.021)	14.81(0.002)	14.37(0.01)
4	15.67(0.017)	15.03(0.021)	14.67(0.012)	14.31(0.02)
5	16.76(0.002)	16.08(0.014)	15.71(0.012)	15.31(0.02)
6	16.73(0.023)	15.95(0.020)	15.52(0.015)	15.08(0.01)
7	16.68(0.010)	16.01(0.026)	15.65(0.008)	15.25(0.02)
8	16.64(0.005)	16.01(0.031)	15.66(0.000)	15.28(0.03)
9	17.08(0.000)	16.40(0.014)	16.05(0.006)	15.68(0.02)
10	17.23(0.003)	16.52(0.009)	16.12(0.004)	15.72(0.01)

*The stars are labeled in the same way as in Figure 3.1.

3.4.2 Light Curves

The light curves of SN 2004A in *BVRI* bands are shown in Figure 3.2. From the light curves it is apparent that the supernova exhibits a distinct plateau in V, R and I bands. During the plateau in V, R and I bands, the B band light curve declines with a decline rate $\beta^B_{100} \sim 2.0$ mag, firmly establishing that SN 2004A is a Type II-P event (Patat et al. 1994). During the first 100 days the B band light curve declines steeply, whereas light curves in V, R and I bands show almost constant brightness.

After the plateau phase there is a steep decline in the brightness of the supernova, marking the transition from the photospheric phase to the nebular phase. The decline in different filters are 2, 2, 1.8 and 1.6 mag in *BVRI*, respectively.

In the nebular phase, the light curves decline linearly in all bands with decline rates of $\gamma_B \sim 0.01$ mag, $\gamma_V \sim 0.01$ mag, $\gamma_R \sim 0.01$ mag, $\gamma_I \sim 0.01$ mag. The photometric evolution of Type II-P SNe at late phases is powered by radioactive decay of ^{56}Co into ^{56}Fe, and the expected decay rate is 0.98 mag (100 days)$^{-1}$, especially in the V band. The decay rates obtained during the nebular phase are close to that of expected rate for ^{56}Co to ^{56}Fe decay, suggesting that during the nebular phase γ-ray trapping was efficient.

A comparison of the light curves of SN 2004A with those of the well studied Type II-P SNe SN 2004et (Sahu et al. 2006) and SN 1999em (Leonard et al. 2002) is made. Light curves of SN 2004A is plotted in Figure 3.2 along with the light curves of SN 2004et and SN 1999em. The *BVRI* light curves of SN 1999em and SN 2004et have been shifted arbitrarily in magnitudes to match the light curves of SN 2004A.

The length of the plateau is 80 days for SN 2004A, 110 days for SN 2004et (Sahu et al. 2006) and 95 days for SN 1999em (Leonard et al. 2002). The overlap of the *BVRI* light curves of the three SNe is fairly good during plateau phase, while some differences are visible in the nebular phase. At the nebular phase the light curves of SN 2004A and SN 1999em match very well, but not that of SN 2004et. The slope of the light curve radioactive tails of all three SNe in the nebular phase is same in V, I bands, while the magnitude of SN 2004A at this phase is similar to SN 1999em, and brighter compared to SN 2004et.

The reddening corrected $B-V$, $V-R$, $R-I$, $V-I$ color curves of SN 2004A are shown in Figure 3.3. Also shown in the same figure are the respective color curves of SN 1999em and SN 2004et. Color curves of SN 1999em and SN 2004et have been corrected for colour excess $E(B-V) = 0.1$ and 0.45 respectively, using interstellar extinction law (Cardelli et al. 1989). The colour evolution of SN2004A in (B-V) is very similar to that of other two supernovae. The (V-R) colour evolution of SN2004A is similar to that of SN2004et

Table 3.3: Journal and results of optical photometry of SN 2004A.

Date	JD (245 0000+)	*Phase (days)	B	V	R	I
27/01/04	3031.53	21	–	15.55(0.01)	15.15(0.01)	14.77(0.04)
01/02/04	3036.50	26	16.16(0.01)	15.57(0.01)	15.17(0.01)	14.92(0.01)
08/02/04	3044.46	34	16.29(0.02)	15.57(0.02)	15.16(0.03)	14.85(0.04)
15/02/04	3051.45	41	16.41(0.01)	15.55(0.02)	15.13(0.01)	14.80(0.01)
28/02/04	3064.48	54	16.59(0.01)	15.56(0.02)	15.09(0.02)	14.78(0.01)
29/02/04	3065.43	55	16.57(0.01)	15.55(0.01)	15.10(0.02)	14.74(0.02)
10/03/04	3075.49	65	16.65(0.01)	15.55(0.01)	15.07(0.01)	14.74(0.01)
16/03/04	3081.34	71	16.70(0.01)	15.56(0.01)	15.09(0.01)	14.75(0.01)
03/04/04	3099.35	89	16.89(0.02)	15.68(0.01)	15.19(0.01)	14.85(0.01)
06/04/04	3102.41	92	16.93(0.02)	15.73(0.03)	15.23(0.02)	14.88(0.01)
14/04/04	3110.30	100	17.14(0.01)	15.86(0.01)	15.36(0.01)	15.00(0.01)
23/04/04	3119.33	109	17.48(0.04)	16.14(0.02)	15.62(0.02)	–
28/04/04	3124.38	114	–	–	15.93(0.01)	–
29/04/04	3125.31	115	18.10(0.01)	16.58(0.02)	16.00(0.01)	15.57(0.03)
03/05/04	3129.31	119	18.60(0.01)	16.99(0.02)	16.33(0.01)	15.88(0.02)
05/05/04	3131.28	121	18.75(0.02)	17.18(0.02)	16.50(0.02)	16.05(0.02)
07/05/04	3133.39	123	–	17.36(0.01)	16.67(0.03)	16.22(0.02)
09/05/04	3135.43	125	19.09(0.02)	17.44(0.01)	16.74(0.01)	16.26(0.02)
11/05/04	3137.36	127	19.16(0.02)	17.06(0.09)	16.77(0.01)	16.30(0.01)
12/05/04	3138.32	128	–	–	16.78(0.01)	16.28(0.01)
13/05/04	3139.43	129	19.12(0.02)	17.49(0.01)	16.80(0.01)	16.32(0.01)
20/05/04	3146.26	136	–	17.58(0.01)	16.85(0.01)	16.40(0.02)
31/05/04	3157.38	147	19.34(0.01)	17.69(0.01)	16.95(0.01)	16.52(0.01)
02/06/04	3159.29	149	–	–	16.97(0.02)	16.50(0.01)
13/06/04	3170.22	160	19.32(0.02)	17.82(0.01)	17.07(0.01)	16.61(0.01)
28/06/04	3185.18	175	–	17.96(0.01)	17.20(0.02)	16.76(0.01)
30/06/04	3187.27	177	19.59(0.03)	18.00(0.02)	17.21(0.02)	16.77(0.01)
15/07/04	3202.14	192	19.59(0.01)	18.17(0.01)	17.32(0.02)	16.92(0.01)
19/07/04	3206.12	196	19.65(0.02)	18.23(0.01)	17.35(0.01)	16.94(0.01)
29/07/04	3216.25	206	19.71(0.02)	18.29(0.01)	17.44(0.01)	17.02(0.01)
05/08/04	3223.31	213	19.82(0.03)	18.45(0.01)	17.51(0.01)	17.13(0.01)
07/08/04	3225.19	215	19.81(0.01)	18.44(0.01)	17.51(0.01)	17.13(0.01)
10/08/04	3228.15	218	19.84(0.01)	18.46(0.01)	17.54(0.01)	17.18(0.01)
11/08/04	3229.14	219	19.79(0.02)	18.47(0.01)	17.55(0.01)	17.15(0.02)
13/08/04	3231.11	221	–	–	17.58(0.02)	–
15/08/04	3233.19	223	19.81(0.01)	18.53(0.01)	17.58(0.01)	17.26(0.01)
27/08/04	3245.23	235	20.07(0.03)	18.69(0.02)	17.68(0.03)	17.31(0.01)
28/08/04	3246.19	236	20.09(0.03)	18.67(0.02)	17.70(0.02)	17.35(0.01)
06/09/04	3255.07	245	–	18.74(0.02)	17.76(0.02)	17.47(0.03)

$*$ Relative to the epoch of date of Explosion(JD = 245 3010)

NOTE: Figures in brackets give the statistical errors associated with the magnitudes.

Table 3.4: Journal of spectroscopic observations of SN 2004A.

Date	JD (245 0000+)	*Phase (days)	Wavelength Range (Å)
2004 Feb 28	3064.5	54	3500−7000; 5200−9200
2004 Feb 29	3065.5	55	3500−7000; 5200−9200
2004 Mar 13	3078.5	68	3500−7000; 5200−9200
2004 Mar 25	3090.5	80	3500−7000; 5200−9200
2004 Apr 03	3099.5	89	3500−7000; 5200−9200
2004 Apr 25	3121.5	111	3500−7000; 5200−9200
2004 May 05	3131.5	121	3500−7000; 5200−9200
2004 May 07	3133.5	123	3500−7000
2004 May 08	3134.5	124	3500−7000; 5200−9200
2004 May 26	3152.5	142	3500−7000; 5200−9200
2004 May 31	3157.5	147	3500−7000; 5200−9200
2004 Jun 13	3170.5	160	3500−7000; 5200−9200
2004 Jun 23	3180.5	170	3500−7000; 5200−9200
2004 Jun 28	3185.5	175	3500−7000; 5200−9200
2004 Jun 30	3187.5	177	3500−7000; 5200−9200

*Relative to the epoch of explosion (JD = 2453010).

and SN1999em until day 200, beyond which SN 2004A trends redward while the other two SNe show a blueward trend. In the (R-I), SN 2004A evolves similar to SN 1999em until day 150, beyond which SN 2004A colors are bluer than SN 1999em. On the other hand, as noted by Sahu et al. (2006), SN 2004et remains bluer than both SN 2004A and SN 1999em throughout. A similar trend is seen in the (V-I) color evolution also.

3.4.3 Spectroscopy

The spectroscopic evolution of SN 2004A is displayed in Figure 3.4, Figure 3.5, and the lines are identified in Figure 3.6. The spectra have been corrected for the redshift of the parent galaxy NGC 6027 and not for reddening. Our first spectrum is taken $\sim$ 54 days after explosion, which corresponds to almost middle of the plateau. At this epoch the spectrum is dominated by strong lines of H with well developed P-Cygni profiles. Numerous other lines due to Ca II (H & K and NIR triplet), Fe II, Na I, Sc II, Ca II, Ba II have also been identified in the spectrum (Leonard et al. 2002). Hα line is emission dominated with P-Cygni profile, which appears to consist of two components. Similar feature is associated with Hβ also, which is seen until $\sim$ 110 days after explosion. The two component P-Cygni profile was termed as "complicated P-Cygni profile" by Baron et al. (2000). The complicated P-Cygni profile is already reported in SN 1999em (Baron et al.

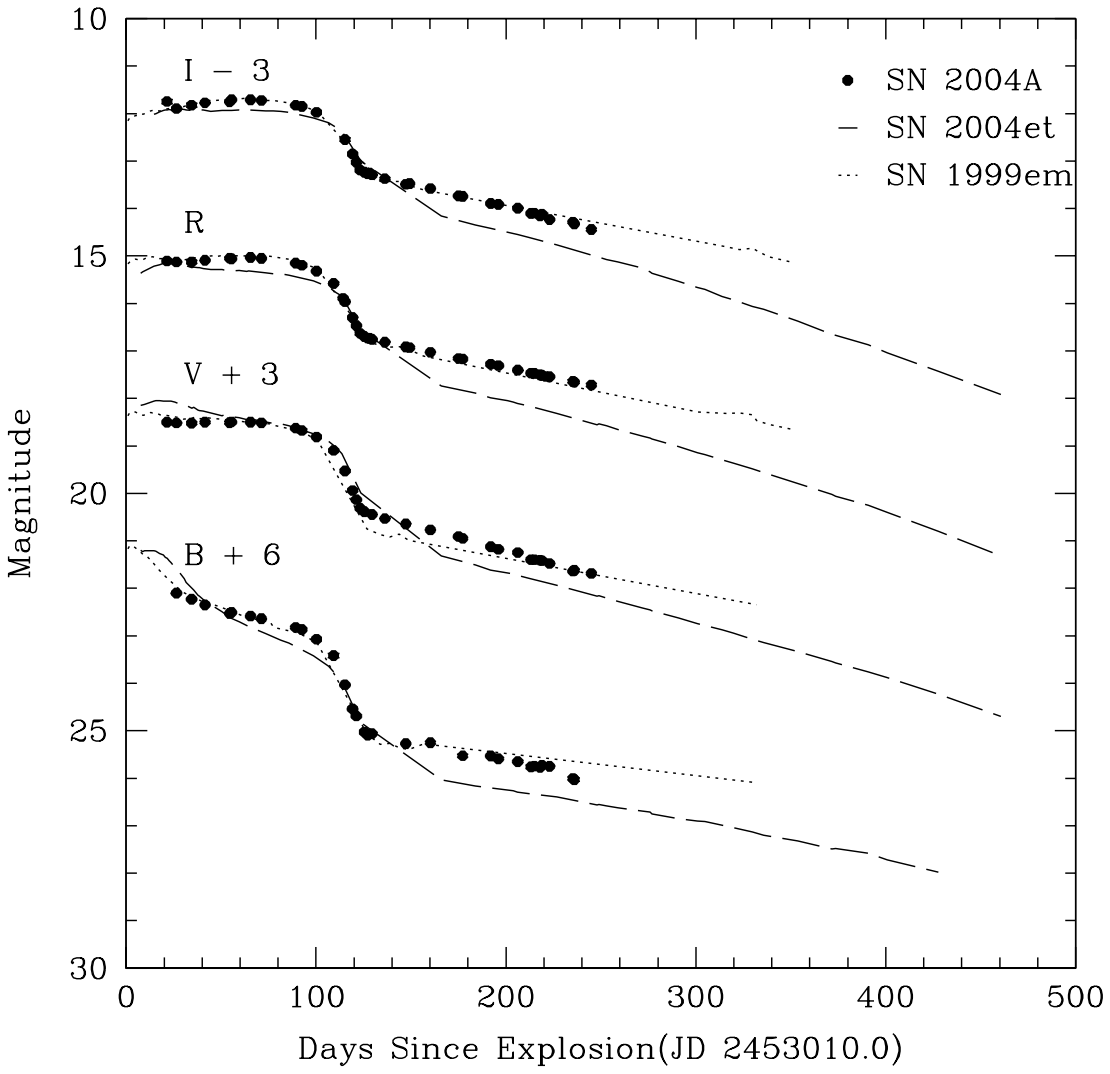

Figure 3.2: BVRI Light curves of SN 2004A plotted with other Type II-P SNe. Light curves of SN 2004A have been shifted by the reported amounts, other light curves have been shifted arbitrarily to match those of SN 2004A.

2000), (Leonard et al. 2002), SN 2004et (Sahu et al. 2006), and SN 2005cs (Pastorello et al. 2006). However, the absorption on blue side of Hα and Hβ lines appears to be much stronger in SN 2004A as compared to other Type II-P SNe. The absorption on the blue side of Hα and Hβ lines could be due to either high-velocity features of H lines or absorption lines of other ions. Based on the velocity estimates of the absorption lines, Pastorello et al. (2006) have shown that the absorption in the blue wing of Hβ line is not due to the

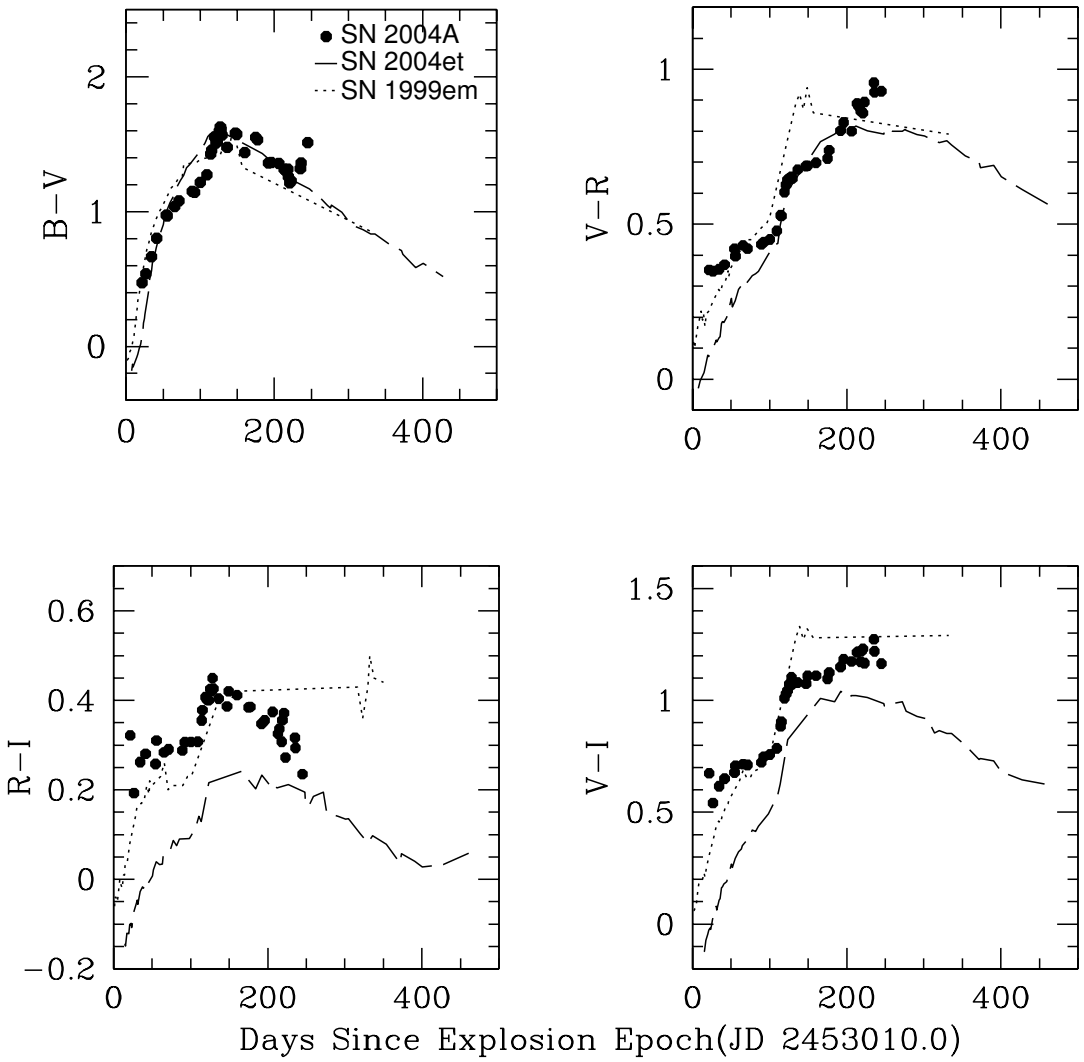

Figure 3.3: Color curves of SN 2004A compared with other SNe

high velocity component of H but is due to N II. However, the sharp absorption blue-ward of Hα and Hβ in SN 2004A are most likely due to the high velocity components. The "complicated P-Cygni profile" is explained as a combination of the usual wide P-Cygni profile and a second P-Cygni profile with a highly blue-shifted absorption corresponding to two line forming regions in the expanding atmosphere of the supernova, which could arise either by an unusual density structure of the progenitor star or by strong mixing and asphericity of the ejecta.

As the supernova ages, the absorption components of Hα, Hβ and the Ca II IR triplet

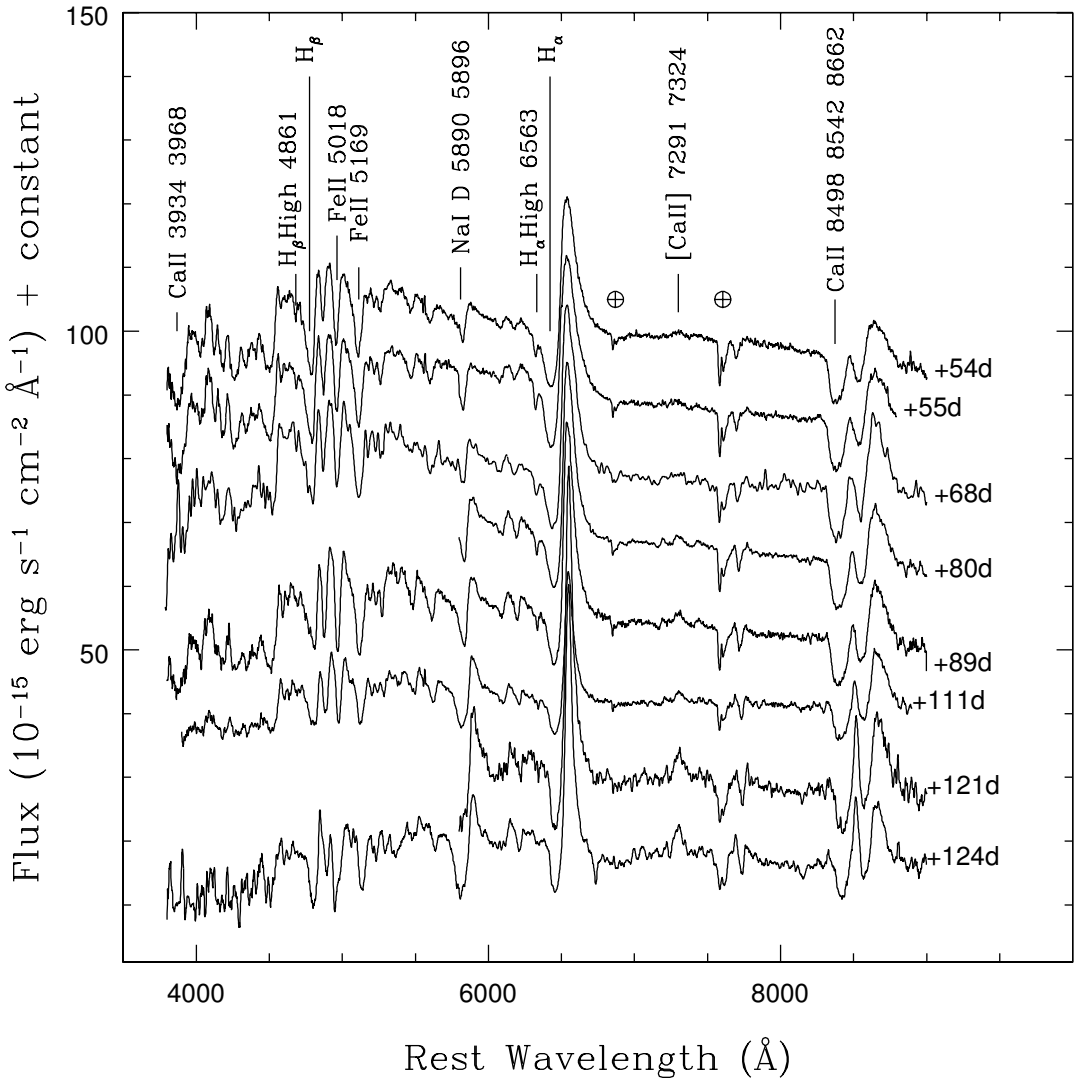

Figure 3.4: Spectroscopic evolution of SN2004A in plateau phase

become narrower and deeper. In the blue region of the spectrum numerous metal lines due to Fe, Sc, Ba and Sr appear and the emission line strength increases with time till the supernova enters into the nebular phase.

The spectra shown in Figure 3.5 indicates that the SN was in pre-nebular phase. During this phase the permitted lines due to metals and P-Cygni profiles gradually fade. The narrow forbidden emission lines [O I] λ 6300, 6363 Å and [Ca II] λ 7291, 7324 Å start appearing in the spectrum, indicating the onset of nebular phase. The lack of prominence of forbidden lines in the spectra indicates that the supernova was not completely transformed

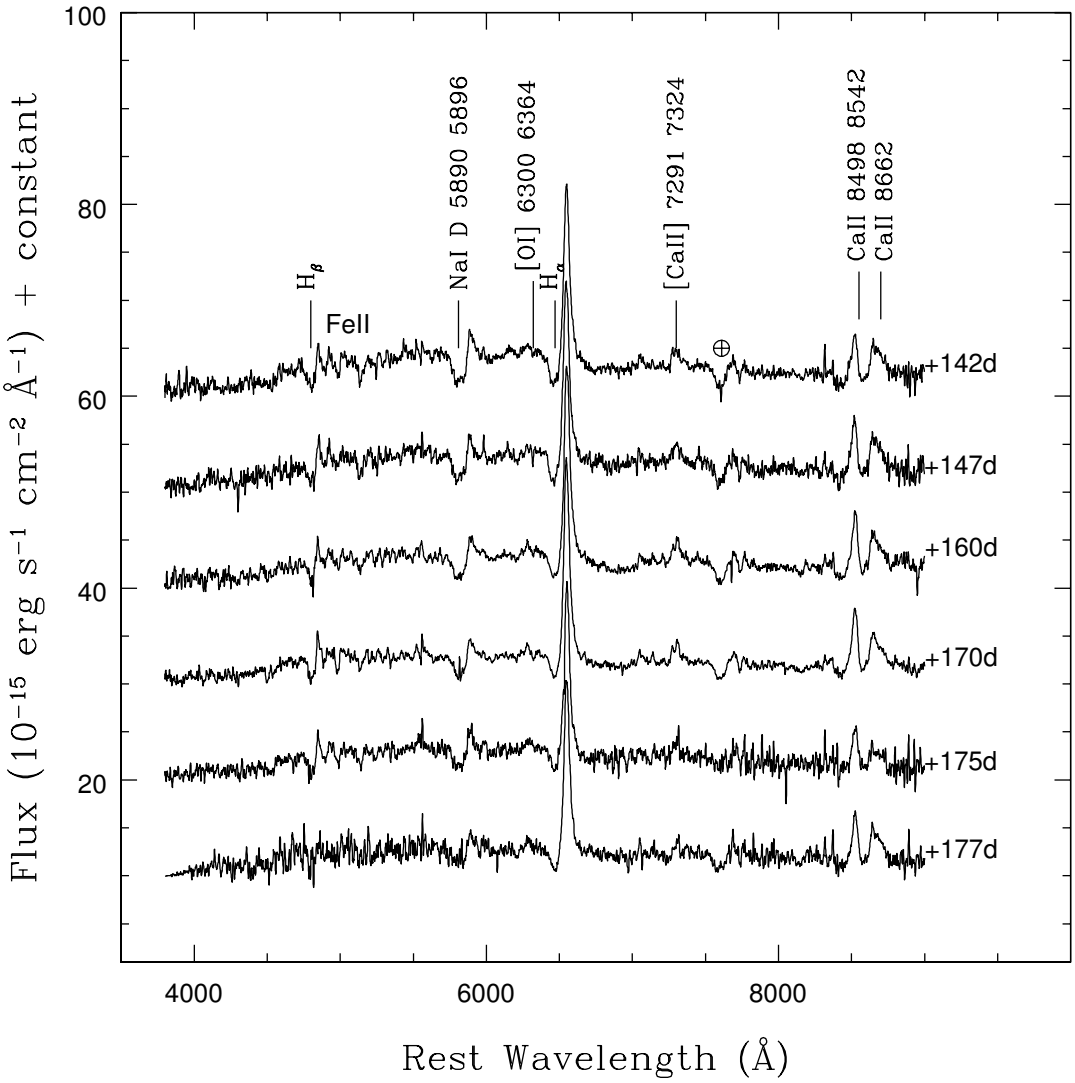

Figure 3.5: Spectroscopic evolution of SN2004A in late phase

into nebular phase.

3.4.4 Expansion Velocity

The velocity evolution of various spectral lines in SN 2004A is presented in Figure 3.7. These expansion velocities were measured from the minimum of the blue-shifted absorption trough of the Fe II $\lambda\lambda$ 4924, 5018, 5169 Å and Hα, Hβ. The velocities have been corrected for the recession velocity of 1300 km s^{-1} for NGC 6207 (Mould et al. 2000).

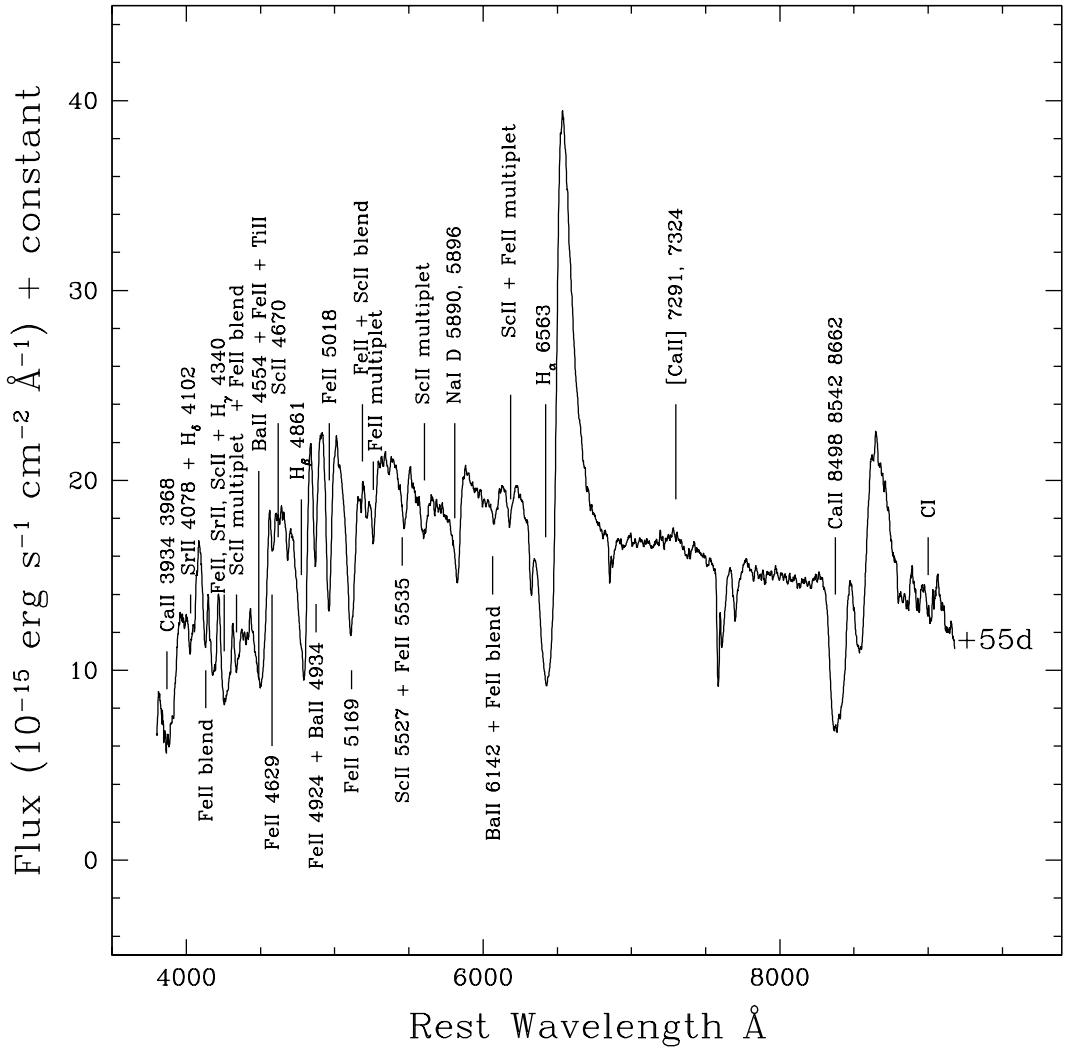

Figure 3.6: Line identification in middle of the plateau.

The expansion velocity measured using different species declines slowly with time. The velocity estimates, derived from Hα, Hβ lines are always higher as compared to those estimated using Fe II (multiplet 42). It is because hydrogen lines are formed at the top of the photosphere and have higher optical depths. However, the velocities derived using the Fe II (multiplet 42) lines are supposed to be good estimate of the photospheric expansion velocity, as they are formed close to the photosphere and are weak and unblended.

The expansion velocity of the high velocity components of Hα and Hβ are seen in the spectra in the nebular phase. The estimated velocity of these lines are consistent with each

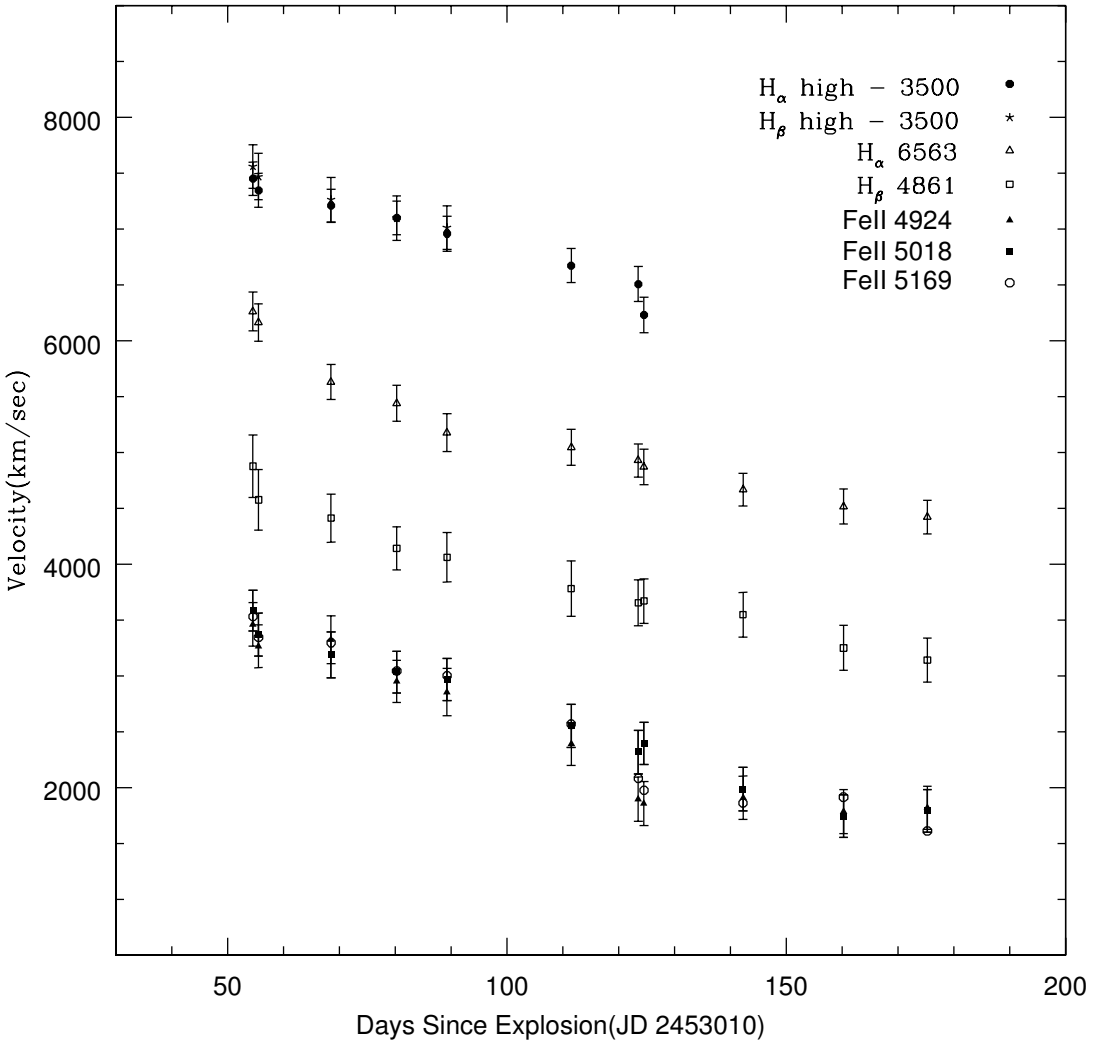

Figure 3.7: Velocity evolution of SN 2004A.

other, indicating that they are formed in the same high velocity region, and the evolution of these lines are very similar to those of other lines namely Hα, Hβ and multiplets of Fe II, with almost constant offset of 4500 km s^{-1}.

Table 3.5: Results from the Least-Square fitting algorithm which adjusts the time, Δt, and apparent magnitude, Δm, of the "model" light curve (SN 1999em) to find the best fit to the data points of SN 2004A.

Filter	Δm (days)	Δt (JD 245 0000)	explosion epoch
B	1.39(0.05)	1531(2)	3010(2)
V	1.61(0.02)	1534(2)	3013(2)
R	1.60(0.01)	1528(2)	3007(2)
I	1.55(0.01)	1530(2)	3009(2)
BVRI		1531(2)	3010(2)

3.4.5 Estimation of explosion epoch and reddening

Explosion epoch

An estimate of the explosion epoch is made by comparing the light curve of SN 2004A with those of SN 1999em (Leonard et al. 2002). Time and apparent magnitudes of the light curves of SN 1999em is adjusted to get the best match to the data points of SN 2004A, by minimizing the χ^2. The data points covering the plateau and the transition to nebular phase have been considered for comparison. The offsets in time Δt and apparent magnitudes Δm between SN 1999em and SN 2004A for each bands have been listed in Table 3.5. The shifted light curves of SN 1999em in *BVRI* bands have been over plotted with the observed points of SN 2004A in Figure 3.8. The explosion epoch of SN 1999em is well constrained by Hamuy et al. (2001) as JD 2451478.8±0.5. Using this and the average offset of 1531 days in explosion epoch between SN 1999em and SN 2004A the explosion epoch of SN 2004A has been estimated as JD 245 3010 ± 2.5, which corresponds to 2004 January 5. The error in the explosion epoch is estimated from the error in the weighted average of Δt.

Reddening estimation

The Galactic reddening in the direction of NGC 6207 is $E(B-V)_G = 0.015$ mag (Schlegel et al. 1998). In the spectrum taken on Feb 28, 2004, the interstellar Na ID line is seen clearly with an equivalent width of 0.4 Å, which corresponds to a total reddening of $E(B-V) = 0.10$, following the calibration by Munari & Zwitter (1997). For a sample of Type Ia supernovae, Turatto et al. (2003) have shown that the relation between equivalent width and reddening is bivariate with most of the less reddened objects following the relation E(B-V) = 0.16 × EW (Na ID). This relation gives an estimate of reddening as

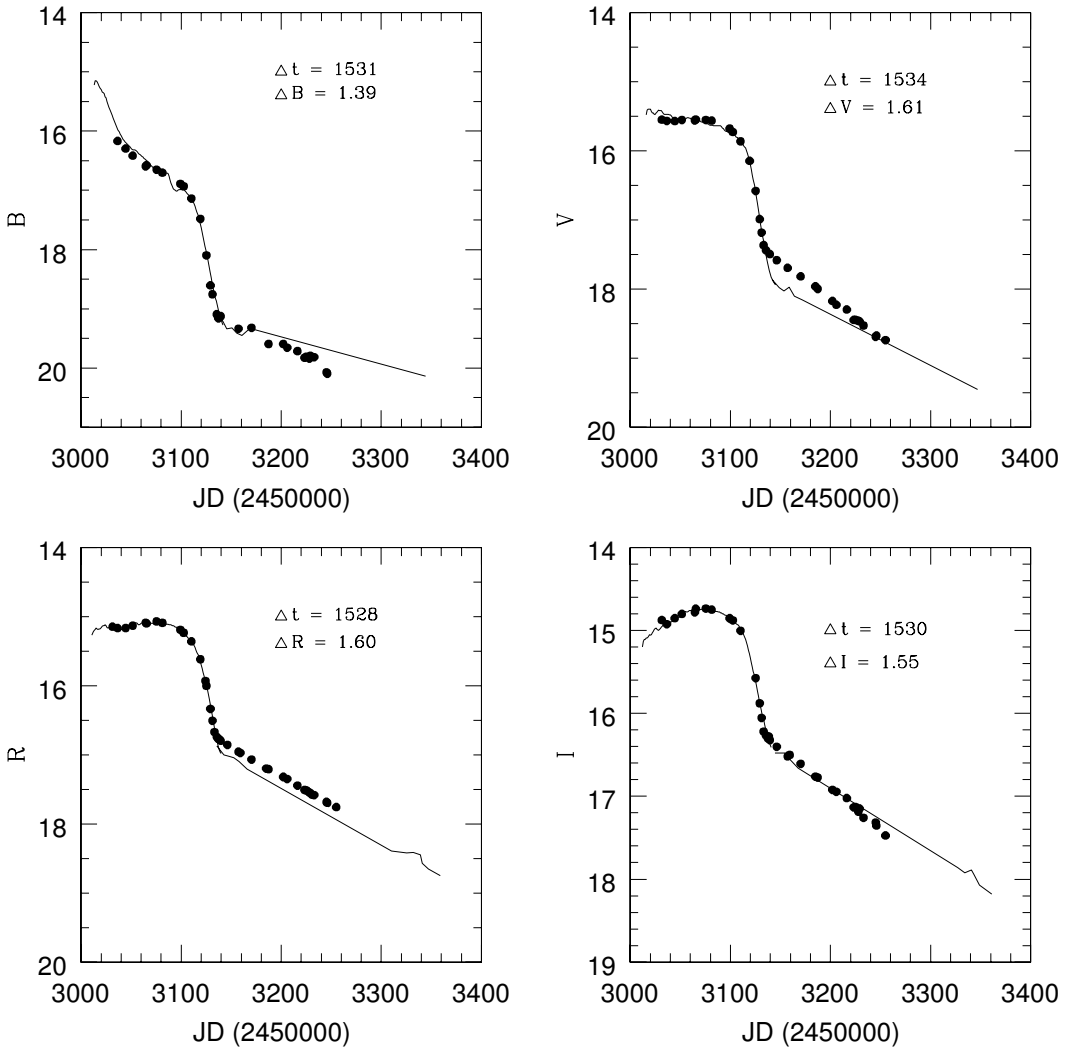

Figure 3.8: *BVRI* light curves of SN 2004A (filled circles), over-plotted with the best fit light curve of SN 1999em (solid line), shifted by Δt days and Δm magnitudes

.

$E(B-V) = 0.06$ towards SN 2004A, which is consistent with the estimate by Hendry et al. (2005) using the neighboring stars. The reddening corrected colours of SN 2004A are similar to those of SN 1999em, indicating that the derived colour excess towards SN 2004A is consistent with the intrinsic colours of Type II-P SNe as all Type II-P SNe are supposed to attain similar intrinsic colour towards the end of plateau (Eastman et al. 1996).

3.4.6 Distance Estimation

The V, I magnitudes and expansion velocity of SN 2004A for phase 54 day is available from our observations. We have linearly extrapolated the expansion velocity and interpolated the magnitudes for phase 50 day. The interpolated magnitudes for phase 50 day are V_{50} = 15.55 ± 0.02 mag and I_{50} = 14.77 ± 0.01 mag, and the expansion velocity for this phase is V_{50} = 3266.0±225.0 km s^{-1}. Using these magnitudes, in the Equations 3.17 and 3.18, distance to the supernova SN 2004A is estimated as D(V) = 20.16± 3.54 Mpc and D(I) = 20.54±2.91 Mpc. Using the refinement of SCM method by Nugent et al. (2006) the distance is estimated as 20.51±1.25 Mpc using Equation 3.19, which is in good agreement with the earlier estimate. A straight average of these results gives a distance of D = $20.35^{+3.35}_{-3.73}$ Mpc, where the errors are estimated from the limits of D(V) and D(I). The average distance of SN 2004A estimated using the standard candle method compares very well with the mean distance of 20.3 ± 3.4 Mpc by Hendry et al. (2006), which is arrived at using three different methods namely the standard candle method, brightest super-giant distance using HST photometry and the kinematic distance available in the literature.

3.4.7 Bolometric light curve

The reddening and distance estimates obtained in the previous sections, along with the *BVRI* photometric data is used to compute the bolometric light curve of SN 2004A. The missing magnitudes in some bands were obtained by interpolating between points adjacent in time. The optical magnitudes have been corrected for reddening $E(B-V)$ =0.06 using interstellar extinction law (Cardelli et al. 1989). The emitted flux is estimated by converting the corrected magnitudes into flux according to Bessell et al. (1998). The *BVRI* fluxes were derived by fitting spline curve to the B, V, R and I fluxes and integrating it over the wavelength range 3600-10600 Å . Unfortunately, U band magnitudes of supernova were not available. The contribution of U flux to the $UBVRI$ bolometric flux was determined using supernovae SN 1999em and SN 2004et, and the same fraction is added to the *BVRI* flux of SN 2004A to get the $UBVRI$ bolometric flux. No corrections have been applied for the missing flux in UV and IR bands. The bolometric light curve of SN 2004A is plotted in Figure 3.9. For the purpose of comparison the bolometric light curves of SN 2004et (Sahu et al. 2006) and SN 1999em (Leonard et al. 2002, Elmhamdi et al. 2003) have also been plotted in the same figure. The bolometric light curves for SN 2004et and SN 1999em have been computed using the photometry reported in the literature while the SN 1987A bolometric curve has been taken from Suntzeff & Bouchet

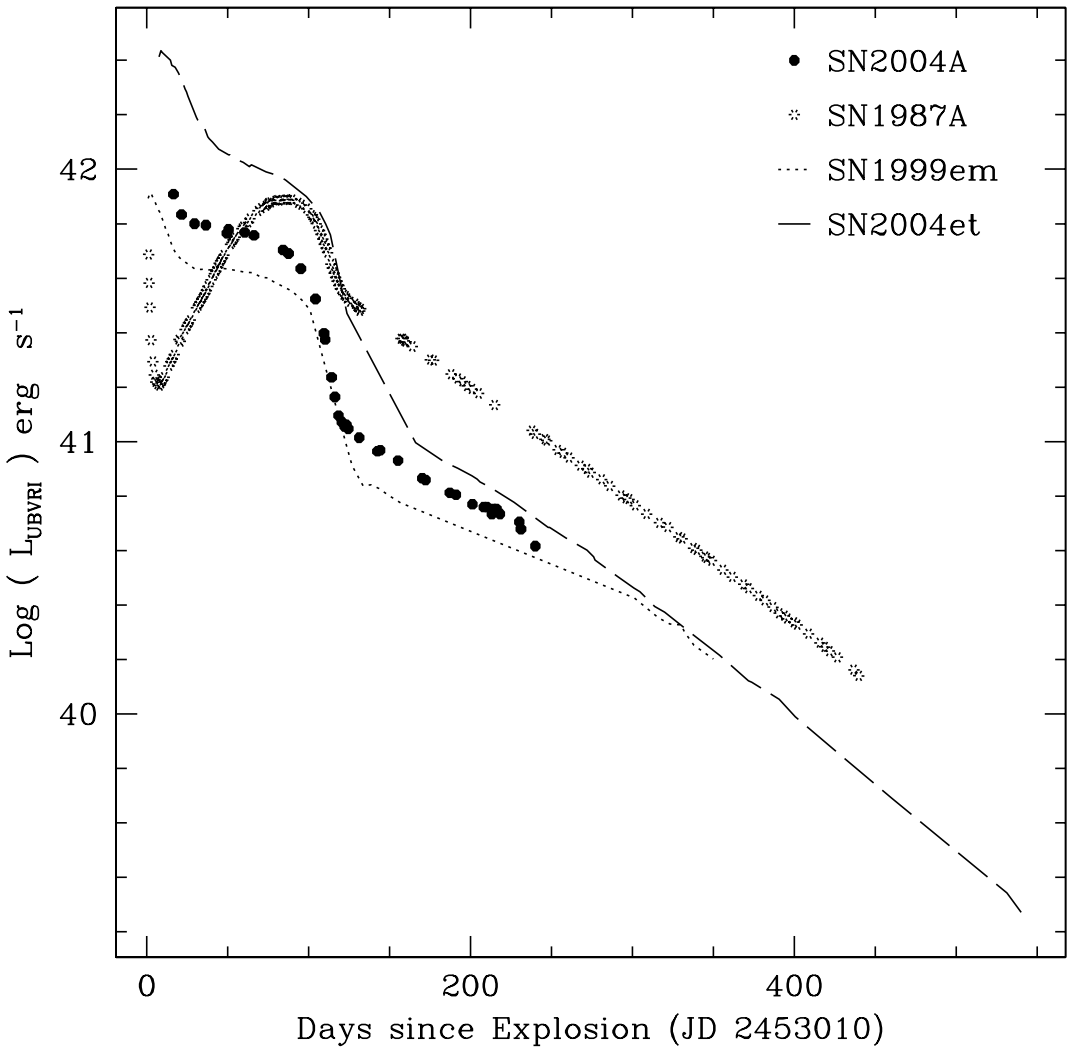

Figure 3.9: Bolometric light curve of SN 2004A.

(1990). The bolometric light curve evolution of SN 2004A is very similar to SN 2004et and SN 1999em. At all epochs the bolometric luminosity of SN 2004A is intermediate between the luminous SN 2004et and normal SN 1999em, it is marginally brighter than SN 1999em.

3.4.8 Nickel mass Estimation

The *V*-band photometric magnitudes of SN 2004A in the nebular phase are converted to the bolometric luminosity using the Equation 3.4. This calculated luminosity then used

in Equation 3.5 to estimate the mass of ^{56}Ni for each point in the nebular part of the light curve. A simple average of these estimates gives $M(56^Ni = 0.034 \pm 0.05\ M_\odot$. The error was calculated in a standard manner.

A good coverage of data points during the transition from plateau to the nebular phase allowed us to estimate the steepness parameter accurately as $S = 0.1(\pm 0.007)$. Hendry et al. (2006) have reexamined the correlation of Elmhamdi et al. (2003) and provided improved co-efficients. With the improved relation given in Equation 3.8, the mass of ^{56}Ni is found to be 0.035 ($\pm$0.01) $M_\odot$, which agrees very well with the mass of ^{56}Ni derived using the V magnitude on the radioactive tail.

3.4.9 Estimation of physical parameters of the progenitor

We applied the methods developed by Litvinova & Nadezhin (1985) which are given in Equations 3.1, 3.2 and 3.3, to SN 2004A, to estimate the explosion energy (E), ejected envelope mass (M), and the progenitor radius (R). The observed parameters for SN 2004A namely, length of the plateau is estimated as 80 $\pm$ 5 days using the date of explosion and the V band light curve, the photospheric velocity at the mid of the plateau was estimated using the weak iron lines as V_{ph} = 3300 $\pm$ 250 km sec^{-1} and the mid-plateau absolute V magnitude Mv is -15.83 $\pm$ 0.47. Using these parameters and the Equations 3.1, 3.2 and 3.3, the explosion energy (E), ejected envelope mass (M), and the progenitor radius (R) are $4.7 \pm 2.7 \times 10^{50}$ erg, 7.2($\pm$ 2.2) $M_\odot$ and 199.7($\pm$ 92.3) $R_\odot$, respectively. Assuming that the compact remnant has mass in the range a $\sim$ 2 - 3 $M_\odot$ we expect the mass of the progenitor before explosion to be $\sim$10 $\pm$ 2.5 $M_\odot$.

3.5 SN 2008in

3.5.1 Introduction

SN 2008in was discovered on 2008 December 26.79 and 27.67 UT by K. Itagaki (CBET 1636), located at R.A. = 12h22m01s.77, Dec = +04:28:47.5 which is 102$''$ east and 22$''$ north of the center of a nearby spiral galaxy M61 (NGC 4303). The identification chart is shown in Figure 3.10. Optical spectra taken on 2008 December 29.0 UT by Chakraborti et al. (2008) reveals broad $H\alpha$ emission and was found to be most similar to that of SN 2005cs at age 1.0 days past maximum and 7 days from the day of explosion. They also report that the spectra was also similar to that of SN 1999em at 1.6 days before maximum and 8.3 days from the date of explosion. Foley (2008, CBET 1638) reported

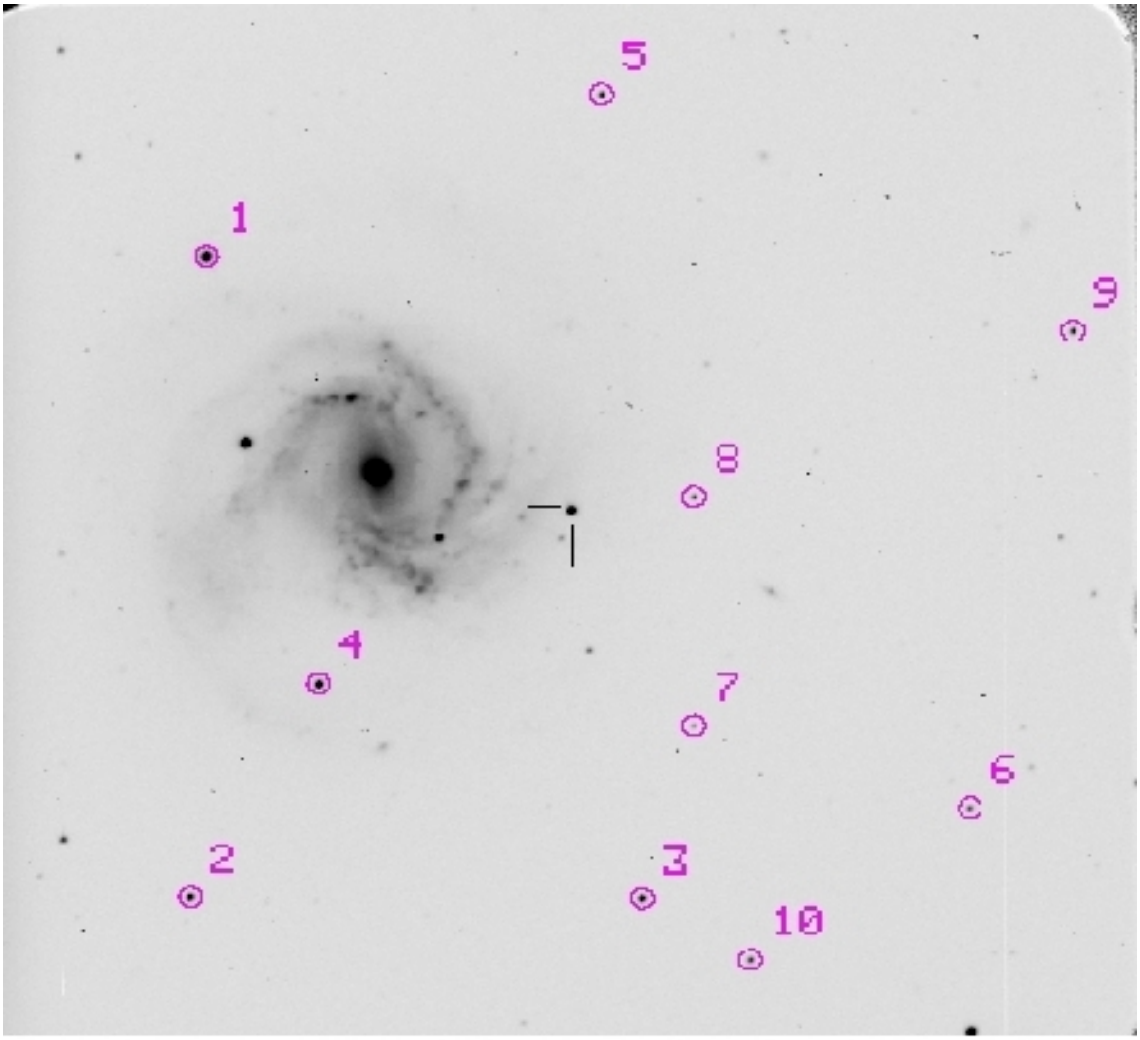

Figure 3.10: Finder chart for SN 2008in. The stars those labeled by numbers are used as local standards to calibrate the supernova.

that spectra taken on 2008 December 29.0 UT shows the Balmer Series, as well as a blue continuum, indicating that the supernova was relatively young. After correcting for the galaxy recesion velocity, the minimum of the $H\alpha$ P-Cyg absorption was reported to be blue-shifted by 9600 km s^{-1}. The same is reported by Stritzinger based on spectra observed on 2008 December 29.2 UT (2008, CBET 1638). The photometric monitoring of SN 2008in began on 2008 December 29 and continued until 2009 May 22. Photometric magnitudes of the standard stars in the supernova field are given in Table 3.6.

The journal of spectroscopic observations of SN 2008in is given in Table 3.7. The spectroscopic observations were started on 2008 December 29 and continued until 2009

Table 3.6: Photometry of the stars in the field of SN 2008in.

Star ID	U	B	V	R	I
1	14.55 (0.03)	14.58 (0.01)	13.96 (0.01)	13.59 (0.01)	13.22 (0.01)
2	18.52 (0.01)	17.39 (0.01)	15.97 (0.01)	15.04 (0.01)	14.10 (0.01)
3	16.77 (0.02)	16.35 (0.01)	15.55 (0.01)	15.05 (0.02)	14.62 (0.01)
4	17.89 (0.01)	16.69 (0.01)	15.53 (0.01)	14.84 (0.01)	14.19(0.01)
5	19.56 (0.05)	18.26 (0.02)	16.94 (0.01)	16.16 (0.01)	15.47 (0.01)
6	17.88 (0.04)	17.83 (0.01)	17.17 (0.01)	16.74 (0.01)	16.36 (0.01)
7	18.14 (0.02)	18.26 (0.02)	17.67 (0.02)	17.29 (0.01)	16.94 (0.01)
8	19.91 (0.17)	18.71 (0.02)	17.50 (0.01)	16.73 (0.01)	16.04(0.01)
9	19.73 (0.06)	18.78 (0.02)	17.28 (0.02)	16.18 (0.02)	14.94 (0.02)
10	17.06 (0.03)	17.34 (0.01)	16.84 (0.01)	16.48 (0.01)	16.13 (0.01)

*The stars are labeled in the same way as in Fig 3.10 .

May 22.

3.5.2 Light Curves

The light curves of SN 2008in in *UBVRI* bands plotted against other Type II-P supernovae are shown in Figure 3.11. Observations started 10 days after explosion and continued till day ~200. The journal of photometric observations and the estimated magnitudes in *UBVRI* bands are given in Table 3.8. During the first 100 days the U and B light curves decline rapidly whereas the V, R and I light curves maintain a constant luminosity. The plateau duration is determined to be 90 ± 10 days. After the plateau there is a steep decline in the B,V,R and I bands marking the transition from plateau phase to nebular phase. The decline to transition phase is found to be $\sim$ 2.5, 1.8, 1.8 and 1.6 mag in *BVRI* respectively.

The photometric evolution of Type II-P SNe at nebular phase is powered by radioactive decay of ^{56}Co to ^{56}Fe, and the expected decay rate is 0.98 mag $(100\mathrm{d})^{-1}$, especially in V band. The decline rates in *BVRI* bands are $\gamma_B \sim 0.038$ mag, $\gamma_V \sim 0.009$ mag, $\gamma_R \sim 0.003$ mag, $\gamma_I \sim 0.001$mag. The decay rate in the V band obtained during the nebular phase is very close to that of expected rate for ^{56}Co to ^{56}Fe decay, suggesting that during the nebular phase the γ-ray trapping was efficient.

The reddening corrected $B - V$, $V - R$, $R - I$, $V - I$ color curves of SN 2008in are shown in Figure 3.12. Also shown in the same figure are the respective colour curves of SN 1999em, SN 2004et and SN 2004A. Colour curves of SN 1999em, SN 2004et and SN 2004A have been corrected for colour excess $E(B - V) = 0.1$, 0.45 and 0.06 respectively, using interstellar extinction law (Cardelli et al. 1989). The color evolution

Table 3.7: Journal of Spectroscopic Observations of SN 2008in.

Date	JD (245 0000+)	*Phase (days)	Wavelength Range
2008 Dec 29	4829.5	11	3500−7000; 5200−9200
2008 Dec 30	4831.5	13	3500−7000; 5200−9200
2008 Dec 31	4832.5	14	3500−7000; 5200−9200
2009 Jan 02	4833.5	15	3500−7000; 5200−9200
2009 Jan 04	4836.5	18	3500−7000; 5200−9200
2009 Jan 06	4838.5	20	3500−7000; 5200−9200
2009 Jan 10	4841.5	23	3500−7000; 5200−9200
2009 Jan 13	4844.5	26	3500−7000; 5200−9200
2009 Jan 23	4855.0	37	3500−7000; 5200−9200
2009 Jan 29	4861.0	43	3500−7000; 5200−9200
2009 Feb 03	4866.5	48	3500−7000; 5200−9200
2009 Feb 11	4874.0	56	3500−7000; 5200−9200
2009 Feb 14	4877.0	59	3500−7000; 5200−9200
2009 Feb 18	4881.0	63	3500−7000; 5200−9200
2009 Feb 19	4882.0	64	3500−7000; 5200−9200
2009 Feb 20	4883.0	65	3500−7000; 5200−9200
2009 Feb 27	4890.0	72	3500−7000; 5200−9200
2009 Mar 01	4892.5	74	3500−7000; 5200−9200
2009 Mar 02	4893.0	75	3500−7000; 5200−9200
2009 Mar 28	4919.0	101	3500−7000; 5200−9200
2009 Mar 31	4922.0	104	3500−7000; 5200−9200
2009 Apr 03	4925.0	107	3500−7000; 5200−9200
2009 Apr 16	4938.0	120	3500−7000; 5200−9200
2009 Apr 30	4952.0	134	3500−7000; 5200−9200
2009 May 15	4967.0	149	3500−7000; 5200−9200
2009 May 22	4974.0	156	3500−7000; 5200−9200

*Relative to the explosion epoch (JD = 2454818).

of all SNe is very much similar and follows same trend during the plateau phase and differs there after.

3.5.3 Spectroscopy

The spectral evolution of SN 2008in is displayed in the Figures 3.13, 3.14 and 3.15. The early spectra was characterized by blue continuum with prominent Balmar lines and He I λ 5876 Å abosorption lines. The position of minima of these lines indicates expansion velocities of the ejecta of 9000 km s^{-1}. The subsequent two spectra shows similar features and in the next one observed on day 15, Fe II λ 5169 Å started appearing and He I line

Table 3.8: Journal and results of optical photometry of SN 2008in.

JD (245 4000+)	*Phase (days)	U	B	V	R	I
830.485	12	13.80 (0.11)	15.14 (0.02)	15.05 (0.02)	14.80 (0.02)	14.72 (0.03)
831.480	13	14.39 (0.07)	15.18 (0.03)	15.04 (0.01)	14.80 (0.02)	14.71 (0.01)
832.415	14	14.36 (0.05)	15.17 (0.04)	15.05 (0.03)	14.81 (0.03)	14.73 (0.02)
834.479	16	14.41 (0.11)	15.24 (0.03)	15.11 (0.04)	14.83 (0.02)	14.76 (0.02)
841.522	23	15.28 (0.08)	15.53 (0.03)	15.14 (0.02)	14.83 (0.01)	14.70 (0.02)
845.455	27	16.57 (0.09)	15.82 (0.09)	15.15 (0.03)	14.84 (0.05)	14.73 (0.05)
861.399	43	–	16.33 (0.02)	15.34 (0.01)	14.92 (0.02)	14.69 (0.01)
865.496	47	16.90 (0.10)	–	15.34 (0.02)	14.90 (0.01)	14.66 (0.03)
866.500	48	–	16.44 (0.99)	15.40 (0.03)	14.94 (0.03)	14.66 (0.01)
877.513	59	–	16.75 (0.12)	15.40 (0.05)	14.92 (0.02)	14.69 (0.05)
881.272	63	17.71 (0.03)	16.75 (0.02)	15.47 (0.01)	14.99 (0.01)	14.69 (0.01)
882.307	64	17.60 (0.04)	16.80 (0.02)	15.48 (0.02)	15.02 (0.02)	14.69 (0.02)
883.375	65	17.68 (0.03)	16.83 (0.03)	15.47 (0.02)	15.01 (0.01)	14.70 (0.02)
884.376	66	17.78 (0.08)	16.80 (0.02)	15.51 (0.01)	15.03 (0.02)	14.71 (0.02)
890.281	72	17.87 (0.05)	16.90 (0.02)	15.55 (0.01)	15.05 (0.01)	14.74 (0.01)
892.379	74	18.14 (0.10)	17.00 (0.04)	15.55 (0.02)	15.09 (0.02)	14.75 (0.02)
906.333	88	18.19 (0.10)	17.14 (0.02)	15.66 (0.02)	15.16 (0.01)	14.85 (0.01)
919.161	101	–	17.36 (0.09)	15.87 (0.01)	15.41 (0.03)	15.03 (0.03)
921.324	103	18.50 (0.08)	17.41 (0.02)	15.91 (0.01)	15.39 (0.01)	15.07 (0.01)
922.224	104	–	17.46 (0.03)	15.95 (0.02)	15.44 (0.01)	15.13 (0.01)
925.339	107	18.64 (0.10)	17.57 (0.02)	16.03 (0.01)	15.50 (0.01)	15.18 (0.01)
934.247	116	20.05 (0.08)	18.67 (0.05)	17.07 (0.02)	16.38 (0.01)	15.95 (0.02)
947.170	129	–	19.93 (0.04)	17.91 (0.02)	17.90 (0.01)	16.59 (0.03)
950.153	132	–	20.36 (0.12)	18.02 (0.03)	17.16 (0.01)	16.62 (0.02)
952.196	134	–	20.10 (0.03)	18.00 (0.01)	17.15 (0.01)	16.60 (0.01)
959.298	141	–	–	18.08 (0.08)	17.22 (0.03)	16.66 (0.02)
962.215	144	–	20.07 (0.06)	17.89 (0.03)	17.15 (0.02)	16.75 (0.03)
965.155	147	–	20.20 (0.02)	18.05 (0.03)	17.20 (0.02)	16.68 (0.02)
974.126	156	–	20.27 (0.03)	18.08 (0.01)	17.28 (0.01)	16.81 (0.01)
992.212	174	–	20.36 (0.10)	18.32 (0.02)	17.47 (0.01)	16.87 (0.02)
1009.131	191	–	–	18.20 (0.02)	17.40 (0.01)	17.06 (0.02)

∗ Relative to the epoch of date of Explosion(JD = 245 4818).

NOTE: Figures in brackets give the statistical errors associated with the magnitudes.

becomes dimmer. In the spectra which is observed just after two days on day 17, all Fe II triplet started appearing and Hα is more prominent. He I is completely disappeared. By the end of one month, spectra observed on day 42, continuum is redder, and overall it looks like a spectrum of typical SN Type II during the recombination phase. Iron lines are prominent and other metal absorption lines started appearing. Since He I is no longer visible, the feature at λ 5800 Å is ascribed to Na ID. Mg I λ 8807 Å and Ca II triplet are very prominent at this phase. The components of Ca II triplet are not blended, confirming

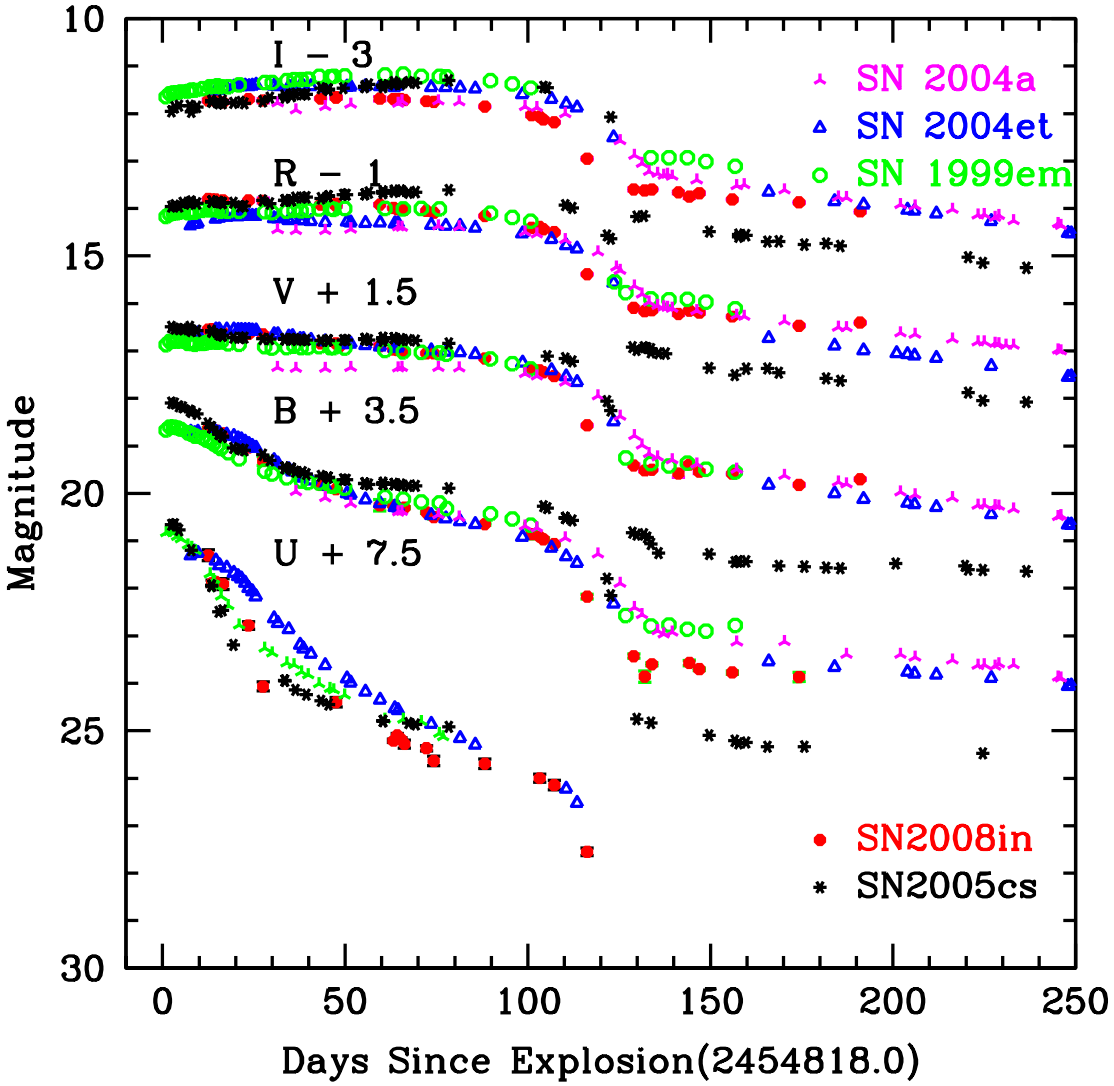

Figure 3.11: BVRI light curves of SN 2008in plotted with other Type II-P SNe. Light Curves of SN 2008in have been shifted by the reported amounts, other light curves have been shifted arbitrarily to match those of SN 2008in

the low ejecta velocity. At the phase day 60, an additional absorption developed blueward of the Hα absorption. This feature, also seen in the spectra of SN 2005cs (Pastorello et. al. 2006) also, is ascribed to Ba II λ 6497 Å.

The line identification based on the spectrum obtained on day ~50 from the day of explosion is shown in Figure 3.16. We followed Pastorello et al. (2006) to identify the lines that are based on spectral modelling. The synthetic spectra support the identification

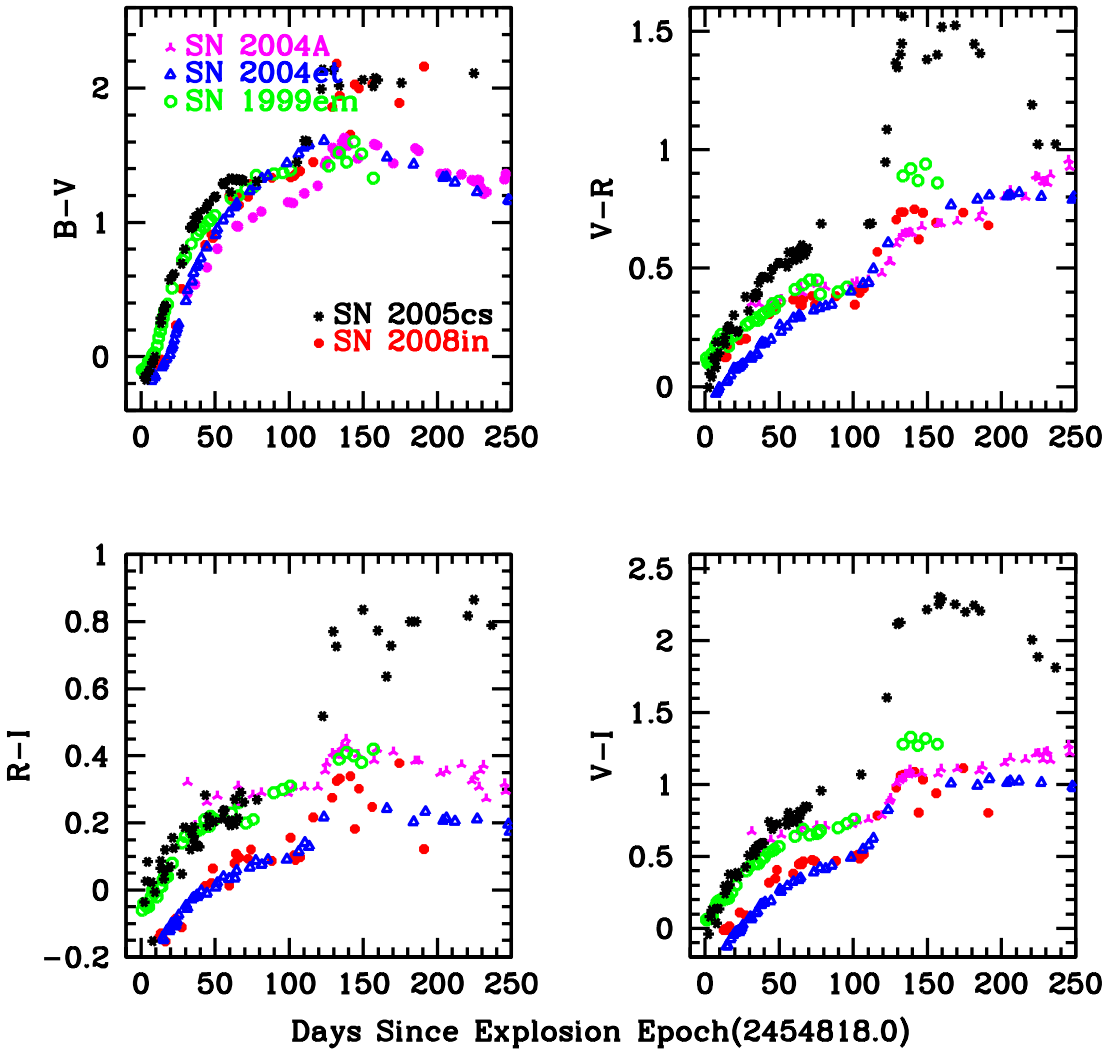

Figure 3.12: Colour curves of SN 2008in compared with other SNe

of the feature near 6300 Å, with the Si II $\lambda\lambda$ 6347, 6371 Å lines instead of high velocity component of Hα. In the region between 5000 and 6400 Å, together with the strong Fe II features, prominent lines of Sc II, Ti II and the Na ID lines are identified. The Ba II lines and other s-process elements (Sc and Sr) are identified and the strength of these lines are found to increase towards the later phase.

The velocities of the Fe II $\lambda\lambda$ 5169, 5018, 4924 Å, Sc II, Ba II lines were measured and are plotted in the Figure 3.18. The Fe II lines are only visible on about day $\sim$ 20 and disappeared on day $\sim$120. The Sc II and Ba II lines appeared in the spectra observed on

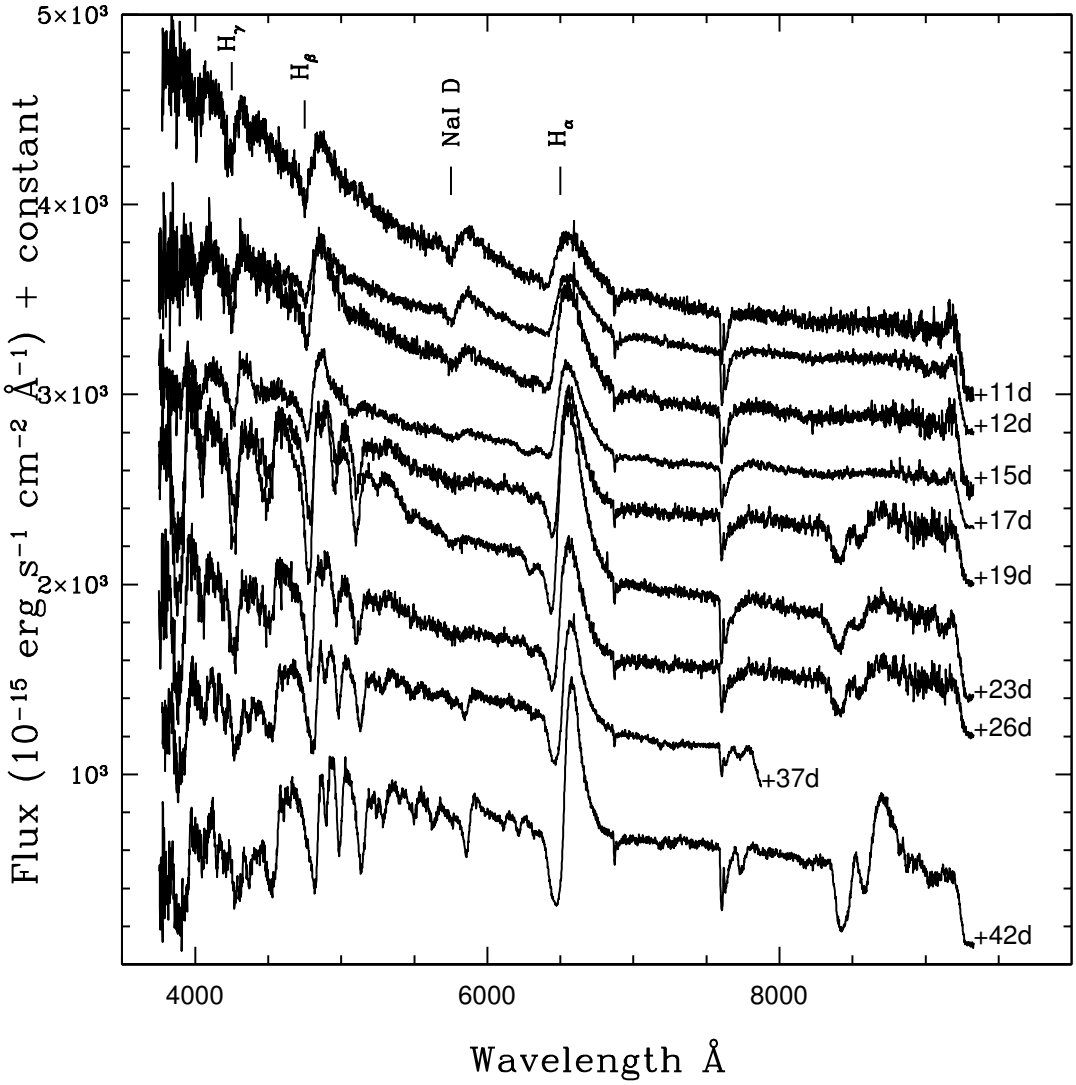

Figure 3.13: Spectroscopic evolution of SN 2008in during early phase. Epoch is relative to the date of explosion(JD 2454 818).

day 25 and slowly submerged in the continuum at around day 150. At late phase, the Hα P-Cygni profile was merged with the Ba II λ 6497 Å which appeared on day 60, quite early compared to other supernovae. The velocities of Sc II λ 6245 Å are measured and plotted in Figure 3.19. These velocities are compared with other SNe, low luminosity (Pastorello et al. 2009) as well as normal supernovae. The velocities of SN 2008in are intermediate when compared with the low luminosity supernovae and the normal ones.

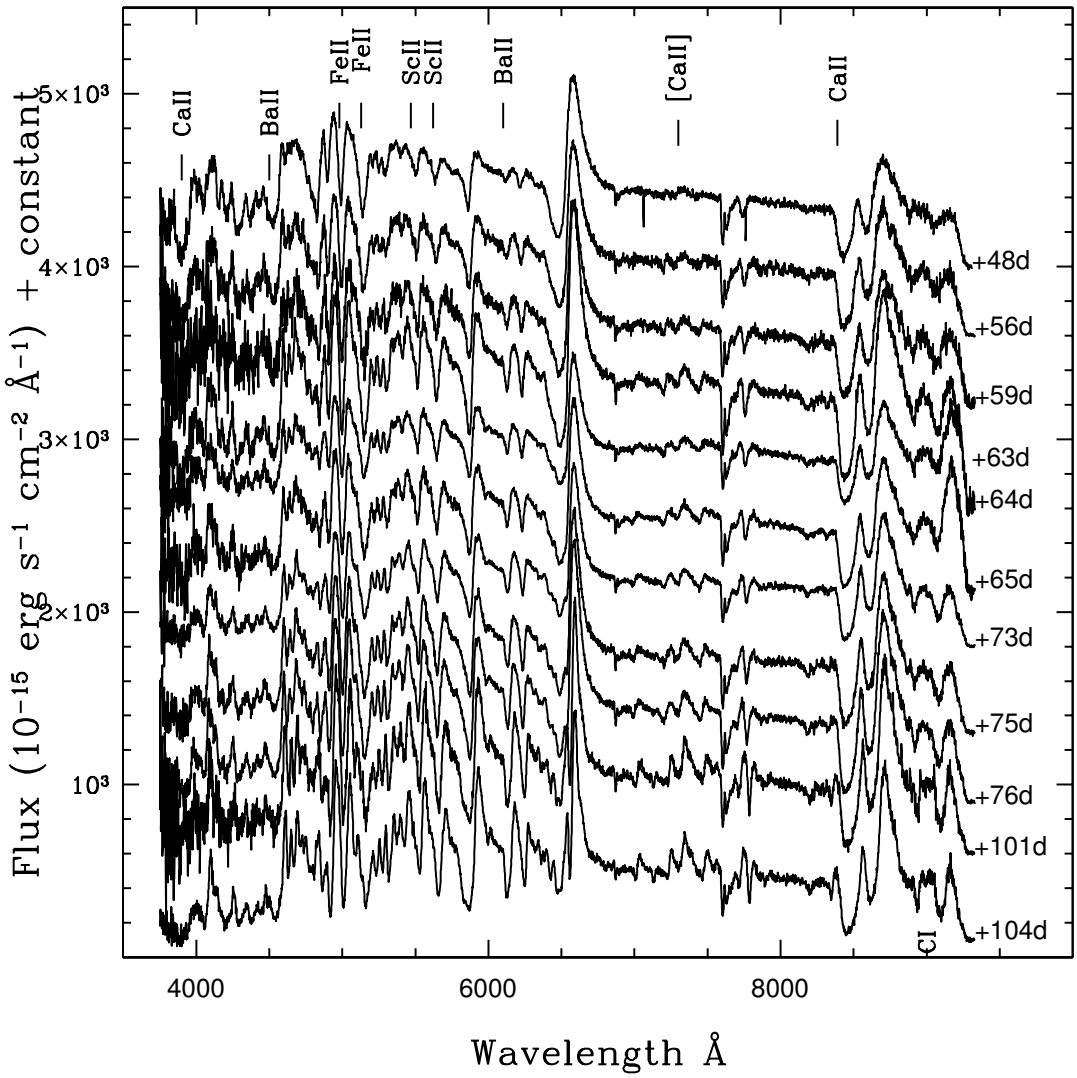

Figure 3.14: Spectroscopic evolution of SN 2008in during mid-plaeau phase. Epoch is relative to the date of explosion(JD 2454 818).

Reddening estimation

The Galactic reddening in the direction of NGC 4303 is $E(B-V)_G = 0.022$ mag (Schlegel et al. 1998). In the spectrum taken on Jan 06, 2009, the interstellar Na ID line is seen clearly with an equivalent width of 0.8 Å, which corresponds to a reddening of $E(B-V)$ = 0.128, following the calibration by Munari & Zwitter (1997). For a sample of Type Ia supernovae, Turatto et al. (2003) have shown that the relation between equivalent width

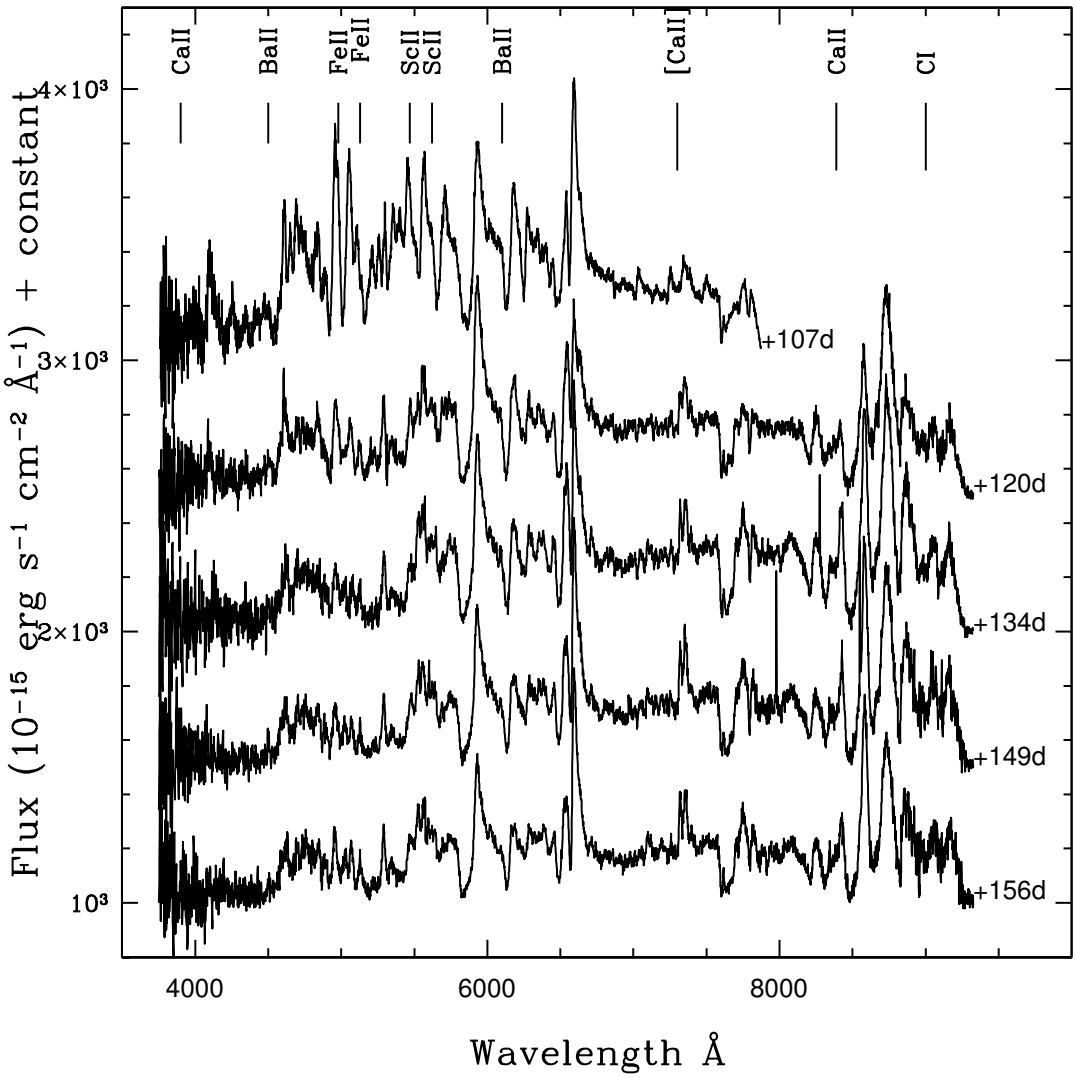

Figure 3.15: Spectroscopic evolution of SN 2008in during late phase. Epoch is relative to the date of explosion(JD 2454 818).

and reddening is bivariate with most of the less reddened objects following the relation $E(B-V) = 0.16 \times$ EW(Na ID). This relation gives an estimate of reddening as $E(B-V)$ = 0.15 towards SN 2008in.

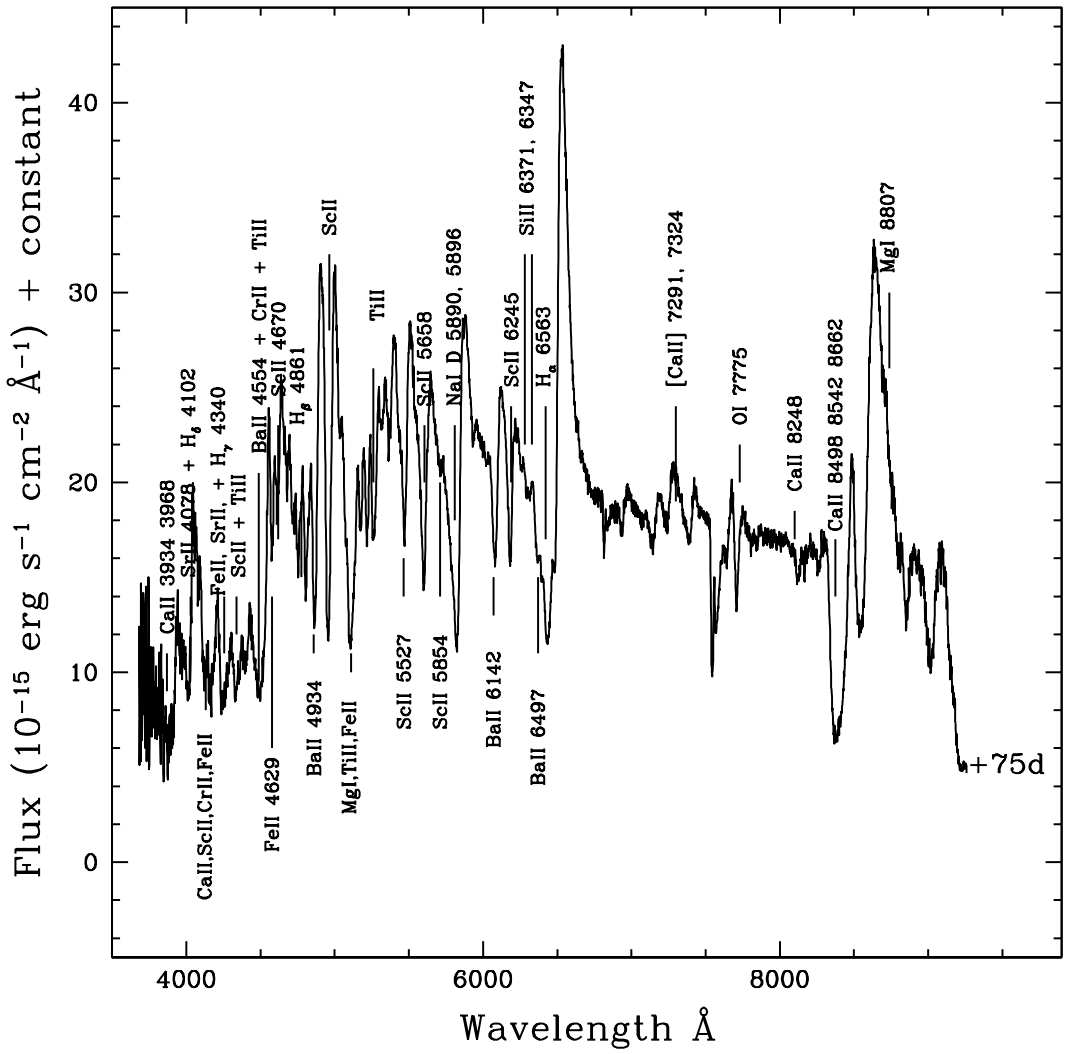

Figure 3.16: Line Identification of SN 2008in. Epoch is relative to the date of explosion(JD 2454 818).

3.5.4 Distance Estimation

We have applied EPM method to estimate the distance to the supernova SN 2008in. We have calculated the angular size (θ), flux dilution factor (ζ), and color temperature (T_c) from the *BVI* magnitudes and velocities (Figure 3.9) by minimizing Equation 3.14 using Levenberg-Marquardt chi-square minimization alogrithm (Press et al. 1992). The angular size (θ) and color temperatures (T_c) for different combinations are given in Table 3.10.

Table 3.9: Quantities that goes as input to EPM analysis

Day (JD)	Velocity (km s^{-1})	B	V	I
2454836.500	6907	15.32	15.15	14.76
2454838.500	6279	15.39	15.14	14.70
2454842.500	5343	15.60	15.14	14.70
2454845.500	4991	15.82	15.15	14.73
2454848.500	4651	16.00	15.20	14.75
2454855.500	3829	16.24	15.33	14.73
2454861.250	3369	16.33	15.34	14.69
2454865.500	3229	16.41	15.34	14.66
2454866.500	3198	16.45	15.40	14.66
2454874.500	2844	16.74	15.42	14.68
2454877.500	2696	16.75	15.40	14.69
2454881.250	2612	16.75	15.47	14.69
2454882.250	2584	16.80	15.48	14.69
2454883.250	2477	16.83	15.47	14.70
2454884.250	2381	16.80	15.52	14.71
2454890.250	2345	16.90	15.55	14.74
2454892.250	2377	17.00	15.55	14.75
2454893.250	2345	17.04	15.56	14.76

By using these values and ejecta velocities measured from Fe II λ 5196 Å line from the spectroscopic data, we fit minimum absolute deviation method to get the distance and explosion dates which are given in the Table 3.11 for different filter combinations. The coefficients of dilution factors from Dessart & Hillier (2005) (termed as D05) and Eastman et al. (1996) (termed as E96) which were later refined by Hamuy et al. (2001) were used to estimate the color temperature and distance. The coefficients of dilution factors provided by Eastman et al. (1996) give consistent distance estimates (see Figure 3.17).

We also have used SCM method to estimate the distance to SN 2008in. The *V*, *I* magnitudes of SN 2008in for phases ~ 49, 53 and 54 days are available from our observations. We have measured the expanding velocities of the ejecta from the spectroscopic observations and linearly interpolated to epoch of day ~ 54. By substituting these magnitudes and velocities in the Equations 3.17 and 3.18, distance to the supernova SN 2008in is estimated and given in the Table 3.12. The last column in the Table 3.12 is the distance derived by Nugent method (Nugent et al. 2006). A straight average of these results gives a distance of D = $15.2^{+3.35}_{-3.73}$ Mpc, where the errors are estimated in the standard manner. The average distance of SN 2008in estimated using the above methods comparable well with

Table 3.10: Quantities derived from the EPM analysis.

BV θ (10^{15} cm)	T_c (K)	BVI θ (10^{15} cm)	T_c (K)	VI θ (10^{15} cm)	T_c (K)
5.46	12888	5.71	11547	5.91	10641
6.36	11454	6.32	10643	6.38	10058
8.36	8914	7.26	9436	6.56	9923
8.91	8145	7.58	9024	6.56	9923
9.76	6495	8.22	8086	6.28	10197
9.83	5777	8.58	7438	6.50	9792
9.47	5283	9.02	6576	7.83	8205
9.60	4973	9.32	6222	8.36	7794
9.81	4697	9.54	5954	8.69	7568
9.49	4763	9.50	5856	9.09	7157
10.43	4007	9.63	5314	9.00	7157
10.70	3939	9.62	5318	8.77	7356
09.99	4103	9.53	5309	9.20	6909
10.15	4007	9.55	5219	9.26	6849
10.42	3917	9.54	5186	9.10	6969
09.77	4103	9.42	5252	9.28	6734
09.99	3939	9.33	5130	9.16	6734
10.65	3730	9.36	4983	9.06	6791
10.85	3672	9.33	4935	9.02	6791

Table 3.11: EPM results.

Filter combination	Distance (Mpc) Using E96	Explosion date (2454000+)	Distance (Mpc) Using D05	Explosion date (2454000+)
BV	14.21	816.0	13.97	825.0
BVI	14.90	817.0	16.53	821.0
VI	14.92	821.0	18.27	821.0

Table 3.12: SCM results.

JD (2454000+)	D(V) (Mpc)	D(I) (MPc)	Nugent method (Mpc)
861.2	15.71 (2.88)	17.14 (2.43)	15.65 (1.50)
865.5	14.89 (2.85)	16.14 (2.37)	14.86 (1.42)
866.5	15.13 (2.93)	15.97 (2.37)	15.23 (1.46)

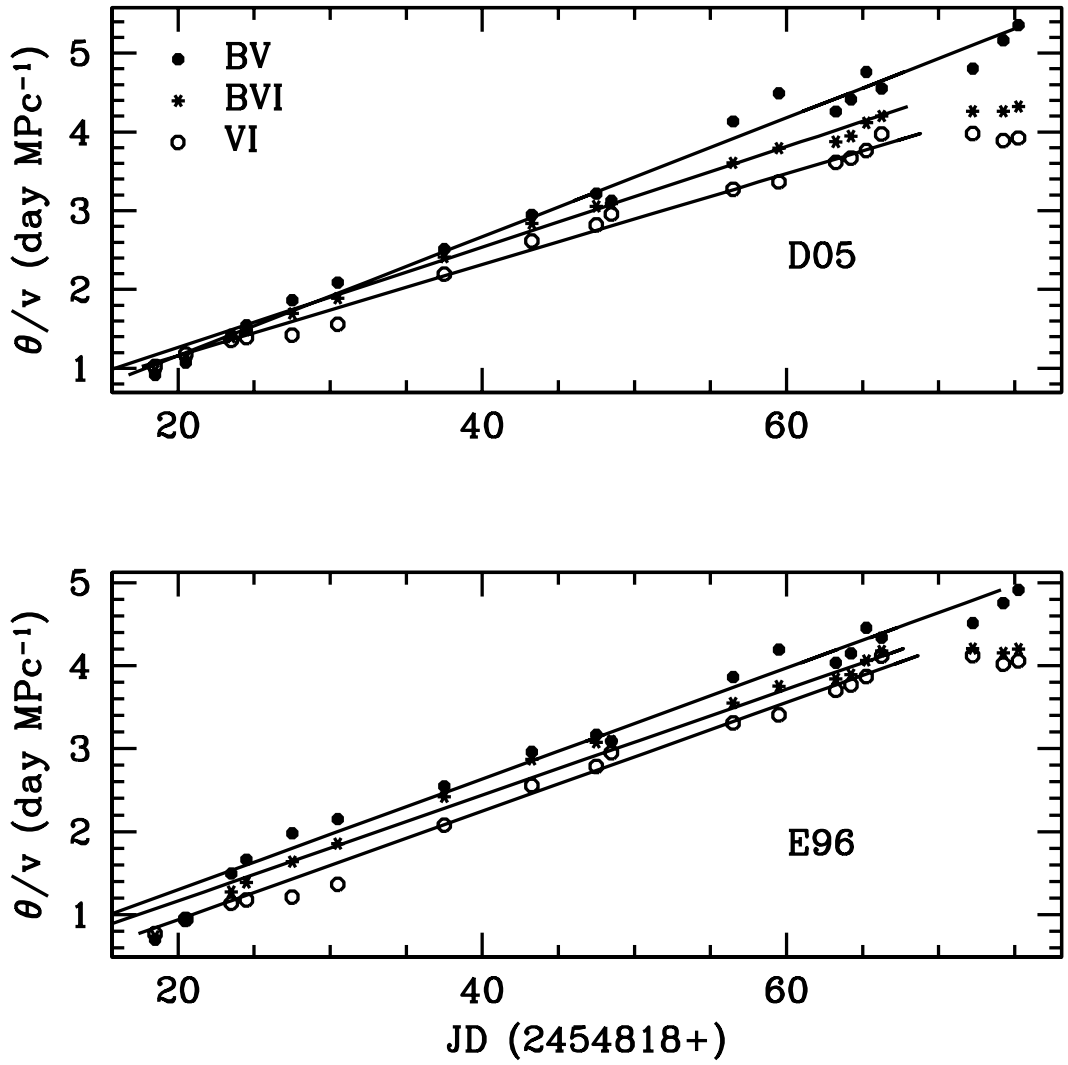

Figure 3.17: The slope of the line gives the distance estimation to supernova. The lines are fitted with minimum absolute deviations method to the data points.

the distance estimation of 13.4 MPc to the host galaxy NGC 4303 (Mould et al. 2000) by different methods.

3.5.5 Bolometric light curve

The reddening and distance estimates obtained in the previous sections, and the photometric data presented in the Table 3.8 are used to compute the bolometric light curve of

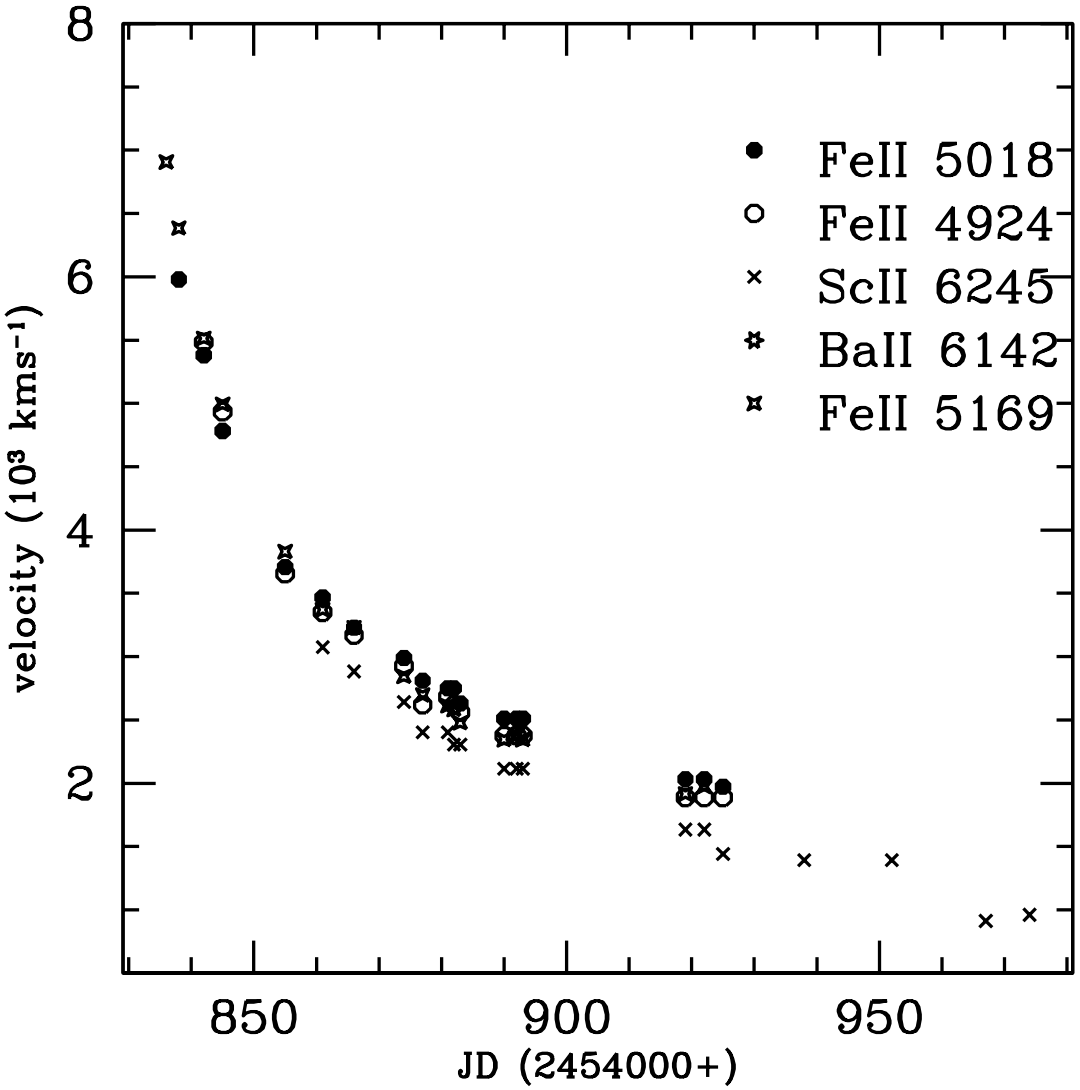

Figure 3.18: Velocity evolution of SN 2008in

SN 2008in. First, the missing magnitudes in some bands were obtained by interpolating between points adjacent in time. The optical magnitudes have been corrected for reddening $E(B-V)$ =0.15 using interstellar extinction law (Cardelli et al. 1989). The emitted flux is estimated by converting the corrected magnitudes into flux according to Bessell et al. (1998). The *UBVRI* fluxes were derived by fitting spline curve to the *U*, *B*, *V*, *R* and *I* fluxes and integrating it over the wavelength range 3600-10600 Å. No corrections have been applied for the missing flux in UV and IR bands. The bolometric light curve of SN 2008in is plotted in Figure 3.20. Other Type II-P supernovae SN 2004et (Sahu et al.

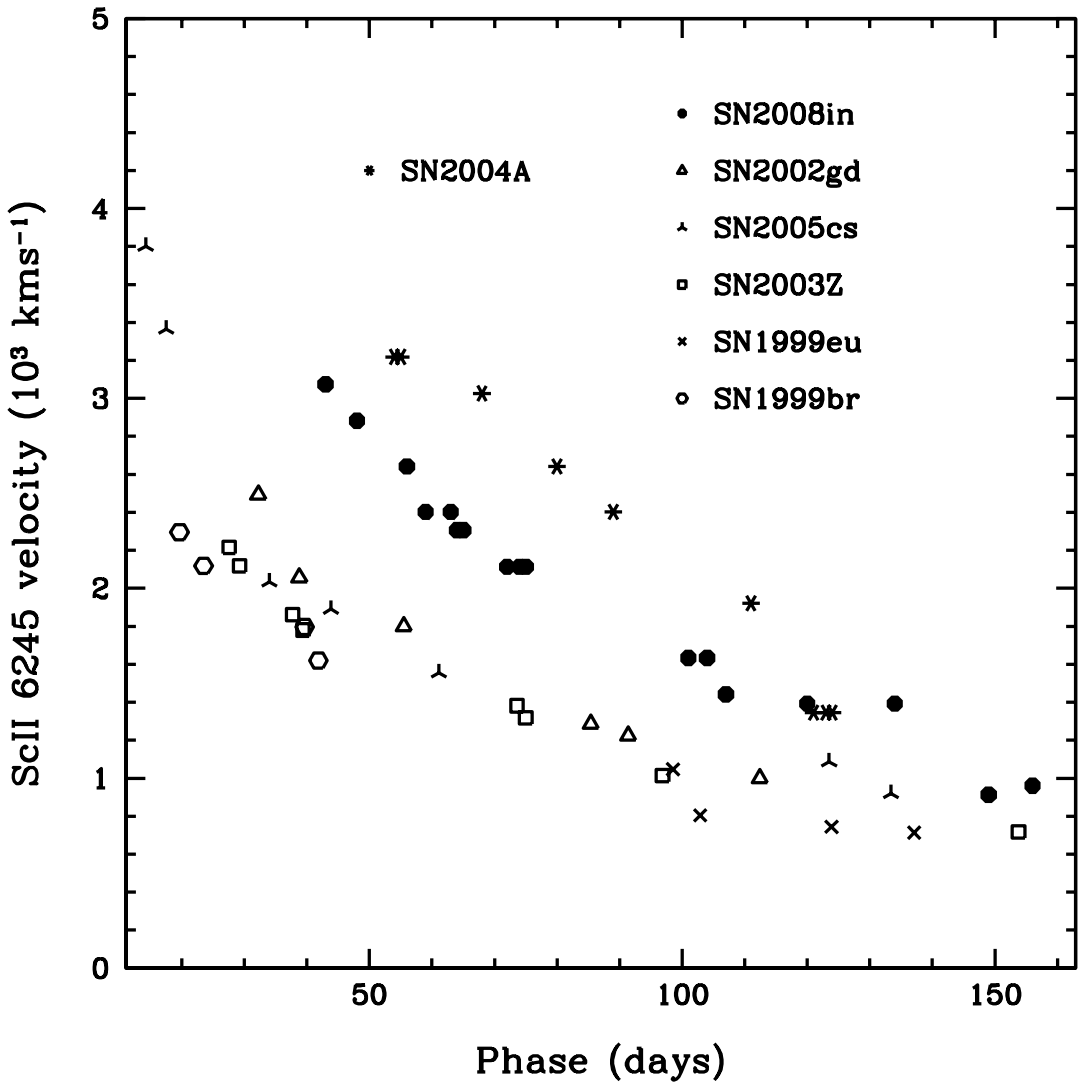

Figure 3.19: Comparision of Sc II line velocity of SN2008in with that of other low luminosity type II-P SNe and normal type II-P SN. The data points are taken from Pastorello et. al (2009) and from Gurugubelli et. al. (2008).

2006), SN 1999em (Leonard et al. 2002, Elmhamdi et al. 2003), SN 1990E, SN 1987A, SN 1999gi, SN 2003gd, SN 2005cs, and SN 2004A have also been plotted in the same figure for the purpose of comparision. The SN 1987A bolometric curve has been taken from Suntzeff & Bouchet (1990). The bolometric curve of SN 2008in matches very well with the SN 1999gi during the plateau phase and with SN 2004A, SN 1999em during the maximum light. The absolute V magnitude light curve is shown in Figure 3.21 and

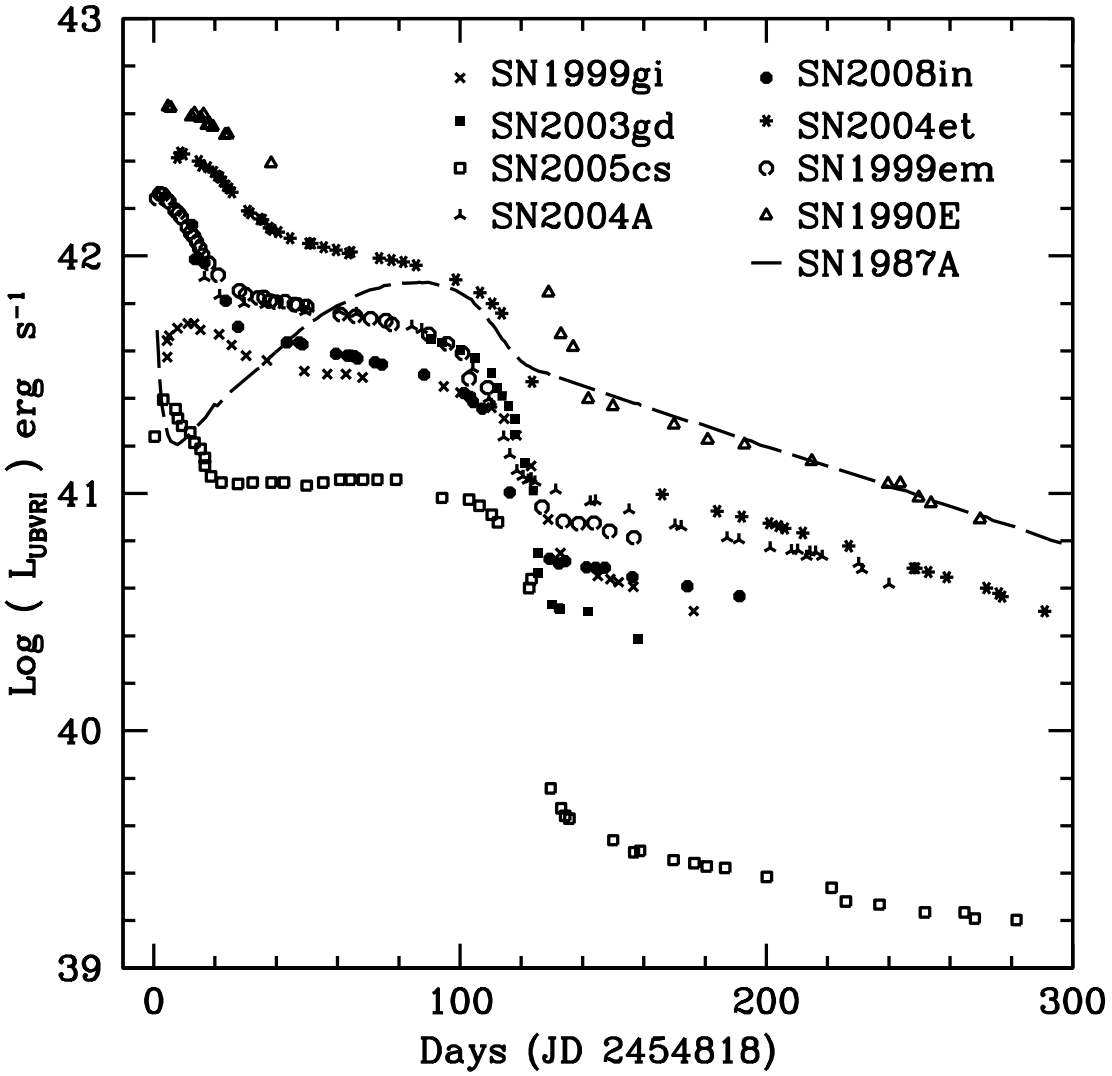

Figure 3.20: Bolometric Light Curve of SN 2008in in comparision with other Type II-P SNe.

compared with other Type II-P supernovae. The Nickel mass estimated from the tail part of the bolometric light curve is discussed in the Section 3.5.6.

3.5.6 Nickel mass Estimation

The *V*-band photometry of SN 2008in in the nebular phase is converted to the bolometric luminosity using the Equation 3.4 and the reddening and distance are estimated in the

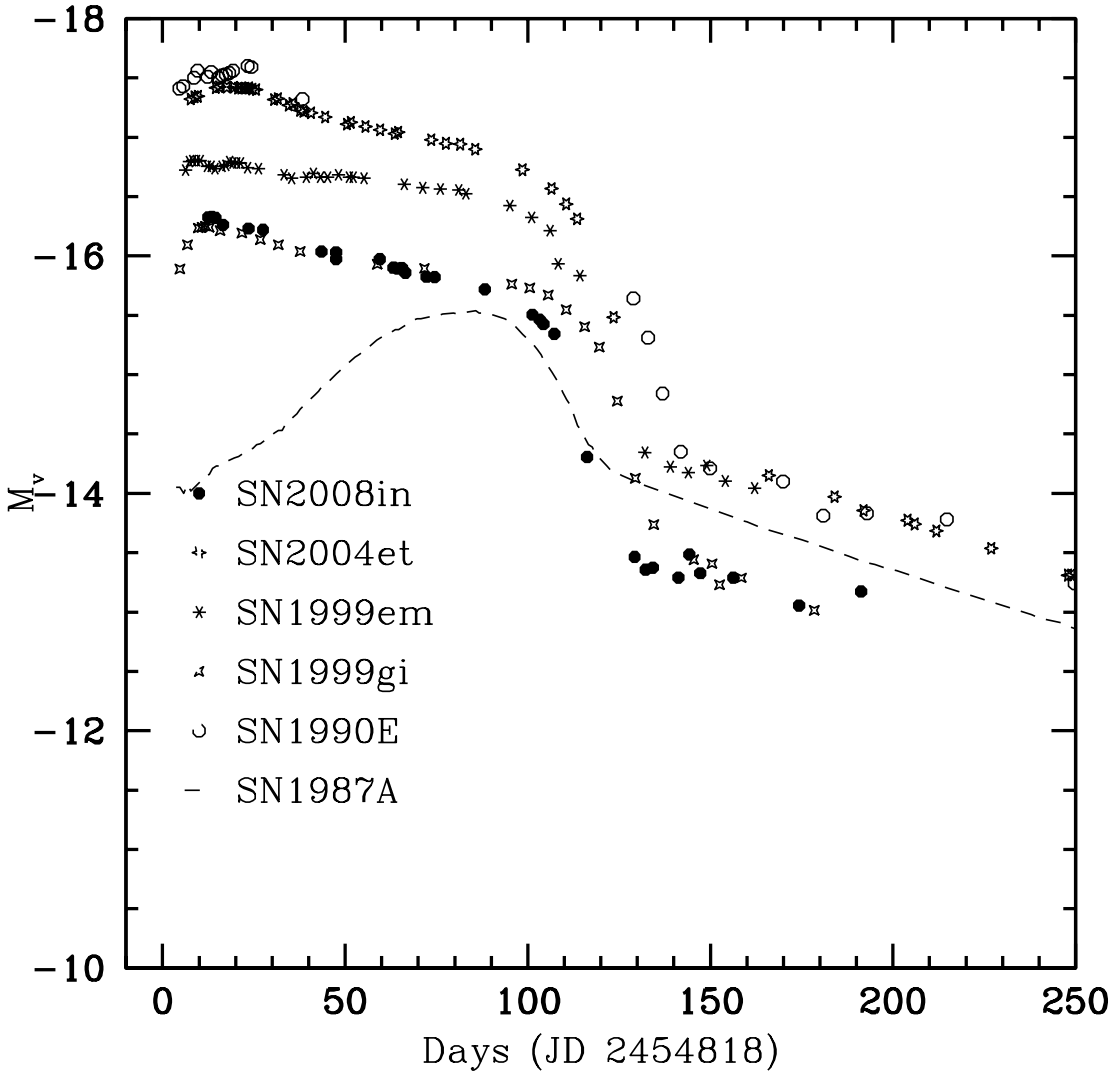

Figure 3.21: Absolute V magnitude Light Curve of SN 2008in in comparision with other Type II-P SNe.

previous Sec. 3.5.3, 3.5.4. The mass of ^{56}Ni was then found using Equation 3.5, for each point in the nebular part of the light curve. A simple average of these estimates give M_{Ni} = 0.021 ± 0.008 $M_{\odot}$. The error was calculated in a standard manner.

A good coverage of data points during the transition from plateau to the nebular phase allowed us to estimate the steepness parameter accurately as S = 0.1(±0.007). Hendry et al. (2006) have reexamined the correlation of Elmhamdi et al. (2003) and provided improved co-efficients. With the improved relation given in Equation 3.8, the mass of

Table 3.13: Pysical parameters of different Type II-P SNe for comparison.

SN	D(Mpc)	Av	plateau duration(days)	vel (km s^{-1})	M_V	E (10^{51} erg)	R ($R_\odot$)	M_{ejec} ($M_\odot$)
1999br	14.1	0.06	100	1541	-13.16	0.20	31	20
1999em	11.7	0.31	120	3046	-16.68	0.84	437	18
1999gi	10.0	0.65	115	2717	-15.67	0.64	183	21
2003gd	09.3	0.43	113	3210	-16.06	1.04	179	24
2004A	20.3	0.19	107	3200	-16.33	0.68	328	15
2004dj	03.3	0.53	105	2957	-16.16	0.65	277	16
2004et	05.9	1.30	110	3462	-17.15	0.88	631	14
2005cs	07.1	0.16	118	1500	-14.66	0.17	208	13
2006my	22.3	0.08	120	2953	-16.26	0.86	274	22
2006ov	12.6	0.07	118	1410	-15.12	0.12	465	09
*2004A	20.3	0.19	80	3266	-16.00	0.50	199	07
*2008in	15.2	0.15	90	3300	-15.88	0.85	144	16

NOTE: Table is taken from the Maguire et al. (2010) and references there in.
* Values are from this work

^{56}Ni is found to be 0.028(±0.005) $M_\odot$, which agrees very well with the mass of ^{56}Ni derived using the V magnitude in the radioactive tail. The Ni mass that is produced during the explosion is 0.025(±0.009) $M_\odot$ which is average of the above two estimates.

3.5.7 Estimation of physical parameters of the progenitor

We applied the methods of Litvinova & Nadezhin (1985) which are given in Equations 3.1, 3.2 and 3.3, to SN 2008in, to estimate the explosion energy (E), ejected envelope mass (M), and the progenitor radius (R). The observed parameters for SN 2008in namely, length of the plateau is estimated as 90±10 days using the date of explosion and the V band light curve, the photospheric velocity at the mid of the plateau was estimated using the weak iron lines as V_{ph} = 3300±250 km s^{-1} and the mid-plateau absolute V magnitude M_V is -15.88±0.47. By substituting these parameters in the Equations 3.1, 3.2 and 3.3 the explosion energy (E), ejected envelope mass M, and the progenitor radius (R) are $8.6 \pm 2 \times 10^{50}$ erg, 16(± 4) $M_\odot$ and 144(± 18) $R_\odot$, respectively.

3.6 Summary

Here, we have presented photometric and spectrocopic studies of two Type II-P supernovae SN 2004A and SN 2008in. We have estimated the expansion velocities of the ejecta and various physical parameters like progenitor mass, radius and explosion energy.

SN 2004A is a normal Type II-P supernova with explosion energy of 4.7×10^{50} erg s^{-1} and progenitor mass of $10 - 15\ M_{\odot}$. SN 2008in is an interesting object, though does not show any individual peculiarity. From the bolometric and velocity plots, it is apparent that, it fills the gap between the low luminosity supernova like SN 2005cs and the normal supernovae, while the explosion enrgies and ejected masses are comparable with normal supernovae. The spectral evolution of SN 2008in is quite similar to normal ones with no pecularities.

The physical parameters that are derived from the observations using Equations 3.1, 3.2 and 3.3 (Litvinova & Nadezhin 1985) for a sample of Type II-P supernovae (Maguire et al. 2010) are given in Table 3.13. From the table, the diversity of these object progenitor stars is quite apparent. Though, we may not accurately determine the progenitor star properties of this kind of supernovae, this kind of study will give a range of values, that can be further constrained by future observations of more Type II-P SNe.

CHAPTER 4

SUPERNOVAE TYPE IIN

4.1 Introduction

The Type IIn subclass of SNe II are those in which the expanding ejecta are believed to be strongly interacting with dense circumstellar gas, whose derived mass loss rates can exceed $10^{-4} M_{\odot}$ yr^{-1}. In these objects, the broad absorption components of all lines are weak or absent throughout their evolution. Instead, their spectra are dominated by strong emission lines, most notably Hα, that have a complex but relatively narrow profile. The emission line Hα typically exhibits a very narrow component (FWHM $\lesssim$ 200 kms^{-1}) superposed on a base of intermediate width (FWHM $\lesssim$ 1000-2000 kms^{-1}); sometimes a very broad component (FWHM $\lesssim$ 5000-10000 kms^{-1}). Schlegel (1990) named this subclass "Type IIn", the "n" denoting "narrow" to emphasize the presence of the intermediate-width or very narrow emission components.

The early-time continuum of SNe IIn tend to be bluer than normal. Occasionally, He I emission lines are present in the first few spectra. Very narrow Balmer absorption lines are visible in the early-time spectra of some of these objects, often with corresponding Fe II, Ca II, O I, or Na I absorption as well. Some of them are unusally luminous at maximum brightness, and they generally fade quite slowly, at least at early times.

Type IIn supernovae exhibit considerable heterogeneity. Some objects like SN 1986J, SN 1988Z, SN 1995N, whose spectra were for many years completely dominated by Hα emission of FWHM $\lesssim$ 1000 km s^{-1}, became strong radio and X-ray sources indicating that they had dense circumstellar material. Other SNe, however, are distinct from the above. Although they exhibit strong Hα emission they do not become luminous radio and X-ray sources.

The late phase total luminosity decline is exceptionally slow and cannot be explained

by a simple radioactive model and is best explained as being powered by the interaction of the supernova ejecta with the circumstellar material.

The Hα and bolometric luminosities of most IIn are large, which can be explained by the shock interaction of supernova ejecta with a very dense circumstellar (CS) gas (Chugai 1990). Many SNe also show an excess late time infrared emission, which is a signature of dense CS dust. CS interaction in SNe is typically observed by radio and X-ray emission (Chevalier & Fransson 2003), however, in many cases, radio emission from SNe IIn has not been detected. The important issue for SNe Type IIn is their wide range of pre-supernova mass loss rates ($\sim 10^{-2}$ - 0.1 $M_\odot$ yr^{-1}). One possibility for these high mass loss rates is that they are related to an explosive event a few years before the SN outburst (Chugai & Danziger 2003; Pastorello et al. 2007). Radio observations may put better constraints on the mass loss of the progenitor stars.

4.2 SN 2005kd: A Type IIn Supernova

4.2.1 Introduction

SN 2005kd was discovered by Puckett et al. (2005) on November 12.22 UT, by the 0.35m automated supernova patrol telescope, located 0.1" west and 5.0 " north of the center of CGCG 327-013 (Zwicky et al. 1968). Optical spectra taken on November 13.3 UT with the MDM 2.4m telescope by an Ohio State University group, shows a blue continuum and strong hydrogen Balmer and He I lines emission lines at the central wavelengths fully consistent with the recession velocity (4509 km s^{-1}) of the host galaxy. The observed features suggest that the supernova found was very young with position coordinates RA = 04^h 03^m $16^s.88$, Dec. = +71^o 43′ 18".9 (equinox 2000.0).

The photometric observations of the SN 2005kd started on 2005 November 14, and continued till 2007 February 17, for an almost one and half year. The identification chart is displayed in the Figure 4.1 and the secondary standard stars which are used to calibrate the supernova are numbered. The secondary standard stars magnitudes are shown in the Table 4.1. Spectroscopic monitoring of SN 2005kd started on 2005 November 14 and continued till 2006 January 8. The log of spectroscopic observations is given in Table 4.2.

4.2.2 Light Curves

The light curves of SN 2005kd in *UBVRI* bands are shown in Figure 4.2. The SN was observed well before the maximum and from the light curves it is apparent that the su-

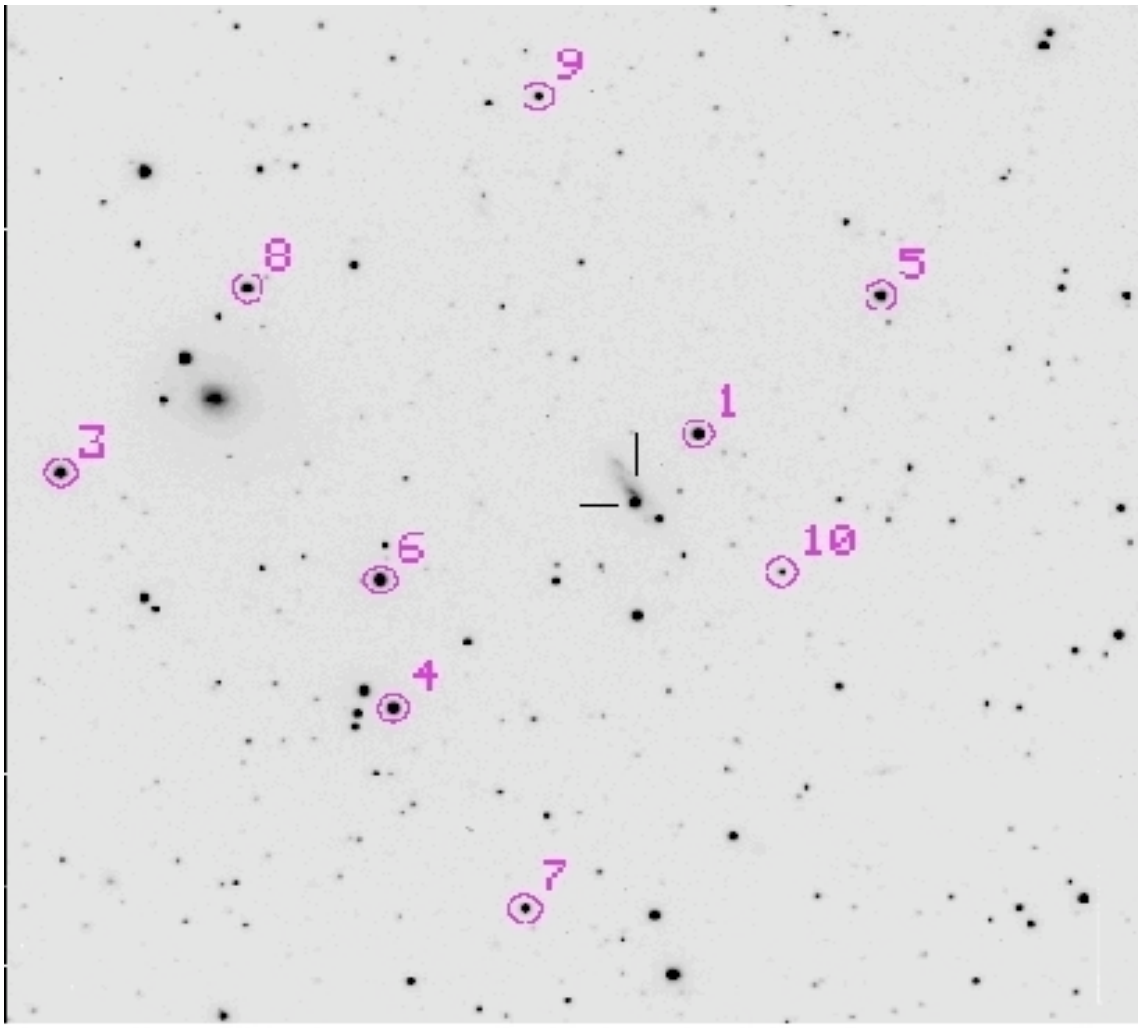

Figure 4.1: SN2005kd identification chart

Table 4.1: Photometry of stars in the field of SN 2005kd. The stars are labeled in the same way as in Figure 4.1

Star ID	*U*	*B*	*V*	*R*	*I*
1	15.30 (0.007)	15.18 (0.015)	14.49 (0.021)	14.05 (0.019)	13.628 (0.021)
2	14.61 (0.019)	14.48 (0.031)	13.79 (0.022)	13.33 (0.017)	12.916 (0.005)
3	14.65 (0.014)	14.55 (0.020)	13.80 (0.021)	13.35 (0.016)	12.884 (0.007)
4	15.26 (0.005)	15.16 (0.014)	14.43 (0.019)	13.98 (0.016)	13.516 (0.018)
5	15.60 (0.020)	15.08 (0.020)	14.16 (0.020)	13.60 (0.016)	13.099 (0.007)
6	15.26 (0.032)	14.73 (0.011)	13.79 (0.012)	13.24 (0.014)	12.726 (0.008)
7	16.10 (0.018)	15.89 (0.014)	15.13 (0.019)	14.68 (0.017)	14.238 (0.022)
8	15.48 (0.017)	15.40 (0.011)	14.65 (0.017)	14.19 (0.011)	13.714 (0.013)
9	16.64 (0.021)	16.59 (0.023)	16.05 (0.036)	15.71 (0.031)	15.335 (0.023)
10	16.90 (0.005)	16.77 (0.013)	16.08 (0.012)	15.64 (0.010)	15.216 (0.019)

Table 4.2: Journal of Spectroscopic observations of SN 2005kd.

Date	JD (245 0000+)	*Phase (days)	Wavelength Range (Å)
2005 Nov 14	3689.5	2	3500−7000; 5200−9200
2005 Nov 16	3691.5	4	3500−7000; 5200−9200
2005 Nov 18	3693.0	6	3500−7000; 5200−9200
2005 Nov 24	3699.0	12	3500−7000; 5200−9200
2005 Dec 08	3713.0	26	3500−7000; 5200−9200
2005 Dec 16	3721.0	34	3500−7000; 5200−9200
2005 Dec 27	3732.0	45	3500−7000; 5200−9200
2006 Jan 05	3741.0	54	3500−7000; 5200−9200
2006 Jan 12	3748.0	61	3500−7000; 5200−9200
2006 Jan 28	3764.0	77	3500−7000; 5200−9200
2006 Feb 11	3778.0	91	3500−7000; 5200−9200
2006 Mar 07	3802.0	112	3500−7000; 5200−9200
2006 Mar 14	3809.0	119	3500−7000; 5200−9200
2006 Mar 26	3821.0	131	3500−7000; 5200−9200
2006 Apr 11	3851.0	161	3500−7000; 5200−9200
2006 Sep 20	3999.5	313	3500−7000; 5200−9200
2006 Sep 25	4004.5	318	3500−7000; 5200−9200
2006 Oct 10	4019.5	333	3500−7000; 5200−9200
2006 Oct 16	4025.0	339	3500−7000; 5200−9200
2006 Nov 04	4044.0	358	3500−7000; 5200−9200
2006 Nov 20	4060.5	374	3500−7000; 5200−9200
2006 Nov 23	4063.0	377	3500−7000; 5200−9200
2006 Dec 28	4098.0	412	3500−7000; 5200−9200
2006 Jan 08	4109.0	424	3500−7000; 5200−9200

*Relative to the epoch of discovery (JD = 2453687).

pernova exhibits a distinct plateau during ∼ 60 days to ∼ 190 days since discovery. This kind of plateau is generally expected in Type II-P supernova and explained by the motion of ionized wavefront through the ejected medium. Similar kind of plateau-like light curve was observed in the IIn SN 1994W (Chugai et al. 2004), which was reproduced by a hydrodynamical model and found to be powered by a combination of internal energy leakage after the explosion of an extended pre-SN and subsequent luminosity from CS interaction. After the plateau phase the light curve declined gradually in all bands.

The peak magnitudes of the *BVRI* light curves at the maximum are 15.18, 14.82, 14.40, 14.14 magnitudes respectively. After reaching the maximum, the light curves decline slowly before entering into the plateau phase. Following the plateau, the light curves continue a slow decline even in the nebular phase at a rate of 0.8, 0.8, 0.7, 0.6 per

Table 4.3: Journal and results of optical photometry of SN 2005kd.

Date	JD (245 0000+)	*U*	*B*	*V*	*R*	*I*
2005-11-14	3689.43	–	15.72 (0.02)	15.56 (0.01)	15.32 (0.01)	15.21 (0.02)
2005-11-15	3690.34	14.84 (0.03)	15.51 (0.02)	15.36 (0.02)	15.11 (0.02)	14.96 (0.02)
2005-11-16	3691.34	14.66 (0.06)	15.36 (0.07)	15.17 (0.03)	14.89 (0.03)	14.72 (0.03)
2005-11-18	3693.34	14.57 (0.05)	15.23 (0.05)	15.05 (0.06)	14.80 (0.04)	14.66 (0.04)
2005-11-23	3698.34	14.63 (0.02)	15.19 (0.01)	14.88 (0.01)	14.55 (0.01)	14.39 (0.01)
2005-12-08	3713.03	15.11 (0.03)	15.48 (0.01)	14.95 (0.01)	14.49 (0.01)	14.22 (0.01)
2005-12-09	3714.03	–	15.45 (0.02)	14.88 (0.03)	14.42 (0.02)	14.11 (0.06)
2005-12-15	3720.28	–	15.65 (0.02)	15.03 (0.01)	14.54 (0.01)	14.23 (0.01)
2005-12-16	3721.28	–	–	–	–	14.20 (0.02)
2005-12-17	3722.28	–	15.66 (0.02)	15.04 (0.01)	14.56 (0.01)	14.23 (0.01)
2005-12-26	3731.27	–	15.79 (0.01)	15.13 (0.01)	14.62 (0.01)	14.23 (0.02)
2005-12-27	3732.27	–	–	15.18 (0.02)	14.64 (0.02)	14.29 (0.02)
2005-12-28	3733.27	–	15.82 (0.02)	15.13 (0.01)	14.62 (0.01)	14.27 (0.01)
2005-12-31	3736.08	–	15.90 (0.03)	15.22 (0.01)	14.66 (0.02)	14.29 (0.03)
2006-01-06	3742.32	15.75 (0.03)	15.97 (0.02)	15.28 (0.01)	14.72 (0.01)	14.35 (0.01)
2006-01-12	3748.29	15.83 (0.02)	16.05 (0.02)	15.33 (0.01)	14.74 (0.02)	14.40 (0.01)
2006-01-28	3764.23	15.82 (0.03)	16.02 (0.02)	15.34 (0.02)	14.76 (0.02)	14.40 (0.01)
2006-02-24	3791.08	15.89 (0.03)	16.11 (0.01)	15.46 (0.01)	14.84 (0.01)	14.49 (0.01)
2006-03-07	3802.12	–	16.10 (0.01)	15.49 (0.01)	14.90 (0.01)	14.49 (0.02)
2006-03-14	3809.12	–	16.13 (0.02)	15.51 (0.01)	14.89 (0.01)	14.51 (0.02)
2006-03-17	3812.10	15.89 (0.02)	16.09 (0.01)	15.50 (0.01)	14.90 (0.01)	14.54 (0.01)
2006-03-26	3821.17	15.88 (0.03)	16.09 (0.02)	15.50 (0.02)	14.87 (0.01)	14.54 (0.02)
2006-03-29	3824.10	–	16.11 (0.01)	15.50 (0.01)	14.90 (0.01)	14.52 (0.01)
2006-04-05	3831.09	15.88 (0.03)	16.10 (0.01)	15.52 (0.01)	14.88 (0.01)	14.54 (0.01)
2006-04-26	3852.11	–	16.10 (0.02)	15.55 (0.01)	14.91 (0.02)	14.56 (0.02)
2006-07-18	3935.43	–	16.44 (0.02)	15.94 (0.02)	–	14.90 (0.01)
2006-09-05	3984.40	–	–	16.16 (0.03)	15.29 (0.02)	15.14 (0.01)
2006-09-06	3985.40	16.42 (0.03)	16.68 (0.01)	16.26 (0.02)	15.34 (0.01)	14.90 (0.03)
2006-09-19	3998.40	–	16.66 (0.02)	16.23 (0.02)	15.37 (0.02	15.23 (0.02)
2006-09-20	3999.40	16.50 (0.03)	16.72 (0.02)	16.26 (0.02)	15.38 (0.01)	15.21 (0.02)
2006-11-06	4046.40	–	17.22 (0.02)	16.80 (0.01)	15.80 (0.01)	15.64 (0.01)
2006-11-23	4063.21	–	17.31 (0.02)	16.83 (0.02)	15.86 (0.01)	15.67 (0.02)
2006-12-14	4084.25	17.38 (0.02)	17.70 (0.02)	17.26 (0.02)	16.19 (0.01)	16.02 (0.01)
2006-12-28	4098.25	–	–	17.02 (0.02)	16.14 (0.02)	15.84 (0.02)
2007-01-08	4109.23	–	17.75 (0.04)	17.21 (0.03)	16.26 (0.02)	16.07 (0.02)
2007-01-13	4114.21	–	17.86 (0.03)	17.46 (0.03)	16.48 (0.02)	16.24 (0.03)
2007-02-17	4149.13	18.55 (0.04)	18.85 (0.03)	18.34 (0.04)	17.10 (0.03)	16.92 (0.04)

NOTE: Figures in brackets give the statistical errors associated with the magnitudes.

100 days respectively in *BVRI*.

SN 2005kd clearly shows a plateau for about ∼ 120 days which is a characteristic feature of type II-P supernova. When compared to Type II-P supernova SN 2004et, SN 2005kd has long duration of decline from maximum to plateau. The overall light curve evolution of SN 2005kd is very similar to the Type IIn supernova SN 1988Z. The pre-maximum light curve is very similar to that of SN 1998S having a short rise time (< 20 days), while SN 1998S (Liu et al. 2000) does not show any plateau. SN 2008iy (Miller et al. 2010) shows an unusually long rise time of ∼ 400 days. The objects SN 1996L (Benetti et al. 1999) and SN 2005ip (Smith et al. 2009) decline rapidly (∼ 0.05 and 0.02 mag day^{-1}), though this decline rate is slower at later times.

The color curves are shown in the Figure 4.3. The color curve of (B-V) clearly shows that the supernova is mush bluer than other supernovae in the early epoch. Later supernova tends to be redder indicating dust formation at the later epochs.

The quasi-bolometric light curve of SN 2005kd using the *UBVRI* is estimated in the following way. The missing magnitudes in some bands were obtained by interpolating between points adjacent in time. The optical magnitudes have been corrected for reddening $E(B-V)$ =0.27 using interstellar extinction law (Cardelli et al. 1989). The emitted monochromatic flux is estimated by converting the corrected magnitudes into flux according to Bessell et al. (1998). The *UBVRI* bolometric flux for each day was then derived by fitting a spline curve to the U, B, V, R and I fluxes and integrating it over the wavelength range λ 3600-10600 Å. No corrections have been applied for the missing flux in UV and IR bands. The bolometric light curve of SN 2005kd is plotted in Figure 4.4 along with other supernovae for comparison. The absolute V magnitude peaks at −20.36 mag, indicating that SN 2005kd is one of the brightest candidates observed after SN 2005gy.

4.2.3 Spectroscopic Evolution

The spectral evolution is shown in Figures 4.6, 4.7, and 4.8. The spectra is not corrected for reddening. There is blue excess present in the spectra till maximum and flattened there after. The first spectra was taken just two days after the discovery which shows strong narrow emission lines on top of the broad lines. In the spectra, all Balmer series lines are prominent. Hδ disappeared around day 50 from the date of maximum where as all other three lines are seen till the day 410 from the date of discovery. Apart from the Balmer lines, He I , O III λ 4648 Å, N III λ 4640 Å and He II λ 4686 Å lines are also present in the spectra. The Ca II triplet is absent in the early time spectra, but started appearing from day 25 since discovery. Around day ∼ 42, O I and Ca III begin to appear in the

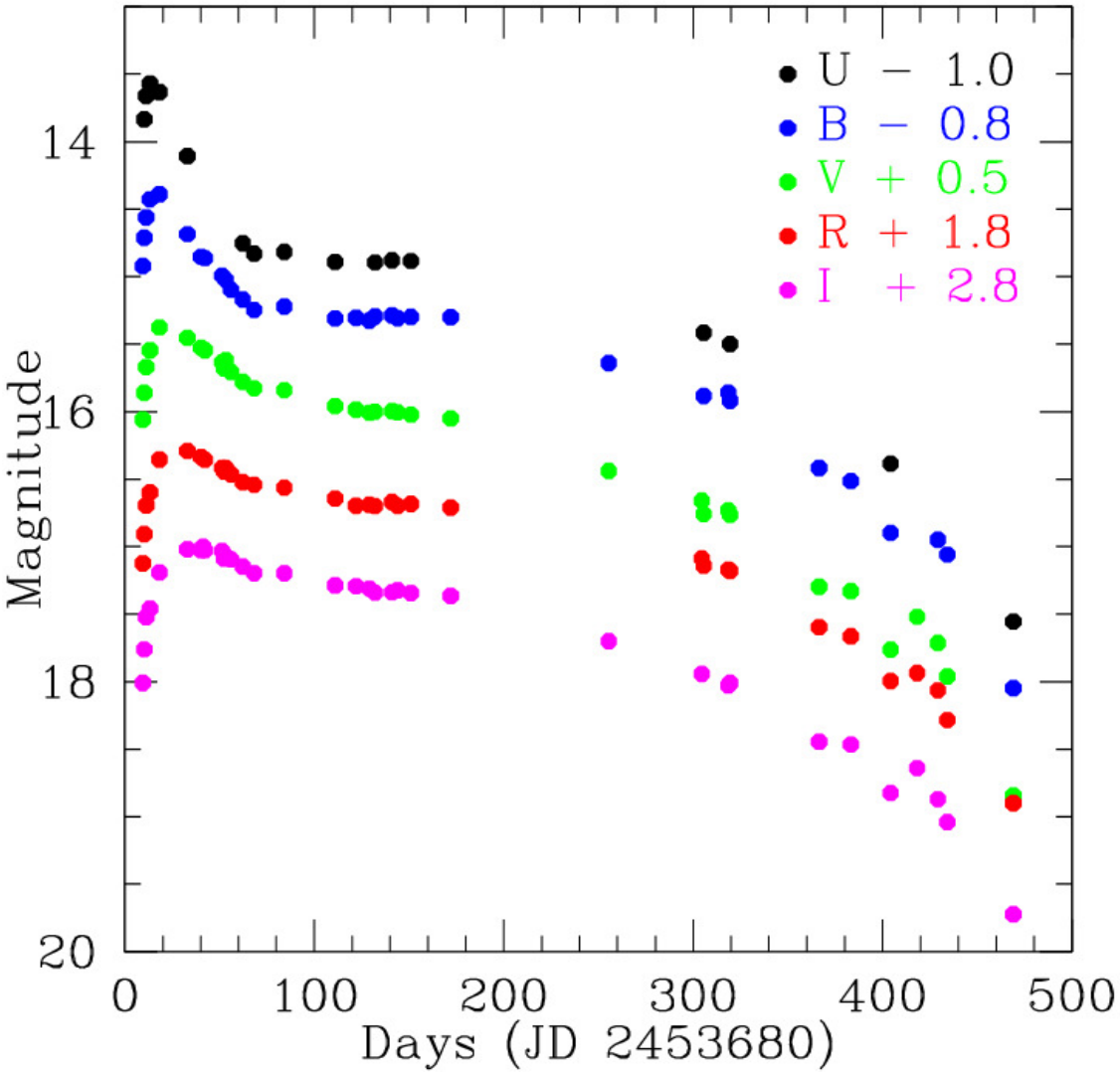

Figure 4.2: SN2005kd UBVRI light curve.

spectra. An asymmetry in the Hα line is clearly observed at later phase (day 103 from day of maximum) indicating asymmetric ejection of mass during the explosion. The iron lines due to Fe II, Fe III and higher ionization lines Fe VII appear at the later phases (after day 100 from maximum) indicating that the ejected material had became optically thin.

The spectral continuum and the bolometric fluxes can be used to estimate the photosphere temperature & radius assuming it to be similar to a black body. The best fit black body temperature using continuum and bolometric fluxes are given in Table 4.4. The corresponding photospheric radius is calculated using the luminosity - temperature

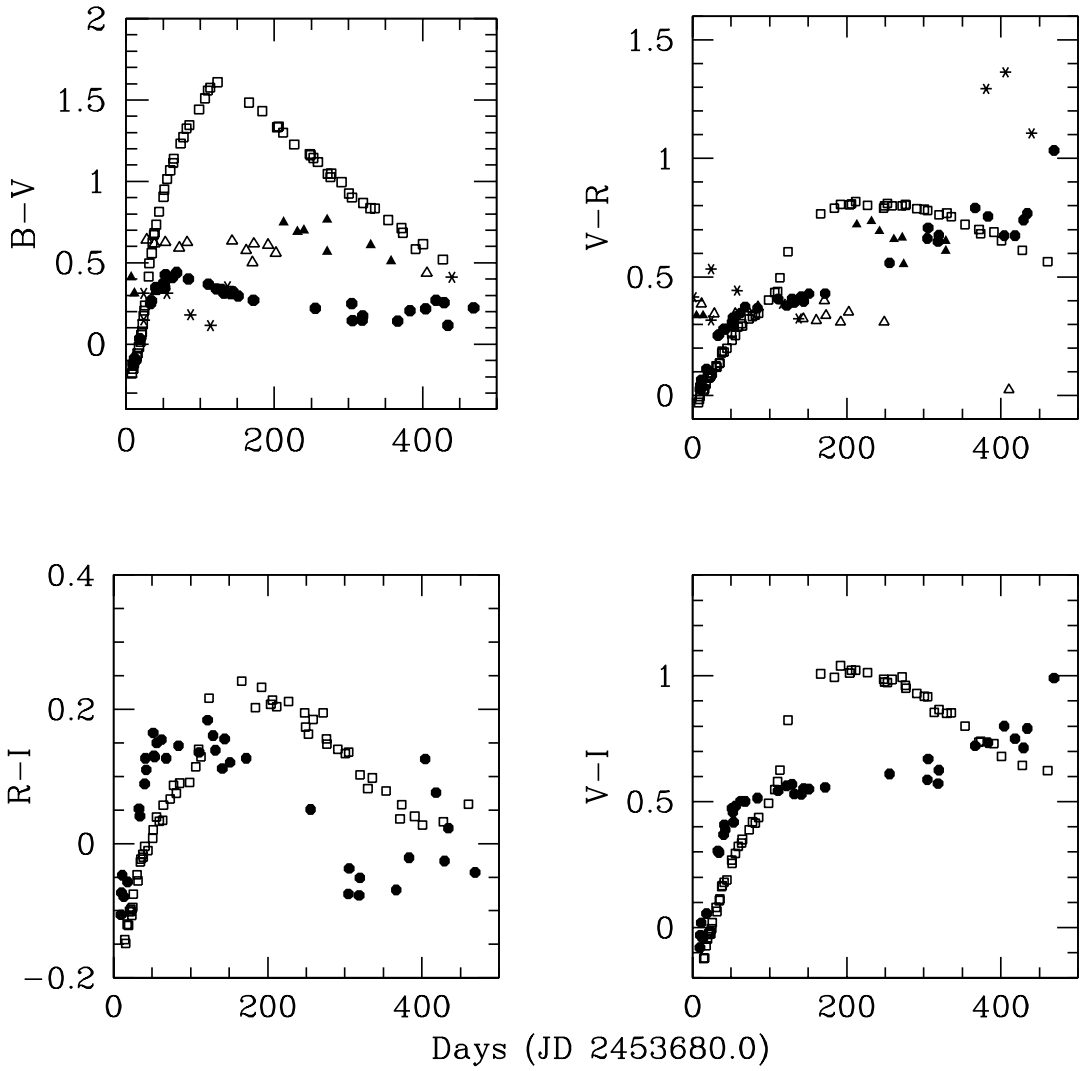

Figure 4.3: SN2005kd color curves in comparision with others. Filled circles correspond to SN 2005kd (IIn), stars correspond to SN 1988Z (IIn), filled triangles correspond to SN 1995G (IIn), open triangles correspond to SN 1997cy (IIn), squares correspond to SN 2004et (II-P).

relation. The estimated black body temperature and radius are plotted in Figure 4.10. The black body temperature shows an unusual rapid decline, decreasing from ∼ 18,000 K before maximum to remains nearly constant temperature of ∼ 8000 K until day 400 since discovery. While the spectral continuum could be fit with a black body during the early phases, it was not possible to fit beyond day 160 since the continuum showed a blue excess with a flat spectrum in the red. SN 2007rt also showed a similar evolution and as

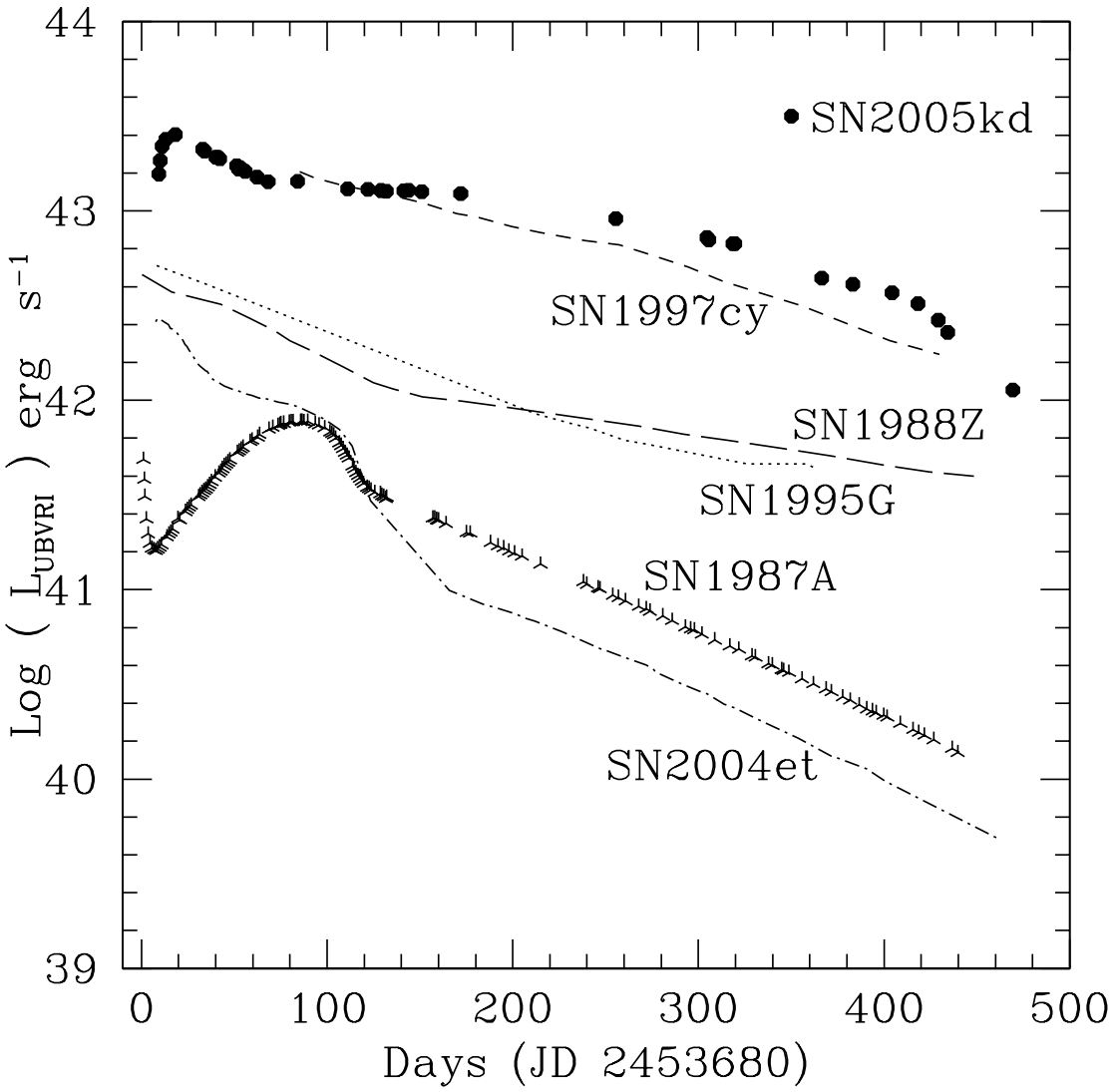

Figure 4.4: SN2005kd bolometric magnitude curve compared with other type IIn and II-P SNe.

shown by Turndle et. al. 2009 that the blackbody fit was poor initially and as the SN evolved it became increasingly difficult to simultaneously reconcile the flat red spectral region and the blue excess with a single blackbody.

To study the spectral properties of the line profiles, we deconvolved the Hα line into separate gaussian components. We fit the gaussian parameters of central amplitude, wavelength and Full Width Half Maximum (FWHM) freely by the NGAUSSFIT task in IRAF data reduction package. Hα was fit by three Gaussians namely broad, intermediate and narrow components. As an illustration, the deconvolved Hα observed on 2006 January

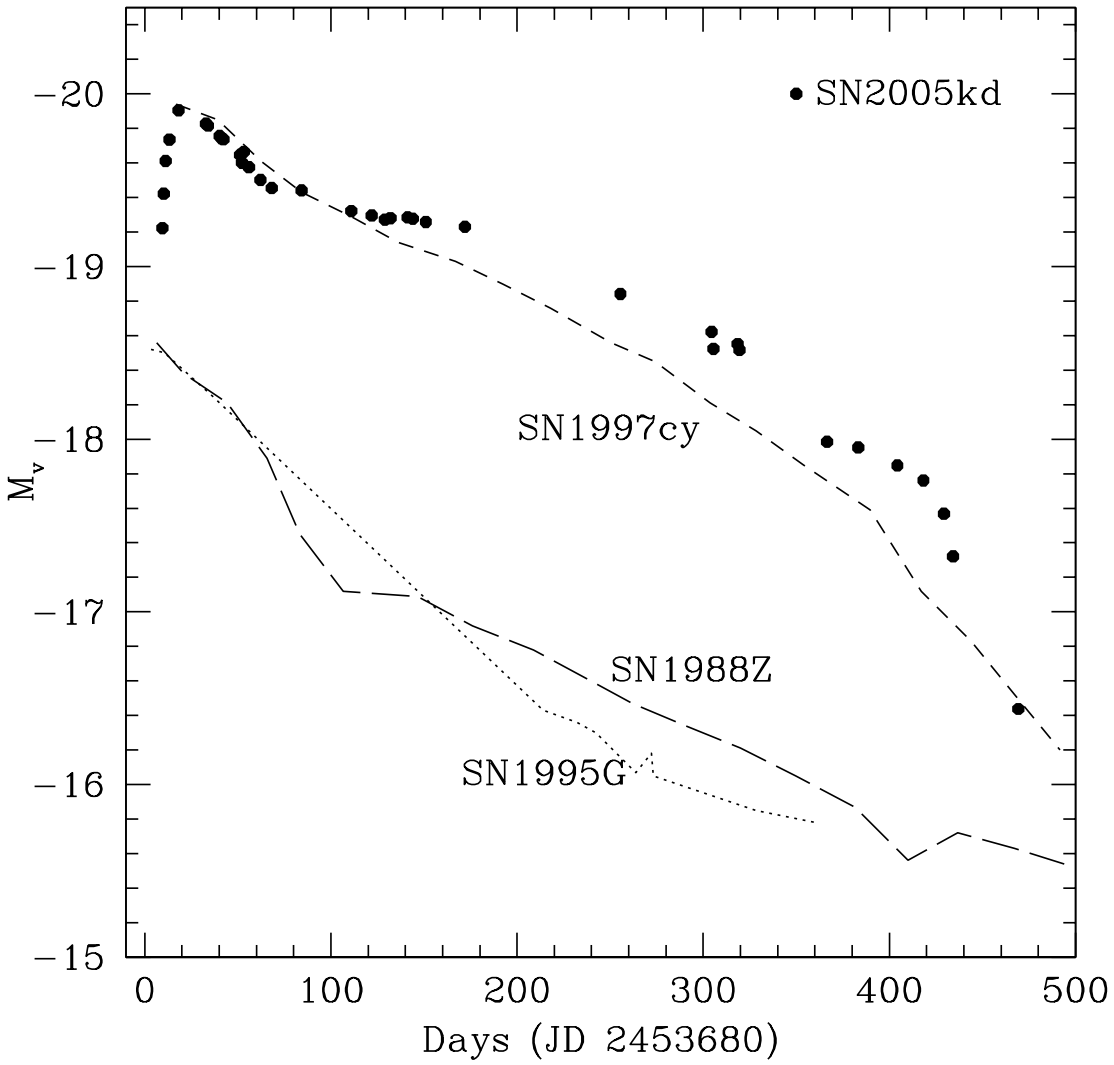

Figure 4.5: SN2005kd absolute V magnitude curve comparing with other Type IIn and II-P SNe.

28 is shown in Figure 4.9. The FWHM velocities derived from the fits are plotted in Figure 4.11. The fit of the broad component at later epoch is poor due to an asymmetry of the line. The narrow and intermediate components maintain constant velocity of 500 km s^{-1} and 2000 km s^{-1} respectively till the day 180. After that, the velocities are found to be 1500 km s^{-1} and 3000 km sec^{-1} respectively. This increment in the velocities can be attributed either to the transfer of energy of the ejecta to the circumstellar material or gradual interaction of the ejecta with the CSM. We are unable to comment further on this as we do not have observations during the days $\sim$ 180 - 300. There is a sharp decline

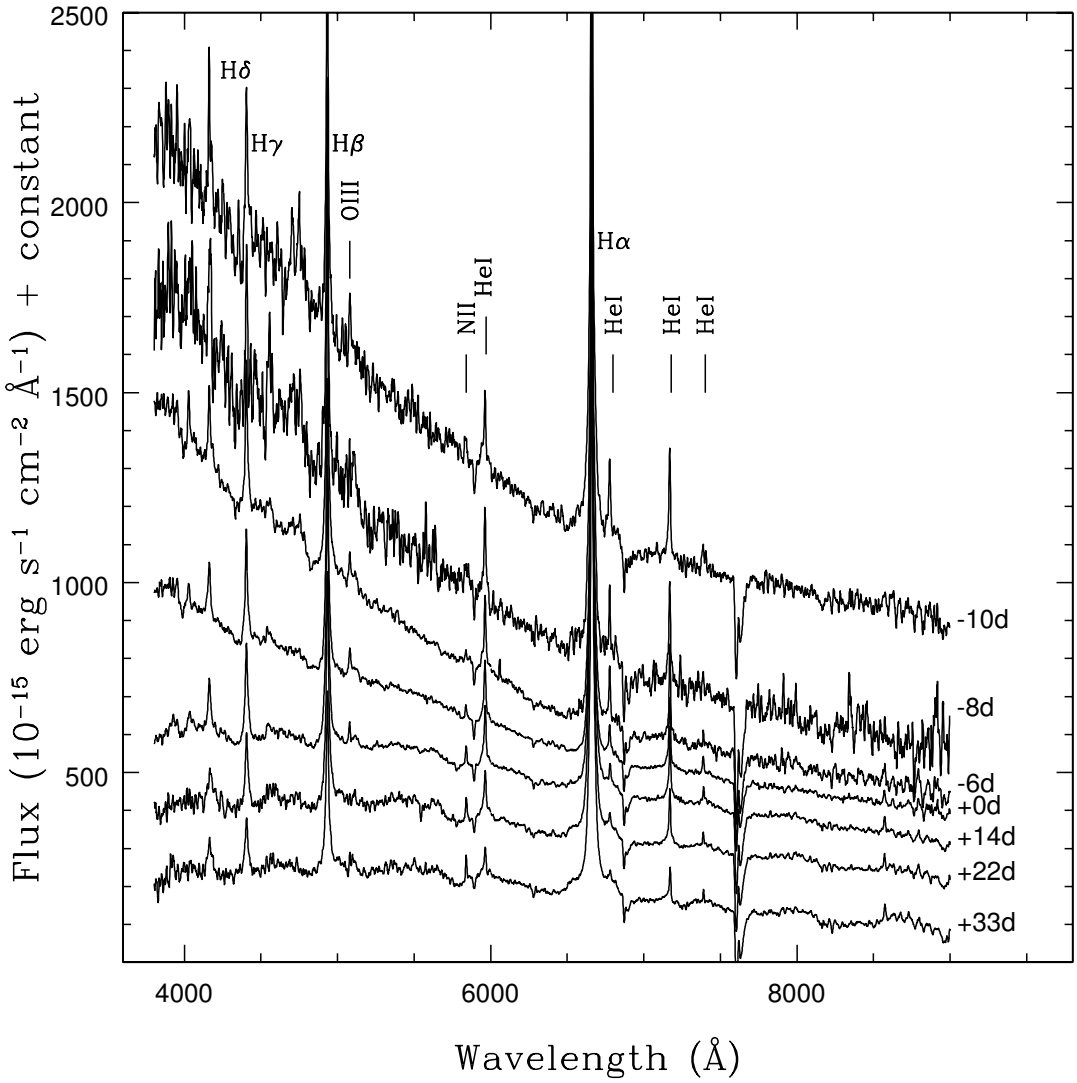

Figure 4.6: Early phase spectral evolution of SN2005kd

in the velocity of broad component of Hα from 9000 km s^{-1} to 7000 km s^{-1} within 10 days just after the discovery, where the light curve reaches the maximum, and the velocity increases thereafter. The broad component of Hα velocity increases to maximum 12000 km s^{-1} around day ∼100 and declines slowly, reaching around 6000 km s^{-1} at the nebular phase. The supernova ejecta velocity i.e the broad component reached maximum when the light curve entered the plateau phase.

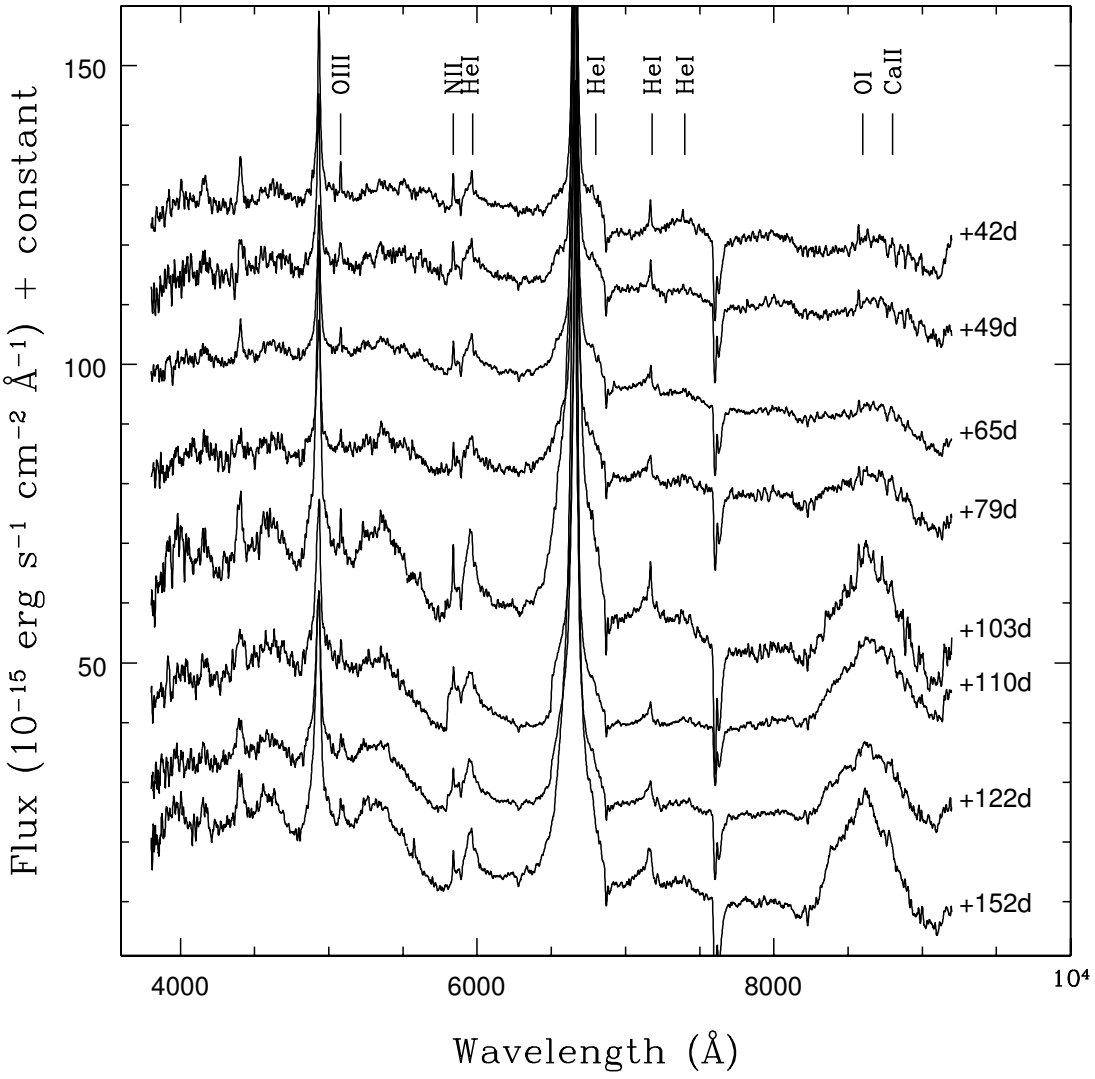

Figure 4.7: Spectral evolution of SN2005kd during the plateau

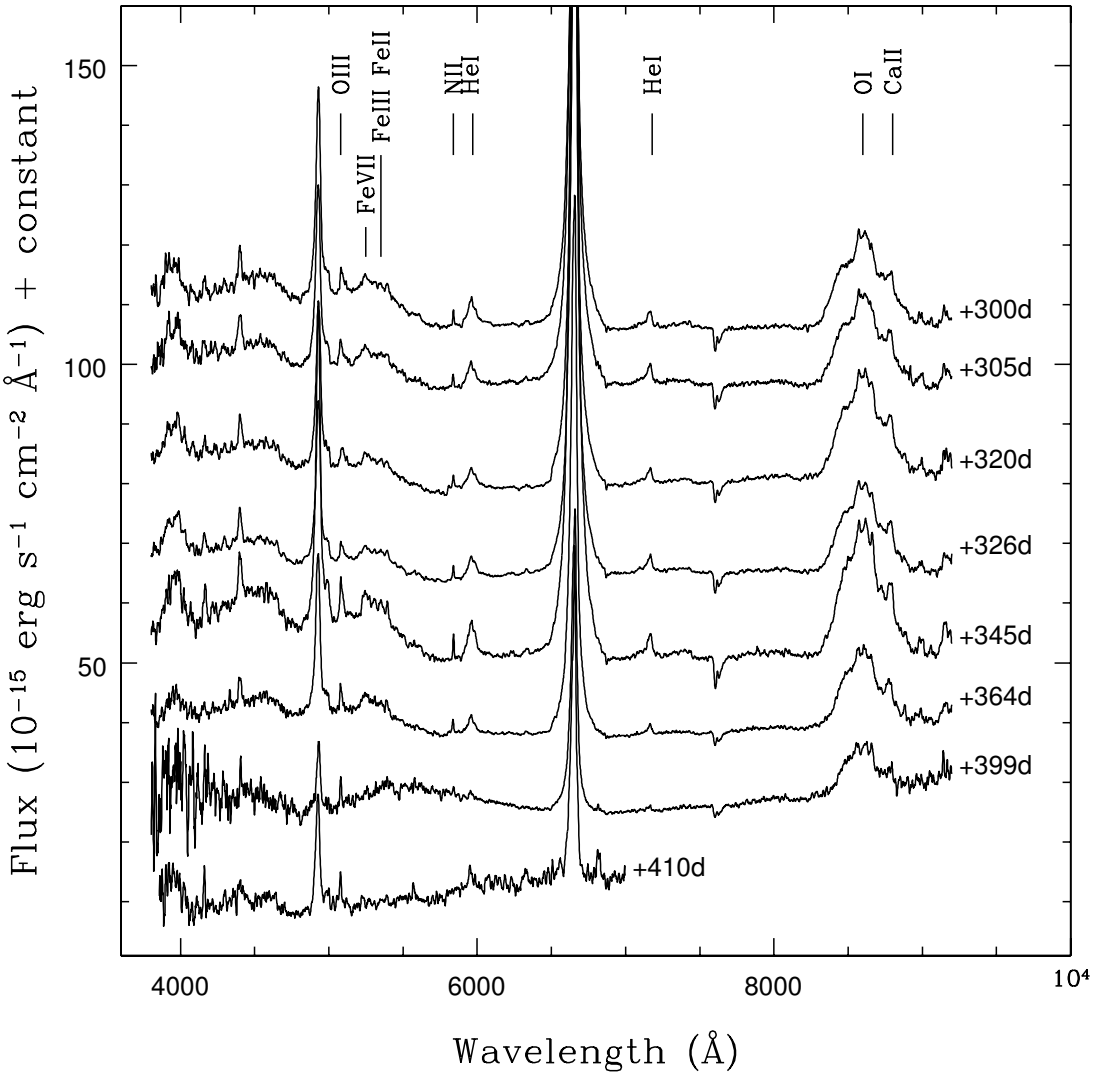

Figure 4.8: SN2005kd Spectral evolution in the nebular phase

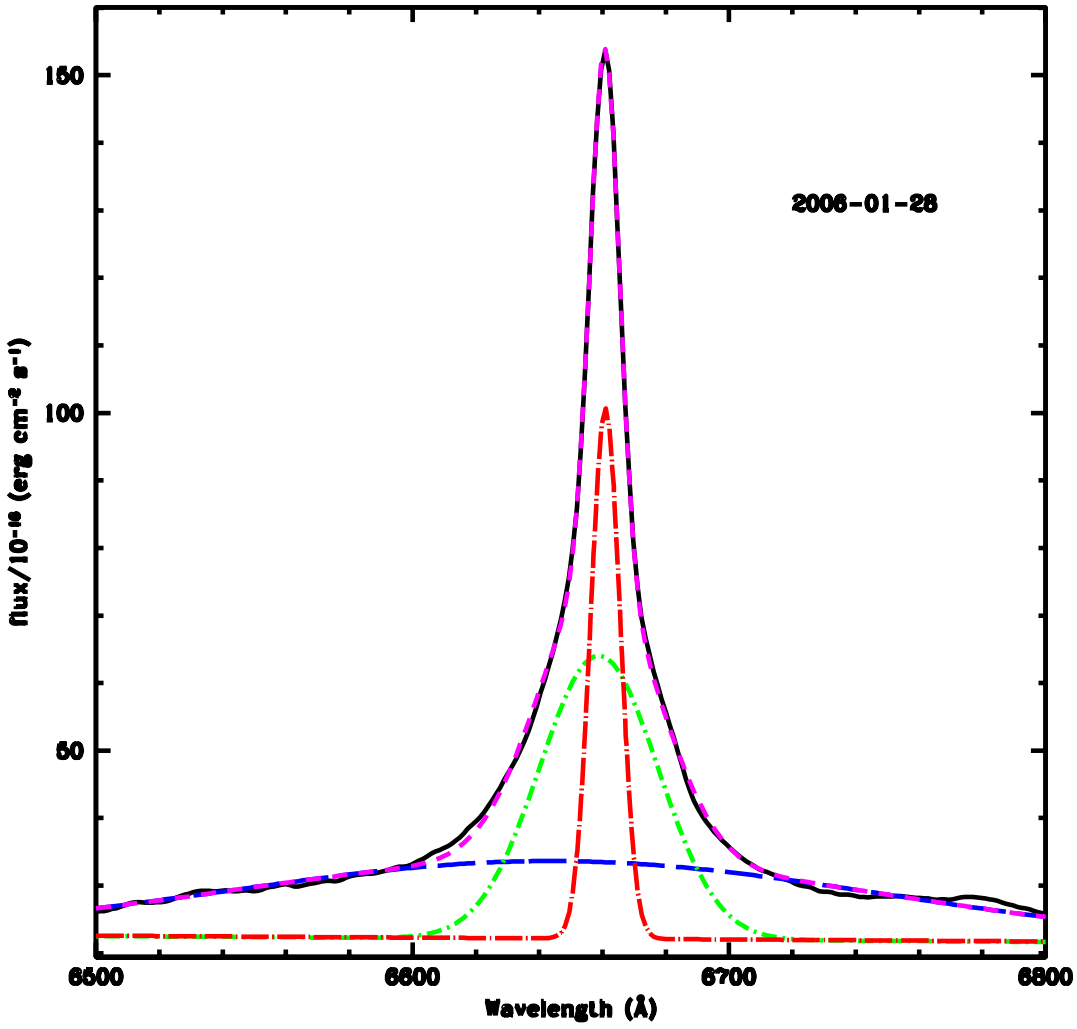

Figure 4.9: Hα deconvolution on three gaussian components. The combined spectra (magenta) of broad (blue), intermediate (green) and narrow (red) is overplotted on top of the observed spectra (black).

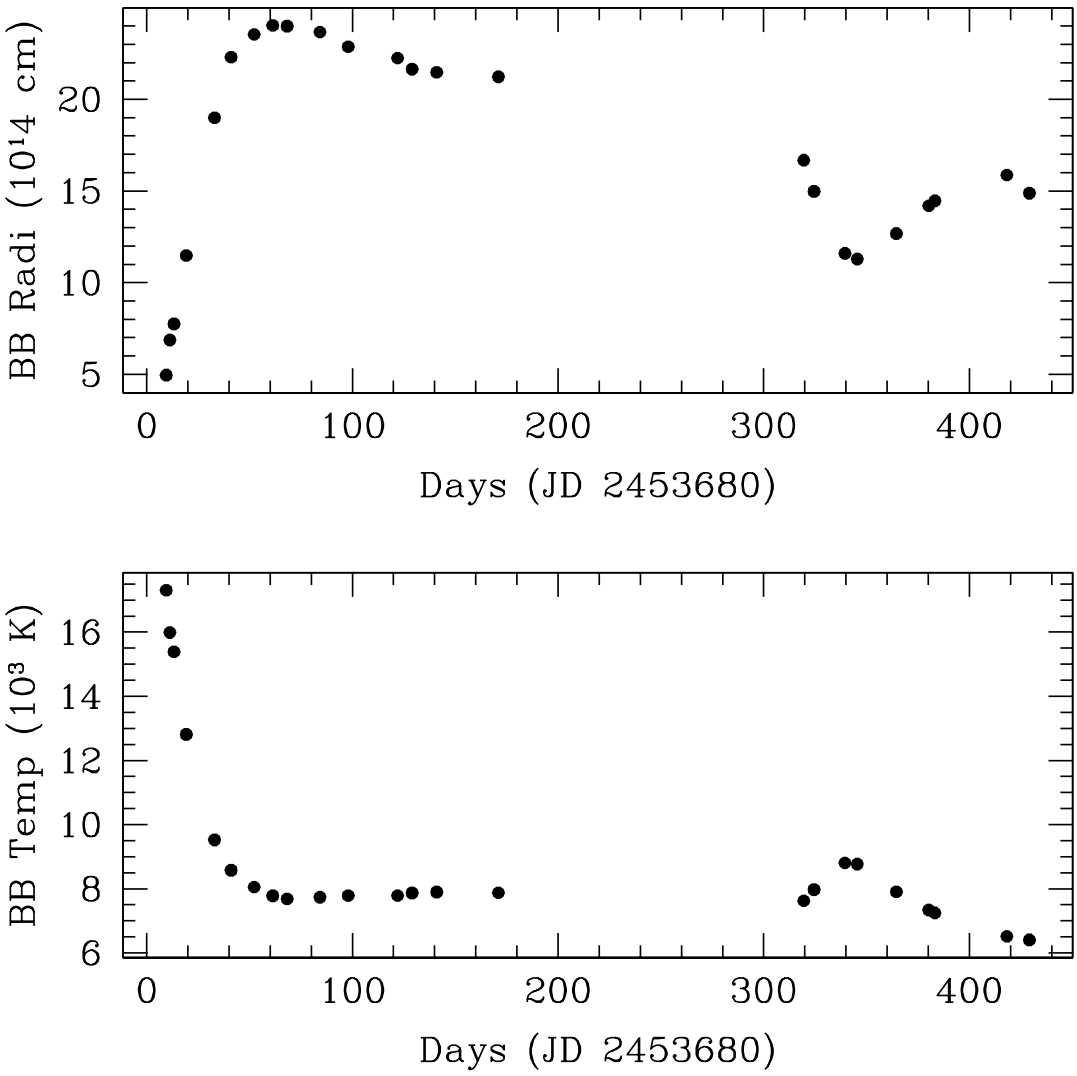

Figure 4.10: SN2005kd blackbody temperature and radius evolution.

Table 4.4: Physical parameters of the supernova SN 2005kd.

Date	JD (245 0000+)	*Phase (days)	BB Temp Spectra (K)	BB Temp from UBVRI mags (K)	Luminosity (10^{43})	Photospheric Radius (10^{15}cm)
2005 Nov 14	3689.5	2	17238.79	17305.76	1.56	0.50
2005 Nov 16	3691.5	4	15123.42	15988.10	2.20	0.70
2005 Nov 18	3693.0	6	16234.08	15389.37	2.39	0.77
2005 Nov 24	3699.0	12	12167.88	12809.57	2.53	1.15
2005 Dec 08	3713.0	26	8540.77	9526.09	2.11	1.89
2005 Dec 16	3721.0	34	7794.71	8579.84	1.92	2.23
2005 Dec 27	3732.0	45	7534.02	8055.67	1.66	2.35
2006 Jan 05	3741.0	54	7172.04	7782.53	1.51	2.40
2006 Jan 12	3748.0	61	7080.31	7683.18	1.43	2.39
2006 Jan 28	3764.0	77	7599.02	7737.58	1.43	2.36
2006 Feb 11	2778.0	91	7292.11	7790.11	1.37	2.28
2006 Mar 07	3802.0	112	7467.02	7788.66	1.30	2.22
2006 Mar 14	3809.0	119	7444.88	7871.21	1.28	2.16
2006 Mar 26	3821.0	131	7811.99	7895.47	1.27	2.14
2006 Apr 11	3851.0	161	7852.38	7876.31	1.23	2.12
2006 Sep 20	3999.5	313	-	7627.14	0.67	1.66
2006 Sep 25	4004.5	318	-	7973.28	0.64	1.49
2006 Oct 10	4019.5	333	-	8804.84	0.57	1.16
2006 Oct 16	4025.0	339	-	8769.40	0.54	1.13
2006 Nov 04	4044.0	358	-	7905.57	0.45	1.27
2006 Nov 20	4060.5	374	-	7341.64	0.42	1.42
2006 Nov 23	4063.0	377	-	7246.22	0.41	1.44
2006 Dec 28	4098.0	412	-	6516.75	0.32	1.58
2007 Jan 08	4109.0	424	-	6404.12	0.26	1.48

*Relative to the epoch of discovery (JD = 2453687).

4.2.4 Discussion

Chugai & Danziger (1994) presented calculations of the dynamical interaction of the ejecta with a dense clumpy circumstellar wind in the case of SN 1988Z. Two alternative models were proposed for the wind structure that are relevant to the three components: broad, intermediate and narrow. These models suggest that the optical emission is a result of the dynamical interaction of the ejecta with two-component wind; the broad lines are identified with emission from the shocked supernova material expanding in a relatively rarefied wind, while the intermediate-width lines originate from a shocked dense wind component. The narrow component velocities ($\sim$ 500 km s^{-1}) may not represent the true velocities of the wind ($\sim$ 100 - 200 km s^{-1}) since they are limited by the resolution instrument.

We envisage that before it exploded, the progenitor of SN 2005kd had undergone two phases of mass-loss, which give rise to two shells of CSM. The early time broad component had a FWHM $\sim$ 9000 km s^{-1}, the lines of this width in SNe are usually associated with the ejecta, the absence of any corresponding P-Cygni absorption is a robust indicator that these lines are driven by the high-energy radiation of the shock resulting from the interaction of the ejecta with dense CSM in the immediate vicinity of the supernova (Chugai 1990). From the Figure 4.11, we can infer that the supernova ejecta started interacting with the nearby shell around the day 80. If we assume that the ejecta is moving with the velocity of 8000 km s^{-1} for 80 days, then the radius of the shell is estimated to be 5.53×10^{15} cm. If we assume that the shell is moving with an average velocity of 2000 km s^{-1}, then the time of mass eruption is estimated to be one year. The spectral lines of SN 2005kd at this phase are similar to those observed in the spectra of normal SNe Type II during their photospheric phase (Blanton et al. 1995; Fassia et al. 1998.

The luminosity evolution of Hα, the luminosity in the individual components as well as the total luminosity is plotted in Figure 4.12. Following Chugai & Danziger (1994), we can derive some important parameters of the progenitor. We assume that the velocity of the broad Hα emission is representative of the velocity of the ejecta, since this component is supposed to originate in the shocked ejecta.

The interaction between the ejecta and the progenitor's wind follows two distinct phases. Initially the outer part of the ejecta, having a power law distribution, collides with the wind. This is the so called free expansion phase. In this phase the shock velocity v (cm s^{-1}) (which is observed as the velocity of the broad component of Hα) is given by

$$v = 7.46 \times 10^8 E_{51}^{2/5} (M_{ej}/M_{\odot})^{-1/5} w_{16}^{-1/5} t_{yr}^{-1/5}, \tag{4.1}$$

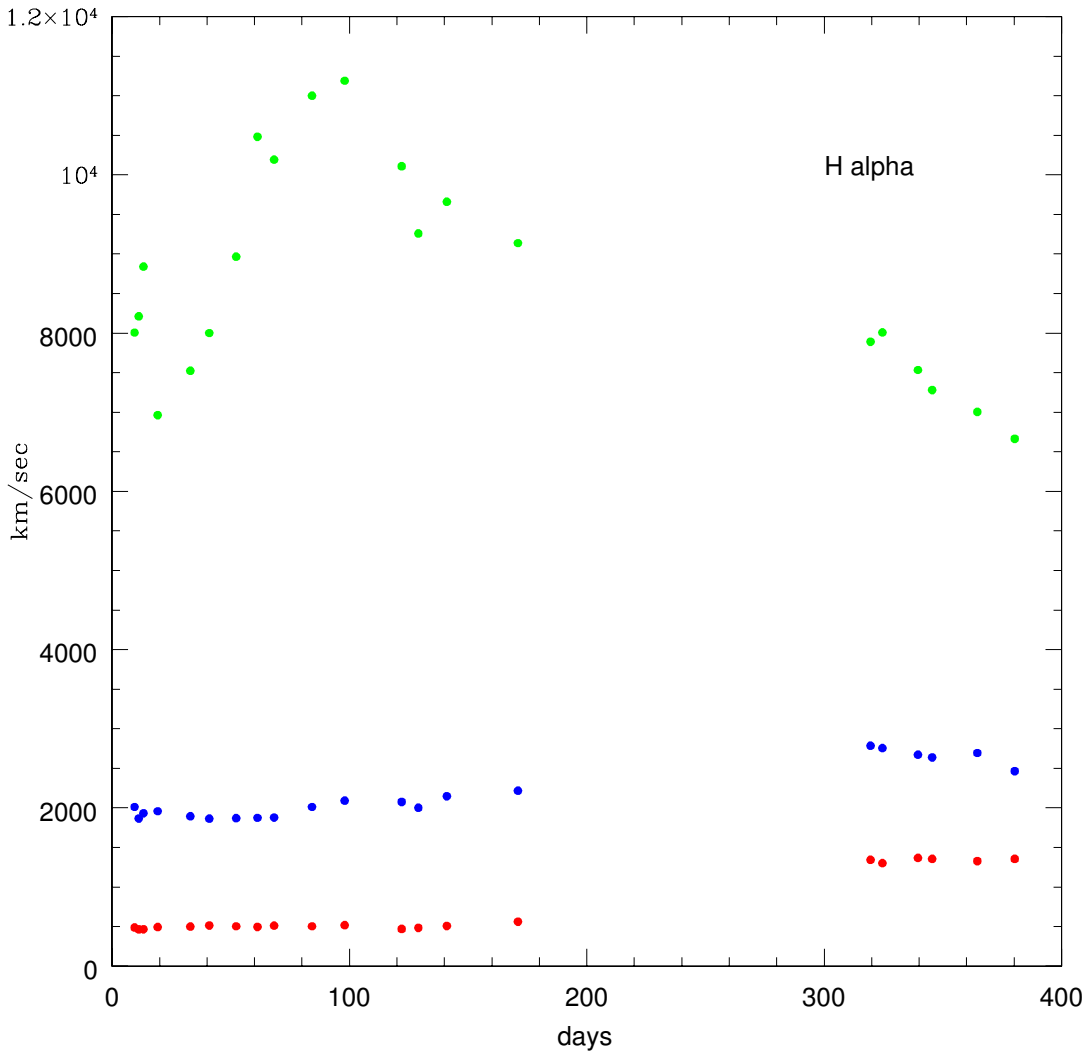

Figure 4.11: Hα FWHM velocities. Broad components are in green, intermediate are in blue and narrow components are in red.

where E_{51} is the kinetic energy of the ejecta in units of 10^{51} erg, t_{yr} is the time elapsed since the explosion in years, w=$\dot{M}/u_w$ is the wind density papameter, u_w is the wind velocity, and $w_{16} = w/10^{16}$g cm^{-1}. A lower limit for w can be obtained from the general expression for the luminosity of the shock wave,

$$L = \frac{1}{2}\psi w v^3, \tag{4.2}$$

where L is the SN luminosity (which is dominated by the interaction) and ψ is the effi-

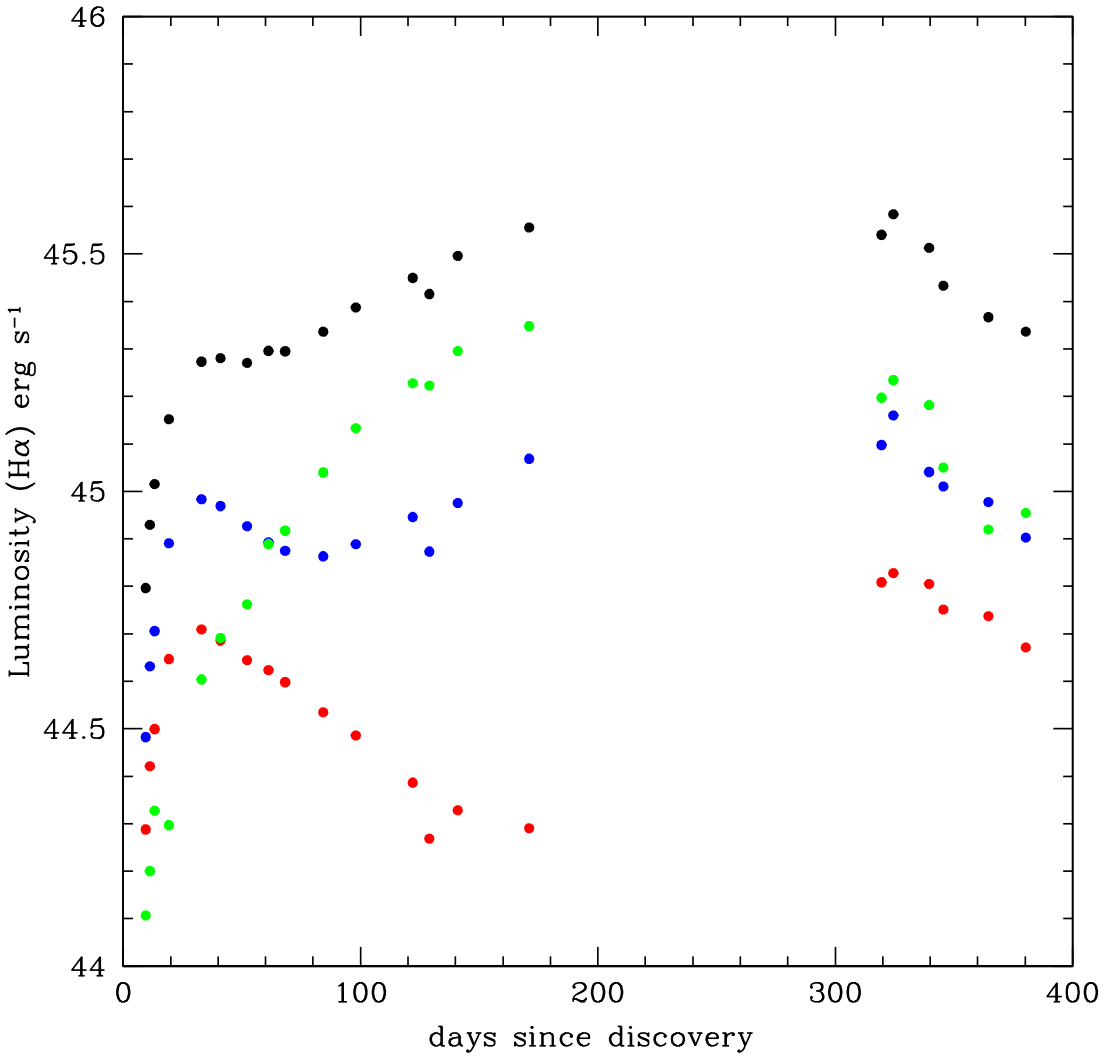

Figure 4.12: The Hα individual broad (green), intermediate (red) and narrow (black) components luminosity evolution along with the total luminosity (black) are shown.

ciency of conversion of mechanical into optical energy.

In the case of SN 2005kd at t = 0.2 years, we estimate L = 2×10^{43} erg s^{-1} (with a considerable uncertainty, because of the paucity of observed data at this epoch) and broad component velocity v = 10000 km s^{-1}. If we assume ψ = 1, Eq. 4.2 gives w_{16} = 4 g cm^{-1}. For a wind velocity of u_w = 500 - 2000 km s^{-1}, from narrow and broad components, we get $\dot{M}$ = 0.02 - 0.08 M$_\odot$ yr^{-1}, which is a lower limit because in general $\psi < 1$. Such large $\dot{M}$ results from the fact that L is large but v is small. For SN 2005kd, the estimated ejecta mass is M_{ej} = 6 M$_\odot$ if we take $E = 10^{51}$ erg.

Table 4.5: Journal of Radio Observations of SN 2005kd.

Date	*Phase	frequency	Flux	RMS	SN 1995N	
	(days)	(MHz)	density (mJy)	Noise (μJy)	phase(d)	flux (mJy)
2007 Nov 16	700	1400	3.3 ± 0.6	200	689	4.37
2008 Feb 25	800	1400	4.0 ± 0.5	150	845	4.26
2008 Oct 31	1050	1280	3.7 ± 0.4	125	936	4.50
2010 Jan 26	1500	1280	4.2 ± 0.5	175	1440	5.21

*Relative to the epoch of discovery (JD = 2453687).

If a higher value of the kinetic energy is used, a larger ejecta mass is obtained. On the otherhand, decreasing ψ leads to a higher wind density and mass-loss rate (and to a larger mass lost in the wind), but it also leads to a smaller ejecta mass through Eq. 4.1.

Kiewe et al. (2010) derived the progenitor star wind velocities and pre-explosion mass loss rates for a considerable sample of SN Type IIn supernovae. The wind velocities range over 600 - 1400 km s^{-1} and the mass loss rates range over 0.026 - 0.12 $M_{\odot}$ yr^{-1}, assuming intermediate velocities of Hα as a velocity of the shock. In the case of SN 2005kd, it is assumed that the broad component of Hα represents the shock velocity.

4.2.5 Radio observations of SN 2005kd

Radio observations of SN 2005kd were carried out with GMRT (Swarup et. al. 1991) in full array configuration mode (all 30 antennas were used in the observations) at 1280 MHz or 1420 MHz with 16 MHz bandwidth. The detailed journal of radio observations is given in Table 4.5. The target source was observed for 30 min followed by 4 - 5 min observation on phase calibrator 0410+769 of 5 Jy in each scan and the same set was repeated through out the observing time slot. The flux calibrator (either 3C48 or 3C147) was observed before and after the observation for 10 - 20 min. The radio contour map of supernova is shown in Figure 4.13 along with the optical image. As can be seen in the figure, the peak of radio flux coincide with the optical position of the supernova.

The estimated flux densities for SN 2005kd are given in Table 4.5, and compared with those of SN 1995N (Chandra et al. 2009) at similar epochs. The light curve is shown in the Figure 4.14 along with that of SN 1995N. The evolution of SN 2005kd is very similar to SN 1995N. A useful way to characterize the radio emission from SNe is by considering their peak radio luminosity and the time of the peak; the more luminous Type II SNe peak at a later time, the more the dense circumstellar medium (Chevalier 2006). The observed data points of SN 2005kd is so sparse that we are unable to estimate the peak and the time of peak. However, comparing with SN 1995N, it appears that the radio flux is around

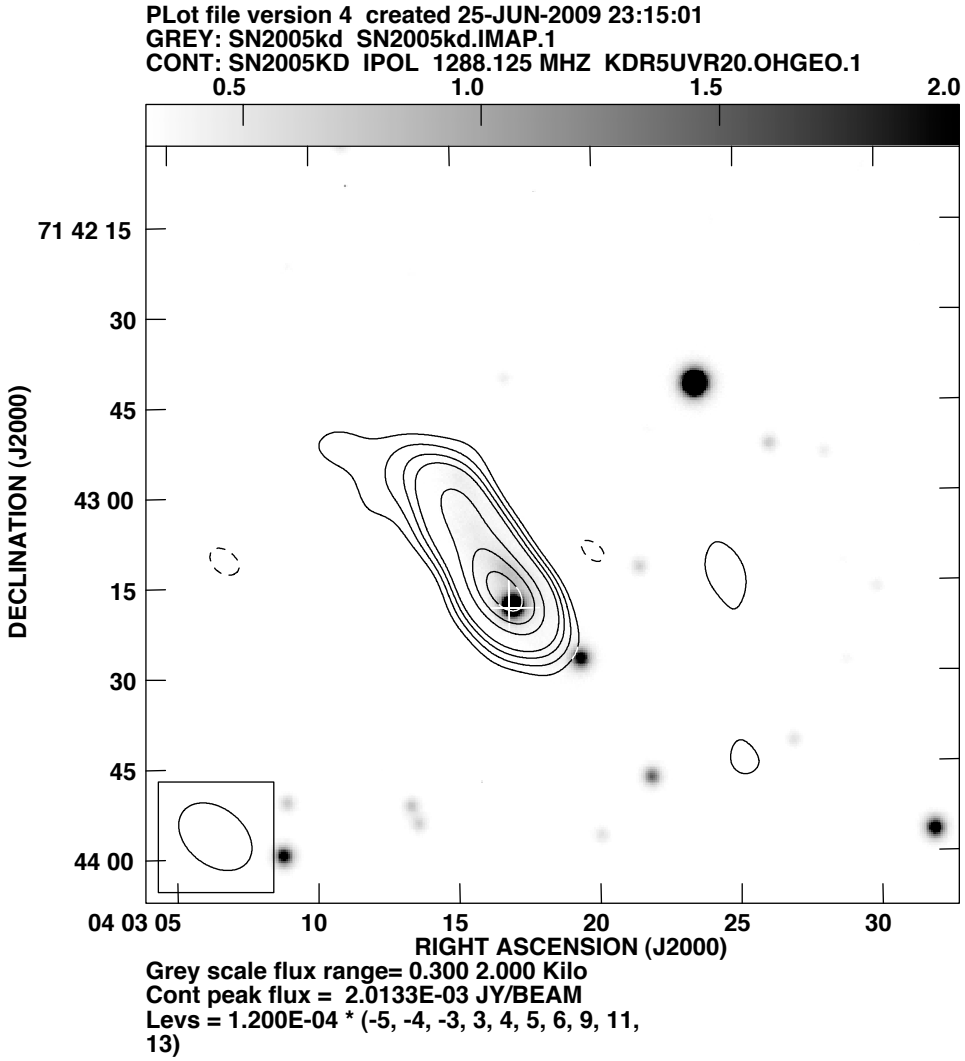

Figure 4.13: SN counter map of radio emission on top of the optical image. The peak of radio flux coincide with the optical position of the supernova.

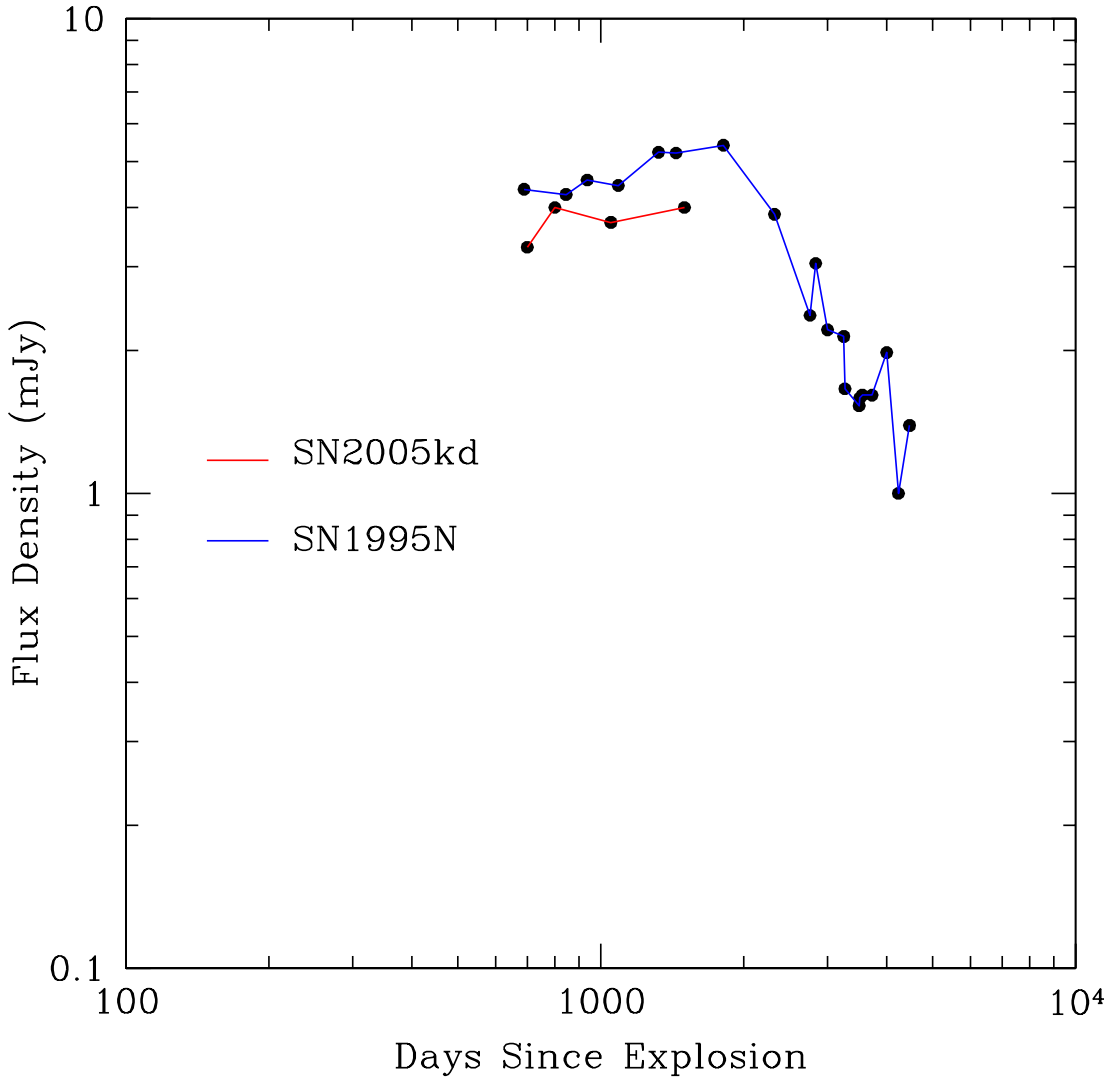

Figure 4.14: SN2005kd radio light curve (black) evolution in 1.4 GHz plotted along with SN 1995N (blue). SN 1995N data are taken from Chandra et al. (2009))

maximum. Clearly, further observations, over a much longer period of time are required before any conclusions can be drawn based on radio fluxes, and further radio observations are planned.

4.3 Summary

Here, we present photometric and spectroscopic studies of supernova Type IIn SN 2005kd. It is unique among these kind of objects by having a plateau for almost 120 days. The narrow emission lines indicate circumstellar material, that is a result of mass loss of the progenitor. We have derived the mass loss rate of the progenitor to be 0.02 - 0.08 $M_{\odot}\ yr^{-1}$. We have also detected and observed SN 2005kd in radio wavelength and compared the flux densities with that of similar kind of object SN 1995N. Further observations in radio regime are planned in future to get the critical parameters like the peak luminosity and the time of the peak to derive the physical parameters of the supernova.

CHAPTER 5

STRIPPED-ENVELOPE CORE COLLAPSE SUPERNOVAE

5.1 Introduction

Supernova Type Ib/c are basically classified spectroscopically by the absence of deep Si 6150Å absorption when compared to type Ia spernovae. These SNe are again categorized spectroscopically as types Ib and Ic by the presence of helium, i.e Type Ib are helium rich and Type Ic are helium poor SNe. For the first time, in their study, Wheeler & Levreault (1985) concluded that the explosion mechanism might be more closely related to that of SNe II than to SN Ia. The other characteristics of this type are (a) preference for galaxies having Hubble types Sbc or later, (b) proximity to H II regions, (c) rather low luminosity, typically 1.5 mag fainter than classical SNe I (d) distinct IR light curves having no secondary maximum around one month past primary maximum (e) reddish colors, and (f) emission of radio waves within a year past maximum.

The progenitors of Type Ib and Ic SNe have been proposed to be massive WR stars (Smartt 2009), as these are massive evolved stars that have shed most, if not all, of their H envelope. An alternative scenario is that the Ibc SNe progenitors are stars of much lower initial mass in close binaries that have had their envelopes stripped through interaction (e.g. SN1993j, Smartt 2009). Hence the Type Ib/c supernovae are commonly referred to as the stripped envelope Core Collapse Supernovae (CCSNe).

Wolf-Rayet stars, i.e., massive stars that have been stripped off their outer hydrogen and/or helium layers due to mass loss during the course of their evolution, are believed to be the progenitors of the stripped-envelope CCSNe (IIb, Ib, Ic). The possibility of yet another class of stripped-envelope CCSNe emerged with the detection of moderately nar-

row helium emission lines in SN 1999cq (Matheson et al. 2000), similar to the presence of narrow hydrogen lines in type IIn. Matheson et al. (2000) suggested an interaction of the supernova ejecta with a dense CSM that had little or no hydrogen. SN 2002ao (Martin et al. 2002, Filippenko & Chornock 2002) was identified to be similar to SN 1999cq. The recent discovery of SN 2006jc with strong, moderately narrow helium emission lines, and weak hydrogen lines has added to the list of this new, interesting class of CCSNe, now designated as Type Ibn (Pastorello et al. 2008a).

Broad-line Type Ic supernovae (SNe Ic) are a subclass of core collapse SNe Type Ic that have broad features in their spectra, indicating unusually high expansion velocities reaching close to $0.1c$ at early times. Only a few candidates of this class are known. Some broad-line SNe Type Ic are associated with Gamma Ray Bursts (GRBs) (Galama et al. 1998; Matheson et al. 2003; Malesani et al. 2004, or X-Ray Flash (XRF) (Pian et al. 2006; Modjaz et al. 2006), while some others do not show any clear evidence of being associated with a GRB or an XRF (Kinugasa et al. 2002; Foley et al. 2003; Valenti et al. 2008).

The broad-line SNe Type Ic exhibit diversity in terms of the explosion energy, ejecta mass and mass of ^{56}Ni produced during the explosion. The photometric and spectral features of SN 1998bw are explained with $\sim 10M_{\odot}$ ejected with a kinetic energy $2 - 5{\times}10^{52}$ ergs, producing $0.4 - 0.5M_{\odot}$ of ^{56}Ni in the explosion (Iwamoto et al. 1998; Nakamura et al. 2001; Maeda et al. 2006, Tanaka et al. 2007). On the other hand, modelling of nebular spectra of SN 2002ap indicates an ejected mass of $\sim 2.5\ M_{\odot}$ with a kinetic energy $\sim 4{\times}10^{51}$ ergs and production of $\sim 0.1M_{\odot}$ of ^{56}Ni (Mazzali et al. 2007), showing a large range in the physical parameters of broad-line SNe Type Ic. Among these, SNe with kinetic energy $E_{\rm K} > 10^{52}$ ergs are termed as "hypernovae (HNe)" (Iwamoto et al. 1998). The broad-line SNe that are not associated with GRBs are found to have smaller values of ejecta mass, explosion energy and lower luminosity as compared to the GRB-associated HNe (Nomoto et al. 2007).

The presence of hydrogen in Type Ib supernovae remains to be an open issue for investigation. There are some Type Ib events which show a deep absorption at $\sim$ 6200 Å in their early spectra, which could be attributed to Hα (Branch et al. 2002, Anupama et al. 2005, Soderberg et al. 2008), whereas some others show a shoulder in the red wing of the [O I] 6300-6364 Å line in their nebular spectra, due to Hα (Sollerman et al. 1998, Stritzinger et al. 2009). Using the SYNOW code, Elmhamdi et al. (2006) have shown the presence of a thin layer of hydrogen ejected at high velocity in almost all the SNe Type Ib in their sample.

Late phase observations of stripped envelope CCSNe have gained special importance as these phases probe deeper into the core of the expanding stars. The nebular spectrum originating from an optically thin ejecta provides important clues to the nature of progenitor star and the explosion mechanism. Asphericity in the explosion of stripped envelope supernovae is confirmed by a higher degree of polarization through spectropolametric studies of these objects during early phases (Leonard et al. 2006). An independent indication of the asphericity in the explosion comes from the asymmetric profile of [O I] 6300-6364 Å line (Mazzali et al. 2001, Maeda et al. 2002).

We discuss in this chapter the observational properties of the stripped envelope core-collapse supernovae through the studies of three diverse examples, the type Ibn SN2006jc, broad lined type Ic SN2007ru and the Type Ib SN2009jf.

5.2 SN2006jc: Type Ib supernova

5.2.1 Introduction

Supernova SN 2006jc was discovered by K. Itagaki, at a magnitude of 13.8, on 2006 October 9.75 UT on an unfiltered image (Nakano et al. 2006). The non-detection of this object on an image obtained on 2006 September 22 suggests the supernova was discovered shortly after explosion. Based on the presence of strong helium features in the early spectra, the event was classified to be of Type Ib (Fesen et al. 2006, Crotts et al. 2006). The similarity of SN 2006jc with SNe 1999cq and 2002ao was first noted by Benetti et al. (2006). The identification chart of SN 2006jc is shown in Figure 5.1.

Multiwavelength observations of this supernova have shown it to be unique in many respects. Early *Swift* UVOT observations on 2006 October 13 by Brown et al. (2006) indicate extremely blue UV-V colours. X-ray emission has also been observed by the *Swift* (X-Ray Telescope) and the *Chandra* satellites (Immler et al. 2008). On the contrary, SN 2006jc was not detected in the early-time radio observation (Soderberg 2006).

Photometric monitoring of SN 2006jc in the $UBVR$ and I bands began on 2006 October 16 (JD 2454025.45) and continued until 2007 January 13 (JD 2454114.40), using the Himalaya Faint Object Spectrograph Camera (HFOSC). Photometric standard fields (Landolt 1992) PG0231+051 and PG0942-029 were observed on 2006 November 23 and the fields PG1047+003, PG0942-029 and PG1323-086 were observed on 2006 December 27 under photometric conditions. These were used to calibrate a sequence of secondary standards in the supernova field. The secondary standard stars magnitudes are given in Table 5.1.

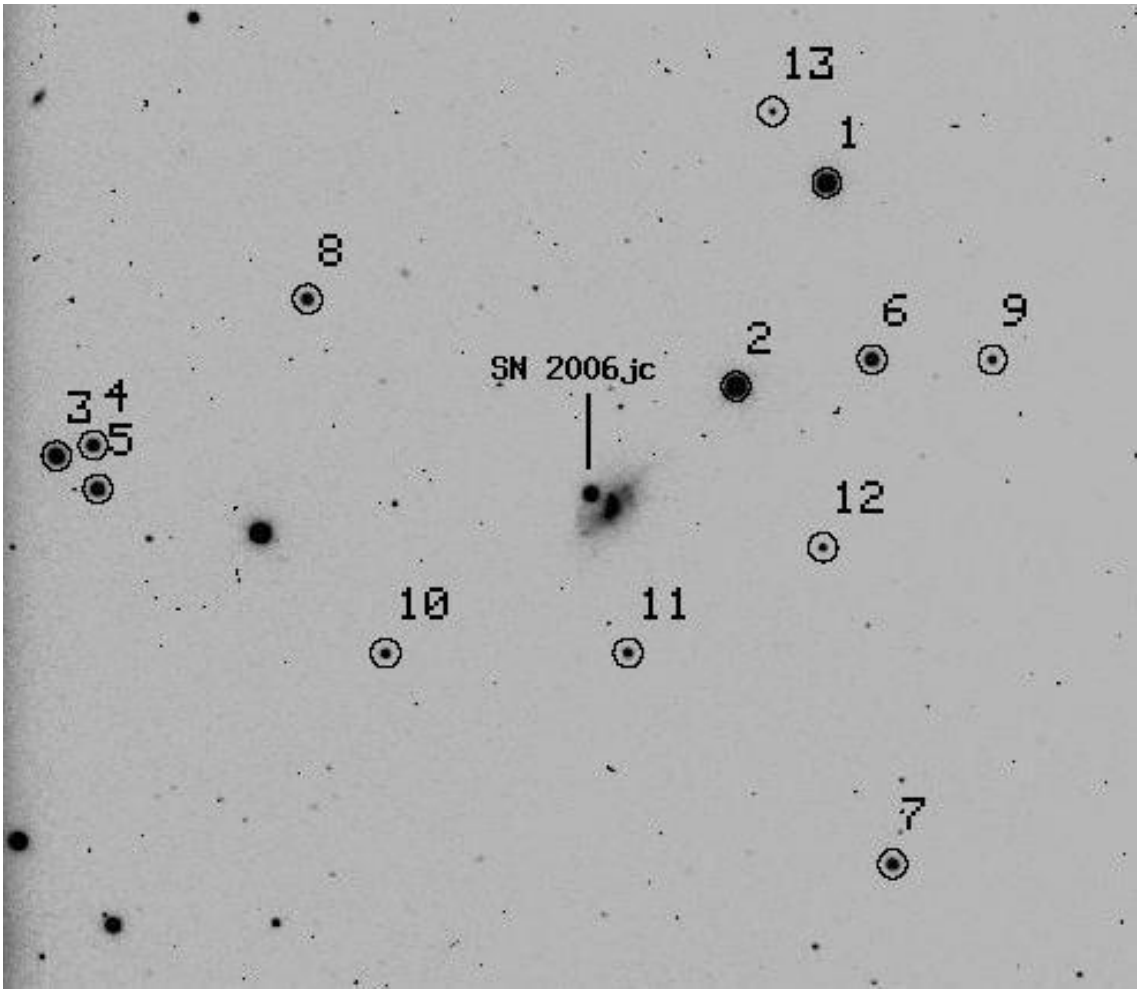

Figure 5.1: The field of SN 2006jc. Stars used as secondary standards and listed in Table 1 are marked.

Spectroscopic monitoring of SN 2006jc began on 2006 October 14 (JD 2454023.47) and continued until 2006 Dec 14 (JD 2454084.35). The log of spectroscopic observations is given in Table 5.2.

5.2.2 Light curves

The *UBVRI* magnitudes of SN 2006jc are tabulated in Table 5.3 and plotted in Figure 5.2. Figure 5.3 shows the light curves of SN 2006jc compared with the light curves of a few SNe Ib/c, namely, SN 1999ex (Ib/c) ($JD_{max,B}$ = 245 1498.1: Stritzinger et al. 2002), SN 1994I (Ic) ($JD_{max,B}$ = 244 9450.56: Richmond et al. 1996), SN 1990I (Ib) (JD_{max} = 244 8010: Elmhamdi et al. 2004) and SN 1990B (Ic) ($JD_{max,B}$ = 244 7909.0: Clocchiatti

Table 5.1: Magnitudes for the sequence of secondary standard stars in the field of SN 2006jc. The stars are identified in Figure 5.1.

ID	U	B	V	R	I
1	13.636 ± 0.020	13.482 ± 0.005	12.884 ± 0.010	12.537 ± 0.031	12.156 ± 0.015
2	13.005 ± 0.020	13.167 ± 0.005	12.795 ± 0.011	12.528 ± 0.020	12.202 ± 0.020
3	14.663 ± 0.030	14.280 ± 0.005	13.534 ± 0.013	13.175 ± 0.029	12.699 ± 0.053
4	15.511 ± 0.050	15.376 ± 0.005	14.749 ± 0.011	14.397 ± 0.006	14.030 ± 0.050
5	15.084 ± 0.030	14.966 ± 0.005	14.307 ± 0.010	13.937 ± 0.008	13.543 ± 0.004
6	15.142 ± 0.030	15.100 ± 0.011	14.503 ± 0.005	14.102 ± 0.003	13.722 ± 0.010
7	16.140 ± 0.037	15.742 ± 0.012	14.994 ± 0.005	14.553 ± 0.005	14.145 ± 0.005
8	16.068 ± 0.033	15.614 ± 0.005	14.739 ± 0.008	14.246 ± 0.003	13.754 ± 0.013
9	17.974 ± 0.041	17.163 ± 0.020	16.240 ± 0.006	15.712 ± 0.005	15.277 ± 0.014
10	16.862 ± 0.046	16.695 ± 0.010	16.055 ± 0.005	15.661 ± 0.005	15.255 ± 0.006
11	16.590 ± 0.032	16.705 ± 0.016	16.207 ± 0.005	15.860 ± 0.005	15.519 ± 0.015
12	18.332 ± 0.058	17.462 ± 0.013	16.545 ± 0.016	16.005 ± 0.007	15.549 ± 0.031
13	19.724 ± 0.070	18.189 ± 0.008	16.912 ± 0.023	16.127 ± 0.007	15.472 ± 0.028

The errors quoted are the statistical errors associated with the magnitudes.

et al. 2001, and the type IIn SN 1998S ($JD_{max,R}$ = 245 0890.0: Fassia et al. 2000. The early decline ($\sim 10-25$ days; JD(max)=2454016*: Pastorello et al. 2007) in the U and B bands is similar to SN 1999ex, while the decline is very similar to SN 1994I in the VRI bands. The R band light curve of SN 2006jc shows a decline during days $\sim 10-20$ which is slower compared with that of the Type Ibn SN 1999cq (Matheson et al. 2000). Between days 30 - 50, a flattening is seen in all the bands, and the decline rate appears very similar to SN 1990B and SN 1990I. However, beyond day 50, SN 2006jc behaves in a quite different manner compared to the other SNe. A sharp decline is seen in all the bands, with the decline being the steepest in the U and B bands.

The $U-B$, $B-V$, $V-R$ and $V-I$ colours of SN 2006jc, reddening corrected using $E(B-V) = 0.05$ (Pastorello et al. 2007) are shown in Figure 5.4. Also shown in the Figure are the colours for SN 1999ex, SN 1994I, SN 1990I, SN 1990B and SN 1998S reddening corrected using $E(B-V)$ values 0.30 (Stritzinger et al. 2002), 0.45 (Richmond et al. 1996), 0.13 (Elmhamdi et al. 2004) , 0.85 (Clocchiatti et al. 2001) and 0.22 (Fassia et al. 2000), respectively. The $U-B$, $B-V$, $V-R$ and $V-I$ colour curves show very little colour evolution until $\sim$ day 60. SN 2006jc had significantly bluer $U-B$, $B-V$ and $V-R$ colours compared to other supernovae, while the $V-I$ colour is similar to other SNe. A

*Comparing the early spectra of SN 2006jc with those of the Type Ibn SN 2000er, Pastorello et al. (2008b) suggest that SN 2006jc was discovered $\sim$ 10 days after maximum light, estimated to have occured on JD 2450008 ± 15. Since the uncertainity in the estimated epoch of maximum is quite large, we choose to follow the epoch estimated by Pastorello et al. (2007)

Table 5.2: Log of spectroscopic observations of SN 2006jc

Date	J.D. 2450000+	Phase* (days)	Resln Å	Range Å
2006 Oct 14	4023.47	7.5	7	3500-7800; 5200-9250
2006 Oct 16	4025.49	9.5	7	3500-7800; 5200-9250
2006 Oct 17	4026.44	10.5	7	3500-7800; 5200-9250
2006 Oct 20	4029.49	13.5	7	3500-7800; 5200-9250
2006 Oct 23	4032.46	16.5	7	3500-7800; 5200-9250
2006 Oct 24	4033.43	17.5	7	3500-7800; 5200-9250
2006 Oct 29	4038.45	22.5	7	3500-7800; 5200-9250
2006 Oct 30	4039.48	23.5	7	3500-7800; 5200-9250
2006 Nov 01	4041.48	25.5	7	3500-7800; 5200-9250
2006 Nov 05	4045.37	29.4	7	3500-7800; 5200-9250
2006 Nov 07	4047.42	31.4	7	3500-7800; 5200-9250
2006 Nov 14	4054.45	37.5	9	3500-7800
2006 Nov 16	4055.51	39.5	7	3500-7800; 5200-9250
2006 Nov 18	4058.41	42.4	7	3500-7800; 5200-9250
2006 Nov 23	4063.34	47.3	7	3500-7800; 5200-9250
2006 Dec 14	4084.35	68.4	9	3500-7800

* With respect to date of maximum, assumed to be JD 2454016 (Pastorello et al. 2007)

dramatic change in all the colours is seen beyond day 60. SN 2006jc begins to get redder, by ~ 0.5 mag. Maximum change is seen in $V-I$ colour, which changes by almost 1 mag by day 100. The reddening of colours observed in SN 2006jc at later phases is not seen in other SNe, except in the case of the IIn SN 1998S.

The sudden decline in the *UBVRI* light curves, coincident with the increase in the luminosities in the near-IR region (Arkharov et al. 2006), with a reddening of the colours are quite similar to the behaviour of dust forming novae (e.g. Gehrz 1988) and a clear indication of the formation of hot dust.

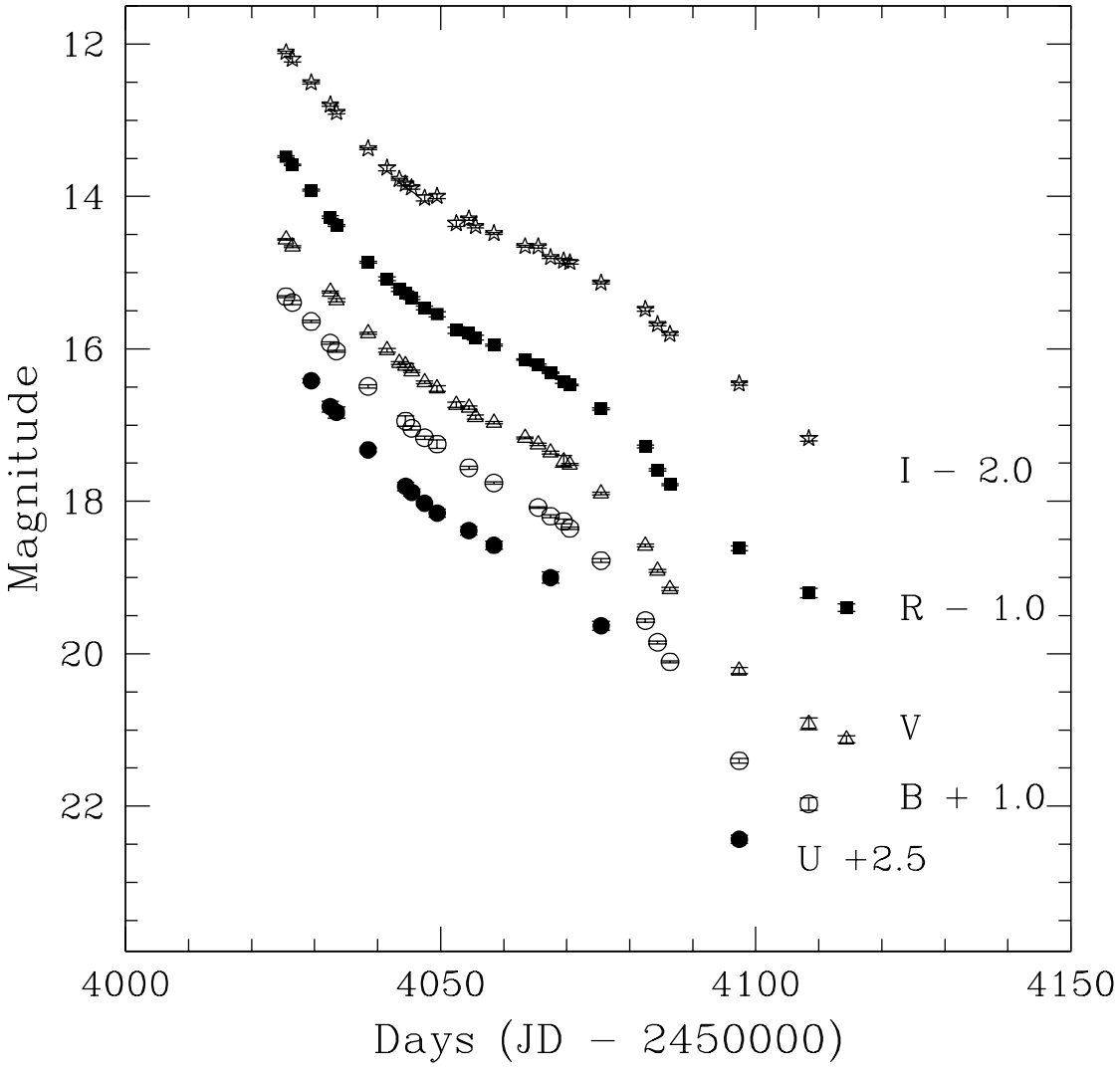

Figure 5.2: *UBVRI* light curves of SN 2006jc obtained with the HCT.

Table 5.3: Photometric observations of SN 2006jc.

Date	J.D. 2450000+	Phase* (days)	U	B	V	R	I
2006 Oct 16	4025.45	9.45		14.314 ± 0.014	14.563 ± 0.011	14.480 ± 0.013	14.107 ± 0.015
2006 Oct 17	4026.49	10.49		14.392 ± 0.026	14.659 ± 0.013	14.587 ± 0.010	14.200 ± 0.037
2006 Oct 20	4029.46	13.46	13.918 ± 0.027	14.641 ± 0.015		14.918 ± 0.013	14.508 ± 0.015
2006 Oct 23	4032.48	16.48	14.256 ± 0.070	14.925 ± 0.016	15.252 ± 0.011	15.271 ± 0.017	14.799 ± 0.018
2006 Oct 24	4033.48	17.48	14.333 ± 0.074	15.030 ± 0.012	15.360 ± 0.023	15.379 ± 0.012	14.897 ± 0.022
2006 Oct 29	4038.49	22.49	14.824 ± 0.025	15.493 ± 0.020	15.794 ± 0.013	15.864 ± 0.012	15.373 ± 0.015
2006 Nov 01	4041.49	25.49			16.018 ± 0.023	16.079 ± 0.026	15.626 ± 0.036
2006 Nov 03	4043.46	27.46			16.187 ± 0.017	16.220 ± 0.026	15.774 ± 0.014
2006 Nov 04	4044.44	28.44	15.304 ± 0.056	15.947 ± 0.069	16.218 ± 0.026	16.265 ± 0.025	15.836 ± 0.026
2006 Nov 05	4045.41	29.41	15.381 ± 0.047	16.041 ± 0.025	16.294 ± 0.017	16.334 ± 0.019	15.883 ± 0.021
2006 Nov 07	4047.45	31.45	15.524 ± 0.028	16.167 ± 0.022	16.438 ± 0.017	16.465 ± 0.025	16.019 ± 0.038
2006 Nov 09	4049.44	33.44	15.654 ± 0.051	16.249 ± 0.055	16.520 ± 0.035	16.545 ± 0.033	15.996 ± 0.030
2006 Nov 12	4052.49	36.49			16.732 ± 0.036	16.756 ± 0.043	16.353 ± 0.040
2006 Nov 14	4054.48	38.48	15.885 ± 0.055	16.559 ± 0.021	16.771 ± 0.020	16.794 ± 0.017	16.295 ± 0.017
2006 Nov 15	4055.52	39.52			16.894 ± 0.025	16.853 ± 0.029	16.392 ± 0.020
2006 Nov 18	4058.46	42.46	16.078 ± 0.053	16.760 ± 0.017	16.969 ± 0.015	16.950 ± 0.011	16.484 ± 0.013
2006 Nov 23	4063.38	47.38			17.168 ± 0.010	17.140 ± 0.010	16.655 ± 0.013
2006 Nov 25	4065.47	49.47		17.079 ± 0.010	17.254 ± 0.016	17.214 ± 0.014	16.658 ± 0.017
2006 Nov 27	4067.44	51.44	18.472 ± 0.074	17.195 ± 0.019	17.360 ± 0.017	17.312 ± 0.011	16.800 ± 0.015
2006 Nov 29	4069.51	53.51		17.263 ± 0.029	17.474 ± 0.078	17.429 ± 0.025	16.844 ± 0.031
2006 Nov 30	4070.50	54.50		17.355 ± 0.015	17.517 ± 0.012	17.473 ± 0.011	16.865 ± 0.024
2006 Dec 05	4075.45	59.45	17.132 ± 0.061	17.777 ± 0.024	17.898 ± 0.016	17.788 ± 0.013	17.133 ± 0.017
2006 Dec 12	4082.49	66.49		18.565 ± 0.021	18.580 ± 0.020	18.281 ± 0.019	17.482 ± 0.026
2006 Dec 14	4084.42	68.42		18.850 ± 0.019	18.912 ± 0.021	18.587 ± 0.014	17.680 ± 0.017
2006 Dec 16	4086.39	70.39		19.106 ± 0.014	19.150 ± 0.020	18.780 ± 0.014	17.805 ± 0.019
2006 Dec 27	4097.38	81.38	19.935 ± 0.052	20.404 ± 0.033	20.220 ± 0.039	19.617 ± 0.030	18.458 ± 0.021
2007 Jan 07	4108.42	92.42		20.971 ± 0.082	20.920 ± 0.077	20.202 ± 0.064	19.173 ± 0.036
2007 Jan 13	4114.40	98.40			21.122 ± 0.046	20.394 ± 0.050	

* With respect to date of maximum, assumed to be JD 2454016.
The errors quoted are the statistical errors associated with the magnitudes.

The optical 'quasi-bolometric' light curve is constructed using the *UBVRI* magnitudes presented here, and those published by Pastorello et al. (2007). Assuming a distance of 25.8 Mpc and a reddening of $E(B-V) = 0.05$ (Pastorello et al. 2007), the observed *UBVRI* magnitudes were converted to monochromatic fluxes and integrated over the observed wavelength range to obtain the optical quasi-bolometric light curve. Likewise, combining the NIR magnitudes (Arkharov et al. 2006, Di Carlo et al. 2008, Mattila et al. 2008) with the UBVRI magnitudes, the optical+NIR (*uvoir*) bolometric light curve was constructed integrating over the *U* to *K* bands (see also Pastorello et al. 2007, Mattila et al. 2008, Di Carlo et al. 2008, Tominaga et al. 2008). Figure 5.5 shows the optical 'quasi-bolometric' light curve as well as the *uvoir* bolometric light curve. Also shown in the Figure 5.5 are the bolometric light curves of type Ib/c SNe 1990I, 1994I and 1999ex and the type IIn SN 1998S. It is evident from the plot that SN 2006jc has a luminosity that is higher than that of other Type Ib/c SNe, while it is about 1.6 magnitudes fainter than the Type IIn SN 1998S.

The optical luminosity of SN 2006jc indicates an early decline rate of 0.092 mag day^{-1} until $\sim$ 30 days since maximum. A flattening is seen in the light curve during $\sim 30-50$ days after maximum, with the decline rate during this period being 0.047 mag day^{-1}. The onset of dust formation is marked by a sharp decline in the optical luminosity, with a decline rate of 0.084 mag day^{-1} during $\sim 50-100$ days after maximum. In contrast to the optical luminosity, the *uvoir* bolometric luminosity shows a flat decline, with a decline rate of 0.026 mag day^{-1} beyond day 35. A comparison with the bolometric light curves of other SNe indicates that the bolometric light curve decline of SN 2006jc is not too different from other normal SNe Type Ib/c. The early decline lies between the rapidly declining SN 1994I (0.106 mag day^{-1}) and the slower SN 1999ex (0.076 mag day^{-1}), while the *uvoir* decline rate at later phases is similar to SN 1994I (0.029 mag day^{-1}).

5.2.3 The spectrum and its evolution

The spectrum of SN 2006jc and its evolution during the phase +7 to +68 days since the estimated maximum on JD 2454016 is presented in Figures 5.6 and 5.8. These spectra provide a fairly dense coverage of the early-time spectral evolution of SN 2006jc and are complementary in phase to those presented by Foley et al. (2007), Smith et al. (2008) and Pastorello et al. (2007, 2008). The spectrum is peculiar and different from that of normal Type Ib/c supernovae (Matheson et al. 2001, Branch et al. 2002). The photospheric P-Cygni profiles that are typically found in the early spectra of Type Ib/c supernovae are absent, and the spectrum is characterized by (a) a steep, blue continuum shortward of

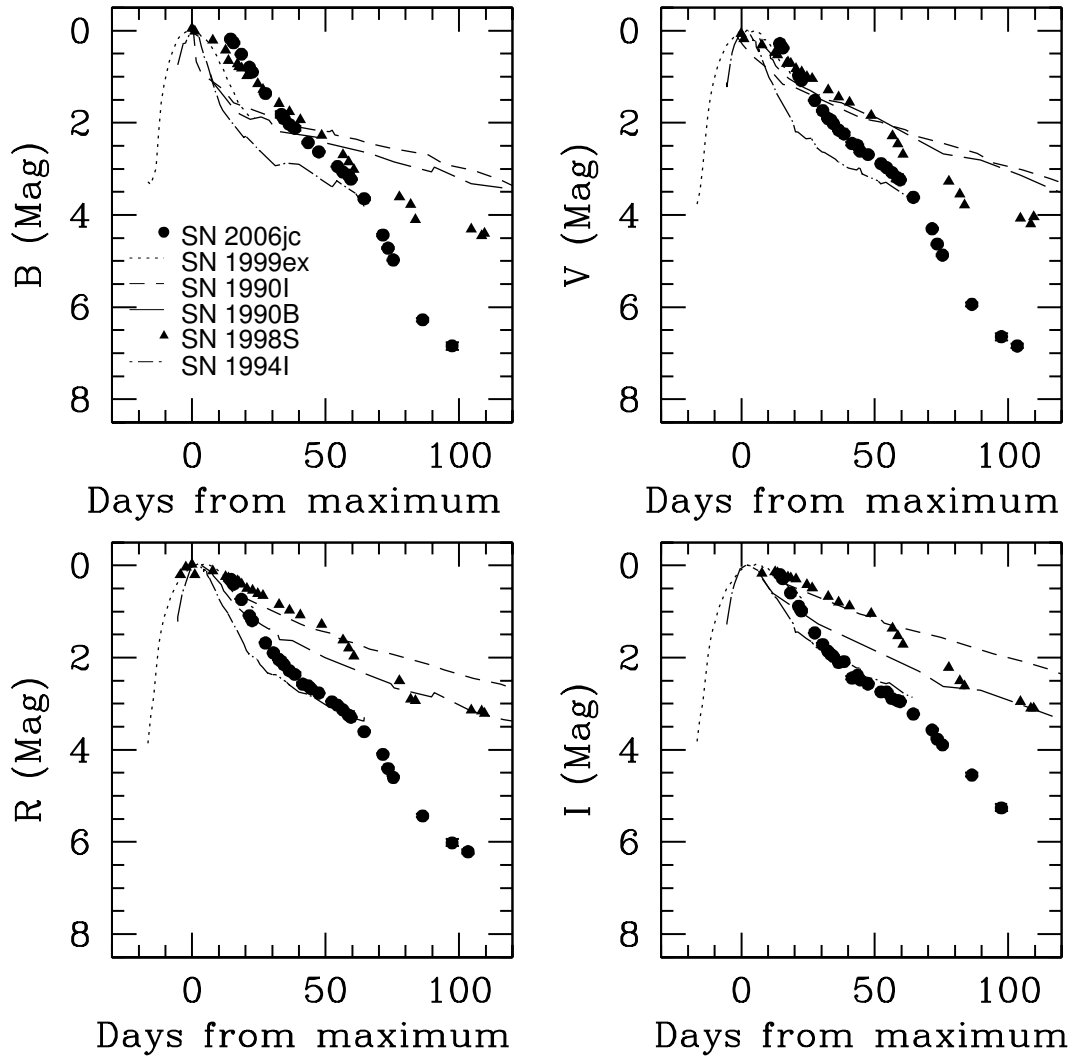

Figure 5.3: Comparison of the *BVRI* light curves with SNe 1999ex (Ib/c), SN 1994I (Ic), SN 1990I (Ib), SN 1990B (Ic), and SN 1998S (IIn). The magnitudes of SN 2006jc are normalized with respect to those on JD 454021.7 (B = 14.13, V = 14.28, R = 14.18 and I = 13.91: Pastorello et al. 2007), while the magnitudes of other SNe are normalized with respect to the magnitudes at their respective maximum (see text).

$\sim$ 5500 Å and (b) dominant moderately narrow helium emission lines.

Broad emission features, due to the expanding supernova material are also seen at $\sim$ $\lambda\lambda$ 3850, 4121, 5950, 6348, 7800, 8214 and 8500 Å. The features at $\lambda\lambda$ 3850, 5950, 7800 and 8214 Å are identified with Mg II 3848, 3850, 5938, 5943, 7790, 7877 Å, and 8214, 8234 Å respectively. The feature at λ 6348 Å is identified with Si II λ 6355 Å,

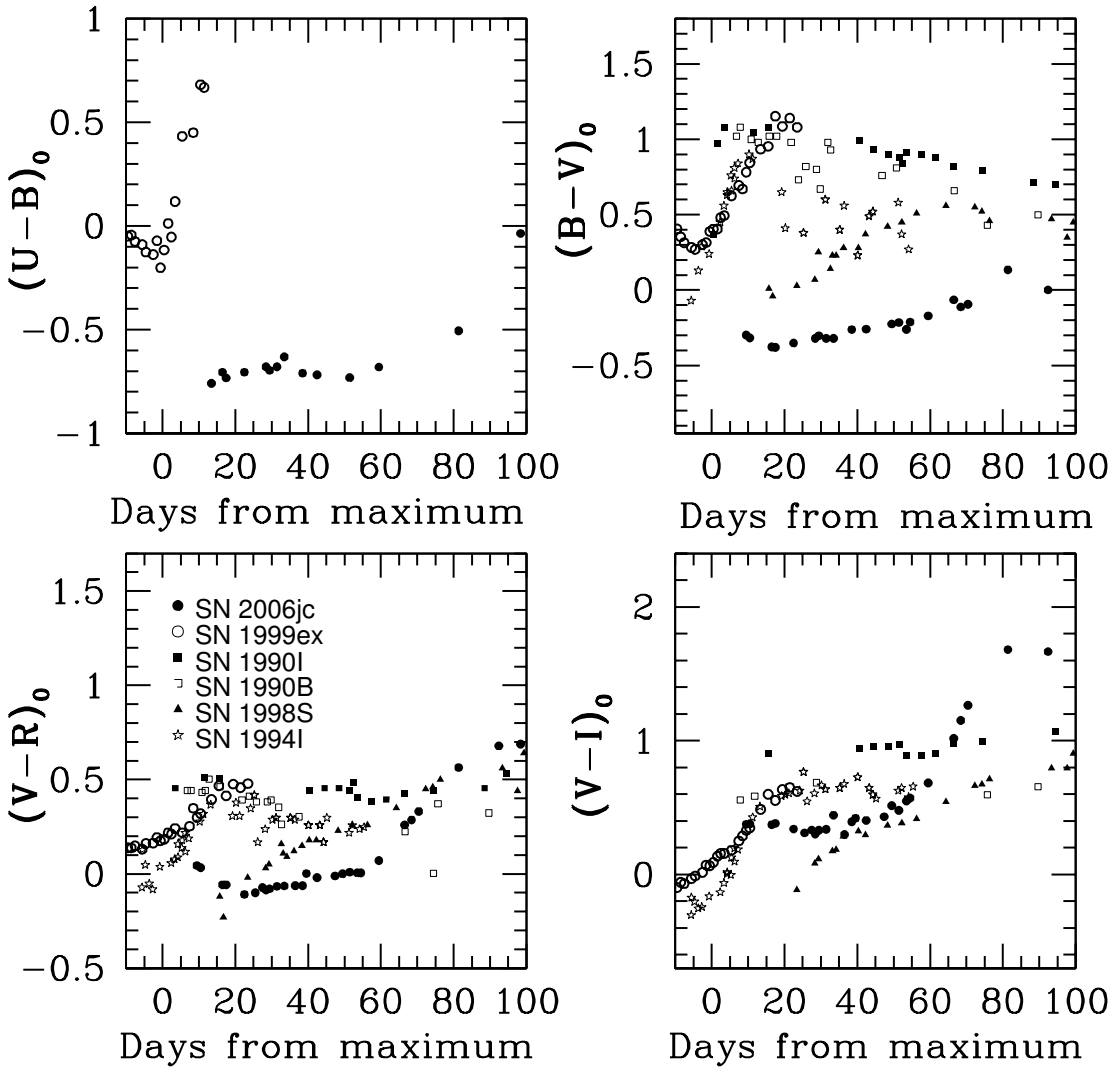

Figure 5.4: Reddening corrected $U-B$, $B-V$, $V-R$ and $R-I$ colour curves of SN 2006jc compared with other type Ib, Ic and IIn supernovae.

probably blended with Mg II 6346 Å, and the feature are 4121 Å could be due to Si II 4128, 4131 Å. Si II $\lambda\lambda$ 5041, 5056 Å could also be present. O I 7774 Å is also present, blended with Mg II. The feature at λ 8500 Å is due to Ca II infrared triplet. Mg II λ 4481 Å could be blended with He I λ 4471 Å. The full width at half maximum of the broad features indicate a velocity of $\sim 5000-6000$ km s^{-1}. The strength of the Mg II and Si II features decrease with time, while that of the Ca II IR triplet and O I 7774 Å increase with time. Fe II features appear to develop in the λ 4500-5500 Å region, around 10 days after B maximum. The O I 7774 Å line shows a sharp P-Cygni absorption during the early

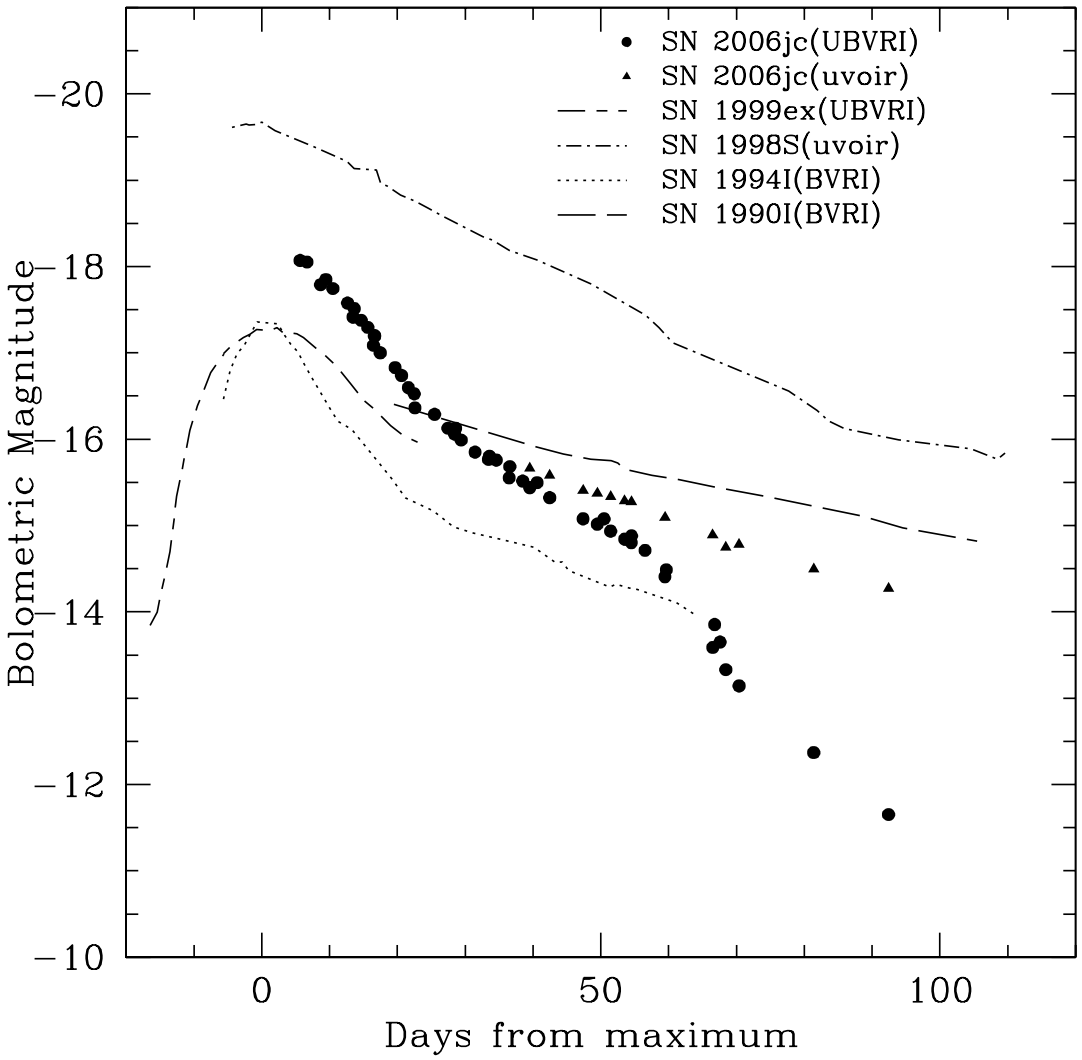

Figure 5.5: The optical 'quasi-bolometric' and the *uvoir* bolometric light curves of SN 2006jc. Also shown in the figure are the *UBVRI* bolometric light curves of the Type Ib/c SN 1999ex and SN 1994I and the *uvoir* bolometric light curve of the Type IIn SN 1998S.

phases, with the absorption minimum indicating a velocity of ~ 620 km s^{-1} (Figure 5.7).

The He I line widths indicate a velocity of $\sim 2200 - 3000$ km s^{-1}. As noted by Foley et al. (2007), a narrow P Cygni component is noticed in the He I 3889 Å line, at a velocity of ~ 620 km s^{-1}. A similar component could be present in the 4471 Å line also, at ~ 670 km s^{-1}. It is interesting to note that the velocity of the narrow P Cygni absorption seen in the O II λ 7774 Å line is very similar to the velocity of this component.

The line profiles of the strongest He I lines at $\lambda\lambda$ 5876, 6678 and 7065 Å are shown in

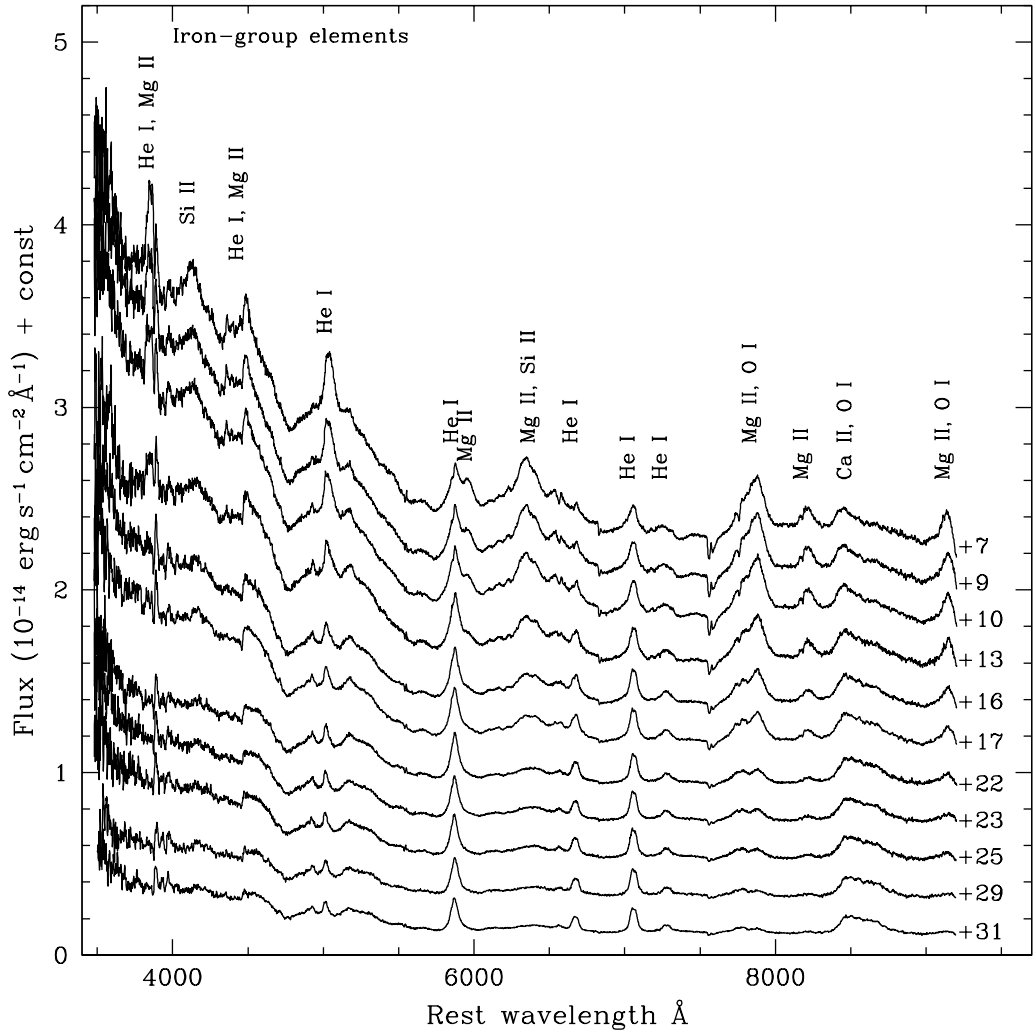

Figure 5.6: Spectroscopic evolution of SN 2006jc during +7–+31 days since maximum on JD 2454016. Note the fading of the broad features, the evolution of Fe II lines in the 4500–5500 Å region, and the development of Hα line from an absorption feature into an emission feature.

Figure 5.9. From the figure, it appears that He I λ 5876 Å may have a contribution from the fast moving supernova material. A broad component could be present in the λ 5876 Å profile in the spectra of days 3, 5, 6 and 9. A simple de-blending of the components, assuming a simple Gaussian profile for both components, indicates the broad component has a velocity $\sim$ 5000 km s^{-1}, similar to the supernova features. The broad component fades with time, in accordance with the evolution of the Mg II and Si II features from the

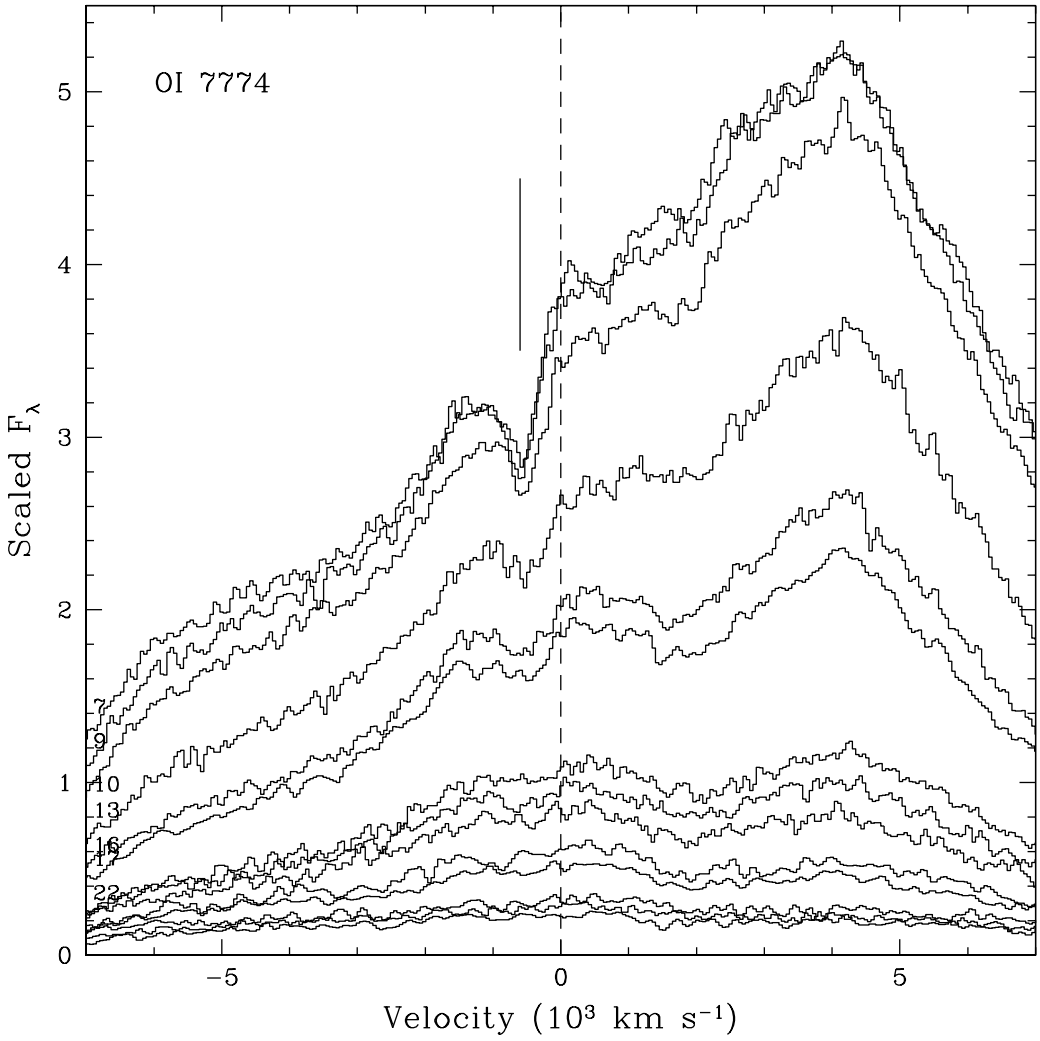

Figure 5.7: The O I 7774 Å line profile. Note the sharp absorption at $\sim$ 620 km s^{-1} (marked by the short vertical line) on days 7, 9 and 10, and its subsequent fading.

supernova material. Pastorello et al (2008) note the presence of helium in the fast moving supernova ejecta in the early phase spectra of SN 2000er which has been found to be very similar to SN 2006jc. This broad feature could also be due to Na I 5893 Å (Pastorello et al. 2007). The peak of the moderately narrow λ 5876 Å component shifts blueward around day 10, and the line profile begins to show asymmetry that is clearly seen by day 20. A similar shift in the peak and asymmetry is seen in the λ 6678 Å line also, while the peak is blueshifted in the λ 7065 Å line all through. The 7065 Å line shows a clear double-peaked structure after day 12. The asymmetry in the line profiles at later phases

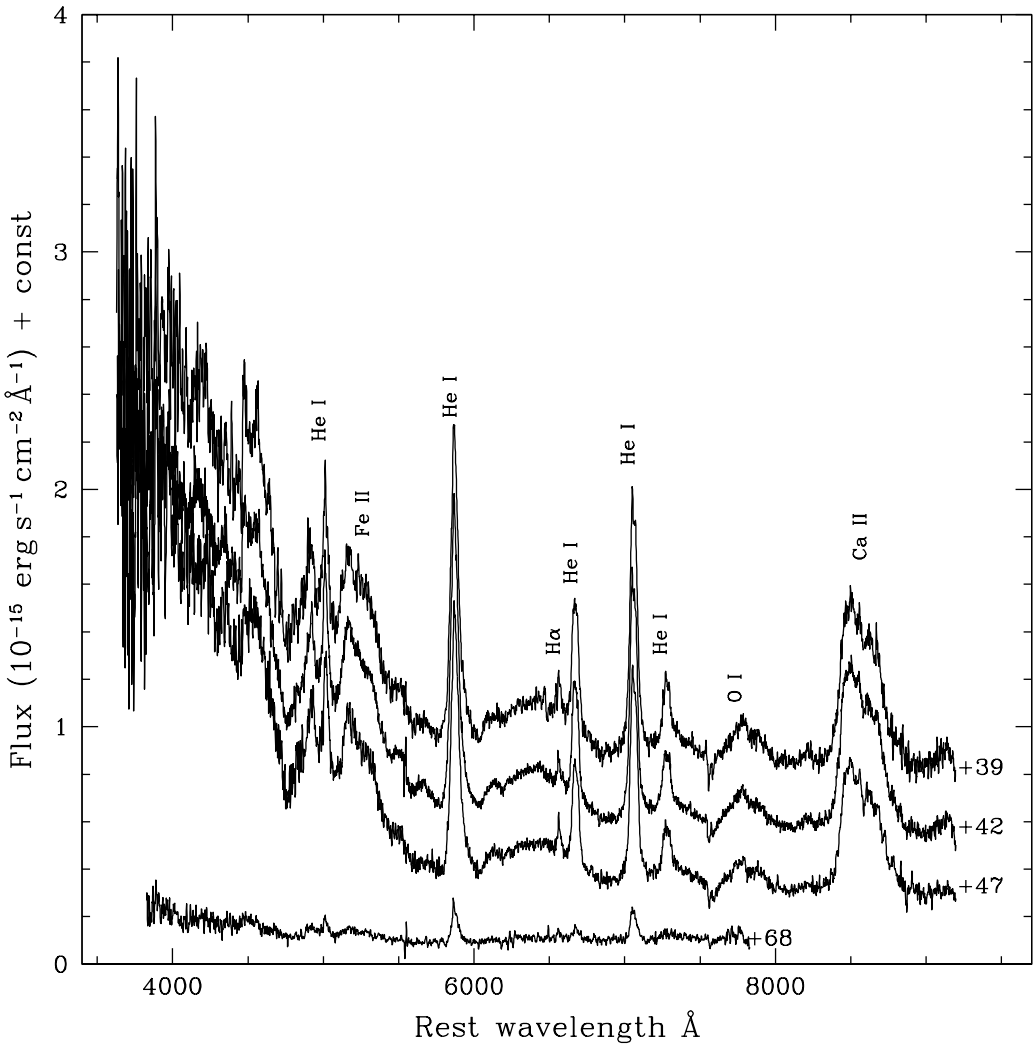

Figure 5.8: Spectroscopic evolution of SN 2006jc during +39–+68 days since maximum on JD 2454016. Note the increase in strength of the O I 7774 Å and Ca II infrared triplet lines.

was first noted by Smith et al. (2008) also, who find the asymmetry more pronounced in the spectra obtained at phases later than presented here, with the strongest decrease in the red side of the lines occuring between $\sim 50 - 75$ days, at the same time during which the red/IR continuum appeared and increased giving rise to a "U-shaped" continuum.

Hα is clearly detected in all the spectra presented here, and is seen to increase in strength at the later phases. While it is seen in absorption during the early days, it evolves into an emission feature around day 18–20 (refer Figures 5.6, 5.8). Pastorello et al (2008)

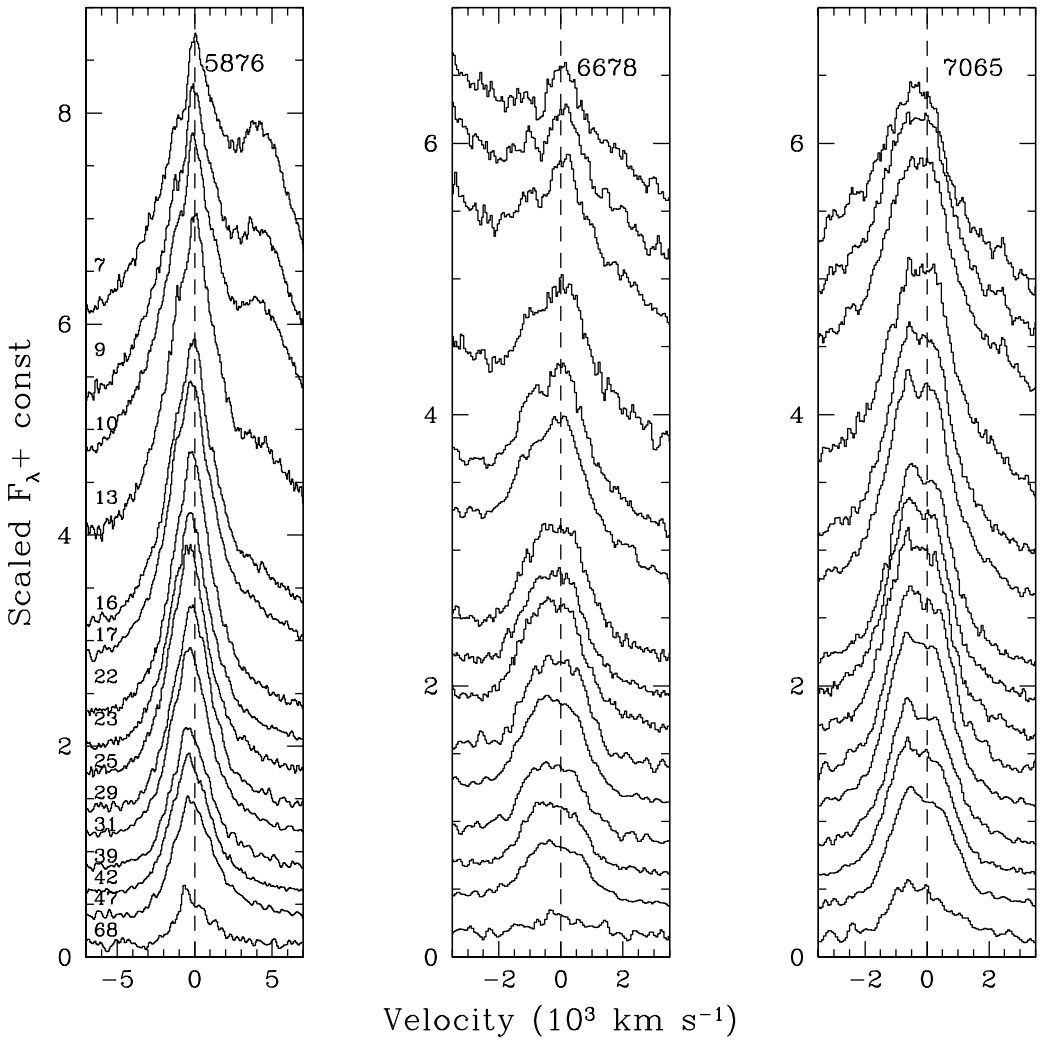

Figure 5.9: Evolution of the line profiles of the He I 5876, 6678 and 7065 Å lines.

note that the supernova features faded completely beyond ∼ 100 days and the spectrum was completely dominated by narrow He I circumstellar lines. They also note that the strength of Hα is almost comparable to that of He I λ 6678 Å line at this phase.

5.2.4 The Helium emitting region

The progenitor of SN 2006jc was observed to undergo a luminous mass loss episode, similar to the giant eruptions seen in LBVs, lasting about 10 days, two years prior to the supernova event (Nakano et al. 2006, Pastorello et al. 2007). If we assume that the helium

emission lines seen in the supernova spectra arise in the shell ejected during the luminous event, and this shell is helium enriched, then, the observed helium line luminosity may be used to estimate the density and mass of the shell. The observed, reddening corrected He Iλ 5876 Å and λ 7065 Å line fluxes are listed in Table 5.4.

If we assume the circumstellar shell (CS) ejected during the luminous mass loss episode had a velocity of 600 km s^{-1}, similar to the velocity of the narrow P Cygni absorption seen in the He I and O I lines, the radius of the shell would be 3.8×10^{15} cm. The corresponding radius for a CS velocity of 2500 km s^{-1}, as observed for the He I emission lines is 1.6×10^{16} cm. We also assume the thickness of the shell to be constant and determined by the observed duration ($\sim$ 10 days) of the luminous mass loss episode (Nakano et al. 2006). Using the observed reddening corrected line fluxes and a distance of 25.8 Mpc, we estimate an average density in the range $(0.54-3.7)\times10^{10}$ cm^{-3} for the shell with a velocity of 600 km s^{-1}. The corresponding mass range for this shell is $M_{\rm He} = 0.001 - 0.008$ M$_\odot$. Likewise, for a shell velocity of 2500 km s^{-1}, the average density lies in the range $(0.6 - 4.0) \times 10^9$ cm^{-3} and the corresponding mass range is $M_{\rm He} = 0.01 - 0.07\ M_\odot$. The helium line emissivities are taken from Almog & Netzer (1989). The density estimates are consistent with that estimated by Smith et al. (2008). Based on the observed X-ray luminosities, Immler et al. (2008) estimate a lower limit to the mass of the X-ray emitting shell to be 0.01M$_\odot$, and the circumstellar density to be $\sim 10^7$ cm^{-3}. These estimates are much lower than the values implied by the helium emission lines. This indicates that the X-ray emitting region could be different from the region emitting the bulk of the helium lines.

5.2.5 Discussion

SN 2006jc shows a very peculiar spectrum with a very steep blue continuum and dominated by moderately narrow He I emission lines. The presence of the moderately narrow emission lines is very similar to that observed in Type IIn supernovae, where the fast moving supernova ejecta interacts with a pre-exisiting circumstellar material. The observed properties of SN 2006jc are very similar to the recent supernovae SN 1999cq, SN 2000er and SN 2002ao (e.g. Pastorello et al. 2008b). A weak X-ray emission and UV excess have also been detected in SN 2006jc, providing further evidence for an interaction with a pre-supernova circumstellar material (Immler et al. 2008). A luminous mass loss episode was observed in the progenitor of SN 2006jc two years prior to the outburst. It is suggested that the strong, intermediate width He I emission lines dominating the optical spectrum arise in the circumstellar shell due to the recent mass loss episode and that it is helium

Table 5.4: He I 5876 and 7065 Å emission line fluxes

Phase	Flux (10^{-14} erg cm^{-2})		Density[1] (10^9 cm^{-3})		Mass[1] ($M_\odot$)	
	5876 Å	7065 Å	A[2]	B[3]	A[2]	B[3]
7.47	4.96[4]	9.44	16.49	1.91	0.003	0.031
9.47	7.64[4]	12.20	19.46	2.25	0.004	0.036
10.46	9.80[4]	11.59	20.48	2.36	0.004	0.038
13.48	12.28	11.12	36.27	4.18	0.008	0.066
16.45	20.24	11.68	36.86	4.24	0.008	0.070
17.44	17.52	11.35	35.24	4.07	0.008	0.066
22.46	15.79	8.70	32.17	3.71	0.007	0.059
23.49	14.48	9.51	32.23	3.71	0.007	0.059
25.49	13.65	8.48	30.83	3.55	0.007	0.057
29.37	12.27	9.30	30.89	3.55	0.007	0.057
31.42	11.29	8.08	28.97	3.34	0.007	0.055
39.51	8.59	6.82	26.14	3.01	0.005	0.049
42.42	8.49	6.25	25.43	2.94	0.005	0.048
47.35	6.95	5.45	23.43	2.70	0.004	0.043
68.36	0.758	0.725	5.41	0.63	0.001	0.011

1: Average of 5876 and 7065 Å
2: Assuming a shell velocity of 600 km s^{-1}
3: Assuming a shell velocity of 2500 km s^{-1}
4: Flux of de-blended narrow component

enriched (Foley et al. 2007, Pastorello et al. 2007, Smith et al. 2008). The fluxes of the He I emission lines indicate a density of $\sim 10^9$ cm^{-3} and a helium mass $\lesssim 0.07\ M_\odot$ in the circumstellar shell that is assumed to have a velocity of 2500 km s^{-1} corresponding to the FWHM width of the He I lines. It is also quite likely that the velocity of the CSM shell was initially low, and accelerated to 2500 km s^{-1} due to the interaction. In such a case, the initial velocity of the shell is more likely to be in between the assumed velocities, and the density of the shell $\sim 10^9 - 10^{10}$ cm^{-3}. The density estimated here is similar to that estimated by Smith et al. (2008). Comparing with type IIn SNe, it is found that the estimated density range for SN 2006jc is somewhat higher than that estimated for IIn SNe, in which the CSM densities are found to range from $\sim 10^6$ (e.g. SN 1995N: Fransson et al. 2002) to $\gtrsim 10^8$ cm^{-3} (e.g. SN 1995G: Pastorello et al. 2002; SN 1997eg: Salamanca et al. 2002.

Dust formation has been observed in SN 2006jc early on, at $\sim$ 50 days past maximum (Di Carlo et al. 2008, Smith et al. 2008, Nozawa et al. 2008b). Dust formation is reflected in the helium emission line profiles, which developed an asymmetric profile, with the red

wing of the profile getting increasingly suppressed with time, and also in the increase in the red to NIR continuum between 65–120 days. Smith et al. (2008) estimate the dust temperature during this phase to be $\sim$ 1600 K. The estimated densities in the shell are high enough to precipitate graphite dust (Clayton 1979).

Based on NIR and MIR observations at $t \sim 200$ days, Sakon et al. (2009) conclude that IR emission orginated from amorphous carbon grains with two temperatures of 800 K and 320 K. Sakon et al. (2008), Nozawa et al. (2008) and Tominaga et al. (2008) suggest the hot carbon dust is newly formed in the supernova ejecta and heated by the ^{56}Ni–^{56}Co decay, while the origin of the warm carbon dust is a supernova light echo of the CSM carbon dust. For the dust to originate in the SN ejecta, it implies an ejecta radius of $\sim 10^{16}$ cm during dust formation. This in turn implies a (constant) velocity $\sim 25,000 - 30,000$ km s^{-1}. No evidence for such a high velocity is seen in the observed spectra. Based on a comparison of the early spectra of SN 2006jc with those of SN 2000er, Pastorello et al. (2008) suggest that SN 2006jc was discovered a couple of weeks after explosion or $\sim$ 10 days after maximum light. Very high initial velocities can thus not be ruled out, as the initial interaction of the supernova material with the CS material can lead to a deceleration of the supernova shell (e.g. Chevalier 1982).

On the basis of spectroscopic evidences, Smith et al. propose the site of dust formation to be a cold dense shell (CDS) behind the blast wave and that the shell was composed of dense CSM ejected by the luminous event, which was then swept up by the forward shock. They, however, do not rule out the possibility of dust formation in a carbon-rich SN ejecta. Mattila et al. (2008) also propose the CDS as the site for formation of the hot dust. However, they argue, based on the intensity, spectral energy distribution and evolution of the IR flux, that the IR emission in SN 2006jc is due to IR echoes. The bulk of the near-IR emission is due to an IR echo from the newly formed dust in the CDS, while a substantial fraction of the MIR flux is due to pre-existing dust in the progenitor wind due to an episodic mass-loss phase that ceased at least $\sim$ 200 years before the recent pre-supernova luminous outburst and the SN event.

The observed optical light curves of SN 2006jc show an early evolution that is quite similar to normal Ib/c supernovae. The initial decline is steep and at about 20 days past maximum, the decline slows, a probable indication of the supernova having reached the exponential tail. Comparing the light curve evolution with Type IIn supernovae (e.g. SN 1998S), it is seen that the early decline is much slower in the case of SNe Type IIn, where the light curve is thought to be powered by the interaction of the supernova material with the CSM (e.g. Rigon et al. 2003). On the other hand, the light curve evolution of SN

2006jc, until the onset of dust formation at $\sim$ 50 days since maximum is very similar to normal Type Ib/c objects. Comparing the bolometric light curve of SN 2006jc with normal Type Ib/c SNe and the Type IIn SNe, it is seen that the *uvoir* bolometric light curve of SN 2006jc is very similar to the normal Type Ib/c objects, with a fast early decline followed by a flattening in the light curve $\sim$ 35 days after maximum.

It is interesting to note that while the spectrum shows clear signatures of circumstellar interaction similar to Type IIn SNe, the bolometric light curve does not show any evidence of being powered by the interaction. We suggest this is possibly a result of a weaker interaction in the case of SN 2006jc due to a shell mass that is lower compared to the mass of the circumstellar material in the case of Type IIn SNe (eg. $\sim$ 0.4 $M_\odot$ in SN 1994W: Chugai et al. 2004; $\sim$ 10$M_\odot$ in 1997eg: Salamanca et al. 2002).

Tominaga et al. (2008) present a detailed theoretical model for SN 2006jc. Their work suggests that the progenitor is WCO Wolf-Rayet star whose total mass has been reduced from M_{MS} = 40 $M_\odot$ to as small as M_{pre-SN} = 6.9 $M_\odot$ through mass loss. The WCO star has a thick C-rich envelope and CSM, consistent with the formation of amorphous carbon grains in the SN ejecta and CSM suggested by AKARP observations (Sakon et al. 2008). This model, however, does not explain the LBV - like outburst observed two years prior to the SN outburst since there is no observations evidence for such luminous outburst in Wolf - Rayet stars.

5.3 SN2007ru: The broad line type Ic supernova

5.3.1 Introduction

SN 2007ru was discovered by Donati et al. (2007) on 2007 November 27.9 and independently by Winslow & Li with KAIT on 2007 November 30.15 in the spiral galaxy UGC 12381. The identification chart of SN 2007ru is shown in Figure 5.10. There was no evidence of the supernova in the KAIT image taken on November 22.16, down to a limiting magnitude of 18.9 (Donati et al. 2007). Based on a spectrum obtained on 2007 December 1, SN 2007ru was classified as peculiar SN Ic at premaximum phase (Chornock et al. 2007). The Ca II H & K and Ca II Near Infrared (NIR) triplet absorption troughs were found to be weak compared to other SNe Type Ic. Further, the O I line at λ 7774 Å indicated an expansion velocity of 19000 km s^{-1}, similar to the expansion velocity seen in the broad-line SN Type Ic SN 2006aj (Pian et al. 2006). A search through the reported discoveries of GRBs during 2007 October 15 to 2007 November 30, does not show any possible association of a GRB with this supernova.

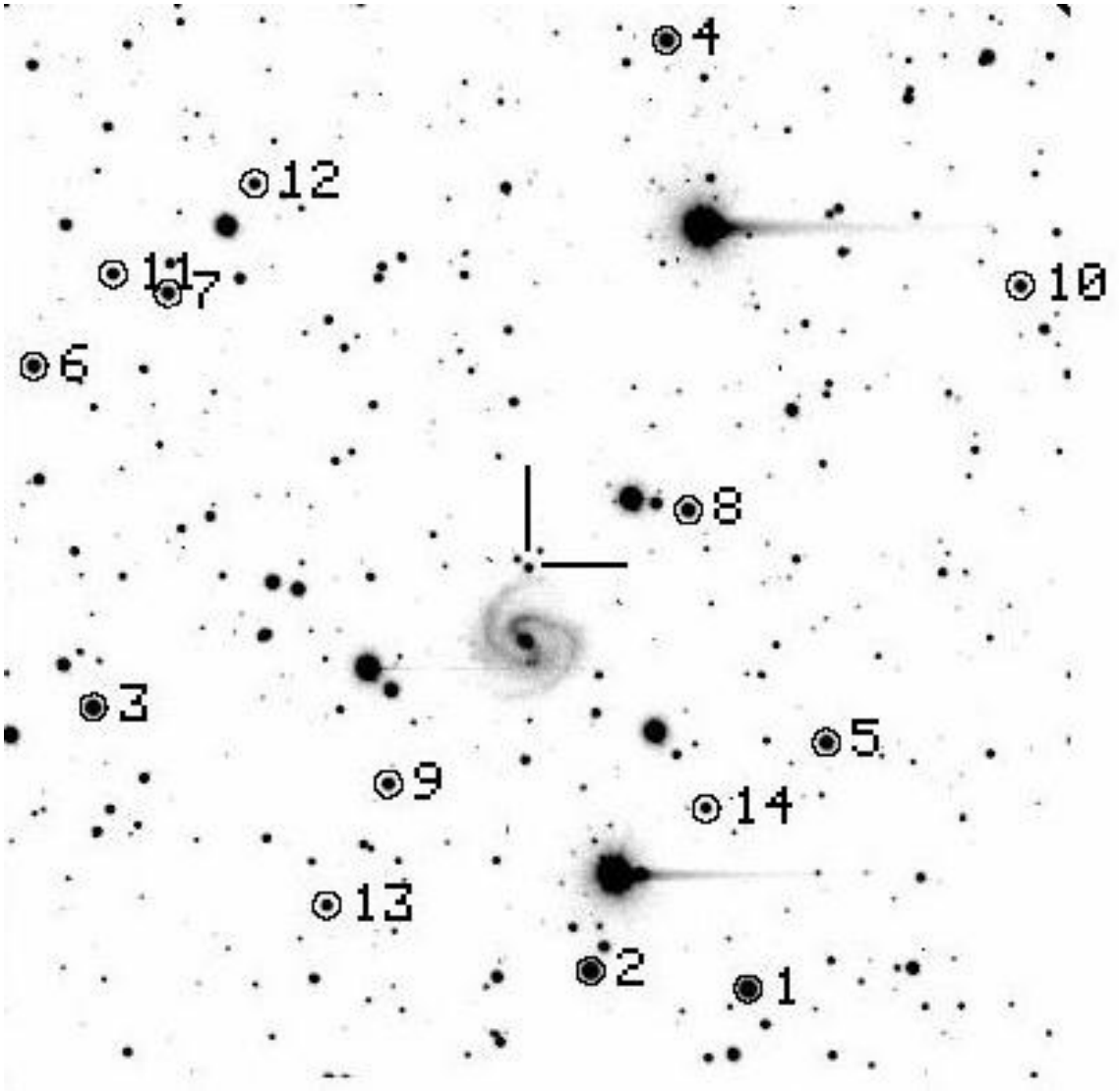

Figure 5.10: Identification chart for SN 2007ru. The stars used as local standards are marked as numbers 1-14.

SN 2007ru was observed in *UBVRI* bands during 2007 December 2 (JD 2454437.09) to 2008 July 03 (JD 2454651.35). Photometric standard regions (Landolt 1992) were observed on 2007 December 25 and December 26 under photometric sky conditions to calibrate a sequence of secondary standards in the supernova field. The *UBVRI* magnitudes of secondary stars are listed in Table 5.6. The supernova magnitudes are listed in Table 5.7.

A series of spectra were taken during 2007 December 3 to 2008 June 12, in the wavelength range (3500 Å - 7000 Å) and (5200 Å - 9200 Å), with a resolution of $\sim$ 7 Å. The

Table 5.5: Log of spectroscopic observations of SN 2007ru.

Date	J.D. 2454000+	Phase* (days)	Range Å
03/12/07	438.21	+8	5200-9100
10/12/07	445.06	+15	3500-7000; 5200-9100
11/12/07	446.07	+16	3500-7000; 5200-9100
15/12/07	450.14	+20	3500-7000; 5200-9100
19/12/07	454.13	+24	3500-7000; 5200-9100
22/12/07	457.09	+27	3500-7000
04/01/08	470.09	+40	3500-7000; 5200-9100
03/02/08	500.08	+70	3500-7000
12/06/08	630.38	+200	5200-9100

* With respect to date of explosion JD = 2454430.

journal of spectroscopic observations is given in Table 5.5. The supernova spectra were corrected for the host galaxy redshift of $z = 0.01546$ (from NED) and dereddened by the total reddening $E(B - V) = 0.27$ as estimated in §5.3.6.

5.3.2 Optical light curves

The *UBVRI* light curves (LC) of SN 2007ru are shown in Figure 5.11. The unfiltered discovery magnitudes and the pre-discovery limiting magnitude are also included in the figure. The LCs indicate that the maximum occurred earlier in the blue, similar to other broad-line SNe Type Ic. The date of explosion can be constrained to $\lesssim 6$ days before discovery (November 25, JD 2454430±3), based on the non-detection on November 22 by KAIT and the subsequent discovery on 2007 November 27.9. The rise time to *B* maximum, which occurred on December 3, is 5-11 (8 ± 3) days, indicating SN 2007ru is a fast rising SN Type Ic with a rise time similar to broad-line SNe 2002ap (Foley et al. 2003), and 2006aj (Modjaz et al. 2008b), marginally faster than SN 2003jd (Valenti et al. 2008) but considerably faster than the GRB-associated SNe 1998bw and 2003dh ((Galama et al. 1998), (Matheson et al. 2003)). .

The light curves of SN 2007ru are compared with those of broad-line SNe SN 2002ap, SN 2003jd, GRB 980425/SN 1998bw, normal SNe Type Ic SN 1994I and SN 2004aw in Figure 5.12. A comparison of the decline in brightness 15 days after maximum light, Δm_{15} in different bands shows that SN 2007ru has a decline similar to other broad-line supernovae. In fact, the decline of SN 2007ru is faster than SN 1998bw but slower than SNe 2003jd and 2006aj (refer Table 5.8). The decline rates are estimated to be $\Delta m_{15}(B)$=1.57,

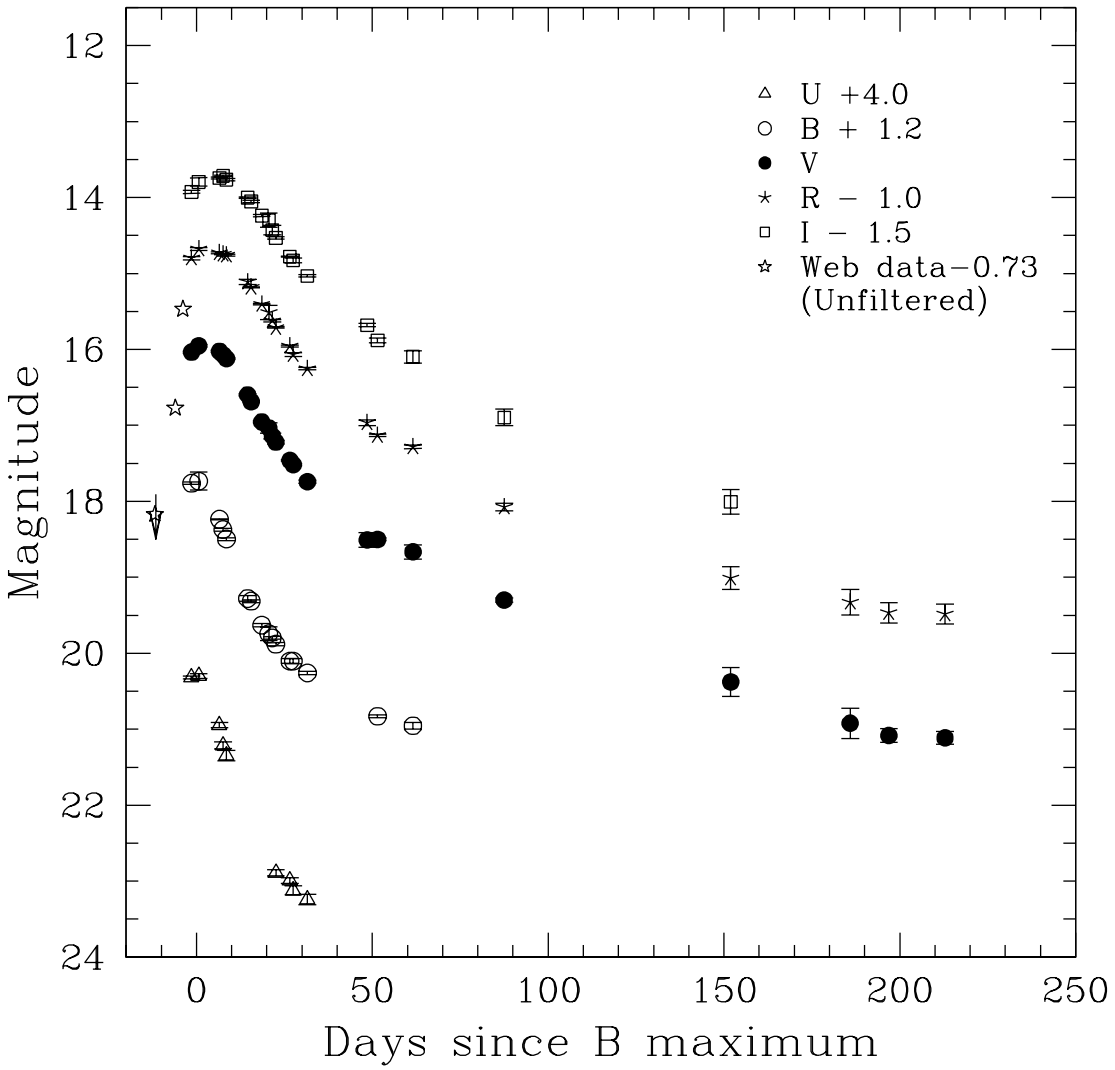

Figure 5.11: The *UBVRI* LCs of SN 2007ru. The LCs have been shifted by the amount indicated in the legend. The unfiltered magnitudes reported by amateurs and the pre-discovery limiting magnitudes have been included with *R* band magnitudes in the figure.

$\Delta m_{15}(V)$=0.92, $\Delta m_{15}(R)$=0.69 and $\Delta m_{15}(I)$=0.50. The light curves of SN 2007ru decline with decline rates of 0.021 mag day^{-1} in *V*, 0.028 mag day^{-1} in *R* and 0.030 mag day^{-1} in *I* bands during days 45 − 80. These decline rates are comparable to the light curve decline rates of the broad-line SN 2003jd and marginally faster than SN 1998bw. The decline rate in *B* cannot be estimated due to a sparse coverage during this period. During the late phases (> 80 days after explosion), the *V* and *R* band light curves of SN 2007ru

Table 5.6: Magnitudes for the sequence of secondary standard stars in the field of SN 2007ru.

ID	U	B	V	R	I
1	14.433 ± 0.015	14.396 ± 0.006	13.877 ± 0.005	13.531 ± 0.005	13.116 ± 0.006
2	14.918 ± 0.017	14.790 ± 0.013	14.073 ± 0.018	13.618 ± 0.016	13.111 ± 0.023
3	15.111 ± 0.020	15.020 ± 0.016	14.343 ± 0.020	13.953 ± 0.017	13.488 ± 0.024
4	15.870 ± 0.030	15.554 ± 0.010	14.714 ± 0.021	14.232 ± 0.012	13.689 ± 0.019
5	16.105 ± 0.030	15.670 ± 0.021	14.796 ± 0.024	14.317 ± 0.002	13.783 ± 0.004
6	15.390 ± 0.025	15.339 ± 0.014	14.780 ± 0.022	14.406 ± 0.021	13.995 ± 0.021
7	15.773 ± 0.032	15.616 ± 0.019	14.869 ± 0.024	14.444 ± 0.024	13.933 ± 0.030
8	16.138 ± 0.030	15.900 ± 0.012	15.046 ± 0.021	14.550 ± 0.023	13.985 ± 0.030
9	16.792 ± 0.036	16.136 ± 0.018	15.139 ± 0.022	14.553 ± 0.014	13.951 ± 0.025
10	17.312 ± 0.045	16.619 ± 0.017	15.631 ± 0.017	15.066 ± 0.014	14.471 ± 0.014
11	17.321 ± 0.040	16.730 ± 0.014	15.739 ± 0.025	15.153 ± 0.014	14.555 ± 0.021
12	17.970 ± 0.052	16.954 ± 0.019	15.766 ± 0.025	15.083 ± 0.024	14.362 ± 0.031
13	16.552 ± 0.045	16.505 ± 0.020	15.796 ± 0.030	15.368 ± 0.026	14.864 ± 0.030
14	17.518 ± 0.050	16.997 ± 0.005	16.045 ± 0.018	15.513 ± 0.018	14.937 ± 0.027

* The stars are identified in Figure. 5.10

decline with decline rates of 0.0152 and 0.0116 mag day^{-1}, respectively, slower than both SN 2003jd and SN 1998bw during the corresponding epochs (Figure 5.12). The decline rate of SN 2007ru during the late phases, is faster than the rate expected due to the radio active decay of ^{56}Co into ^{56}Fe. This indicates inefficient trapping of γ-rays by the ejecta, which suggests a low column density.

The peak absolute magnitudes were estimated using the apparent magnitude at maximum in different bands (see §5.3.6 for reddening and distance estimate). From a comparison of the absolute magnitude, SN 2007ru appears to lie at the brighter end of the observed SNe Ic. With an absolute V magnitude of -19.06 ± 0.2, SN 2007ru is fainter than GRB 031203/SN 2003lw [M_V=-19.75 ± 0.5; Malesani et al. (2004)], comparable in brightness with SN 1998bw [M_V=-19.12 ± 0.05, Galama et al. (1998)], and brighter than XRF 060218/SN 2006aj [M_V=-18.67 ± 0.08; Modjaz et al. (2006)], broad-line SNe 2002ap [M_V=-17.37 ± 0.05; Foley et al. (2003), Tomita et al. (2006)], 2003jd [M_V=-18.9 ± 0.3; Valenti et al. (2008)] and normal SNe Ic 1994I [M_V=-17.62 ± 0.3; Richmond et al. (1996), Sauer et al. (2006)], and 2004aw [M_V=-18.02 ± 0.3; Taubenberger et al. (2006)].

5.3.3 Spectral evolution

The spectral evolution of SN 2007ru is presented in Figure 5.13. The first spectrum, obtained on 2007 December 3, at $t \sim 8$ days, where t is days after explosion, (the rise time

Table 5.7: Photometric observations of SN 2007ru

Date	J.D. 2454000+	Phase* (days)	U	B	V	R	I
02/12/2007	437.086	-2	16.318 ± 0.021	16.562 ± 0.016	16.036 ± 0.011	15.798 ± 0.022	15.426 ± 0.020
04/12/2007	439.155	0	16.299 ± 0.029	16.533 ± 0.120	15.951 ± 0.015	15.678 ± 0.019	15.296 ± 0.056
10/12/2007	445.029	6	16.943 ± 0.034	17.036 ± 0.008	16.025 ± 0.012	15.726 ± 0.012	15.244 ± 0.014
11/12/2007	446.047	7	17.211 ± 0.045	17.172 ± 0.019	16.070 ± 0.011	15.746 ± 0.008	15.215 ± 0.011
12/12/2007	447.027	8	17.346 ± 0.067	17.296 ± 0.019	16.121 ± 0.011	15.759 ± 0.014	15.265 ± 0.016
18/12/2007	453.046	14		18.078 ± 0.039	16.598 ± 0.014	16.111 ± 0.035	15.501 ± 0.010
19/12/2007	454.056	15		18.114 ± 0.019	16.687 ± 0.012	16.184 ± 0.007	15.553 ± 0.017
22/12/2007	457.067	18		18.430 ± 0.024	16.954 ± 0.011	16.404 ± 0.011	15.738 ± 0.013
24/12/2007	459.097	20		18.540 ± 0.090	17.034 ± 0.070	16.512 ± 0.095	15.799 ± 0.095
25/12/2007	460.069	21		18.596 ± 0.017	17.140 ± 0.035	16.621 ± 0.016	15.929 ± 0.060
26/12/2007	461.079	22	18.889 ± 0.040	18.681 ± 0.021	17.221 ± 0.024	16.711 ± 0.010	16.031 ± 0.016
30/12/2007	465.061	26	18.990 ± 0.038	18.902 ± 0.032	17.460 ± 0.008	16.956 ± 0.013	16.278 ± 0.008
31/12/2007	466.029	27	19.118 ± 0.060	18.902 ± 0.036	17.517 ± 0.014	17.069 ± 0.024	16.329 ± 0.031
04/01/2008	470.045	31	19.241 ± 0.069	19.057 ± 0.021	17.741 ± 0.024	17.252 ± 0.015	16.532 ± 0.016
21/01/2008	487.041	48			18.509 ± 0.096	17.964 ± 0.037	17.181 ± 0.022
24/01/2008	490.063	51		19.629 ± 0.021	18.501 ± 0.019	18.130 ± 0.014	17.382 ± 0.031
03/02/2008	500.055	61		19.754 ± 0.044	18.665 ± 0.0924	18.282 ± 0.023	17.597 ± 0.082
29/02/2008	526.068	87			19.300 ± 0.026	19.075 ± 0.050	18.395 ± 0.109
03/05/2008	590.431	151			20.377 ± 0.19	20.007 ± 0.15	19.506 ± 0.164
06/06/2008	624.400	185			20.921 ± 0.20	20.325 ± 0.169	
17/06/2008	635.360	196			21.083 ± 0.088	20.466 ± 0.133	
03/07/2008	651.348	212			21.115 ± 0.084	20.483 ± 0.128	

* Observed phase with respect to the epoch of maximum in *B* band (JD 2454438.8).

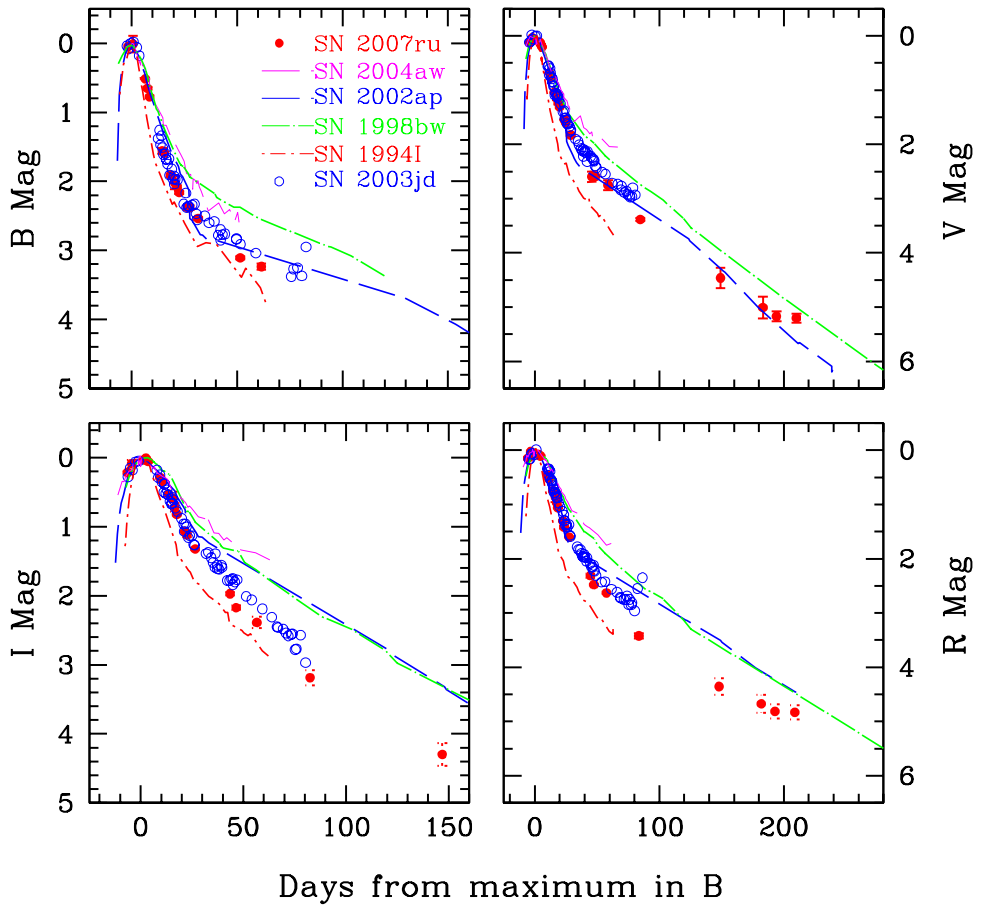

Figure 5.12: Comparison of LCs of SN 2007ru with other Type Ib/c SNe. The LCs of the supernovae in comparison have been shifted arbitrarily to match the date of maximum and magnitude at maximum.

is assumed to be 8 days, see §5.3.2) shows broad absorption features at $\sim \lambda$ 6000 Å due to Si II (and a possible contamination as discussed by Valenti et al. 2008), at $\sim \lambda$ 7200 Å due to O I and at $\sim \lambda$ 8200 Å due to weak Ca II NIR triplet. The spectrum at $t \sim 20$ days shows well developed broad absorptions due to Mg II λ 4481 Å, blends of Fe II at $\sim \lambda$ 4700 Å, Si II λ 6355 Å, O I λ 7774 Å and Ca II NIR triplet. The continuum gets redder by $t \sim 20$ days. No significant evolution is seen in the spectrum taken at $t \sim 41$ days. The last spectrum presented here, obtained $\sim$ 200 days after explosion indicates the supernova

to be in the nebular phase.

Comparing the spectrum and its evolution with that of the broad-line SN 2003jd and the 'normal spectrum' Ic supernova SN 2004aw (Figure 5.14 and Figure 5.15), it is seen that SN 2007ru is very similar to the broad-line SN Type Ic, indicating high expansion velocities. The spectral features continue to remain broad and similar to those of SN 2003jd even at $t \sim 41$ days.

5.3.4 Photospheric velocity

The high velocity of the supernova ejecta usually results in blending of the spectral lines, making direct measurement of the photospheric velocity difficult. The photospheric velocity of SN 2007ru is estimated by fitting a Gaussian profile to the minimum of the absorption trough of Si II λ 6355 Å line, in the redshift corrected spectra. In the first spectrum, ~8 days after the explosion, the absorption feature at λ 6200 Å consists of two components, similar to that seen in the premaximum spectra of the broad-line SN 2003jd (Valenti et al. 2008). Assuming the blue component is due to Si II and the red wing is due to possible contamination by other species, the photospheric velocity is estimated to be 20,000 km sec^{-1}. This is consistent with the velocity estimate by Chornock et al. (2007) using OI line in the spectrum.

The photospheric velocity of SN 2007ru, measured using Si II lines, and its evolution is compared with other SNe Type Ic in Figure 5.16. The photospheric velocity of SN 2007ru at ~ 8 days after explosion is lower than GRB 980425/SN 1998bw (Patat et al. 2001), but comparable to XRF 060218/SN 2006aj (Pian et al. 2006) and broad-line SN 2002ap (Foley et al. 2003). However, at the later epochs, the photospheric velocity of SN 2007ru is comparable to those of SN 1998bw and SN 2003jd and higher than other SNe Ic in comparison. Except for the early phase (< 15 days after explosion) the photospheric velocity evolution of SN 2007ru is very similar to that of the broad-line SN 2003jd.

5.3.5 Nebular spectrum

The spectrum of SN 2007ru taken ~ 200 days after explosion (refer Figure 5.17) is dominated by the forbidden emission lines of [O I] $\lambda\lambda$ 6300, 6364 Å and [Ca II] $\lambda\lambda$ 7291, 7323 Å, possibly blended with [O II] $\lambda\lambda$ 7320, 7330 Å(Taubenberger et al. 2006). These lines show a broad profile. Due to poor signal-to-noise ratio of our spectrum it is difficult to identify other spectral lines in the spectrum. However, narrow lines due to Hα, [N II] λ 6583Å, [S II] $\lambda\lambda$ 6713, 6731 Å, originating from the underlying HII region at the su-

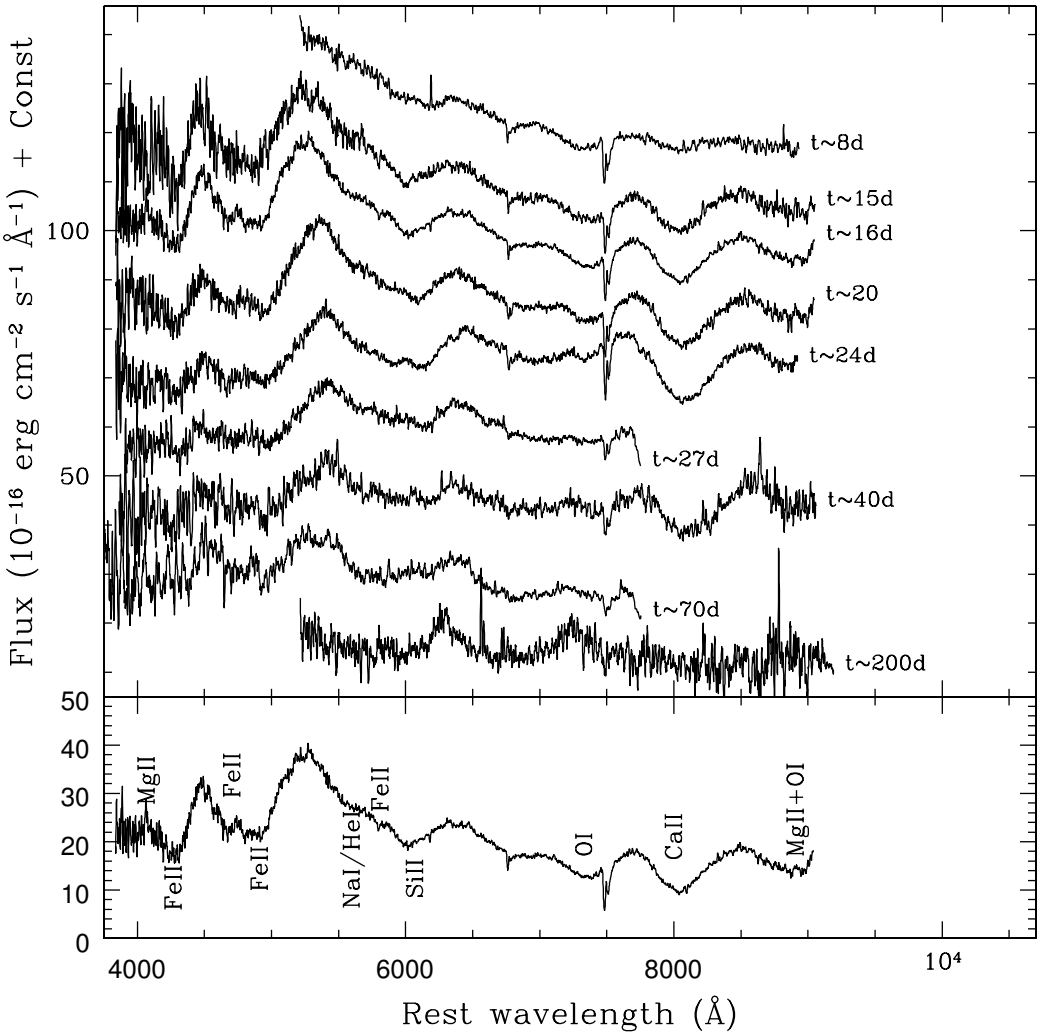

Figure 5.13: Optical spectral evolution of SN 2007ru (top panel). The spectra are corrected for the host galaxy redshift. Time in days since the day of explosion (2008 November 25) is indicated for each spectrum. For clarity, the spectra have been displaced vertically. Main spectral features are identified and marked in the spectrum taken $\sim$ 16 days after explosion (bottom panel).

pernova location and superimposed on the spectrum of the supernova, are clearly seen in the spectrum, and are identified in Figure 5.17.

A comparison of the nebular spectrum of SN 2007ru is made with those of other SNe Type Ic in Figure 5.17. The line profile of the [O I] $\lambda\lambda$ 6300, 6364 Å lines shows a sharp peak, very similar to that seen in SN 1998bw, SN 2004aw and SN 2007ru. Interestingly,

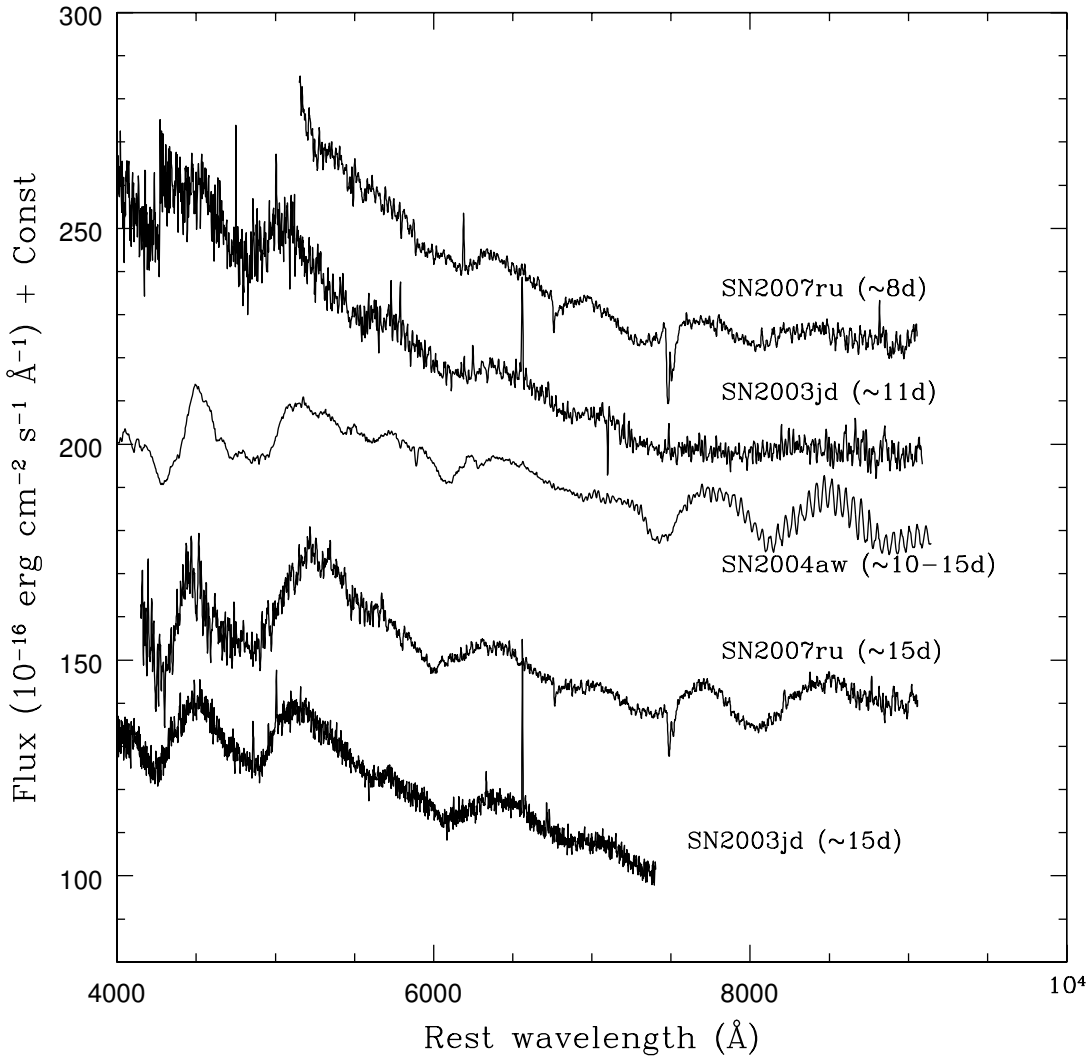

Figure 5.14: Comparison of spectra of SN 2007ru with broad-line Type Ic SN 2003jd and normal spectrum Type Ic SN 2004aw at different epochs.

despite the spectral similarity between SN 2007ru and SN 2003jd at early phase, the [OI] line profile in the nebular spectra is different: SN 2003jd shows a double peaked structure (see §4.3.8 for implications). The profile of [Ca II] $\lambda\lambda$ 7291, 7323/[O II] $\lambda\lambda$ 7320, 7330 Å line is similar to the [O I] line profile, as seen in SN 2004aw (Taubenberger et al. 2006), but different from the profiles seen in SNe 1998bw and 2003jd, which show a flat topped profile.

The [O I] $\lambda\lambda$ 6300, 6364 and [Ca II] $\lambda\lambda$ 7291, 7323 Å lines show a blueshift of 2300±300 km sec^{-1} and 1200 ± 200 km sec^{-1}, respectively. This could be due to a kine-

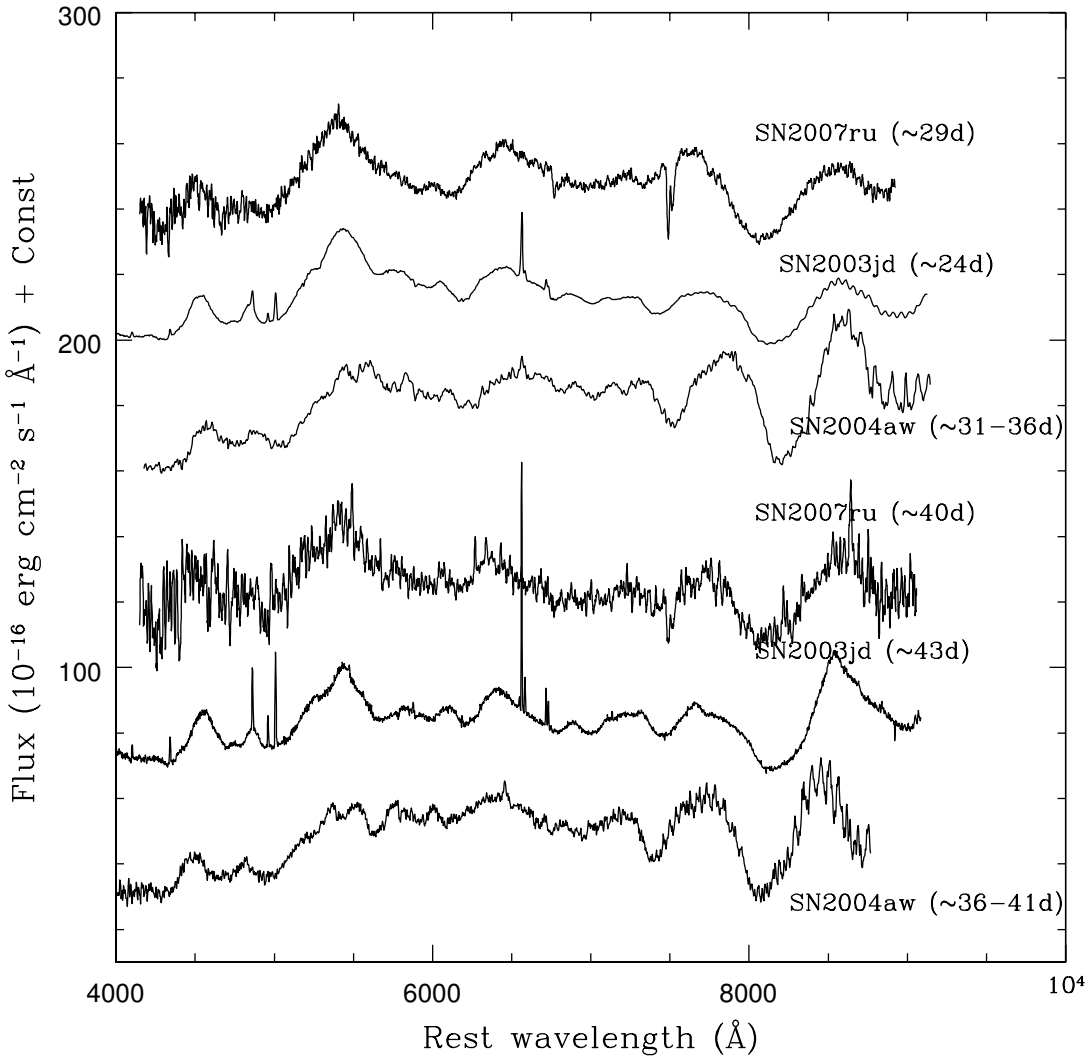

Figure 5.15: Same as figure 5.14 but at different epochs.

matic offset (Maeda et al. 2007), optical depth effect (Filippenko et al. 1994), or extinction by the dust formed in the SN ejecta (although there is no strong indication of the dust formation in the light curve.)

The velocities derived from full width at half maximum of [O I] and [Ca II] lines are found to be 14000±2200 km sec^{-1} and 13500±1300 km sec^{-1}, respectively. These values are comparable to those seen in SN 1998bw and SN 2003jd. The reddening corrected [O I]/[Ca II] flux ratio is found to be $\sim$ 1.6, which is again comparable to the ratios in SN 1998bw and SN 2003jd. Thus, though the profile of the [O I] and [Ca II] lines in the the

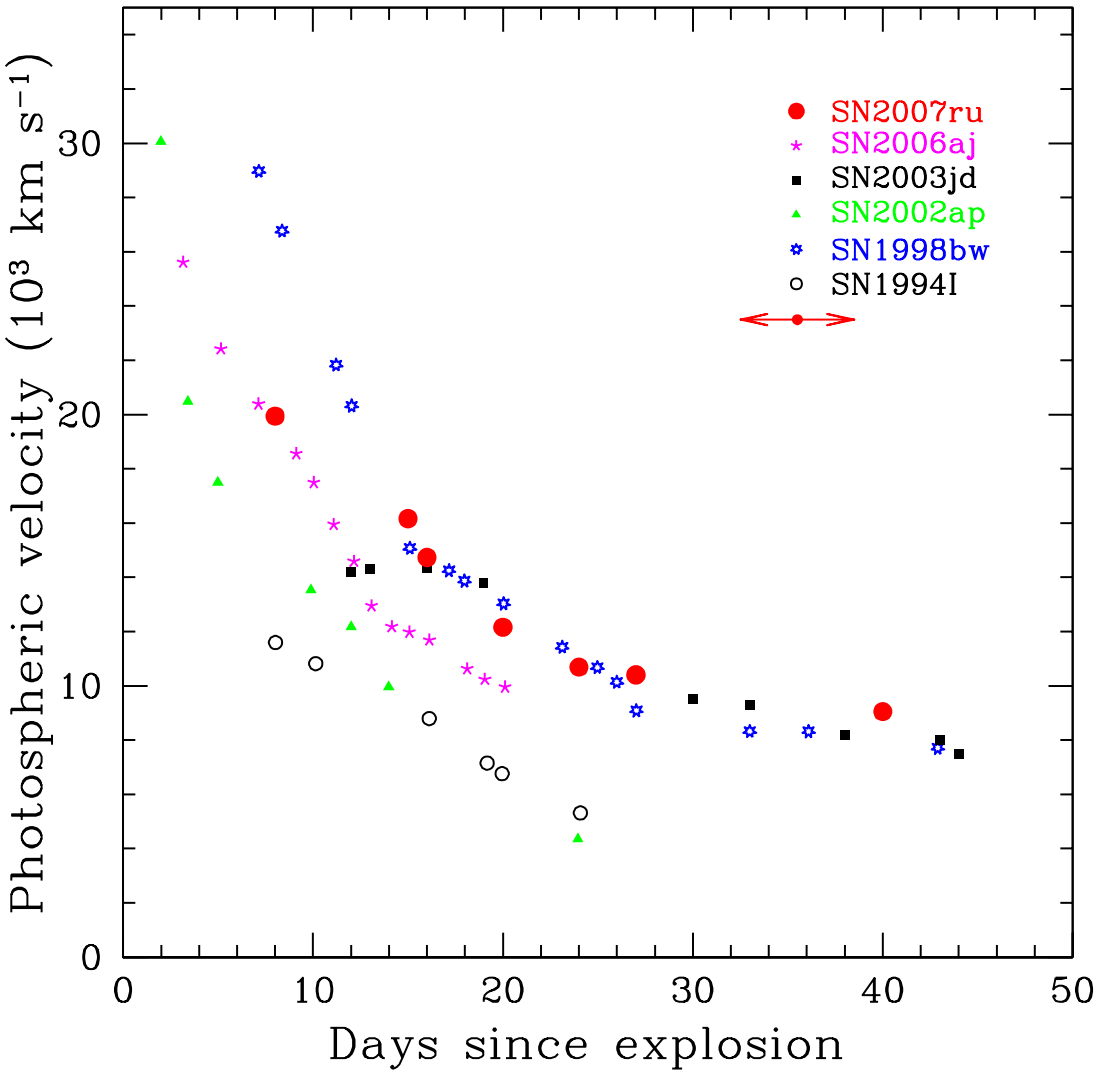

Figure 5.16: Evolution of the photospheric velocity of SN 2007ru and other SNe Ic inferred from Si II λ 6355 Å line. Uncertainty in estimating days since explosion for SN 2007ru due to error in the date of explosion (JD 2454430±3) is indicated by the horizontal arrow.

nebular spectrum of SN 2007ru and SN 2003jd differ, other properties like line width and [O I]/[Ca II] flux ratio are similar.

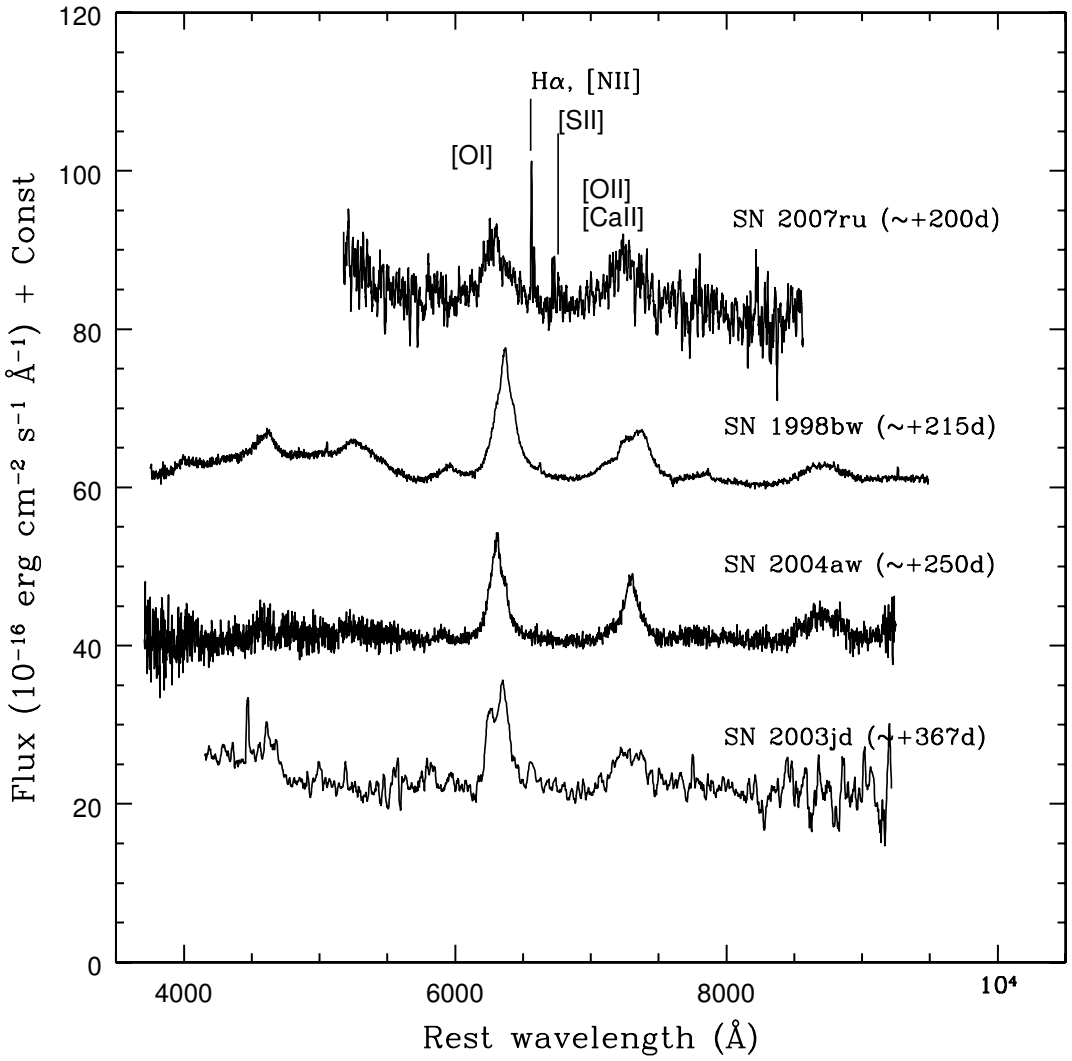

Figure 5.17: Comparison of the nebular spectrum of SN 2007ru with other Type Ic supernovae.

5.3.6 Bolometric light curve

Direct distance estimates to the host galaxy of SN 2007ru are not available in the literature. The radial velocity of UGC 12381, corrected for Local Group infall onto the Virgo Cluster is 4832 km sec^{-1} (LEDA). For H_0 = 72 km sec^{-1} Mpc^{-1}, the distance modulus to UGC 12381 is 34.15 ± 0.10, where the error is estimated taking into account the errors in HI velocity measurement of the galaxy (Paturel et al. 2003) and the uncertainty in H_0 .

The Na ID absorption line is clearly seen in the spectrum with an average equivalent

width of 1.67 ± 0.37 Å. Based on the equivalent widths of Na ID absorption seen in several SNe, Turatto et al. (2003) find two distinct relations between Na ID equivalent width and the reddening $E(B-V)$. Using these relations, the observed Na ID equivalent width indicates $E(B-V)$ values of 0.85 ± 0.19 and 0.27±0.06. The Galactic interstellar reddening in the direction of UGC 12381 is estimated to be 0.26 (Schlegel et al. 1998). The Na ID absorption seen in the spectra of SN 2007ru is clearly from the Milky Way galaxy and no component due to the host galaxy is detected. Hence, an $E(B-V)$ value of 0.27 is used for extinction correction.

The quasi bolometric LC of SN 2007ru is estimated using the *UBVRI* magnitudes corrected for reddening with $E(B-V)$=0.27 and the Cardelli et al. (1989) extinction law. The magnitudes were converted to the monochromatic flux, using zero points from Bessell et al. (1998). The fluxes were then spline interpolated and integrated from 3100 Å to 1.06 μm. Since *U* band observations are not available beyond 35 days since *B* maximum, the bolometric LC is estimated by integrating the *BVRI* fluxes only. The contribution of *U* band to the bolometric flux at phases $\sim$ 35 days is estimated to be $\lesssim$ 10%. In the later phases when only *V*, *R*, *I* or *V*, *R* magnitudes are available, the bolometric magnitudes are derived by applying a bolometric correction to the available magnitudes. The bolometric corrections were estimated based on the last four points for which *B*, *V*, *R* and *I* measurements are available.

The quasi bolometric LC is shown in Figure 5.18. Adding a conservative uncertainty of ±0.2, the bolometric magnitude at maximum is estimated as −18.78 ± 0.2. The quasi bolometric LCs, estimated in a similar manner, for SN 1998bw, SN 2002ap, SN 2004aw and SN 1994I, are also plotted in Figure 5.18. The quasi bolometric LC of SN 2007ru is brighter than the other well studied non-GRB broad-line SN 2002ap and normal SNe Ic, and comparable to SN 1998bw. The decline in the bolometric LC of SN 2007ru is considerably faster than SN 1998bw and comparable to SN 2002ap.

Using Arnett's rule (Arnett 1982), the mass of ^{56}Ni required to power the quasi bolometric LC of SN 2007ru is estimated to be $0.33 M_{\odot}$, whereas it is $0.36 M_{\odot}$ for SN 1998bw (Figure 5.18). It is to be noted here that the contribution due to NIR bands is not included in the bolometric LC. The NIR contribution to bolometric flux for broad-line SNe 2002ap and 1998bw is $\sim$ 30% (2006ApJ...644..400T, Valenti et al. 2008, whereas for SN 1994I it is only $\sim$ 10%, while for SN 2004aw the NIR contribution increases from $\sim$ 31% to $\sim$ 45% between +10 and +30 days (Taubenberger et al. 2006). Assuming an NIR contribution to the bolometric flux similar to SNe 2002ap and 1998bw ($\sim$ 30%), the mass of ^{56}Ni for SN 2007ru is estimated to be $\sim$ 0.4 $M_{\odot}$. The total rate of energy production via ^{56}Ni

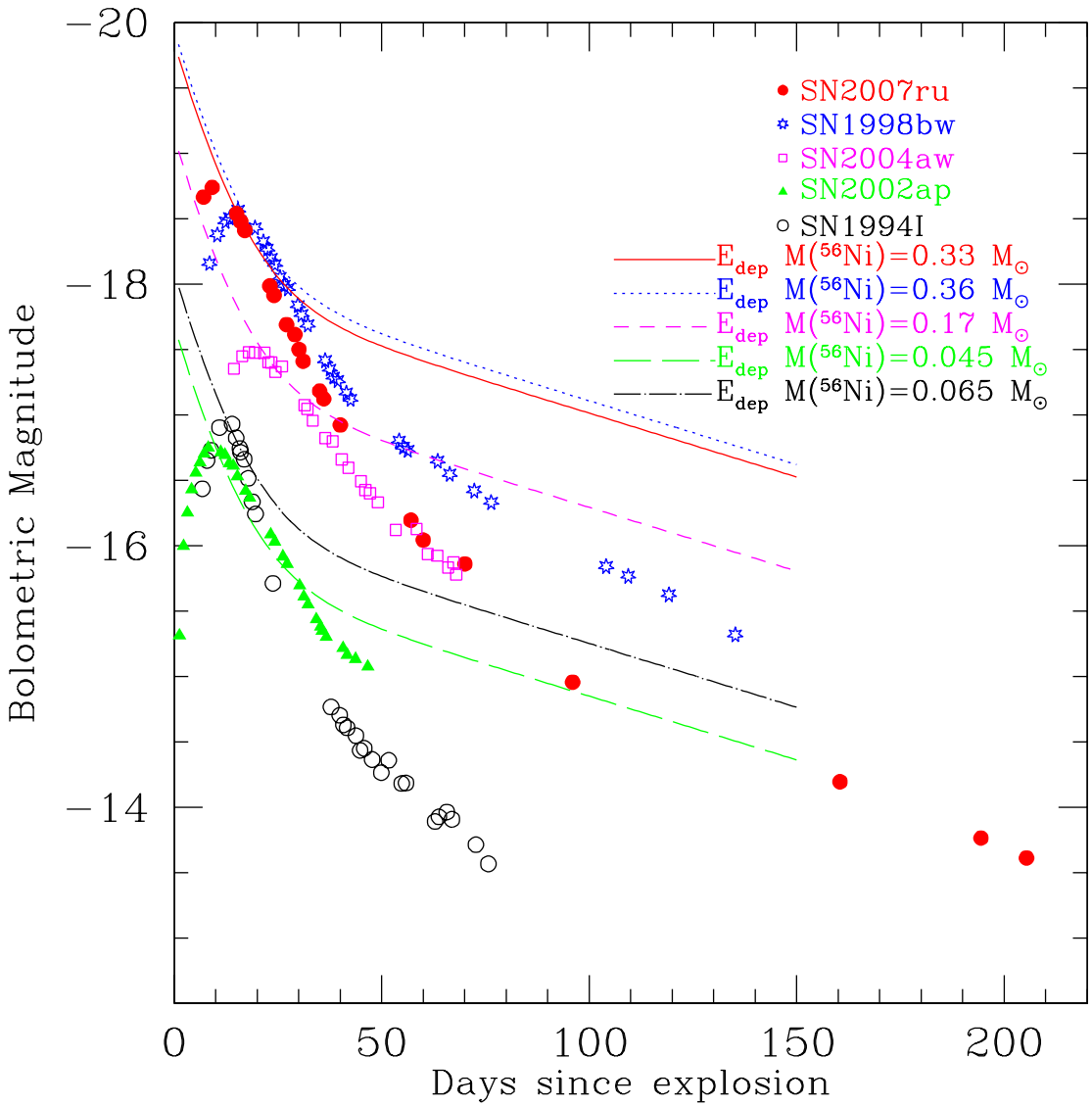

Figure 5.18: Quasi bolometric light curves of SN 2007ru, SN 1998bw, SN2002ap, SN1994I and SN 2004aw, estimated as explained in text. The lines represent the rate of energy production via ^{56}Ni $\rightarrow$ ^{56}Co chain for different values of $M(^{56}\mathrm{Ni})$.

$\rightarrow$ ^{56}Co chain estimated using the analytical formula by Nadyozhin (1994), for different values of mass of ^{56}Ni synthesized during the explosion and are plotted with the quasi bolometric LC (thin lines) in Figure 5.18. The plots indicate a good match of the energy production rate for $0.33 M_{\odot}$ of ^{56}Ni with the initial decline of the quasi-bolometric light curve of SN 2007ru, in agreement with the estimate based on Arnett's rule.

5.3.7 Properties of the host galaxy of SN 2007ru

The supernova region

An attempt is made to estimate the metallicity of the region where the supernova exploded, based on the observed [N II]/Hα flux ratio, from the underlying HII region, superimposed in the nebular spectrum of the supernova. Following Pettini & Pagel (2004), the N2 index (log[N II]/Hα) is estimated to be -0.36. Using this, an oxygen abundance of $12 + \log(O/H) = 8.78$ is derived. Another way of deriving oxygen abundance is using the $\log([N\ II]/H\alpha)$ diagnostic diagram (Kewley & Dopita 2002), which requires an estimate of the ionization parameter q or U ($U = q/c$; c is the speed of light) also. The ionization parameter U can be estimated from the [S II]/[S III] ratio following Diaz et al. (1991). The observed flux of [S II] lines $\lambda\lambda$ 6717, 6731 Å and [S III] line λ 9069 Å, seen in the nebular spectrum can be used to estimate the ionization parameter, however, our spectrum does not cover the [S III] λ 9532 Å region. In the extragalactic HII regions ratio ([S III]λ 9532/[S III]λ 9069 Å) is found to vary in the range 1.58 to 3.77 with an observed mean of 2.66±0.46, against the theoretical value of 2.44 (Diaz et al. 1985, Vilchez & Pagel 1988, Kennicutt & Garnett 1996) This indicates that the ionization parameter q can vary in the range $\sim 10^6$ to 3×10^6. Using the log([N II]/Hα) diagnostic diagram for the above estimated range of the ionization parameter, the oxygen abundance 12 + log(O/H) is found to lie close to 8.8, which is in good agreement with the independent estimate of 12 + log(O/H) = 8.78. This indicates the oxygen abundance in region where the supernova SN 2007ru occurred is close to solar.

In a recent study Modjaz et al. (2008a) have concluded that the broad-line supernovae associated with GRBs are generally found in metal poor environments as compared to the broad-line supernovae without GRBs. They have shown that, in their sample, the oxygen abundance $12 + \log(\mathrm{O/H})_{KD2} = 8.5$ can be treated as the boundary between galaxies that have GRBs associated supernovae and those without GRBs. The estimated oxygen abundance of ~ 8.8 at the location of SN 2007ru fits well in the range expected for a broad-line supernova without GRB.

The nuclear region

The nuclear spectrum of the host galaxy of SN 2007ru (obtained on 2008 October 29) is shown in Figure 5.19. The nuclear spectrum shows strong hydrogen lines of the Balmer series, permitted as well as forbidden lines of oxygen, lines due to helium and the calcium NIR triplet (refer Figure 5.19). The FWHM velocities of the lines indicate velocities of

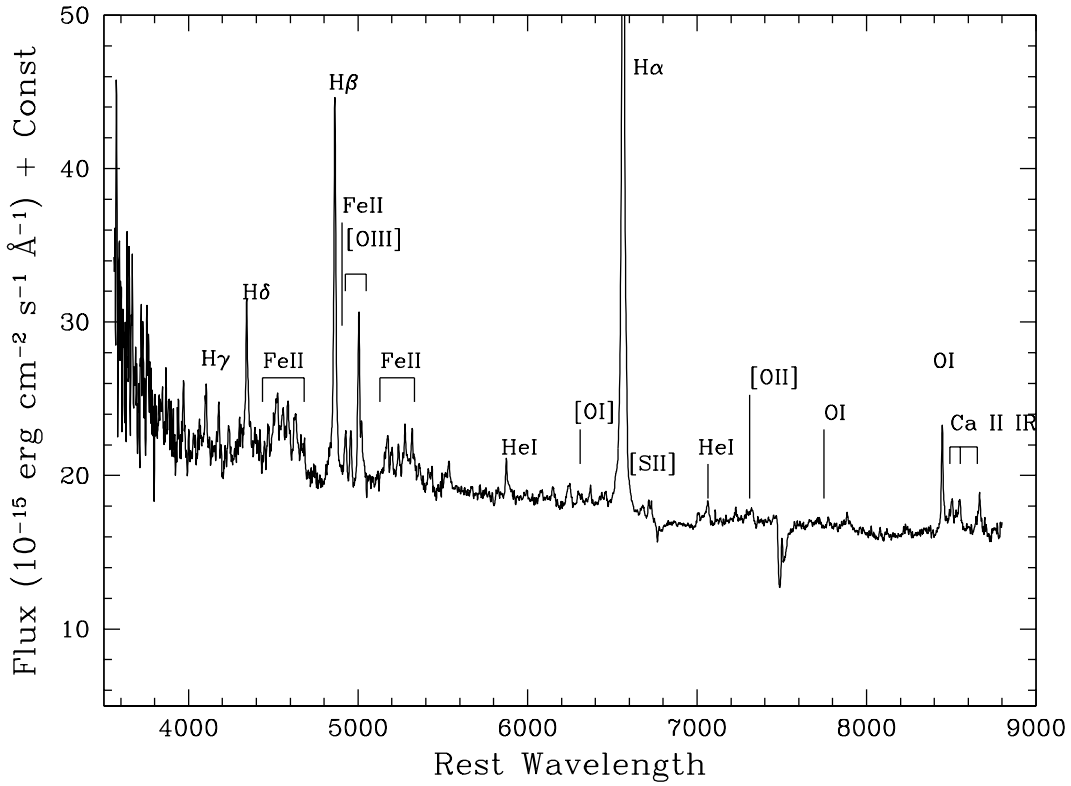

Figure 5.19: Nuclear spectrum of the host galaxy UGC 12381 of SN 2007ru.

the order of 500-700 km sec^{-1}. The hydrogen Balmer lines show broad wings, with a noticable asymmetry in the blue wing. Such broad wings are not seen in the forbidden lines. Another interesting feature of the nuclear spectrum of the host galaxy is the presence of numerous FeII lines seen at wavelengths λ 4400–4600 Å, 4924 Å, 5018 Å and λ 5100–5400 Å, similar to the spectra of Active Galactic Nuclei (Véron-Cetty et al. 2004, Véron-Cetty et al. 2006).

Using the diagnostic diagram (Ho et al. 1997) based on the line ratio $\log([O\ \textsc{iii}]\lambda\,5007/H\beta)$ versus $\log([O\ \textsc{i}]\lambda\,6300/H\alpha)$ and $\log([O\ \textsc{iii}]\lambda\,5007/H\beta)$ versus $\log([S\ \textsc{ii}]\lambda\lambda\,6717,6731/H\alpha)$

the nucleus of UGC 12381 can be classified as belonging to the HII region class, with very weak [S II] and [N II] lines.

It thus appears that the host galaxy of SN 2007ru probably hosts a mild AGN with a nuclear HII region, which needs further detailed study.

5.3.8 Discussion

The optical spectra of SN 2007ru presented here show broad spectral features similar to that seen in GRB-associated SN 1998bw, XRF-associated SN 2006aj and the broad-line SN 2003jd. The expansion velocity of the ejecta of SN 2007ru is higher than that of the normal SN Type Ic SN 1994I and SN 2006aj, but comparable to that of SN 1998bw and SN 2003jd.

The maximum luminosity of SN 2007ru is comparable to SN 1998bw. The light curve reaches a peak in only $\sim 8 \pm 3$ days, which is remarkably faster than in SN 1998bw (~ 20 days). The mass of ^{56}Ni ejected in SN 2007ru is estimated as $\sim 0.4 M_{\odot}$, which is similar to that estimated for SNe 1998bw and 2003jd, slightly larger than that for SN 2004aw, and much larger than that for the broad-line SNe 2002ap and 2006aj and the normal SN Type Ic 1994I (Table 5.8).

From the rise time of the light curve (τ) and the expansion velocity (v), we estimate mass of SN ejecta ($M_{\rm ej}$) and the kinetic energy of the ejecta ($E_{\rm K}$). If the opacity is assumed to be constant, the timescale of the light curve is expressed as $\tau \propto M_{ej}^{3/4} E_{\rm K}^{-1/4}$ (Arnett 1982). The expansion velocity is given by $v \propto M_{ej}^{-1/2} E_{\rm K}^{1/2}$. The rise time of SN 2007ru (8 ± 3 days) is comparable to that of the well studied SN 1994I, while the expansion velocity ($v = 20,000$ km sec^{-1} at maximum) is about twice. Assuming $M_{ej} = 1.0 M_{\odot}$ and $E_{\rm K} = 1.0 \times 10^{51}$ ergs for SN 1994I (see Table 5.8), and the observed expansion velocity of SN 2007ru, we estimate $M_{ej} = 1.3^{+1.1}_{-0.8} M_{\odot}$ and $E_{\rm K} = 5^{+4.7}_{-3.0} \times 10^{51}$ ergs for SN 2007ru. A similar analysis for SN 1998bw, assuming the rise time and the velocity of SN 1998bw to be twice that of SN 1994I, leads to $M_{ej} \approx 8 M_{\odot}$ and $E_{\rm K} \approx 30 \times 10^{51}$ergs, qualitatively consistent with the results of detailed modelling (Iwamoto et al. 1998, Nakamura et al. 2001) [†]. If we take SN 2003jd as a reference (Valenti et al. 2008), $M_{ej} = 1.7^{+1.5}_{-1.0} M_{\odot}$ and $E_{\rm K} = 8.6^{+7.2}_{-5.2} \times 10^{51}$ ergs are derived for SN 2007ru. It should however be noted, that a detailed modelling is required to derive accurate values of M_{ej} and E_K [‡].

[†]Given the very high $M_{\rm Ni}/M_{\rm ej}$ ratio (~ 0.3), the higher end of the ejecta mass may be preferred ($M_{ej} \sim 2.4 M_{\odot}$, and $E_{\rm K} \sim 9.7 \times 10^{51}$ erg). Since the explosion with a larger kinetic energy can produce a larger amount of ^{56}Ni, the large ^{56}Ni mass in SN 2007ru may also support this.

[‡]An attempt was made to estimate the mass of the ejecta M_{ej} and kinetic energy M_K using the width of the light curve. The width is defined as the time from peak of the bolometric light curve to the time when

SN 2007ru has a large kinetic energy while the ejecta mass is close to that of normal SNe Ic. Studies of SNe Type Ic (e.g. Nomoto et al. 2006a) have shown a trend, although weak, wherein SNe having massive ejecta tend to have a larger kinetic energy and eject more ^{56}Ni, connecting normal SNe to GRB-associated SNe. In contrast to this trend, SN 2007ru which resides at the higher energy end has a lower mass ejecta, leading to a higher E/M. SN 2007ru thus adds to the diversity of SNe Ic.

The spectroscopic properties of SN 2007ru at early phases are most similar to SN 2003jd. Also if we take the higher end of M_{ej}, the ejecta properties of SN 2007ru are also close to those of SN 2003jd (although the estimated E/M is higher for SN 2007ru). However, the [O I] line profiles in the nebular spectra are dissimilar. SN 2007ru shows a single peaked profile while SN 2003jd shows a double-peaked profile. In aspherical explosions, we would expect a single-peaked [O I] profile for the polar-viewed case, and a double-peaked profile for the side-viewed case (Mazzali et al. 2005; Maeda et al. 2008; Modjaz et al. 2008b). Also, the polar-viewed aspherical explosion tends to show a brighter peak (Maeda et al. 2006) and faster velocity (Tanaka et al. 2007). This matches with the properties of SN 2007ru. Thus, we suggest that SN 2007ru could be an aspherical explosion viewed from the polar direction. Detailed multidimensional modelling is required to answer if the high E/M derived for SN 2007ru results from the effect of asphericity.

The nebular spectrum of SN 2007ru shows narrow emission lines due to Hα, [N II], [S II] and [S III], arising from the underlying/neighbouring host galaxy HII region. The flux ratios indicate an oxygen abundance of $\sim$ 8.8 in the region of the supernova. The nearly solar oxygen abundance at the location of the supernova matches well with earlier abundance studies for supernova host galaxies.

The nuclear spectrum of the host galaxy of SN 2007ru shows broad hydrogen Balmer lines, with an asymmetric blue wing. Emission lines due to FeII are also fairly prominent. Low ionization emission lines are also present. It appears that the galaxy hosts a mild AGN with nuclear HII region.

the luminosity is equal to the $1/e$ times the peak luminosity, which is equivalent to a decline of 1.1 mag from peak. The derived width is $\sim$ 18 days for SN 2007ru. With this value, we have estimated M_{ej} and E_K in the same manner and derived larger values of M_{ej} and $E_{\rm K}$ ($M_{\rm ej} \sim 4.5 M_\odot$ and $E_{\rm K} \sim 20 \times 10^{51}$ erg). Our conclusion of large E/M is thus not affected.

Table 5.8: Comparison of parameters of SNe Ic

	M_V	Δm_{15}(V)	γ_V	γ_R	γ_I	$E_K/10^{51}$ergs	$M_{ej}/M_\odot$	$M_{Ni}/M_\odot$	E_K/M_{ej}	References
SN 1994I	−17.62	1.65	0.029	0.028	0.026	1	0.9–1	0.07(0.07)	∼ 1	1, 2, 3
SN 2004aw	−18.02	0.62	0.014	0.017	0.015	3.5–9.0	3.5–8.0	0.25–0.35(0.2)	∼ 1	4
SN 2003jd	−18.9	1.44	0.022	0.022	0.029	$7^{+3}_{-2.0}$	3.0±1.0	0.36	∼ 2.3	5
SN 2002ap	−17.35	0.87				4	2.5	0.1(0.06)	∼ 1.6	6, 7, 8
SN 2007ru	−19.06	0.92	0.021	0.028	0.030	$5^{+4.7}_{-3.0}$	$1.3^{+1.1}_{-0.8}$	0.4	∼ 3.8	This work
SN 1998bw	−19.13	0.75	0.020	0.022	0.022	30	10	0.40(0.5)	∼ 3	9, 10, 11
SN 2006aj	−18.7	1.14				2	2	0.21	∼ 1	12, 13

*M_{Ni} given in parenthesis are the values estimated using the Arnett's rule (including NIR contribution in the bolometric light curves, see text), γ represents the magnitude decline rates (mag/day) between 45 - 80 days (1) Richmond et al. 1996; (2) Nomoto et al. 1994; (3) Sauer et al. 2006; (4) Taubenberger et al. 2006; (5) Valenti et al. 2008; (6) Mazzali et al. 2007; (7) Foley et al. 2003; (8) Tomita et al. 2006; (9) Galama et al. 1998; (10) Iwamoto et al. 1998; (11) Nakamura et al. 2001; (12) Modjaz et al. 2006; (13) Mazzali et al. 2006

Table 5.9: Magnitudes for the sequence of secondary standard stars in the field of SN 2009jf.

ID	U	B	V	R	I
1	14.846 ± 0.063	14.717 ± 0.010	14.052 ± 0.019	13.639 ± 0.003	13.218 ± 0.016
2	16.260 ± 0.087	15.757 ± 0.006	14.878 ± 0.015	14.340 ± 0.011	13.834 ± 0.006
3	16.197 ± 0.079	15.885 ± 0.004	15.148 ± 0.024	14.739 ± 0.001	14.317 ± 0.013
4	16.366 ± 0.061	16.040 ± 0.005	15.289 ± 0.011	14.849 ± 0.010	14.421 ± 0.020
5	16.228 ± 0.082	16.156 ± 0.006	15.463 ± 0.023	15.061 ± 0.002	14.620 ± 0.012
6	19.942 ± 0.181	18.271 ± 0.010	16.915 ± 0.014	16.071 ± 0.005	15.320 ± 0.013
7	18.775 ± 0.096	17.387 ± 0.001	16.203 ± 0.017	15.475 ± 0.003	14.860 ± 0.016
8	17.128 ± 0.077	16.729 ± 0.004	15.939 ± 0.022	15.455 ± 0.000	14.996 ± 0.021
9	16.054 ± 0.059	15.350 ± 0.021	14.464 ± 0.030	13.958 ± 0.000	13.519 ± 0.019
10	16.446 ± 0.057	16.088 ± 0.005	15.266 ± 0.024	14.764 ± 0.004	14.264 ± 0.017
11	17.209 ± 0.094	17.182 ± 0.007	16.555 ± 0.015	16.139 ± 0.009	15.720 ± 0.012
12	15.440 ± 0.065	15.332 ± 0.010	14.659 ± 0.020	14.232 ± 0.005	13.791 ± 0.012

* The stars are identified in Figure 5.20.

5.4 Type Ib Supernova: SN 2009jf

5.4.1 Introduction

SN 2009jf was discovered by Li et al. (2009) in the Seyfert 2, barred spiral galaxy NGC 7479 on 2009 September 27.33. This supernova was classified as a young Type Ib supernova by Kasliwal et al. (2009), and Sahu et al. (2009a), based on early spectra obtained on 2009 September 29. Itagaki et al. (2009) reported the detection of a dim object at an unfiltered magnitude of $\sim$ 18.2 in an image obtained on 2006 November 8.499 and at a magnitude of $\sim$ 18.3 in an image obtained on 2007 August 13.74. They also report the presence of the object at $\sim$ 18 magnitude in the DSSS images. They have estimated the absolute magnitude of the object as -14.5 and suggested that these may be recurring outbursts of a luminous blue variable.

Photometric observations of SN 2009jf began on 2009 September 29, using the 2m Himalayan Chandra Telescope (HCT) of the Indian Astronomical Observatory, immediately after discovery, and continued until 2010 June 21, with a break during the period the supernova was behind the Sun. The supernova was observed in Bessell U, B, V, R and I filters. Standard fields PG0231+051, PG1657+078 and PG2213-006 (Landolt 1992) observed under photometric sky condition on 2008 September 30 and October 14, are used for photometric calibration of the supernova magnitudes. The magnitudes of the local standards in the supernova field are listed in Table 5.9 and the supernova field with the local standards marked is shown in Figure 5.20.

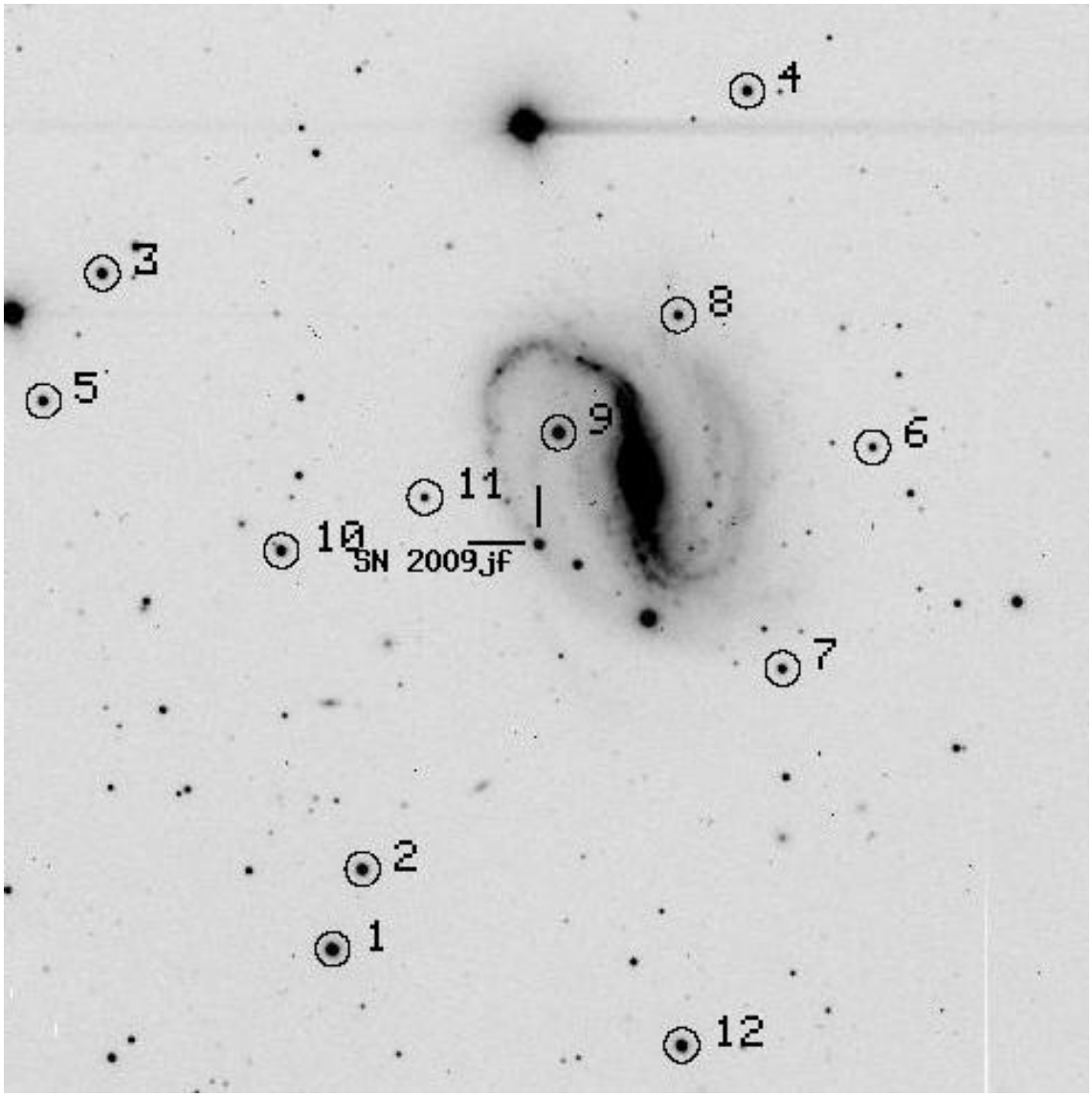

Figure 5.20: Identification chart for SN 2009jf. The stars used as local standards are marked with numbers 1-12. South is up and east to the right. The field of view is $10' \times 10'$.

Spectroscopic observations of SN 2009jf were obtained during 2009 September 29 (JD 2455104.16) and 2010 June 22 (JD 2455370.38). The log of spectroscopic observations is given in Table 5.10. The supernova spectra were corrected for the host galaxy redshift of $z = 0.007942$ and dereddened for a total reddening of $E(B-V) = 0.112$, as estimated in Section 5.4.3. The telluric lines have not been removed from the spectra.

Table 5.10: Log of spectroscopic observations of SN 2009jf.

Date	J.D. 2450000+	Phase* days	Range Å
29/09/2009	5104.16	-15.30	3500-7800; 5200-9250
30/09/2009	5105.13	-14.33	3500-7800; 5200-9250
01/10/2009	5106.17	-13.29	3500-7800; 5200-9250
07/10/2009	5112.09	-7.37	3500-7800; 5200-9250
08/10/2009	5113.07	-6.39	3500-7800; 5200-9250
15/10/2009	5120.17	+0.71	3500-7800; 5200-9250
24/10/2009	5129.22	+9.76	3500-7800; 5200-9250
10/11/2009	5146.19	+26.73	3500-7800; 5200-9250
17/11/2009	5153.17	+33.71	3500-7800; 5200-9250
03/12/2009	5169.17	+49.71	3500-7800; 5200-9250
23/12/2009	5189.06	+69.60	3500-7800; 5200-9250
08/01/2010	5205.04	+85.58	3500-7800; 5200-9250
21/01/2010	5218.07	+98.61	3500-7800; 5200-9250
31/05/2010	5348.40	+228.94	5200-9250
22/06/2010	5370.38	+250.92	5200-9250

* Observed phase with respect to the epoch of maximum in the *B* band (JD 2455119.46).

5.4.2 Optical light curves and colour curves

The supernova magnitudes in U, B, V, R and I bands are given in Table 5.11. The light curves of SN 2009jf in the $UBVRI$ bands are presented in Figure 5.21. Also included in the figure are the unfiltered discovery magnitude and the pre-discovery limiting magnitudes (Li et al. 2009). Our observations began two days after discovery, $\sim$ 15 days before maximum in B band and continued till $\sim$ 250 days after maximum. The date of maximum brightness and the peak magnitude in the different bands have been estimated by fitting a cubic spline to the points around maximum and are listed in Table 5.12. Similar to other type Ib/c supernovae, the light curve of SN 2009jf peaks early in the bluer bands than the redder bands. The maximum in B occurred on JD 2455119.46 (2009 October 14.9), at an apparent magnitude of 15.56 ± 0.02.

The light curves of SN 2009jf are compared with those of a few well studied core-collapse supernovae, namely, SN 2008D (Modjaz et al. 2009), SN 2007Y (Stritzinger et al. 2009), SN 1999ex (Stritzinger et al. 2002), SN 1990I (Elmhamdi et al. 2004), broad lined Type Ic SN 1998bw and the fast declining broad-line Type Ic SN 2007ru (Sahu et al. 2009b), in Figure 5.22. The observed magnitudes of the supernovae have been normalized to their respective peak magnitudes and shifted in time to the epoch of maximum

brightness in B band. From the figure, it is seen that the initial rise to maximum and post-maximum decline of SN 2009jf is slower in comparison with other supernovae, making the light curve of SN 2009jf broader. The post-maximum decline of the light curve in 15 days *i.e.* Δm_{15} estimated for different bands are $\Delta m_{15}(U) = 0.971$, $\Delta m_{15}(B) = 0.908$, $\Delta m_{15}(V) = 0.503$, $\Delta m_{15}(R) = 0.311$ and $\Delta m_{15}(I) = 0.303$. These estimates indicate the decline rate in V to be similar to that of SN 2008D, but considerably slower than other type Ib and type Ic supernovae.

Table 5.11: Photometric observations of SN 2009jf.

Date	J.D. 2454000+	Phase* (days)	U	B	V	R	I
29/09/2009	2455104.171	−15.29	17.557 ± 0.030	17.622 ± 0.020	17.047 ± 0.019	16.733 ± 0.024	16.578 ± 0.027
30/09/2009	2455105.173	−14.29	17.168 ± 0.067	17.275 ± 0.026	16.739 ± 0.023	16.443 ± 0.016	16.317 ± 0.016
01/10/2009	2455106.104	−13.36	16.945 ± 0.033	16.990 ± 0.037	16.508 ± 0.025	16.219 ± 0.026	16.077 ± 0.019
03/10/2009	2455108.261	−11.20		16.441 ± 0.032	16.001 ± 0.038	15.774 ± 0.031	15.594 ± 0.032
04/10/2009	2455109.194	−10.27	16.078 ± 0.040	16.275 ± 0.035	15.842 ± 0.034	15.611 ± 0.032	15.458 ± 0.028
08/10/2009	2455113.119	−6.34	15.572 ± 0.043	15.752 ± 0.032	15.365 ± 0.012	15.159 ± 0.013	14.980 ± 0.026
14/10/2009	2455119.308	−0.15	15.582 ± 0.042	15.594 ± 0.021	15.092 ± 0.011	14.857 ± 0.015	14.643 ± 0.010
15/10/2009	2455120.120	+0.66	15.517 ± 0.028	15.575 ± 0.025	15.078 ± 0.019	14.826 ± 0.024	14.638 ± 0.020
16/10/2009	2455121.313	+1.85	15.580 ± 0.044	15.618 ± 0.027	15.082 ± 0.014	14.816 ± 0.015	14.600 ± 0.037
22/10/2009	2455127.171	+7.71	15.992 ± 0.035	15.855 ± 0.011	15.136 ± 0.009	14.832 ± 0.020	14.588 ± 0.025
24/10/2009	2455129.265	+9.81	16.153 ± 0.030	15.988 ± 0.016	15.186 ± 0.020	14.864 ± 0.023	14.597 ± 0.025
27/10/2009	2455132.288	+12.83	16.574 ± 0.039	16.277 ± 0.028	15.318 ± 0.024	14.950 ± 0.034	14.649 ± 0.038
31/10/2009	2455136.187	+16.73		16.687 ± 0.027	15.604 ± 0.029	15.132 ± 0.024	14.777 ± 0.021
06/11/2009	2455142.047	+22.59		17.118 ± 0.018	15.933 ± 0.021	15.403 ± 0.021	15.024 ± 0.044
10/11/2009	2455146.146	+26.69	17.534 ± 0.056	17.291 ± 0.018	16.108 ± 0.019	15.565 ± 0.013	15.138 ± 0.043
14/11/2009	2455150.057	+30.60	17.598 ± 0.087	17.421 ± 0.031	16.268 ± 0.012	15.720 ± 0.020	15.246 ± 0.014
17/11/2009	2455153.156	+33.70		17.454 ± 0.013	16.353 ± 0.022	15.823 ± 0.017	15.328 ± 0.029
21/11/2009	2455157.21	+37.75		17.547 ± 0.020	16.455 ± 0.017	15.946 ± 0.021	15.439 ± 0.019
25/11/2009	2455161.048	+41.59		17.603 ± 0.025	16.510 ± 0.032	16.026 ± 0.031	15.537 ± 0.034
30/11/2009	2455166.188	+46.73		17.647 ± 0.032	16.594 ± 0.034	16.116 ± 0.024	15.596 ± 0.017
03/12/2009	2455169.030	+49.57		17.654 ± 0.031	16.624 ± 0.014	16.173 ± 0.032	15.653 ± 0.031
18/12/2009	2455184.040	+64.58		17.751 ± 0.020	16.815 ± 0.020	16.393 ± 0.016	15.855 ± 0.023
23/12/2009	2455189.036	+69.58		17.812 ± 0.033	16.890 ± 0.017	16.478 ± 0.025	15.964 ± 0.029
29/12/2009	2455195.151	+75.69		17.847 ± 0.024	16.947 ± 0.028	16.541 ± 0.012	16.061 ± 0.045
09/01/2010	2455206.041	+86.58		17.887 ± 0.022	17.079 ± 0.021	16.692 ± 0.022	16.213 ± 0.043
20/01/2010	2455217.073	+97.61		18.003 ± 0.020	17.203 ± 0.019	16.819 ± 0.016	16.326 ± 0.016
27/01/2010	2455224.073	+104.61		18.151 ± 0.040	17.295 ± 0.036	16.946 ± 0.012	16.464 ± 0.020
01/02/2010	2455229.071	+109.61		18.181 ± 0.049	17.410 ± 0.019	17.011 ± 0.014	16.563 ± 0.016
01/05/2010	2455318.442	+198.98			18.524 ± 0.038	17.979 ± 0.025	17.785 ± 0.033
24/05/2010	2455341.418	+221.96		19.212 ± 0.046	18.753 ± 0.024	18.126 ± 0.022	18.013 ± 0.039
26/05/2010	2455343.406	+223.95		19.296 ± 0.029	18.808 ± 0.031	18.177 ± 0.052	18.019 ± 0.051
11/06/2010	2455359.430	+239.97		19.456 ± 0.034	19.075 ± 0.032	18.427 ± 0.036	18.336 ± 0.038
21/06/2010	2455369.353	+249.89		19.462 ± 0.028	19.109 ± 0.026	18.539 ± 0.026	18.373 ± 0.034

* Observed phase with respect to the epoch of maximum in the *B* band (JD 2455119.46).

Table 5.12: Light curve maximum parameters

Filter	J.D. at max. 2455000+	Peak obs mag.	Peak abs mag.
U	116.60±0.65	15.458±0.014	-17.759±0.19
B	119.46±0.50	15.558±0.020	-17.579±0.19
V	120.98±0.48	15.056±0.022	-17.964±0.19
R	121.44±1.03	14.813±0.032	-18.121±0.19
I	124.10±0.60	14.586±0.010	-18.253±0.19

The decline rates estimated for the later phases (> 40 days) are 0.008 day^{-1} in B, 0.0126 mag day^{-1} in V, 0.0141 mag day^{-1} in R and 0.0145 mag day^{-1} in I. These rates are slower in comparison with other type Ib supernovae. The broader light curves and slower decline rates suggest that the ejecta of SN 2009jf is relatively efficient in trapping the γ-rays produced in the radioactive decay. This also indicates that the progenitor of SN 2009jf was able to retain more of an envelope prior to the core-collapse, thus increasing the diffusion time for the energy produced from the radio active decay of ^{56}Ni to ^{56}Co (Stritzinger et al. 2002, Arnett 1982).

There are only a few cases of Type Ib supernovae where the rise time to B band maximum is constrained somewhat accurately. For example, the rise time for SN 1999ex and SN 2008D is found to be 18 days (Stritzinger et al. 2002) and 16.8 days (Modjaz et al. 2009), respectively. The rise time could be constrained for these two supernovae as they occurred in galaxies which were already being monitored to follow up other events. SN 1999ex was detected in IC 5179 which hosted SN 1999ee (Martin et al. 1999). The data obtained as a part of monitoring of SN 1999ee had the detection of the initial shock breakout due to SN 1999ex. Similarly, the shock breakout of SN 2008D was detected by the *Swift* satellite, as an X-ray transient XRT 080109, during a routine follow up observation of SN 2007uy in NGC 2770 (Berger & Soderberg 2008). The peak of the X-ray transient is expected to occur shortly after the supernova explosion (Li 2007). SN 2009jf was discovered on September 27.33, around 17.5 days before maximum in B band. Comparing with SN 1999ex and SN 2008D, it appears that SN 2009jf was most likely discovered almost immediately after explosion. However, since we are unable to constrain the shock breakout precisely, a rise time of 18 days is assumed in this work.

The colour evolution of SN 2009jf is plotted in Figure 5.23. The colour curves of SN 2008D, SN 2007Y and SN 1999ex are also included in the figure for comparison. The colour curves have been corrected for total reddening values of $E(B-V)$ of 0.112 for SN 2009jf, 0.65 for SN 2008D (Mazzali et al. 2008), 0.112 for SN 2007Y (Stritzinger et al.

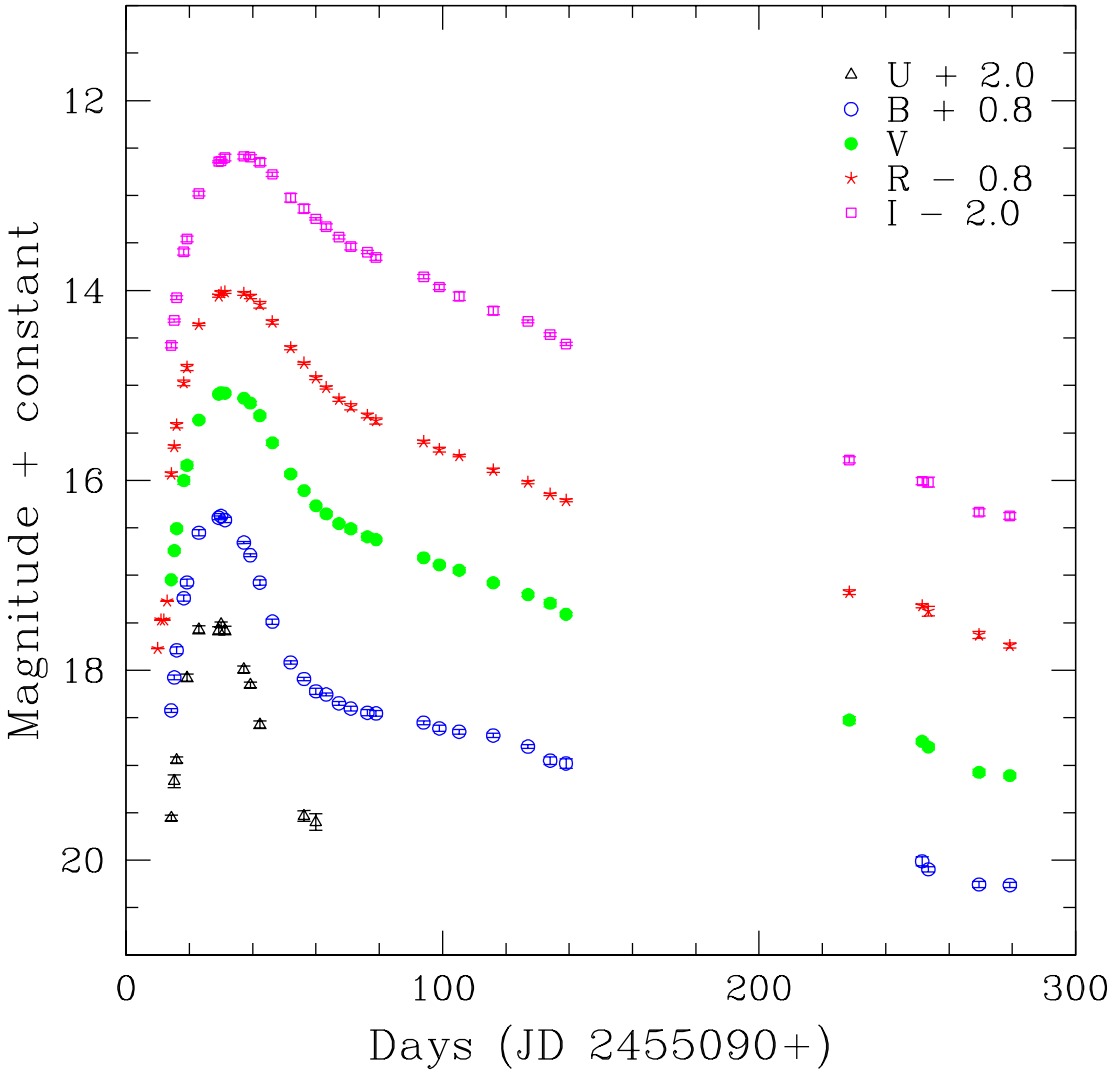

Figure 5.21: *UBVRI* light curves of SN 2009jf. The light curves have been shifted by the amount indicated in the legend.

2009) and 0.3 for SN 1999ex (Stritzinger et al. 2002). The reported magnitudes of SN 2007Y are in the u', g', B, V, r' and i' bands. These magnitudes have been transformed to the *UBVRI* system using transformation equations given in Jester et al. (2005). The $(U-B)$, $(B-V)$ and $(V-R)$ colour curves of SN 2009jf evolve from red to blue in the pre-maximum epoch. This colour change can be attributed to an increase in the photospheric temperature with brightening of the supernova in the pre-maximum phase. The $(B-V)$ colour attains a value of 0.25 mag at $\sim$ 5 days before maximum in B band, after that it monotonically becomes redder till $\sim$ 20 days after B maximum, indicating cooling due

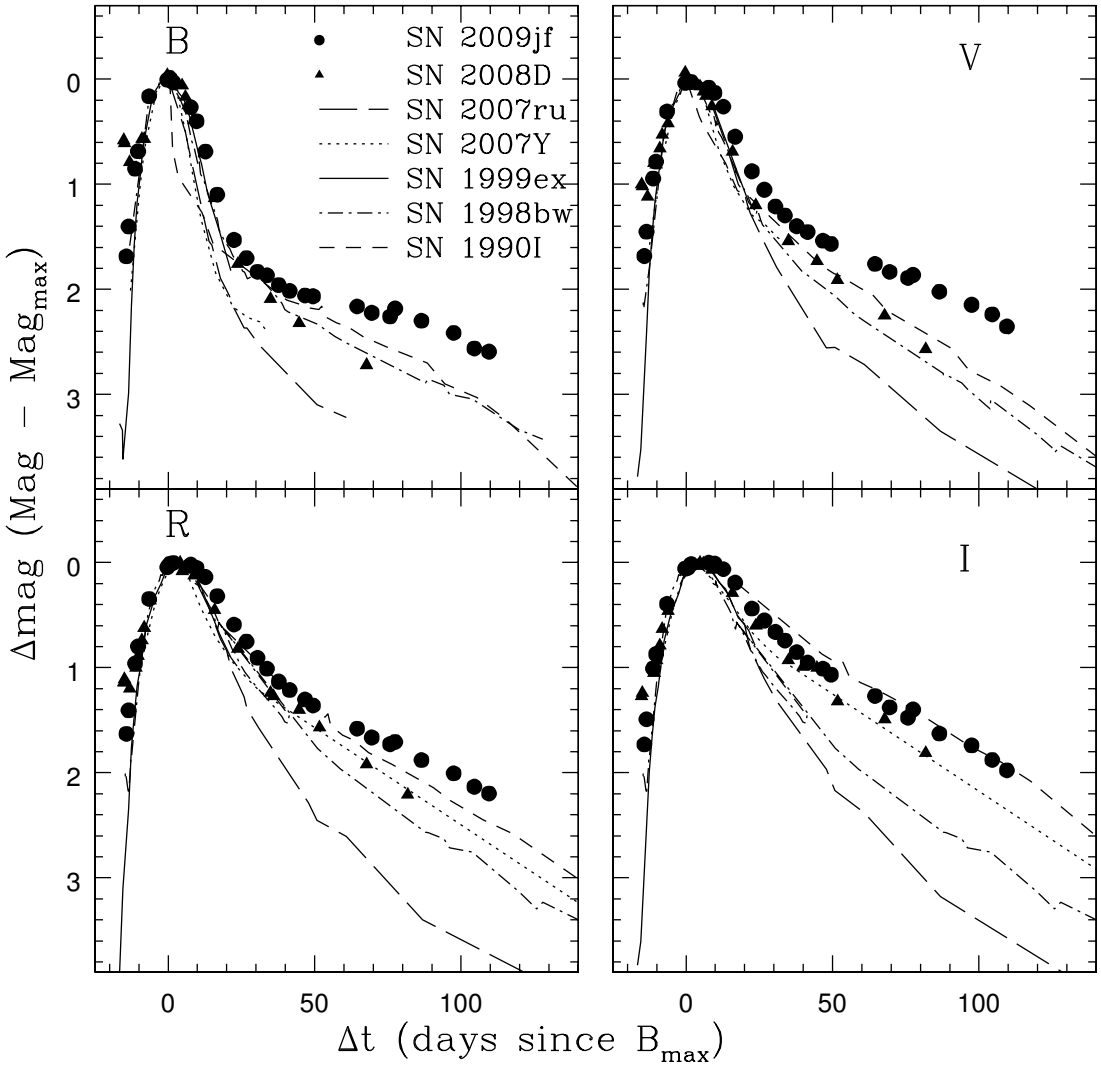

Figure 5.22: Comparison of *UBVRI* light curves of SN 2009jf with those of SN 2008D, SN 2007Y, SN 1999ex, SN 1990I, SN 1998bw and SN 2007ru. The light curves have been normalized as described in the text.

to envelope expansion. It again starts becoming blue at later epochs. The $(V - R)$ colour follows a similar trend, while the $(R - I)$ colour evolves towards red monotoically. The $(B - V)$ and $(V - R)$ colour evolution of SN 2009jf is quite similar to that of SN 1999ex, while the $(U - B)$ colour is always bluer and the $(R - I)$ colour redder than SN 1999ex. While SN 2009jf is redder than both SN 2007Y and SN 2008D in the pre-maximum epoch, the post maximum colour evolution is similar in all three SNe, except for the $(U - B)$ colour, which remains bluer in SN 2009jf.

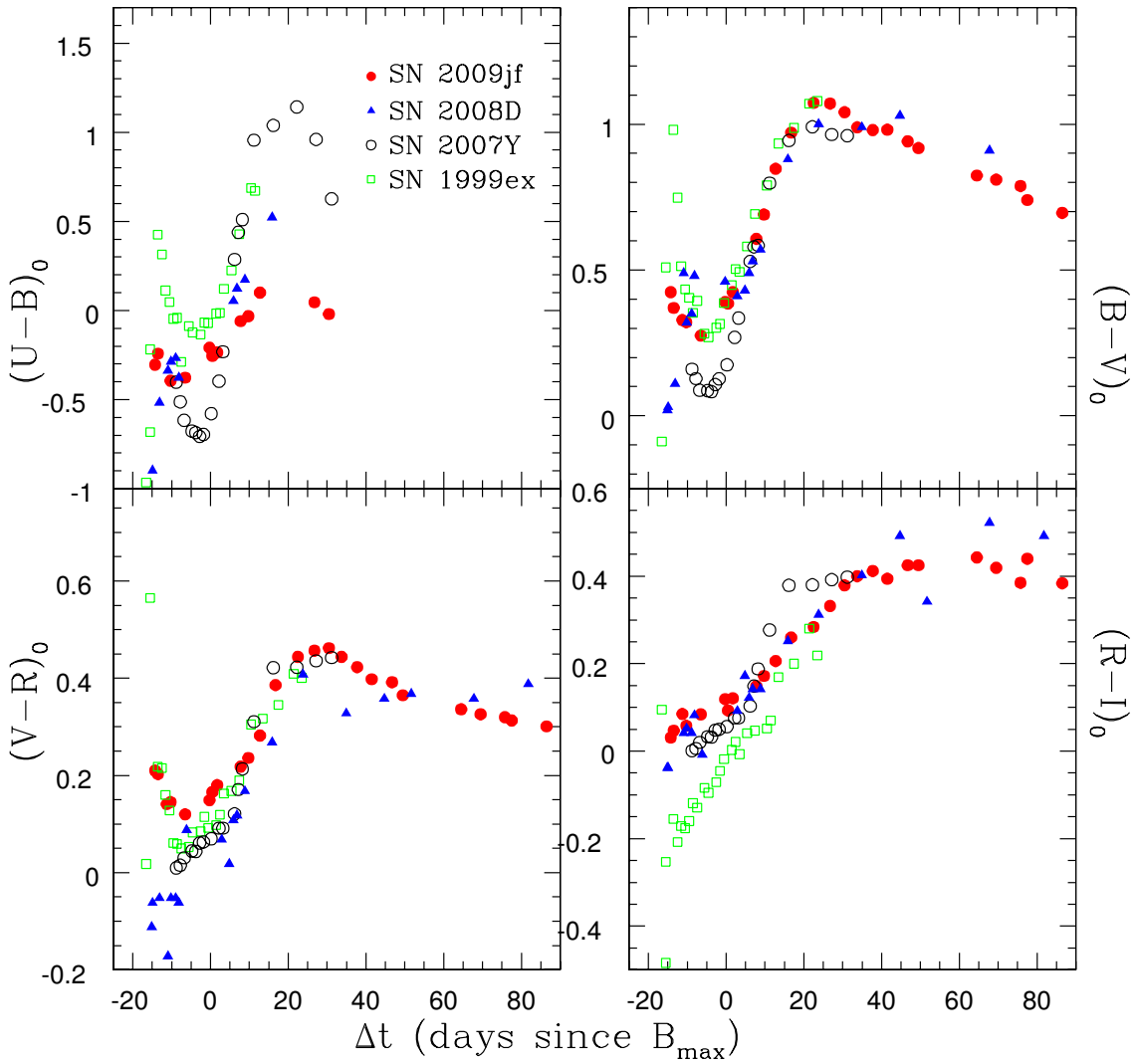

Figure 5.23: $(U-B)$, $(B-V)$, $(V-R)$ and $(R-I)$ colour curves of SN 2009jf compared with those of SN 2008D, SN 2007Y and SN 1999ex.

5.4.3 Distance and Reddening

SN 2009jf is located at 54 ″ west and 37 ″ north of the nucleus of NGC 7479, at the edge of the outer arm of the host galaxy. From the infrared dust maps of Schlegel et al. (1998), the Galactic interstellar reddening in the direction of NGC 7479 is $E(B-V)_{\rm Gal} = 0.112$ mag. The spectrum of SN 2009jf obtained close to maximum light shows the presence of weak Na ID absorption from the Milky Way. We do not detect any Na ID absorption due to the host galaxy. The low reddening of the supernova is also evident from its optical

colours (see Figure 5.23). We therefore conclude there is no additional extinction due to the host galaxy and use a value of $E_(B-V) = 0.112$ mag for extinction correction.

The radial velocity of NGC 7479, corrected for Local Group infall onto the Virgo Cluster is 2443 km s^{-1} (LEDA), which implies a distance modulus of 32.70 ± 0.18 for an H_0 value of 71±6 km s^{-1} Mpc^{-1}. This leads to a distance of 34.66 ± 2.9 Mpc for NGC 7479. The errors in distance modulus and distance are estimated taking into account the uncertainty in H_0. The redshift independent distance estimate using Tully-Fisher relation is 33.85 ± 3.1 (NED), which is in close agreement with the distance estimates using the radial velocity. We use the mean of the two estimates, 34.25 ± 4.2 Mpc as the distance to NGC 7479 for further analysis.

5.4.4 Absolute magnitude, bolometric light curve and mass of ^{56}Ni

The absolute peak magnitudes estimated using a distance of 34.25 Mpc and a reddening correction for an $E(B-V)$ of 0.112 mag are listed in Table 5.12. The errors in the absolute magnitudes have been estimated using uncertainties in the peak magnitude and the distance modulus of the host galaxy. Comparing the absolute magnitude of SN 2009jf with the absolute magnitude distribution of other SNe Type Ib (Richardson et al. (2006) and references therein), SN2009jf lies close to the mean of the distribution. It is fainter than the extremely luminous Type Ib supernova SN 1991D (Benetti et al. 2002), and comparable in brightness to SN 1984L, SN1990I (Elmhamdi et al. 2004), SN1999ex (Stritzinger et al. 2002, Hamuy et al. 2002) and SN 2000H (Krisciunas & Rest 2000). SN 2009jf is ∼ 1.5 magnitude brighter than SN 2007Y (Stritzinger et al. 2009) and ∼ 1 magnitude brighter than SN 2008D, which was associated with the X-ray transient 080909 (Modjaz et al. 2009).

The quasi-bolometric light curve of SN 2009jf is estimated using the reddening corrected $UBVRI$ magnitudes presented here. The reddening corrected magnitudes were converted to monochromatic fluxes using the zero points from Bessell et al. (1998). The quasi-bolometric fluxes were derived by fitting a spline curve to the U, B, V, R and I fluxes and integrating over the wavelength range 3100 Å to 1.06μm, determined by the response of the filters used. There are a few missing magnitudes in the U band light curve, which were estimated by interpolating between the neighbouring points. The quasi-bolometric light curve of SN 2009jf plotted in Figure 5.24 is compared with the bolometric light curves of type Ib supernovae SN 2008D, SN 2007Y, SN 1999ex and the type Ic supernova SN 1994I, also plotted in the figure. The bolometric light curves of supernovae SN 2008D, SN 2007Y, SN 1999ex and SN 1994I were constructed in a manner similar to

SN 2009jf. The bolometric light curve of SN 2007Y (Stritzinger et al. 2009), SN 1999ex (Stritzinger et al. 2002) and SN 1994I (Richmond et al. 1996) are based on the published *UBVRI* magnitudes, while the bolometric light curve of SN 2008D includes the *Swift* UVOT (U-band) and NIR data also (Tanaka et al. 2009). The bolometric light curve of SN 1998bw is taken from Patat et al. (2001) which includes optical and NIR data. A total reddening $E(B-V)$ of 0.45, 0.3, 0.11, 0.65, 0.06 mag and, distances of 8.32, 48.31, 19.31 31.0 and 37.8 Mpc were adopted for SN 1994I, SN 1999ex, SN 2007Y, SN 2008D and SN 1998bw, respectively.

The bolometric light curve of SN 2009jf is fainter than SN 1998bw and brighter than all other Type Ib/c supernovae in comparison. Adding a conservative uncertainty of ±0.2, mainly due to the uncertainty in H_0, the peak bolometric magnitude for SN 2009jf is estimated as -17.48 ± 0.2 mag, which is $\sim$ 1.4 magnitude brighter than SN 2007Y and $\sim$ 0.4 magnitude brighter than SN 1999ex. The contribution of NIR and UV fluxes to the bolometric flux for Type Ib/c supernovae is not well constrained. For SN 2007Y Stritzinger et al. (2009) have estimated that close to the peak brightness, $\sim$ 70% of the flux is in the optical bands, $\sim$ 25% in the UV bands and $\sim$ 5% in the NIR bands. However, by two weeks past maximum the UV contribution comes down to $<$ 10% and NIR contribution rises up to $\sim$ 20%. In the case of SN 2008D, the bolometric flux has an NIR contribution of about $<$ 24% at $\sim$ 12 days after maximum light in *V* (Modjaz et al. 2009). Thus, the UV and NIR bands, together, contribute as much as $\sim$ 30% to the bolometric flux. Even without considering the UV and NIR contribution to the bolometric light curve, it is seen that SN 2009jf is 0.6 magnitude brighter than SN 2008D at peak. Further, as seen in the *UBVRI* light curves, the decline rate of bolometric light curve of SN 2009jf is slower than other supernovae in comparison. While the initial decline rate of SN 2009jf is comparable to SN 2008D, it is much slowler than SN 2008D in the later phases. The slope of the bolometric light curve $\sim$ 45 days after *B* maximum is found to be 0.013 mag day^{-1}. For SN 2008D the same quantity is 0.023 mag day^{-1}.

The mass of ^{56}Ni synthesized during explosion can be estimated using the peak bolometric flux, following Arnett's law (Arnett 1982). The peak *UBVRI* bolometric flux for SN 2009jf is 2.99×10^{42} erg s^{-1}. Assuming a rise time of 18 days, the mass of ^{56}Ni is estimated to be 0.15 $M_\odot$ for SN 2009jf. If we assume the UV and NIR bands contribute a total of 30% to the bolometric luminosity, the mass of ^{56}Ni required to power the peak bolometric flux would be 0.20 $M_\odot$.

Another way for estimating mass of ^{56}Ni synthesized during the explosion is to fit the energy deposition rate via ^{56}Ni $\rightarrow$ ^{56}Co chain, to the observed bolometric light curve.

The total rate of energy production via ^{56}Ni $\rightarrow$ ^{56}Co chain estimated using the analytical formula by Nadyozhin (1994), for different values of mass of ^{56}Ni synthesized during the explosion is plotted with the bolometric light curves in Figure 5.24. The energy deposition rate corresponding to ^{56}Ni mass of 0.18 $M_\odot$ fits the initial decline of the quasi-bolometric light curve of SN 2009jf. If contribution due to UV and NIR bands is also included in the bolometric flux, the energy production rate corresponding to 0.22 $M_\odot$ of ^{56}Ni fits the initial decline of bolometric light curve well. The mass of ^{56}Ni estimated using Arnett's law and the energy deposition rate are in good agreement with each other.

5.4.5 Spectral evolution

Our spectroscopic observations began 15 days before *B* maximum and continued till 99 days after *B* maximum, when the object went in solar conjunction. Subsequently, two spectra were obtained in the nebular phase, at 229 days and 251 days after *B* maximum.

Early phase

The spectral evolution of SN 2009jf is plotted in Figure 5.25. Our first spectrum is one of the earliest spectrum for type Ib supernovae, along with SN 2007Y (Stritzinger et al. 2009) and SN 2008D (Modjaz et al. 2009). All spectra have been corrected for the heliocentric velocity 2381 km sec^{-1} of the host galaxy.

The pre-maximum spectra of SN 2009jf are plotted in the upper panel of Figure 5.25. These spectra are characterized by a broad P-Cygni profile, indicative of high expansion velocity of the ejecta. The first spectrum taken on JD 2455104.16 (15 days before *B* maximum) shows distinctive broad absorption due to He I 5876 Å with an expansion velocity of $\sim$ 16 300 km sec^{-1} and possible contribution from Na ID λ 5890, 5896 Å. The other well developed features seen in the first spectrum are due to Ca II H & K 3934, 3968 Å, Fe I between 4100 to 5000 Å, Si II/Hα at $\sim$ 6250 Å, O I 7774 Å and Ca II NIR triplet between 8000 and 9000 Å. Clear signature of other He II lines 4471 Å (possibly blended with Fe II 4924 Å and Mg II 4481 Å), 5015, 6678 and 7065 Å is present in the spectrum taken $\sim$ 13 days before *B* maximum. The He I 7065 Å line is affected by the telluric H_2O band. The first spectrum also shows the double absorption, the "W" feature, at $\sim$ 4000 Å seen in the very early spectra of the Type II supernova SN 2005ap (Quimby et al. 2007), the Type Ib supernova SN 2008D (Modjaz et al. 2009) and the Type IIb supernova SN 2001ig (Silverman et al. 2009). This feature is identified as a combination of C III, N III and O III lines at high velocities (Modjaz et al. 2009, Silverman et al.

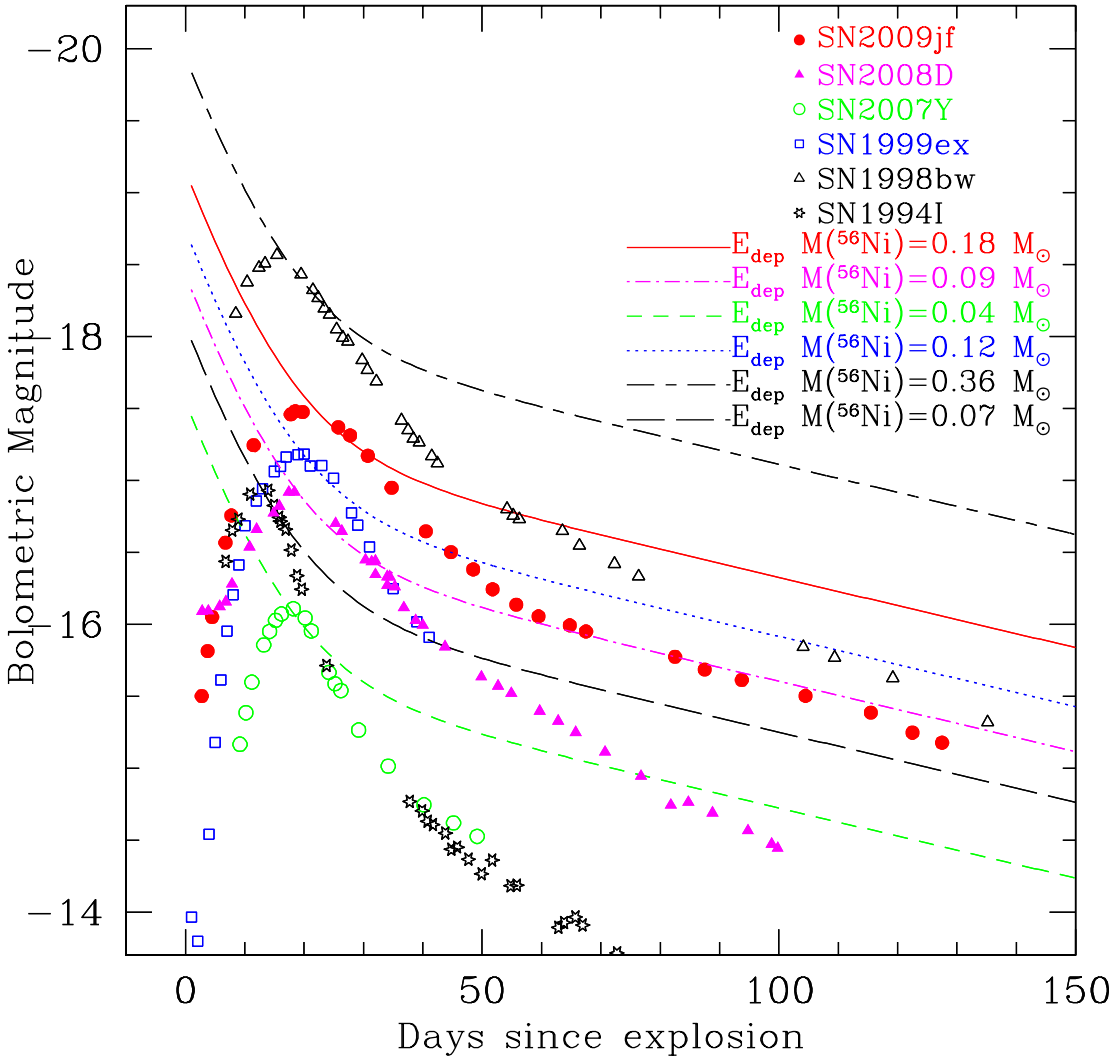

Figure 5.24: Bolometric light curve of SN 2009jf. Also plotted in the figure, for comparison, are the bolometric light curves of SN 2008D, SN 1999ex, SN 1998bw, SN 2007Y and SN 1994I. The continuous curves correspond to the rate of energy production for different masses of ^{56}Ni synthesized during the explosion, based on the analytical formulation by Nadyozhin (1994)

.

2009). The continuum becomes bluer as the supernova evolves towards maximum, as also indicated by colour curves (Figure 5.23).

The pre-maximum spectra of SN 2009jf are compared with those of SN 2007Y and SN 2008D at similar epochs and shown in Figure 5.26. The spectrum of SN 2009jf at 15

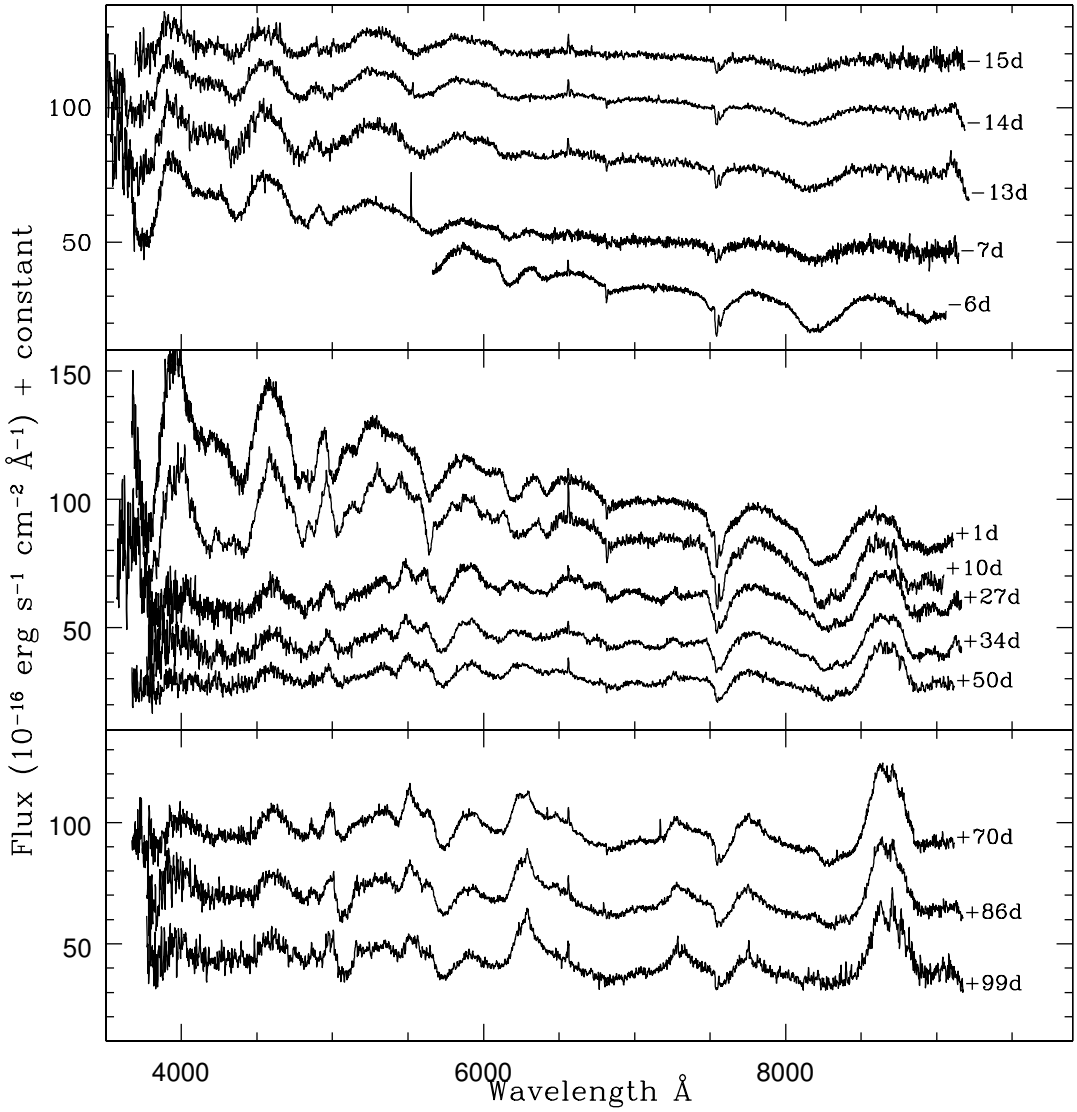

Figure 5.25: Spectral evolution of SN 2009jf during -15 to +99 days with respect to maximum in *B* band.

days before *B* maximum (top panel), shows well developed absorptions at 4100–5500 Å due to Fe II and He II 5876 Å. In comparison, SN 2008D shows a nearly featureless spectrum around the same time. While the Fe II features are clearly identifiable in SN 2007Y, the He II 5876 Å feature is absent. The spectra of SN 2009jf and SN 2007Y at ∼ 7 days before *B* maximum (lower panel) are very similar, except for the differences in the expansion velocities, while in SN 2008D, lines due to He I are identified, but Fe II lines are still not well developed.

The post-maximum spectra are shown in the middle and lower panels of Figure 5.25.

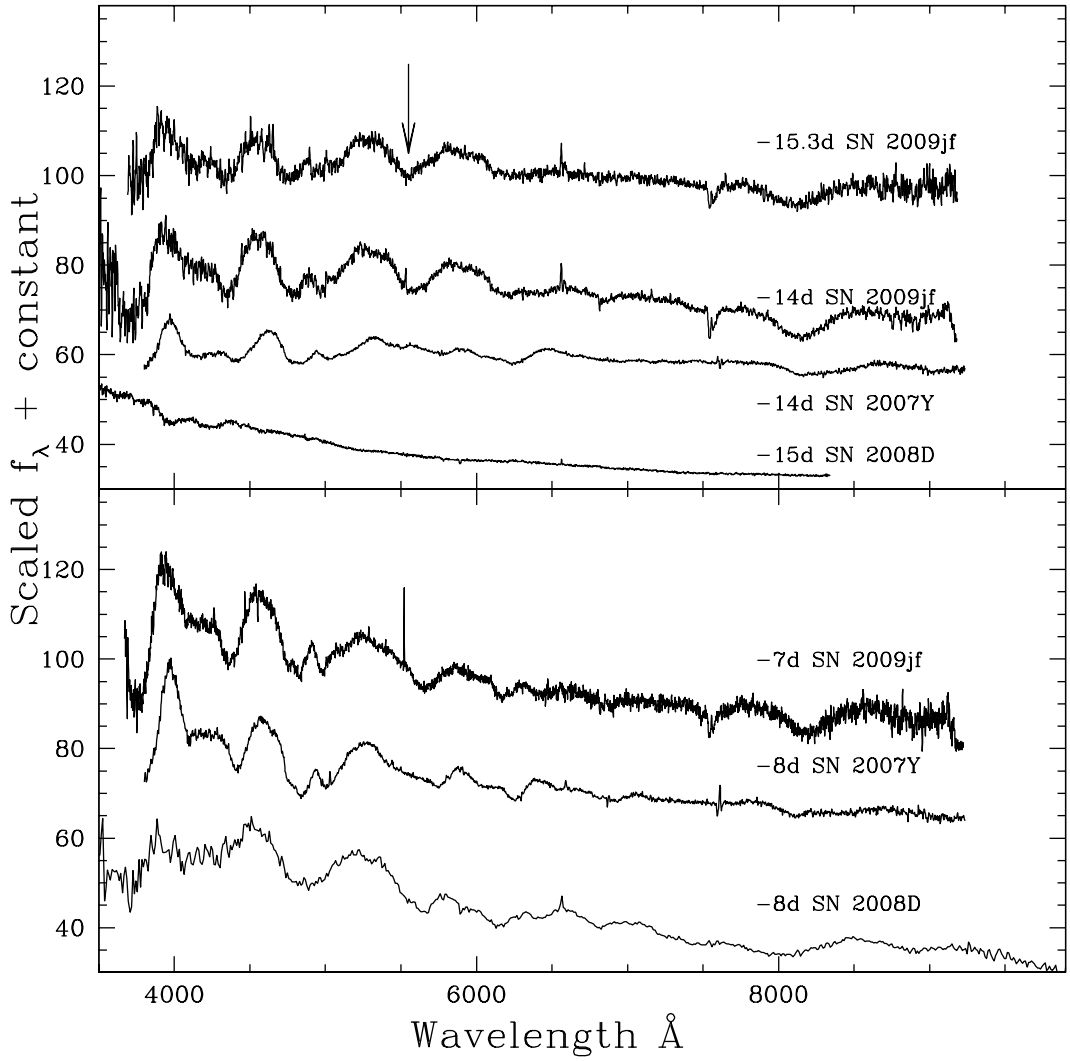

Figure 5.26: Comparison of pre-maximum spectra of SN 2009jf with SN 2008D and SN 2007Y. Note the early emergence of He I line, marked by arrow.

The spectrum of SN 2009jf obtained 1 day after *B* maximum shows a bluer continuum, with well developed lines due to Ca II H & K, He I, Fe II and a broad P-Cygni profile of Ca II near-IR triplet. The prominent absorption at ∼ 6250 Å in the pre-maximum phase weakens, and is not seen in the spectra beyond day 10. The continuum of the post-maximum spectrum on day 27 again becomes redder. Later on, the evolution of the spectrum is slow, with further suppression of the flux in blue and an increase in the flux of Ca II NIR triplet.

The spectra of SN 20090jf, SN 2007Y and SN 1999ex close to maximum are plotted

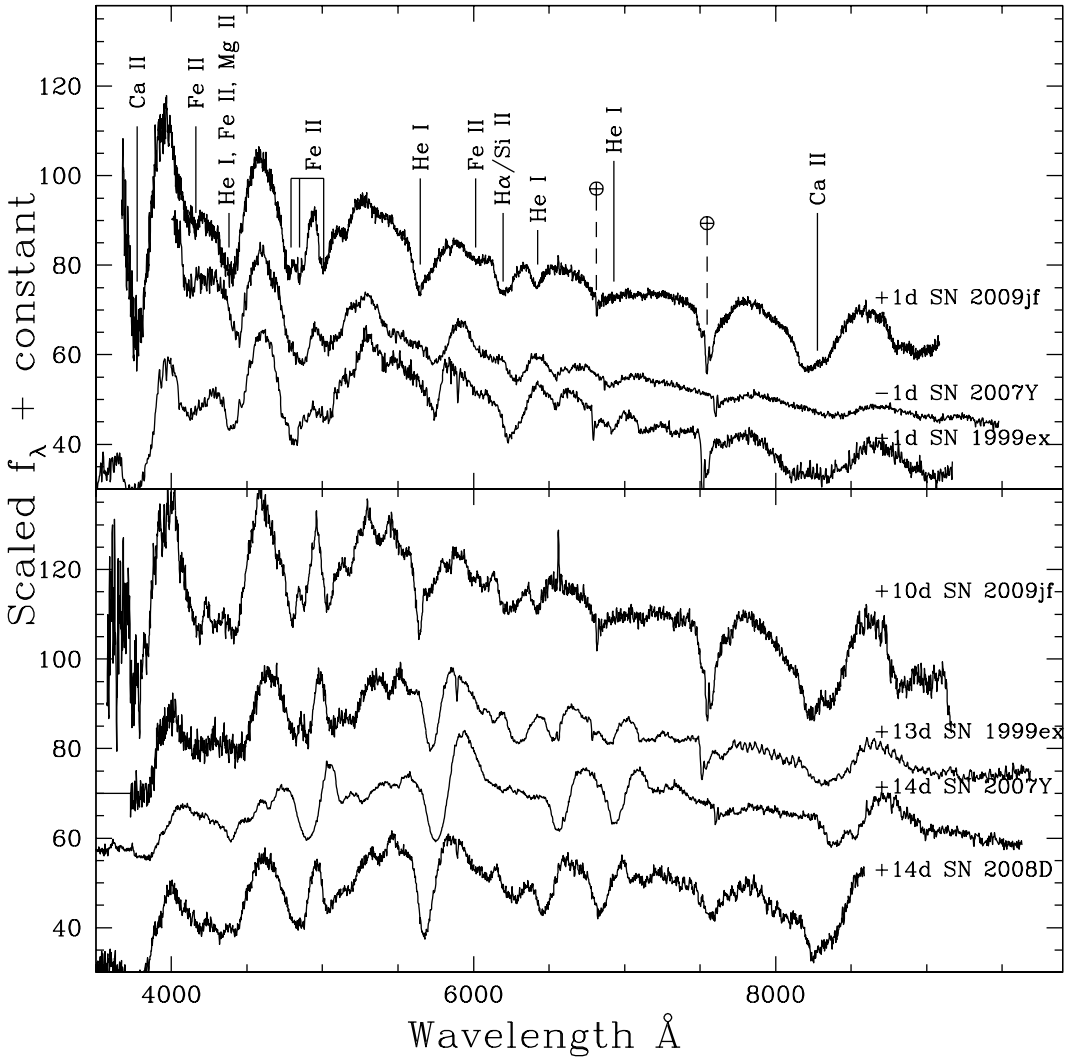

Figure 5.27: Spectral comparison of SN 2009jf around maximum and immediate post-maximum phase.

in Figure 5.27 (top panel). The main features in the spectra are identified and marked in the figure. While the general characteristics of the spectrum in the three SNe are similar, it is seen that the Fe II lines around $\sim$ 5000 Å are somewhat underdeveloped in SN 1999ex. In the phase $\sim$ 10 days after *B* maximum (Figure 5.27: lower panel), the spectral features in SN 2009jf appear to be narrower compared to the other supernovae. Around a month after maximum, all three supernovae show identical features (Figure 5.28: top panel).

Forbidden emission lines of [O I] 6300-6364 Å and [Ca II] 7291, 7324 Å are seen

in the spectrum of day 70 (Figure 5.25: lower panel), marking the onset of the nebular phase. The spectra of +86 and +99 days after *B* maximum show a strenghtening of the [O I] and [Ca II] features. The other features identified in these spectra are [Mg I] 4570 Å, [Fe II] blend at λ 5200 Å, Na I doublet λ 5890, 5896 Å, O I 7774 Å and the blend at $\sim$ 8700 Å, which has contributions from O I λ 8446 Å, Ca II λ 8498–8662 Å, and [C I] 8727 Å (Fransson & Chevalier 1989). The features have been identified in Figure 5.28 (bottom panel). The [O I] profile at this phase is single peaked and asymmetric, with the emission peaking redwards. The asymmetry is more evident in the spectrum of day 99. In comparison, the +93 day spectrum of SN 2008D shows a symmetric double peaked [O I] line.

Nebular phase

The spectra of +229 and +251 days after maximum are presented in Figure 5.29. The spectrum during these days is dominated by the [O I] and [Ca II] features. The [Ca II] emission is blended with [Fe II] lines at $\lambda\lambda$ 7155, 7172, 7388 and 7452 Å and possibly with [O II] λ 7320, 7330 Å (Stritzinger et al. 2009). Na I λ 5890, 5896 Å doublet, O II λ 7774 Å, and the λ 8700 Å blend are also identified in these spectra, but with a decreased strength compared to the spectra of 86 and 99 days after maximum. The FWHM of a Gaussian fit to the [O I] emission line indicates a velocity dispersion of $\sim$ 7300 km sec^{-1}, whereas the corresponding velocity dispersion estimated for the [Ca II] line is $\sim$ 6500 km sec^{-1}. The FWHM velocities measured for SN 2009jf are higher than those for SN 2007Y (Stritzinger et al. 2009), SN 1996N (Sollerman et al. 1998), SN 1984L (Schlegel & Kirshner 1989) and the sample of Type Ib supernovae discussed in (Matheson et al. 2001), at similar epochs. The blend at $\sim$ 8700 Å has a FWHM of $\sim$ 8000 km sec^{-1} on day 229, which decreases to $\sim$ 7300 km sec^{-1} on day 251. The Ca II NIR/[Ca II] line ratio measured in the two nebular spectra indicates that the Ca II NIR is getting weaker as compared to the [Ca II] line, a feature noticed in SN 1996N (Sollerman et al. 1998) and interpreted as due to decreasing density (Filippenko et al. 1990). However, the blend at λ 8700 Å has contribution from O I, Ca II and [C I], hence the measured velocity and flux using this blend must be viewed with caution.

The emission line profiles are multi-peaked and asymmetric. The [O I] line shows a sharp and stronger blue peak. A similar profile is clearly apparent in the [Ca II] profile of day 229. The sharp emission component appears to be present in all the emission lines. In addition to the broad features due to the supernova ejecta, the nebular spectra also show narrow lines due to Hα, [N II] λ 6548, 6583 Å and [S II] λ 6717, 6731 Å, originating

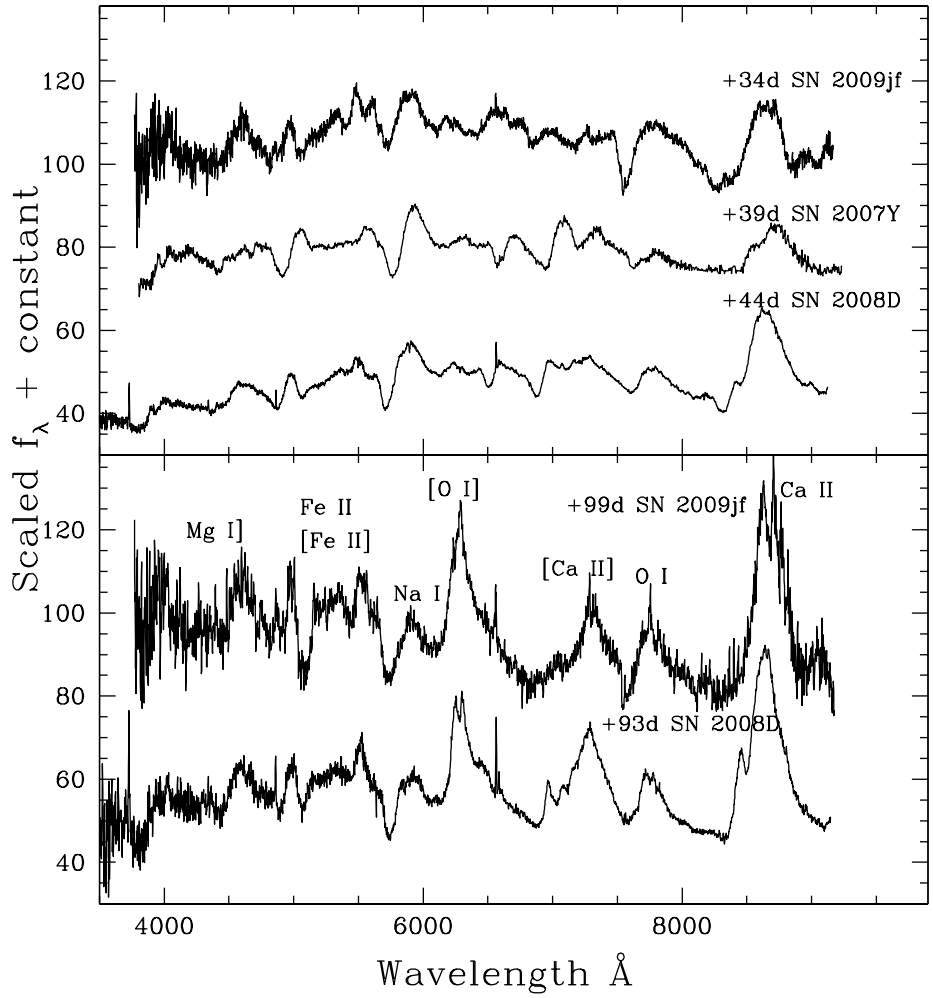

Figure 5.28: Spectral comparison of SN 2009jf at later phases.

from the underlying H II region.

Expansion velocity of the ejecta

Expansion velocities of the prominent features seen in the spectra are estimated by fitting a Gaussian profile to the minimum of the absorption trough in the redshift corrected spectra. The velocity evolution of the prominent ions, seen in the spectra of SN 2009jf, is plotted in Figure 5.30a. The expansion velocity of He I 5876 Å line, determined using the pre-maximum spectra, rapidly decreases from a value of $\sim$ 16000 km sec^{-1} on

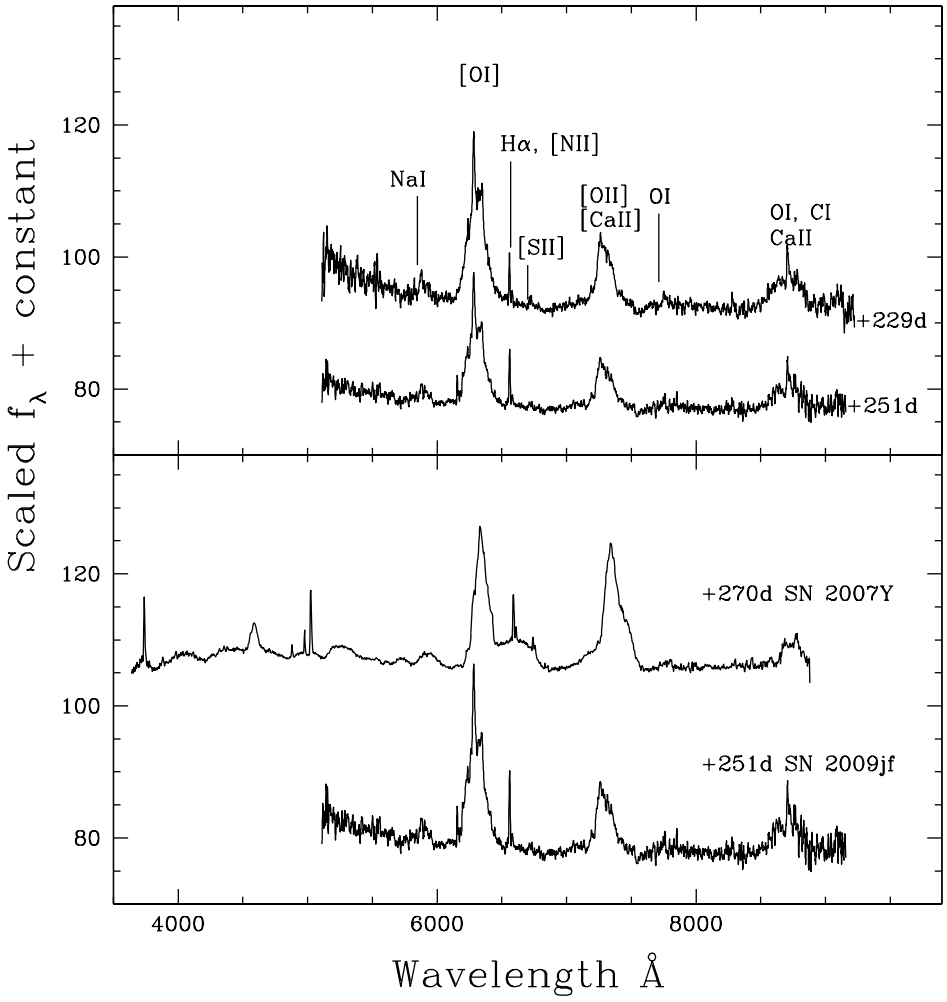

Figure 5.29: Nebular spectra of SN 2009jf (top). Hα+[N II] and [S II] features from the underlying H II region are also marked in the spectra. The bottom panel shows the comparison with the nebular spectrum of SN 2007Y.

day 15 to $\sim$ 12000 km sec^{-1} close to B maximum. The velocity further declines in the post-maximum phase and levels off at $\sim$ 7000 km sec^{-1}. The expansion velocity of Fe II λ 5169 Å feature remains low as compared to that of He I λ 5876 Å line all through its evolution, and also declines at a slower rate, as seen in most Type Ib supernovae (Branch et al. 2002). The expansion velocities of Ca II near-IR triplet follows the evolution of He I λ 5876 Å line, with a marginally higher velocity in the pre-maximum phase. While the velocity of the He I line decreases to $\sim$ 7000 km sec^{-1} in the pre-maximum phase, the

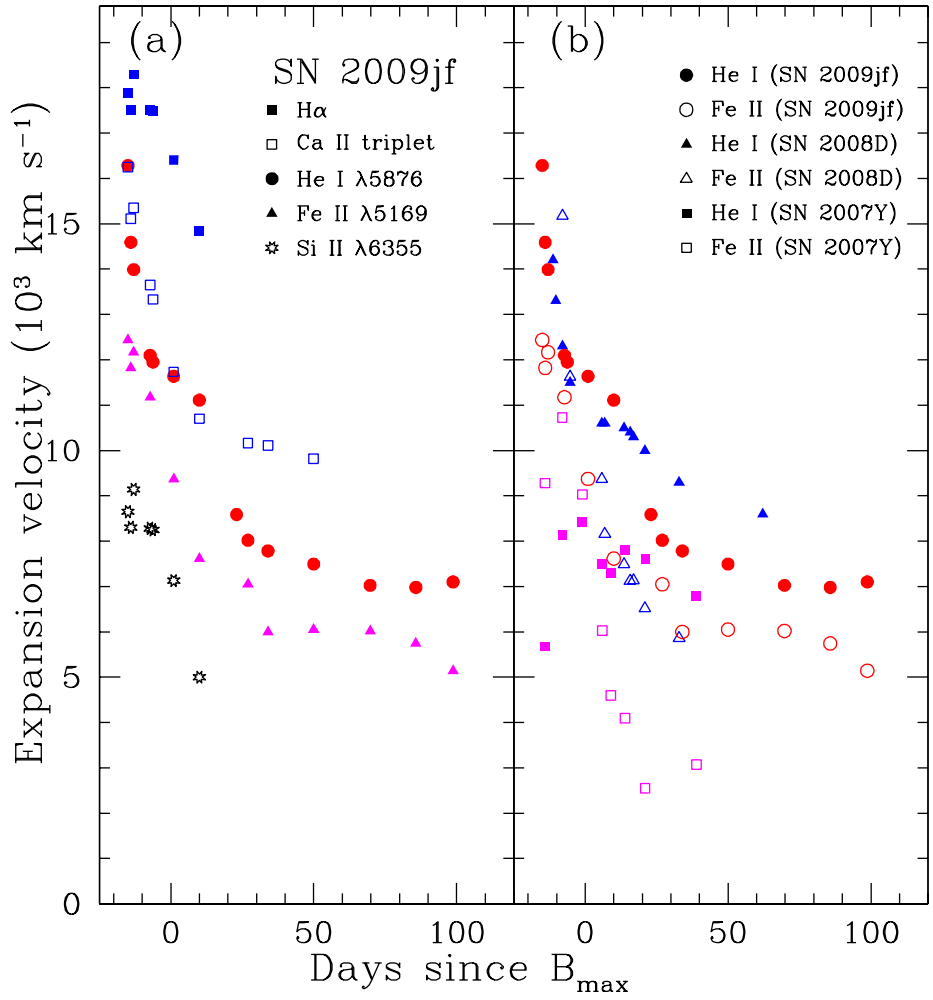

Figure 5.30: Left: Temporal velocity evolution of the prominent ions in SN 2009jf spectra. Right: Comparison of the He I and Fe II lines velocities in SN 2009jf with those observed in SN 2007Y and SN 2008D.

velocity of Ca II near-IR triplet remains higher at $\sim$ 10000 km sec^{-1}.

The feature seen at 6250 Å in the spectrum of some Type Ib supernovae, has been identified with Hα (Branch et al. 2002, Anupama et al. 2005, Pastorello et al. 2008a), or with Si II (Hamuy et al. 2002), or as a blend of C II 6580 Å and Hα (Deng et al. 2000), or as a blend of Si II and Hα (Tanaka et al. 2009). In case of SN 2005bf, identification of the 6250 Å feature with Hα was supported by the presence of a blueshifted Hβ line in the early spectrum (Anupama et al. 2005). Similarly, in SN 2007Y Stritzinger et al.

(2009) have identified the 6250 Å feature with Hα possibly blended with Si II based on the presence of Hα in the nebular spectrum and a possible presence of Hβ in the early spectrum. Identifying the feature with Hα indicates expansion velocities much higher than He I, while identification with Si II indicates velocities that are lower than Fe II (see Figure 5.30). The presence of a high velocity Hα feature in the early phase is usually accompanied by the presence of a broad shoulder redward of the [O I] λ 6300-6364 Å feature, as seen in the spectrum of SN 2007Y. Such a feature is not identified in the nebular spectra of SN 2009jf that are presented here. We therefore prefer to identify the 6250 Å feature with Si II.

The He I 5876 Å and Fe II 5169 Å line velocities estimated for SN 2009jf are compared with those of SN 2008D and SN 2007Y in Figure 5.30b. The velocity evolution of SN 2009jf is similar to that of SN 2008D. The He I velocity in both these objects is higher than the Fe II line velocity, whereas SN 2007Y has a higher Fe II velocity (Stritzinger et al. 2009). The He I velocity in SN 2009jf during the pre-maximum and early post-maximum phases is higher than SN 2008D, but $\sim$ 20 days after B maximum, the velocity in SN 2009jf becomes lower than SN 2008D. On the other hand, the Fe II line velocity is initially lower in SN 2009jf and becomes similar to SN 2008D at later epochs. SN 2007Y has lower velocities compared to both SN 2009jf and SN 2008D at all phases.

5.4.6 The Oxygen mass

The nebular spectra of Type Ib supernovae are dominated by [O I] emission, considered the prime cooling path during the late phases (Uomoto & Kirshner 1986, Fransson & Chevalier 1987). The absolute flux of this line line can be used to estimate the mass of neutral oxygen producing the line emission, following the expression by Uomoto & Kirshner (1986),

$$M_O = 10^8 \times D^2 \times \mathrm{F([O\,I])} \times \exp\left(2.28/T_4\right) \ , \tag{5.1}$$

where M_{O} is the mass of neutral oxygen in $\mathrm{M}_\odot$, D is the distance to the supernova in Mpc, F([O I]) is the flux of the [O I] line in ergs s^{-1} and T_4 is the temperature of the oxygen emitting region in 10^4 K units. The above equation holds in the high density regime ($N_e \geq 10^6$ cm^{-3}), which is met in the ejecta of Type Ib supernovae (Schlegel & Kirshner 1989, Elmhamdi et al. 2004, Gomez & Lopez 1994). An estimate of the temperature of the line emitting region can be made using the [O I] λ 5577/6300-6364 flux ratio. [O I] λ 5577 Å line is not detected in the nebular spectrum of SN 2009jf. This implies a limit on

the [O I] λ 5577/6300-6364 Å flux ratio of ≤ 0.1. At this limit, the emitting region should either be at a relatively low temperature ($T_4 \leq 0.4$) for the high density limit, and/or at low electron density ($n_e \leq 5 \times 10^6$ cm^{-3}) if $T_4 = 1$ (Maeda et al. 2007).

Elmhamdi et al. (2004) estimate a temperature of $\sim 3200 - 3500$ K for SN 1990I at $\sim$ 237 days after maximum light, using an upper limit of the flux of [O I]λ 5577 line, while Schlegel & Kirshner (1989), have estimated the mass of oxygen in Type Ib supernovae SN 1984L and SN 1985F by assuming $T_4 = 0.4$. In all cases, a density 10^6 cm^{-3} is assumed. Assuming that the high density regime is valid for SN 2009jf also, a value of $T_4 = 0.4$ appears to be a good approximation. Using the [O I] flux of 3.74×10^{-14} erg s^{-1} cm^{-2} measured in the spectrum of day 251, and the assumed distance of 34.25 Mpc, the mass of oxygen is estimated to be 1.34 $M_\odot$. This estimate is the upper limit on the mass of oxygen producing the [O I] line. The presence of O I 7774 Å line in the spectrum is indicative of the presence of ionized oxygen also as this line is mainly due to recombination (Begelman & Sarazin 1986). Thus the oxygen mass estimate of 1.34 $M_\odot$ may be considered as a lower limit of the total mass of oxygen ejected during the explosion.

5.4.7 Discussion

The light curve and spectral evolution of SN 2009jf show some peculiarities compared to other SNe Type Ib. The light curves indicate a post-maximum decline that is slower compared to other Type Ib supernovae. This slow decline continues even during the late phases, making the light curve of SN 2009jf broad. The absolute V magnitude at peak is comparable to the mean of the absolute magnitude distribution of Type Ib supernovae. Using the bolometric light curve and the energy deposition rate via ^{56}Ni $\rightarrow$ ^{56}Co, the mass of ^{56}Ni synthesized during the explosion is estimated to be 0.21 $M_\odot$. SN 2009jf shows a very early emergence of He I lines in the spectrum. He II λ 5876 Å line is identified in the first spectrum obtained 15.3 days before B maximum. Other lines due to He I at λ 4471 Å, and λ 6678 Å were identified in the -13 day spectrum. Further, the expansion velocity estimated using He I line $\sim 16,000$ km sec^{-1}, indicating that helium is excited at high velocity. In case of SN 2008D, He I lines became apparent around 11.5 days before B maximum, and were prominent only around 5 days before B maximum (Modjaz et al. 2009). The He I lines seen in the spectra of Type Ib supernovae require non-thermal excitation and ionization, as the temperature present in the ejecta is too low to cause any significant absorption (Lucy 1991). γ-rays, emitted by newly synthesized ^{56}Ni during the explosion, accelerate electrons that act as a source of non-thermal excitation for He

(Harkness et al. 1987, Lucy 1991). For exciting helium at such a high velocity as seen in SN 2009jf, the γ-rays need to be close to the helium layer, which can be possible either through the escape of γ-rays from the ^{56}Ni dominated region, or through some large scale instability causing substantial mixing of ^{56}Ni to the outer layers. The slower decline of the light curves of SN 2009jf gives an indication that it has a massive ejecta and the probability of γ-rays escaping will be low. Hence, substantial mixing of different inner layers appears to be the most probable way for an early excitation of helium at high velocities.

The profile of [O I] λ 6300-6364 Å feature in the nebular spectrum is multi-peaked and asymmetric with a sharp, stronger blue peak. The peak of this feature is blueshifted by $\sim$ 30 Å around day +85, which reduces to a blueshift of $\sim$ 15 Å by day +98. Such observed blueshifts are explained as a result of residual opacity in the core of the ejecta (Taubenberger et al. 2009). The asymmetric and multi-peaked profile seen at phases later than 200 days can be produced by additional components of arbitrary width and shift with respect to the main component. Asymmetric and multi-component profiles cannot be reproduced within spherical symmetry (Maeda et al. 2007, Taubenberger et al. 2009). Such profiles are indicative of an ejecta with large-scale clumping, a single massive blob, or a unipolar jet. The asymmetric [O I] line profile of SN 2009jf with a stronger blue peak is very similar to the line profiles of SNe 2000ew and 2004gt. Taubenberger et al. (2009) have explored a possible configuration which can give rise to this asymmetric line profile, and interpretated the profile as originating from the deblended λ 6300 Å and λ 6364 Å lines of a single narrow, blueshifted component. This, however, does not account for the stronger blue peak of the λ 6300 Å line. The stronger blue peak is explained with a complex ejecta structure with additional blueshifted emission on top of an otherwise symmetric profile. Alternatively, the asymmetry in the profile is explained by a damping of the redshifted emission component in an originally toroidal distribution, caused by the optically thick inner ejecta. The light curve evolution of SN 2009jf indicates the presence of an ejecta more massive than other stripped core collapse supernovae. Hence, it is quite likely that in the case of SN 2009jf also the redward component is damped by an optically thick inner ejecta. This needs further investigation with observations at phases later than presented here, as well as spectrophotometric observations.

The brightness and width of Type Ib light curves are determined by the interplay of nickel mass, opacity and gamma-ray deposition. In general, a greater amount of ^{56}Ni will make the light curve brighter. A more massive ejecta will have a larger optical depth, and it will take longer for the trapped decay energy to diffuse through the envelope, which will

broaden the light curve (Ensman & Woosley 1988). The time taken for the bolometric light curve to decline from peak to the moment when the luminosity is equal to $1/e$ times the peak luminosity (which is equivalent to a decline of 1.1 mag from peak), is known as effective diffusion time $\tau_{\rm m}$. The effective diffusion time is related to the mass of the ejecta $\rm M_{ej}$ and the kinetic energy $\rm E_k$ of the ejecta $\tau_{\rm m} \propto \kappa_{\rm opt}^{1/2} M_{\rm ej}^{3/4} K_{\rm E}^{-1/4}$ (Arnett 1982), where $\kappa_{\rm opt}$ is optical opacity. The expansion velocity v can be expressed in terms of $\rm M_{ej}$ and $\rm E_k$ as $v \propto M_{\rm ej}^{-1/2} K_{\rm E}^{1/2}$. The broad peak and slower decline rates of the light curves of SN 2009jf in comparison to other supernovae indicates that SN 2009jf has a massive ejecta. Further, the broader emission lines at late phase indicates a larger explosion energy.

There are several core-collapse supernovae for which the progenitor mass has been constrained using hydrodynamical modelling. With this approach, Nomoto et al. (2003) constructed the $E_{\rm K} - M_{\rm MS}$ diagram and introduced a hypernova branch. Recent updates of this approach include SN 1998bw (Maeda et al. 2006), SN 2008D (Tanaka et al. 2009), and SN 2003bg (Mazzali et al. 2009). For the well studied bright hypernova SN 1998bw ($M_V = -19.35$, Galama et al. 1998), the main sequence mass of the progenitor is constrained by Maeda et al. (2006) as ~ 40 $\rm M_\odot$. Though SN 2009jf has a brighter peak compared to SN 2008D, the fact that the light curves of SN 2009jf around maximum and the initial decline rate $\Delta m_{15}(V)$ are similar to those of SN 2008D can be used to estimate the mass of the ejecta $\rm M_{\mathit{ej}}$ and kinetic energy $\rm E_k$ of the ejecta, using SN 2008D as the reference, assuming the optical opacity $\kappa_{\rm opt}$ to be the same. The effective diffusion time $\tau_{\rm m}$ for SN 2009jf and SN 2008D are estimated to be 30 days and 26 days, respectively. The photospheric expansion velocity estimated using the Fe II λ 5169 Å line at maximum is ~ 10000 km sec^{-1}, similar for both the objects. Tanaka et al. (2009) have calculated the hydrodynamics of explosion and explosive nucleosynthesis for SN 2008D with varying mass for the He core of the progenitor and concluded that the progenitor star of SN 2008D had a He core mass $6 - 8$ $\rm M_\odot$ prior to explosion. This corresponds to a main sequence mass of $M_{\rm MS} = 20 - 25$ $\rm M_\odot$. The explosion energy and mass of ejecta for SN 2008D were estimated to be $E_{\rm k} = 6.0 \pm 2.5 \times 10^{51}$ erg and $M_{\rm ej} = 5.3 \pm 1.0$ $\rm M_\odot$, respectively. Using the observed photospheric velocity and the estimated diffusion time for SN 2009jf, and using SN 2008D as a reference, we estimate $M_{\rm ej} = 6.9 \pm 1.3$ $\rm M_\odot$ and $E_{\rm k} = 7.8 \pm 3.0 \times 10^{51}$ erg for SN 2009jf. This indicates that SN 2009jf was an energetic explosion of a star having a mass similar, or somewhat more massive than the progenitor of SN 2008D ($M_{\rm MS} 20 - 25$ $\rm M_\odot$). The physical parameters of SN 2009jf may also be compared with those of the type IIb supernova SN 2003bg, which had an absolute peak magnitude of $M_V = -17.5$ (Hamuy et al. 2009) and an oxygen mass estimate of 1.3 $\rm M_\odot$. Mazzali et al. (2009) have

estimated the physical parameters for SN 2003bg based on detailed light curve and spectral modelling. The best fit model gives an ejected mass of $\sim$ 4.8 $M_\odot$, kinetic energy $\sim 5 \times 10^{51}$ erg and mass of ^{56}Ni $\sim$ 0.15 – 0.17 $M_\odot$. The mass of the progenitor for SN 2003bg is estimated as 20 – 25 $M_\odot$. Our qualitative analysis of light curve and spectra of SN 2009jf hints towards a higher kinetic energy and a slightly more massive ejecta than SN 2003bg, and in turn a progenitor with $M_{\rm MS}$20 – 25 $M_\odot$.

The mass of oxygen M(O) in the ejecta of the core collapse SNe is very sensitive to the main-sequence mass $M_{\rm MS}$ of the progenitor. For $M_{\rm MS}$ = 15, 18, 20, 25, 30, and 40 $M_\odot$, M(O) = 0.16, 0.77, 1.05, 2.35, 3.22, and 7.33 $M_\odot$, respectively (Nomoto et al. 2006b). These values are obtained for $E_{\rm k} = 1.0 \times 10^{51}$ erg and the metallicity $z = 0.02$, but are not so sensitive to $E_{\rm k}$ and z. In fact, for ($M_{\rm MS}/M_\odot$, $E_{\rm k}/10^{51}$ erg) = (20, 10), (25, 10), and (30, 20), and (40, 30), M(O)/$M_\odot$ = 0.98, 2.18, 2.74, and 7.05, respectively (Nomoto et al. 2006b). Therefore, the lower limit of the oxygen mass M(O) 1.34 $M_\odot$ estimated from the nebular spectra is quite consistent with the progenitor mass of $M_{\rm MS}$20 – 25 $M_\odot$ estimated from the light curve shape and the photometric velocities.

The [Ca II] λ 7291-7324/[O I] λ 6300-6364 line ratio is also a good diagnostic of $M_{\rm MS}$, because the mass of the explosively synthesized Ca in the ejecta, M(Ca), is not sensitive to $M_{\rm MS}$. For $M_{\rm MS}/M_\odot$ = 15, 18, 20, 25, 30, and 40, M(Ca)/$10^{-2}M_\odot$ = 0.40, 0.45, 0.37, 0.66, 1.6, and 1.6, respectively (Nomoto et al. 2006b). Also, for ($M_{\rm MS}/M_\odot$, $E_{\rm k}/10^{51}$ erg) = (20, 10), (25, 10), and (30, 20), and (40, 30), M(Ca)/$10^{-2}M_\odot$ = 0.50, 0.57, 0.93, and 1.4, respectively (Nomoto et al. 2006b). This is in contrast to M(O), which sensitively increases with $M_{\rm MS}$. Thus a smaller [Ca II]/[O I] ratio indicates a massive core. The [Ca II]/[O I] ratio for SN 2009jf is estimated as 0.51 and 0.49 on days 229 and 251, respectively. For SN 2007Y, SN 1996N, SN 1990I and SN 1998bw, this ratio was found to be 1.0, 0.9, 0.7 and 0.5, respectively, at similar epochs (Elmhamdi et al. 2004, Stritzinger et al. 2009 and references therein). Fransson & Chevalier (1989) have theoretically calculated the [Ca II]/[O I] line ratio for progenitor masses of 15 and 25 $M_\odot$. The observed [Ca II]/[O II] ratio for SN 2009jf is very close to the ratio expected for a star with $M_{\rm MS}$ = 25 $M_\odot$, as indicated by Model 1b in Fransson & Chevalier (1989).

The estimates of the mass of ^{56}Ni synthesized during the explosion, the kinetic energy of explosion and the main sequence mass of the progenitor star places SN 2009jf between the normal core-collapse supernovae and the hypernovae branch in the $E_K - M_{MS}$ diagram of Tanaka et al. (2009), at the upper end of the normal core-collapse supernovae branch. It is however to be noted that the [O I] line profile during the nebular phase indicates asymmetry of the explosion. This can have some effect in the kinetic energy estimate,

as shown by Maeda et al. (2006) and Tanaka et al. (2007) for SN 1998bw. A detailed modelling is therefore required for a better estimate of the various parameters.

Itagaki et al. (2009) suggest the progenitor could have undergone luminous blue variable type mass loss events, based on their detection of a dim object at the location of the supernova on three occasions. There is however, no report of a non-detection of the object on other occasions. Pre-supernova images of the host galaxy obtained in the ultraviolet by the *Swift* satellite, and available in the *Swift* data archives, clearly indicate the presence of a bright HII region at the supernova location. It is hence quite likely that the object detected by Itagaki et al. (2009) corresponds to the underlying HII region.

5.5 Summary

We present in this chapter the potometric and spectroscopic evolution of three different types of supernovae, Type Ibn SN 2006jc, type broad-Ic SN2007ru, and Type Ib SN2009jf. A brief summary of each individal object is gien below:

SN 2006jc: The optical spectrum of SN 2006jc shows a blue continuum and is dominated by moderately narrow He I emission lines, similar to Type IIn SNe. It indicates interaction of the supernova ejecta with a pre-supernova circumstellar material. The moderately narrow He I emission lines arise in the pre-supernova circumstellar shell that is helium enriched.

The optical light curves show a clear signature of dust formation as indicated by a sharp decrease in the magnitudes around day 50, accompanied by a reddening of the colours. The evolution of the optical light curve during the early phases is very similar to normal Type Ib/c SNe. The *uvoir* bolometric light curve evolution of SN 2006jc is reasonably similar to normal Type Ib/c SNe at all phases.

The He I emission line fluxes indicate the circumstellar shell is dense, with a density of $\sim 10^9 - 10^{10}$ cm^{-3}. The helium mass in this shell is estimated to be 0.07 M$_\odot$. The estimated main sequence mass of the progenitor and explosion energies are 40 $M_\odot$ and 10×10^{51}, respectively.

SN 2007ru: The light curve evolution of SN 2007ru indicates a fast rise time of 8 days to *B* band maximum and post-maximum decline more rapid than any other broad-Ic supernovae. The spectra show broad spectral features due to very high expansion velocity (20,000 kms$^-$), normally seen in hypernovae. The ejected mass of ^{56}Ni is estimated to be $0.4M_\odot$.

The early phase spectra are most similar to those of broad line SN 2003jd, the [O I]

line profile in the nebular spectrum of SN 2007ru shows a singly-peaked profile, in contrast to the doubly-peaked profile in SN 2003jd. By taking SN 2003jd as a reference, the estimated ejected mass and explosion energies are M_{ej}=1.7 $M_\odot$ and E_K=8.6×10^{51} ergs. SN 2007ru has a large kinetic energy and lower mass ejecta, leading to a higher E/M.

SN 2009jf: The light curves of SN 2009jf are broad, with a slow decline. The late phase decline rate is slower than other studied type Ib supenovae. The slow evolution of the light surves indicate the presence of massive ejecta. This indicates inefficient γ-ray trapping by the ejecta, suggesting low column density. The peak bolometric flux implies $\sim$ 0.21 $M_\odot$ of ^{56}Ni was synthesized during the explosion.

The spectral evolution of SN 2009jf is typical of Type Ib class, but with an early emergence of helium lines. He I λ 5876 Å is clearly identified in the first spectrum obtained 15 days before maximum, at a velocity of $\sim$ 16000 km s^{-1}. This early emergence of helium lines is likely due to a substantial mixing of the inner layers of the ejecta. The [O I] λ 6300-6364 Å line seen in the nebular spectrum is multi-peaked and asymmetric, with a sharp, stronger blue peak. The absolute flux of this line indicates the mass of oxygen ejected during the explosion to be 1.34 $M_\odot$.

A qualitative analysis of the light curve and spectra of SN 2009jf indicates that SN 2009jf is an energetic explosion of a massive star. The mass of the ejecta and kinetic energy of explosion are estimated to be $M_{\rm ej} = 6.9 \pm 1.3$ $M_\odot$ and $K_{\rm E} = 7.8 \times 10^{51}$ erg, respectively. The main sequence mass of the progenitor star is estimated to be 20 − 25 $M_\odot$.

The three examples presented here highlight the diversity that is seen in these class of supernovae due to various factors that include amongst others, the progenitor mass and composition and the supernova environment such as the host galaxy metallicity and/or the immediate circumstellar environment.

CHAPTER 6

SUMMARY AND FUTURE PROSPECTS

6.1 Summary

Supernovae provide vital clues to the study of stellar evolution and chemical evolution of galaxies, and also provide in situ, real time information about various physical processes such as nuclear reactions in stars, accretion processes, explosion mechanisms, dust formation under various environments, line formation under different environment, physics of expanding material, shock interaction and shock physics. This thesis provides a glimpse of how observations help in understanding some of these aspects.

We present in this thesis the observational properties of core collapse supernovae. The diversity in the observed properties amongst the different types of CCSNe, as well as within a given type are highlighted through the examples of supernovae SN 2004A (IIP), SN 2008in (IIP), SN 2005kd (IIn), SN 2006jc (Ibn), SN 2007ru (BL Ic) and SN 2009jf (Ib). The study is based on extensive monitoring of the optical light curves and spectra of these objects. The data present dense, extensive temporal coverage of all phases in the evolution of the SNe.

The thesis contains six chapters. Chapter 1 gives a general introduction to the evolution of massive stars and supernovae. Chapter 2 describes the telescope and instrument, observations and reduction procedures. All data were obtained using the 2m Himalayan Chandra Telescope (HCT), Hanle, India. The technical details of telescope and instrument are given in the chapter. This chapter also discusses in detail, the various techniques used in photometric and spectroscopic data reductions.

Chapter 3 discusses the properties of Type IIP supernovae with a detailed study of SN 2004A and SN 2008in. The distances to the supernovae are estimated using the Standard Candle Method (SCM) (Hamuy & Pinto, 2002) and the Expanding Photosphere Method

(EPM)(Krishner & Kwan, 1974, 1975, Hamuy et al. 2001) . In addition, the explosion energy, radius of progenitor, the nickel mass and the mass ejected, during the explosion are estimated using the observed light curves and the spectra (Hamuy 2003, Elmahamdi 2003, Litvinova & Nadyozhin 1985). The progenitor mass is also estimated based on the estimate of the ejected mass. Chapter 4 describes the evolution of the Type IIn supernova SN 2005kd, which is characterized by narrow emission lines in the early spectra. Some Type IIn supernovae show a plateau phase in the light curve, and SN 2005kd is of this kind. The narrow emission lines in the spectra show that the SN ejecta interacted with the pre-supernova circumstellar material that is a result of of mass loss from the progenitor during its evolution.

Chapter 5 discusses the properties of stripped envelope core collapse supernovae using the observations of type Ib/c supernovae SN 2006jc, SN 2007ru, and SN 2009jf. SN 2006jc was found to be peculiar, with narrow He I emission lines arising due to the SN ejecta interaction with a helium enriched pre-supernova circumstellar material. SN 2007ru shows very broad lines in the spectra indicating velocity of 20,000 km s^{-1}. The light curve evolution of SN 2007ru indicates a fast rise time and post-maximum decline more rapid than other broad-line Ic supernovae. The light curves of SN 2009jf are broad, with slow decline, indicate the presence of massive ejecta. He I line is identified with velocity of 16,000 km s^{-1}.

The photometric and spectroscopic evolution of all the above SNe are described in detail and compared with other similar supernovae. The various physical parameters related to the explosion and progenitors are also estimated.

6.2 Future scope

The study of supernovae has gained impetus in the recent couple of decades, beginning with the discovery of SN 1987A. The location of this SN in our nearest neighbour, the Large Magellanic Cloud has allowed the study of a core collapse supernova from the time of explosion to several decades since.

A major goal in the study of supernovae has been to understand the progenitors and their evolution. The advent of telescopes capable of providing high spatial resolution images has led to the direct detection of the progenitors of several CCSNe. In a recent review, Smartt (2009) summarizes our understanding of the progenitors of various types of CCSNe. The minimum initial mass required for production of a SN, based on direct detections of red supergiant progenitors is 8 ± 1 $M_{\odot}$. These stars produce the Type II-

P SNe and the most massive white dwarf progenitors (Type Ia). The Type Ib/c and IIb occur with a wide range in physical parameters for the progenitors. The progenitors could be either single stars or moderate mass interacting binaries. The highly energetic, broad-lined SNe Ic are more likely to be produced by massive, Wolf-Rayet progenitors. Such massive progenitors are also thought to be the progenitors of the type IIn and Ibn supernovae.

The observational characteristics of core collapse events strongly depend on the final stage of the progenitor object and on the properties of the circumstellar medium at the time of explosion. The observed spectral classes of core collapse supernovae follow the sequence IIP-IIL-IIb-Ib-Ic, representing different degrees of envelope stripping from the progenitor star (Nomoto et al. 1995).

Supernovae are the best probes to study the early universe as they occur at cosmological distances. To be able to effectively use these objects as cosmological probes, it is essential to understand the diversity of these objects in terms of their progenitors and environment. This is best done by the study of several such objects in the nearby universe. Detailed observations at various phase of the supernova are required for this. Diversity is more prominent during the early phases of a supernova explosion, while observations of supernovae during the late phase is important as the spectra at late epochs probe more deeply into the core of the expanding star. Since the energy source for late time spectra is probably decay of radioactive elements synthesized in the explosion, the energetics at late time provide direct clues to the energy source and to the physics of explosion.

Supernovae are powered by radioactive decay of 56Ni to 56Co and 56Fe. Theoretical modelling of the observed light curve near maximum provides information about the ejected mass Mej, the explosion kinetic energy E, and the mass and distribution of ^{56}Ni, that can be constrained from light curve brightness and shape. Light curve modeling only gives a family of possible models with different values of (M_{ej}, E), and modelling of the spectrum is required to break the degeneracy. Spectral fitting helps in constraining the abundance distribution within the ejecta, the explosion velocity and explosion energy.

The existing 2 - 4 m class facilities will help in detailed observations of several nearby supernovae, while the 8-m class facilities will provide vital observations during the late, nebular phases. Also, the larger facilities will help in the study of SNe at higher redshifts. These studies are important to to understand the properties of the SNe that would be discovered at redshifts around 4 - 6 by the proposed extremely large aperture ground based telescopes and the James Webb Space Telescope.

REFERENCES

Almog, Y. & Netzer, H. 1989, MNRAS, 238, 57

Anupama, G. C., Sahu, D. K., Deng, J., Nomoto, K., Tominaga, N., Tanaka, M., Mazzali, P. A., & Prabhu, T. P. 2005, ApJ, 631, L125

Arkharov, A., Efimova, N., Leoni, R., di Paola, A., di Carlo, E., & Dolci, M. 2006, The Astronomer's Telegram, 961, 1

Arnett, W. D. 1982, ApJ, 253, 785

Baade, W. 1926, Astronomische Nachrichten, 228, 359

Baron, E., Branch, D., Hauschildt, P. H., Filippenko, A. V., Kirshner, R. P., Challis, P. M., Jha, S., Chevalier, R., Fransson, C., Lundqvist, P., Garnavich, P., Leibundgut, B., McCray, R., Michael, E., Panagia, N., Phillips, M. M., Pun, C. S. J., Schmidt, B., Sonneborn, G., Suntzeff, N. B., Wang, L., & Wheeler, J. C. 2000, ApJ, 545, 444

Begelman, M. C. & Sarazin, C. L. 1986, ApJ, 302, L59

Benetti, S., Branch, D., Turatto, M., Cappellaro, E., Baron, E., Zampieri, L., Della Valle, M., & Pastorello, A. 2002, MNRAS, 336, 91

Benetti, S., Cappellaro, E., Elias-Rosa, N., Harutyunyan, A., Chornock, R., Filippenko, A. V., Foley, R. J., Pastorello, A., & Andreuzzi, G. 2006, Central Bureau Electronic Telegrams, 674, 2

Benetti, S., Turatto, M., Cappellaro, E., Danziger, I. J., & Mazzali, P. A. 1999, MNRAS, 305, 811

Berger, E. & Soderberg, A. M. 2008, GRB Coordinates Network, 7159, 1

Bertoldi, F., Carilli, C. L., Cox, P., Fan, X., Strauss, M. A., Beelen, A., Omont, A., & Zylka, R. 2003, A&A, 406, L55

Bessell, M. S., Castelli, F., & Plez, B. 1998, A&A, 333, 231

Blanton, E. L., Schmidt, B. P., Kirshner, R. P., Ford, C. H., Chromey, F. R., & Herbst, W. 1995, AJ, 110, 2868

Branch, D., Benetti, S., Kasen, D., Baron, E., Jeffery, D. J., Hatano, K., Stathakis, R. A., Filippenko, A. V., Matheson, T., Pastorello, A., Altavilla, G., Cappellaro, E., Rizzi, L., Turatto, M., Li, W., Leonard, D. C., & Shields, J. C. 2002, ApJ, 566, 1005

Brown, P. J., Immler, S., & Modjaz, M. 2006, The Astronomer's Telegram, 916, 1

Cardelli, J. A., Clayton, G. C., & Mathis, J. S. 1989, ApJ, 345, 245

Chakraborti, S., Prabhu, T., Anupama, G. C., Kaur, A., Uday Kumar, G., & Ray, A. 2008, Central Bureau Electronic Telegrams, 1638, 1

Chandra, P., Stockdale, C. J., Chevalier, R. A., Van Dyk, S. D., Ray, A., Kelley, M. T., Weiler, K. W., Panagia, N., & Sramek, R. A. 2009, ApJ, 690, 1839

Chevalier, R. A. 1982, ApJ, 259, 302

—. 2006, ArXiv Astrophysics e-prints

Chevalier, R. A. & Fransson, C. 2003, in Lecture Notes in Physics, Berlin Springer Verlag, Vol. 598, Supernovae and Gamma-Ray Bursters, ed. K. Weiler, 171–194

Chevalier, R. A. & Fransson, C. 2006, ApJ, 651, 381

Chevalier, R. A., Fransson, C., & Nymark, T. K. 2006, ApJ, 641, 1029

Chornock, R., Serduke, F. J. D., Wang, X., Filippenko, A. V., & Li, W. 2007, Central Bureau Electronic Telegrams, 1151, 1

Chugai, N. N. 1990, Soviet Astronomy Letters, 16, 457

Chugai, N. N., Blinnikov, S. I., Cumming, R. J., Lundqvist, P., Bragaglia, A., Filippenko, A. V., Leonard, D. C., Matheson, T., & Sollerman, J. 2004, MNRAS, 352, 1213

Chugai, N. N. & Chevalier, R. A. 2006, ApJ, 641, 1051

Chugai, N. N. & Danziger, I. J. 1994, MNRAS, 268, 173

—. 2003, Astronomy Letters, 29, 649

Clayton, D. D. 1979, Ap&SS, 65, 179

Clocchiatti, A., Suntzeff, N. B., Phillips, M. M., Filippenko, A. V., Turatto, M., Benetti, S., Cappellaro, E., Avilés, R., Covarrubias, R., DeGioia-Eastwood, K., Dickinson, M., Gouiffes, C., Guhathakurta, P., Hamuy, M., Heathcote, S. R., Leibundgut, B., Matheson, T., Navarrete, M., Perez, M., Phillips, A., Piemonte, A., Ruiz, M. T., Shields, J. C., Smith, C., Spinrad, H., Sturch, C. R., Tyson, J. A., & Wells, L. 2001, ApJ, 553, 886

Colgate, S. A. 1968, in Nucleosynthesis, ed. W. D. Arnett, C. J. Hansen, J. W. Truran, & A. G. W. Cameron , 169

Colgate, S. A., Grasberger, W. H., & White, R. H. 1961, AJ, 66, 280

Colgate, S. A. & White, R. H. 1966, ApJ, 143, 626

Crotts, A., Eastman, J., Depoy, D., Prieto, J. L., & Garnavich, P. 2006, Central Bureau Electronic Telegrams, 672, 1

Deng, J. S., Qiu, Y. L., Hu, J. Y., Hatano, K., & Branch, D. 2000, ApJ, 540, 452

Dessart, L. & Hillier, D. J. 2005, A&A, 439, 671

Di Carlo, E., Corsi, C., Arkharov, A. A., Massi, F., Larionov, V. M., Efimova, N. V., Dolci, M., Napoleone, N., & Di Paola, A. 2008, ApJ, 684, 471

Diaz, A. I., Terlevich, E., & Pagel, B. E. J. 1985, MNRAS, 214, 41P

Diaz, A. I., Terlevich, E., Vilchez, J. M., Pagel, B. E. J., & Edmunds, M. G. 1991, MNRAS, 253, 245

Donati, S., Ciabattari, F., Winslow, D., & Li, W. 2007, Central Bureau Electronic Telegrams, 1149, 1

Eastman, R. G., Schmidt, B. P., & Kirshner, R. 1996, ApJ, 466, 911

Elmhamdi, A., Danziger, I. J., Branch, D., Leibundgut, B., Baron, E., & Kirshner, R. P. 2006, A&A, 450, 305

Elmhamdi, A., Danziger, I. J., Cappellaro, E., Della Valle, M., Gouiffes, C., Phillips, M. M., & Turatto, M. 2004, A&A, 426, 963

Elmhamdi, A., Danziger, I. J., Chugai, N., Pastorello, A., Turatto, M., Cappellaro, E., Altavilla, G., Benetti, S., Patat, F., & Salvo, M. 2003, MNRAS, 338, 939

Ensman, L. M. & Woosley, S. E. 1988, ApJ, 333, 754

Fassia, A., Meikle, W. P. S., Geballe, T. R., Walton, N. A., Pollacco, D. L., Rutten, R. G. M., & Tinney, C. 1998, MNRAS, 299, 150

Fassia, A., Meikle, W. P. S., Vacca, W. D., Kemp, S. N., Walton, N. A., Pollacco, D. L., Smartt, S., Oscoz, A., Aragón-Salamanca, A., Bennett, S., Hawarden, T. G., Alonso, A., Alcalde, D., Pedrosa, A., Telting, J., Arevalo, M. J., Deeg, H. J., Garzón, F., Gómez-Roldán, A., Gómez, G., Gutiérrez, C., López, S., Rozas, M., Serra-Ricart, M., & Zapatero-Osorio, M. R. 2000, MNRAS, 318, 1093

Fesen, R., Milisavljevic, D., & Rudie, G. 2006, Central Bureau Electronic Telegrams, 672, 2

Filippenko, A. V. 1997, ARA&A, 35, 309

Filippenko, A. V. & Chornock, R. 2002, IAU Circ., 7825, 1

Filippenko, A. V., Matheson, T., & Barth, A. J. 1994, AJ, 108, 2220

Filippenko, A. V., Porter, A. C., & Sargent, W. L. W. 1990, AJ, 100, 1575

Foley, R. J., Papenkova, M. S., Swift, B. J., Filippenko, A. V., Li, W., Mazzali, P. A., Chornock, R., Leonard, D. C., & Van Dyk, S. D. 2003, PASP, 115, 1220

Foley, R. J., Smith, N., Ganeshalingam, M., Li, W., Chornock, R., & Filippenko, A. V. 2007, ApJ, 657, L105

Fransson, C. & Chevalier, R. A. 1987, ApJ, 322, L15

—. 1989, ApJ, 343, 323

Fransson, C., Chevalier, R. A., Filippenko, A. V., Leibundgut, B., Barth, A. J., Fesen, R. A., Kirshner, R. P., Leonard, D. C., Li, W., Lundqvist, P., Sollerman, J., & Van Dyk, S. D. 2002, ApJ, 572, 350

Galama, T. J., Vreeswijk, P. M., van Paradijs, J., Kouveliotou, C., Augusteijn, T., Böhnhardt, H., Brewer, J. P., Doublier, V., Gonzalez, J., Leibundgut, B., Lidman, C., Hainaut, O. R., Patat, F., Heise, J., in't Zand, J., Hurley, K., Groot, P. J., Strom, R. G., Mazzali, P. A., Iwamoto, K., Nomoto, K., Umeda, H., Nakamura, T., Young, T. R., Suzuki, T., Shigeyama, T., Koshut, T., Kippen, M., Robinson, C., de Wildt, P., Wijers, R. A. M. J., Tanvir, N., Greiner, J., Pian, E., Palazzi, E., Frontera, F., Masetti, N.,

Nicastro, L., Feroci, M., Costa, E., Piro, L., Peterson, B. A., Tinney, C., Boyle, B., Cannon, R., Stathakis, R., Sadler, E., Begam, M. C., & Ianna, P. 1998, Nature, 395, 670

Gehrz, R. D. 1988, ARA&A, 26, 377

Gomez, G. & Lopez, R. 1994, AJ, 108, 195

Hamuy, M. 2003, ApJ, 582, 905

—. 2004, Measuring and Modeling the Universe

Hamuy, M., Deng, J., Mazzali, P. A., Morrell, N. I., Phillips, M. M., Roth, M., Gonzalez, S., Thomas-Osip, J., Krzeminski, W., Contreras, C., Maza, J., González, L., Huerta, L., Folatelli, G., Chornock, R., Filippenko, A. V., Persson, S. E., Freedman, W. L., Koviak, K., Suntzeff, N. B., & Krisciunas, K. 2009, ApJ, 703, 1612

Hamuy, M., Maza, J., Pinto, P. A., Phillips, M. M., Suntzeff, N. B., Blum, R. D., Olsen, K. A. G., Pinfield, D. J., Ivanov, V. D., Augusteijn, T., Brillant, S., Chadid, M., Cuby, J., Doublier, V., Hainaut, O. R., Le Floc'h, E., Lidman, C., Petr-Gotzens, M. G., Pompei, E., & Vanzi, L. 2002, AJ, 124, 417

Hamuy, M. & Pinto, P. A. 2002, ApJ, 566, L63

Hamuy, M., Pinto, P. A., Maza, J., Suntzeff, N. B., Phillips, M. M., Eastman, R. G., Smith, R. C., Corbally, C. J., Burstein, D., Li, Y., Ivanov, V., Moro-Martin, A., Strolger, L. G., de Souza, R. E., dos Anjos, S., Green, E. M., Pickering, T. E., González, L., Antezana, R., Wischnjewsky, M., Galaz, G., Roth, M., Persson, S. E., & Schommer, R. A. 2001, ApJ, 558, 615

Harkness, R. P. & Wheeler, J. C. 1990, in Supernovae, ed. A. G. Petschek, 1–29

Harkness, R. P., Wheeler, J. C., Margon, B., Downes, R. A., Kirshner, R. P., Uomoto, A., Barker, E. S., Cochran, A. L., Dinerstein, H. L., Garnett, D. R., & Levreault, R. M. 1987, ApJ, 317, 355

Hendry, M. A., Smartt, S. J., Crockett, R. M., Maund, J. R., Gal-Yam, A., Moon, D., Cenko, S. B., Fox, D. W., Kudritzki, R. P., Benn, C. R., & Østensen, R. 2006, MNRAS, 369, 1303

Hendry, M. A., Smartt, S. J., Maund, J. R., Pastorello, A., Zampieri, L., Benetti, S., Turatto, M., Cappellaro, E., Meikle, W. P. S., Kotak, R., Irwin, M. J., Jonker, P. G., Vermaas, L., Peletier, R. F., van Woerden, H., Exter, K. M., Pollacco, D. L., Leon, S., Verley, S., Benn, C. R., & Pignata, G. 2005, MNRAS, 359, 906

Ho, L. C., Filippenko, A. V., & Sargent, W. L. W. 1997, ApJS, 112, 315

Immler, S., Modjaz, M., Landsman, W., Bufano, F., Brown, P. J., Milne, P., Dessart, L., Holland, S. T., Koss, M., Pooley, D., Kirshner, R. P., Filippenko, A. V., Panagia, N., Chevalier, R. A., Mazzali, P. A., Gehrels, N., Petre, R., Burrows, D. N., Nousek, J. A., Roming, P. W. A., Pian, E., Soderberg, A. M., & Greiner, J. 2008, ApJ, 674, L85

Itagaki, K., Kaneda, H., & Yamaoka, H. 2009, Central Bureau Electronic Telegrams, 1955, 3

Iwamoto, K., Mazzali, P. A., Nomoto, K., Umeda, H., Nakamura, T., Patat, F., Danziger, I. J., Young, T. R., Suzuki, T., Shigeyama, T., Augusteijn, T., Doublier, V., Gonzalez, J., Boehnhardt, H., Brewer, J., Hainaut, O. R., Lidman, C., Leibundgut, B., Cappellaro, E., Turatto, M., Galama, T. J., Vreeswijk, P. M., Kouveliotou, C., van Paradijs, J., Pian, E., Palazzi, E., & Frontera, F. 1998, Nature, 395, 672

Jester, S., Schneider, D. P., Richards, G. T., Green, R. F., Schmidt, M., Hall, P. B., Strauss, M. A., Vanden Berk, D. E., Stoughton, C., Gunn, J. E., Brinkmann, J., Kent, S. M., Smith, J. A., Tucker, D. L., & Yanny, B. 2005, AJ, 130, 873

Kasliwal, M. M., Howell, J. L., Fox, D., Quimby, R., & Gal-Yam, A. 2009, The Astronomer's Telegram, 2218, 1

Kawakita, H., Kinugasa, K., Ayani, K., & Yamaoka, H. 2004, IAU Circ., 8266, 2

Kennicutt, Jr., R. C. & Garnett, D. R. 1996, ApJ, 456, 504

Kewley, L. J. & Dopita, M. A. 2002, ApJS, 142, 35

Kiewe, M., Gal-Yam, A., Arcavi, I., Leonard, D. C., Emilio Enriquez, J., Cenko, S. B., Fox, D. B., Moon, D., Sand, D. J., & Soderberg, A. M. 2010, ArXiv e-prints

Kinugasa, K., Kawakita, H., Ayani, K., Kawabata, T., Yamaoka, H., Deng, J. S., Mazzali, P. A., Maeda, K., & Nomoto, K. 2002, ApJ, 577, L97

Kirshner, R. P. & Kwan, J. 1974, ApJ, 193, 27

Kozasa, T., Hasegawa, H., & Nomoto, K. 1989, ApJ, 344, 325

—. 1991, A&A, 249, 474

Kozasa, T., Nozawa, T., Tominaga, N., Umeda, H., Maeda, K., & Nomoto, K. 2009, in Astronomical Society of the Pacific Conference Series, Vol. 414, Astronomical Society of the Pacific Conference Series, ed. T. Henning, E. Grün, & J. Steinacker, 43

Krisciunas, K. & Rest, A. 2000, IAU Circ., 7382, 2

Landolt, A. U. 1992, AJ, 104, 340

Leonard, D. C., Filippenko, A. V., Ganeshalingam, M., Serduke, F. J. D., Li, W., Swift, B. J., Gal-Yam, A., Foley, R. J., Fox, D. B., Park, S., Hoffman, J. L., & Wong, D. S. 2006, Nature, 440, 505

Leonard, D. C., Filippenko, A. V., Gates, E. L., Li, W., Eastman, R. G., Barth, A. J., Bus, S. J., Chornock, R., Coil, A. L., Frink, S., Grady, C. A., Harris, A. W., Malkan, M. A., Matheson, T., Quirrenbach, A., & Treffers, R. R. 2002, PASP, 114, 35

Li, L. 2007, MNRAS, 375, 240

Li, W., Cenko, S. B., & Filippenko, A. V. 2009, Central Bureau Electronic Telegrams, 1952, 1

Litvinova, I. I. & Nadezhin, D. K. 1983, Ap&SS, 89, 89

Litvinova, I. Y. & Nadezhin, D. K. 1985, Soviet Astronomy Letters, 11, 145

Liu, Q., Hu, J., Hang, H., Qiu, Y., Zhu, Z., & Qiao, Q. 2000, A&AS, 144, 219

Lucy, L. B. 1991, ApJ, 383, 308

Maeda, K., Kawabata, K., Mazzali, P. A., Tanaka, M., Valenti, S., Nomoto, K., Hattori, T., Deng, J., Pian, E., Taubenberger, S., Iye, M., Matheson, T., Filippenko, A. V., Aoki, K., Kosugi, G., Ohyama, Y., Sasaki, T., & Takata, T. 2008, Science, 319, 1220

Maeda, K., Mazzali, P. A., & Nomoto, K. 2006, ApJ, 645, 1331

Maeda, K., Nakamura, T., Nomoto, K., Mazzali, P. A., Patat, F., & Hachisu, I. 2002, ApJ, 565, 405

Maeda, K., Tanaka, M., Nomoto, K., Tominaga, N., Kawabata, K., Mazzali, P. A., Umeda, H., Suzuki, T., & Hattori, T. 2007, ApJ, 666, 1069

Maguire, K., di Carlo, E., Smartt, S. J., Pastorello, A., Tsvetkov, D. Y., Benetti, S., Spiro, S., Arkharov, A. A., Beccari, G., Botticella, M. T., Cappellaro, E., Cristallo, S., Dolci, M., Elias-Rosa, N., Fiaschi, M., Gorshanov, D., Harutyunyan, A., Larionov, V. M., Navasardyan, H., Pietrinferni, A., Raimondo, G., di Rico, G., Valenti, S., Valentini, G., & Zampieri, L. 2010, MNRAS, 404, 981

Malesani, D., Tagliaferri, G., Chincarini, G., Covino, S., Della Valle, M., Fugazza, D., Mazzali, P. A., Zerbi, F. M., D'Avanzo, P., Kalogerakos, S., Simoncelli, A., Antonelli, L. A., Burderi, L., Campana, S., Cucchiara, A., Fiore, F., Ghirlanda, G., Goldoni, P., Götz, D., Mereghetti, S., Mirabel, I. F., Romano, P., Stella, L., Minezaki, T., Yoshii, Y., & Nomoto, K. 2004, ApJ, 609, L5

Martin, P., Li, W. D., Qiu, Y. L., & West, D. 2002, IAU Circ., 7809, 3

Martin, R., Williams, A., Woodings, S., Biggs, J., & Verveer, A. 1999, IAU Circ., 7310, 1

Matheson, T., Filippenko, A. V., Chornock, R., Leonard, D. C., & Li, W. 2000, AJ, 119, 2303

Matheson, T., Filippenko, A. V., Li, W., Leonard, D. C., & Shields, J. C. 2001, AJ, 121, 1648

Matheson, T., Garnavich, P. M., Stanek, K. Z., Bersier, D., Holland, S. T., Krisciunas, K., Caldwell, N., Berlind, P., Bloom, J. S., Bolte, M., Bonanos, A. Z., Brown, M. J. I., Brown, W. R., Calkins, M. L., Challis, P., Chornock, R., Echevarria, L., Eisenstein, D. J., Everett, M. E., Filippenko, A. V., Flint, K., Foley, R. J., Freedman, D. L., Hamuy, M., Harding, P., Hathi, N. P., Hicken, M., Hoopes, C., Impey, C., Jannuzi, B. T., Jansen, R. A., Jha, S., Kaluzny, J., Kannappan, S., Kirshner, R. P., Latham, D. W., Lee, J. C., Leonard, D. C., Li, W., Luhman, K. L., Martini, P., Mathis, H., Maza, J., Megeath, S. T., Miller, L. R., Minniti, D., Olszewski, E. W., Papenkova, M., Phillips, M. M., Pindor, B., Sasselov, D. D., Schild, R., Schweiker, H., Spahr, T., Thomas-Osip, J., Thompson, I., Weisz, D., Windhorst, R., & Zaritsky, D. 2003, ApJ, 599, 394

Mattila, S., Meikle, W. P. S., Lundqvist, P., Pastorello, A., Kotak, R., Eldridge, J., Smartt, S., Adamson, A., Gerardy, C. L., Rizzi, L., Stephens, A. W., & van Dyk, S. D. 2008, MNRAS, 389, 141

Mazzali, P. A., Deng, J., Hamuy, M., & Nomoto, K. 2009, ApJ, 703, 1624

Mazzali, P. A., Kawabata, K. S., Maeda, K., Foley, R. J., Nomoto, K., Deng, J., Suzuki, T., Iye, M., Kashikawa, N., Ohyama, Y., Filippenko, A. V., Qiu, Y., & Wei, J. 2007, ApJ, 670, 592

Mazzali, P. A., Kawabata, K. S., Maeda, K., Nomoto, K., Filippenko, A. V., Ramirez-Ruiz, E., Benetti, S., Pian, E., Deng, J., Tominaga, N., Ohyama, Y., Iye, M., Foley, R. J., Matheson, T., Wang, L., & Gal-Yam, A. 2005, Science, 308, 1284

Mazzali, P. A., Nomoto, K., Patat, F., & Maeda, K. 2001, ApJ, 559, 1047

Mazzali, P. A., Valenti, S., Della Valle, M., Chincarini, G., Sauer, D. N., Benetti, S., Pian, E., Piran, T., D'Elia, V., Elias-Rosa, N., Margutti, R., Pasotti, F., Antonelli, L. A., Bufano, F., Campana, S., Cappellaro, E., Covino, S., D'Avanzo, P., Fiore, F., Fugazza, D., Gilmozzi, R., Hunter, D., Maguire, K., Maiorano, E., Marziani, P., Masetti, N., Mirabel, F., Navasardyan, H., Nomoto, K., Palazzi, E., Pastorello, A., Panagia, N., Pellizza, L. J., Sari, R., Smartt, S., Tagliaferri, G., Tanaka, M., Taubenberger, S., Tominaga, N., Trundle, C., & Turatto, M. 2008, Science, 321, 1185

McCray, R. 1993, ARA&A, 31, 175

McCray, R. 2005, in IAU Colloq. 192: Cosmic Explosions, On the 10th Anniversary of SN1993J, ed. J.-M. Marcaide & K. W. Weiler, 77

Meikle, W. P. S., Mattila, S., Pastorello, A., Gerardy, C. L., Kotak, R., Sollerman, J., Van Dyk, S. D., Farrah, D., Filippenko, A. V., Höflich, P., Lundqvist, P., Pozzo, M., & Wheeler, J. C. 2007, ApJ, 665, 608

Miller, A. A., Silverman, J. M., Butler, N. R., Bloom, J. S., Chornock, R., Filippenko, A. V., Ganeshalingam, M., Klein, C. R., Li, W., Nugent, P. E., Smith, N., & Steele, T. N. 2010, MNRAS, 404, 305

Minkowski, R. 1941, PASP, 53, 224

—. 1964, ARA&A, 2, 247

Modjaz, M., Kewley, L., Kirshner, R. P., Stanek, K. Z., Challis, P., Garnavich, P. M., Greene, J. E., Kelly, P. L., & Prieto, J. L. 2008a, AJ, 135, 1136

Modjaz, M., Kirshner, R. P., Blondin, S., Challis, P., & Matheson, T. 2008b, ApJ, 687, L9

Modjaz, M., Li, W., Butler, N., Chornock, R., Perley, D., Blondin, S., Bloom, J. S., Filippenko, A. V., Kirshner, R. P., Kocevski, D., Poznanski, D., Hicken, M., Foley, R. J., Stringfellow, G. S., Berlind, P., Barrado y Navascues, D., Blake, C. H., Bouy, H., Brown, W. R., Challis, P., Chen, H., de Vries, W. H., Dufour, P., Falco, E., Friedman, A., Ganeshalingam, M., Garnavich, P., Holden, B., Illingworth, G., Lee, N., Liebert, J., Marion, G. H., Olivier, S. S., Prochaska, J. X., Silverman, J. M., Smith, N., Starr, D., Steele, T. N., Stockton, A., Williams, G. G., & Wood-Vasey, W. M. 2009, ApJ, 702, 226

Modjaz, M., Stanek, K. Z., Garnavich, P. M., Berlind, P., Blondin, S., Brown, W., Calkins, M., Challis, P., Diamond-Stanic, A. M., Hao, H., Hicken, M., Kirshner, R. P., & Prieto, J. L. 2006, ApJ, 645, L21

Mould, J. R., Huchra, J. P., Freedman, W. L., Kennicutt, Jr., R. C., Ferrarese, L., Ford, H. C., Gibson, B. K., Graham, J. A., Hughes, S. M. G., Illingworth, G. D., Kelson, D. D., Macri, L. M., Madore, B. F., Sakai, S., Sebo, K. M., Silbermann, N. A., & Stetson, P. B. 2000, ApJ, 529, 786

Munari, U. & Zwitter, T. 1997, A&A, 318, 269

Nadyozhin, D. K. 1994, ApJS, 92, 527

Nakamura, T., Mazzali, P. A., Nomoto, K., & Iwamoto, K. 2001, ApJ, 550, 991

Nakano, S., Itagaki, K., Puckett, T., & Gorelli, R. 2006, Central Bureau Electronic Telegrams, 666, 1

Nomoto, K., Maeda, K., Mazzali, P. A., Umeda, H., Deng, J., & Iwamoto, K. 2003, ArXiv Astrophysics e-prints

Nomoto, K., Tominaga, N., Tanaka, M., Maeda, K., Suzuki, T., Deng, J. S., & Mazzali, P. A. 2006a, Nuovo Cimento B Serie, 121, 1207

Nomoto, K., Tominaga, N., Umeda, H., Kobayashi, C., & Maeda, K. 2006b, Nuclear Physics A, 777, 424

Nozawa, T., Kozasa, T., Habe, A., Dwek, E., Umeda, H., Tominaga, N., Maeda, K., & Nomoto, K. 2008a, in IAU Symposium, Vol. 255, IAU Symposium, ed. L. K. Hunt, S. Madden, & R. Schneider, 254–259

Nozawa, T., Kozasa, T., Tominaga, N., Sakon, I., Tanaka, M., Suzuki, T., Nomoto, K., Maeda, K., Umeda, H., Limongi, M., & Onaka, T. 2008b, ApJ, 684, 1343

Nozawa, T., Kozasa, T., Umeda, H., Maeda, K., & Nomoto, K. 2003, ApJ, 598, 785

Nugent, P., Sullivan, M., Ellis, R., Gal-Yam, A., Leonard, D. C., Howell, D. A., Astier, P., Carlberg, R. G., Conley, A., Fabbro, S., Fouchez, D., Neill, J. D., Pain, R., Perrett, K., Pritchet, C. J., & Regnault, N. 2006, ApJ, 645, 841

Pastorello, A., Kasliwal, M. M., Crockett, R. M., Valenti, S., Arbour, R., Itagaki, K., Kaspi, S., Gal-Yam, A., Smartt, S. J., Griffith, R., Maguire, K., Ofek, E. O., Seymour, N., Stern, D., & Wiethoff, W. 2008a, MNRAS, 389, 955

Pastorello, A., Mattila, S., Zampieri, L., Della Valle, M., Smartt, S. J., Valenti, S., Agnoletto, I., Benetti, S., Benn, C. R., Branch, D., Cappellaro, E., Dennefeld, M., Eldridge, J. J., Gal-Yam, A., Harutyunyan, A., Hunter, I., Kjeldsen, H., Lipkin, Y., Mazzali, P. A., Milne, P., Navasardyan, H., Ofek, E. O., Pian, E., Shemmer, O., Spiro, S., Stathakis, R. A., Taubenberger, S., Turatto, M., & Yamaoka, H. 2008b, MNRAS, 389, 113

Pastorello, A., Sauer, D., Taubenberger, S., Mazzali, P. A., Nomoto, K., Kawabata, K. S., Benetti, S., Elias-Rosa, N., Harutyunyan, A., Navasardyan, H., Zampieri, L., Iijima, T., Botticella, M. T., di Rico, G., Del Principe, M., Dolci, M., Gagliardi, S., Ragni, M., & Valentini, G. 2006, MNRAS, 370, 1752

Pastorello, A., Smartt, S. J., Mattila, S., Eldridge, J. J., Young, D., Itagaki, K., Yamaoka, H., Navasardyan, H., Valenti, S., Patat, F., Agnoletto, I., Augusteijn, T., Benetti, S., Cappellaro, E., Boles, T., Bonnet-Bidaud, J., Botticella, M. T., Bufano, F., Cao, C., Deng, J., Dennefeld, M., Elias-Rosa, N., Harutyunyan, A., Keenan, F. P., Iijima, T., Lorenzi, V., Mazzali, P. A., Meng, X., Nakano, S., Nielsen, T. B., Smoker, J. V., Stanishev, V., Turatto, M., Xu, D., & Zampieri, L. 2007, Nature, 447, 829

Pastorello, A., Valenti, S., Zampieri, L., Navasardyan, H., Taubenberger, S., Smartt, S. J., Arkharov, A. A., Bärnbantner, O., Barwig, H., Benetti, S., Birtwhistle, P., Botticella, M. T., Cappellaro, E., Del Principe, M., di Mille, F., di Rico, G., Dolci, M., Elias-Rosa, N., Efimova, N. V., Fiedler, M., Harutyunyan, A., Höflich, P. A., Kloehr, W., Larionov, V. M., Lorenzi, V., Maund, J. R., Napoleone, N., Ragni, M., Richmond, M., Ries, C., Spiro, S., Temporin, S., Turatto, M., & Wheeler, J. C. 2009, MNRAS, 394, 2266

Patat, F., Barbon, R., Cappellaro, E., & Turatto, M. 1994, A&A, 282, 731

Patat, F., Cappellaro, E., Danziger, J., Mazzali, P. A., Sollerman, J., Augusteijn, T., Brewer, J., Doublier, V., Gonzalez, J. F., Hainaut, O., Lidman, C., Leibundgut, B., Nomoto, K., Nakamura, T., Spyromilio, J., Rizzi, L., Turatto, M., Walsh, J., Galama, T. J., van Paradijs, J., Kouveliotou, C., Vreeswijk, P. M., Frontera, F., Masetti, N., Palazzi, E., & Pian, E. 2001, ApJ, 555, 900

Paturel, G., Theureau, G., Bottinelli, L., Gouguenheim, L., Coudreau-Durand, N., Hallet, N., & Petit, C. 2003, A&A, 412, 57

Pettini, M. & Pagel, B. E. J. 2004, MNRAS, 348, L59

Pian, E., Mazzali, P. A., Masetti, N., Ferrero, P., Klose, S., Palazzi, E., Ramirez-Ruiz, E., Woosley, S. E., Kouveliotou, C., Deng, J., Filippenko, A. V., Foley, R. J., Fynbo, J. P. U., Kann, D. A., Li, W., Hjorth, J., Nomoto, K., Patat, F., Sauer, D. N., Sollerman, J., Vreeswijk, P. M., Guenther, E. W., Levan, A., O'Brien, P., Tanvir, N. R., Wijers, R. A. M. J., Dumas, C., Hainaut, O., Wong, D. S., Baade, D., Wang, L., Amati, L., Cappellaro, E., Castro-Tirado, A. J., Ellison, S., Frontera, F., Fruchter, A. S., Greiner, J., Kawabata, K., Ledoux, C., Maeda, K., Møller, P., Nicastro, L., Rol, E., & Starling, R. 2006, Nature, 442, 1011

Press, W. H., Teukolsky, S. A., Vetterling, W. T., & Flannery, B. P. 1992, Numerical recipes in FORTRAN. The art of scientific computing, ed. Press, W. H., Teukolsky, S. A., Vetterling, W. T., & Flannery, B. P.

Puckett, T., Pelloni, A., Baek, M., Prasad, R. R., & Li, W. 2005, IAU Circ., 8630, 1

Quimby, R. M., Aldering, G., Wheeler, J. C., Höflich, P., Akerlof, C. W., & Rykoff, E. S. 2007, ApJ, 668, L99

Richardson, D., Branch, D., & Baron, E. 2006, AJ, 131, 2233

Richmond, M. W., van Dyk, S. D., Ho, W., Peng, C. Y., Paik, Y., Treffers, R. R., Filippenko, A. V., Bustamante-Donas, J., Moeller, M., Pawellek, C., Tartara, H., & Spence, M. 1996, AJ, 111, 327

Rigon, L., Turatto, M., Benetti, S., Pastorello, A., Cappellaro, E., Aretxaga, I., Vega, O., Chavushyan, V., Patat, F., Danziger, I. J., & Salvo, M. 2003, MNRAS, 340, 191

Sahu, D. K., Anupama, G. C., & Gurugubelli, U. K. 2009a, Central Bureau Electronic Telegrams, 1955, 2

Sahu, D. K., Anupama, G. C., Srividya, S., & Muneer, S. 2006, MNRAS, 372, 1315

Sahu, D. K., Tanaka, M., Anupama, G. C., Gurugubelli, U. K., & Nomoto, K. 2009b, ApJ, 697, 676

Sakon, I., Onaka, T., Wada, T., Ohyama, Y., Kaneda, H., Ishihara, D., Tanabé, T., Minezaki, T., Yoshii, Y., Tominaga, N., Nomoto, K., Nozawa, T., Kozasa, T., Tanaka, M., Suzuki, T., Umeda, H., Ohyabu, S., Usui, F., Matsuhara, H., Nakagawa, T., & Murakami, H. 2009, ApJ, 692, 546

Salamanca, I., Terlevich, R. J., & Tenorio-Tagle, G. 2002, MNRAS, 330, 844

Sauer, D. N., Mazzali, P. A., Deng, J., Valenti, S., Nomoto, K., & Filippenko, A. V. 2006, MNRAS, 369, 1939

Schlegel, D. J., Finkbeiner, D. P., & Davis, M. 1998, ApJ, 500, 525

Schlegel, E. M. 1990, MNRAS, 244, 269

Schlegel, E. M. & Kirshner, R. P. 1989, AJ, 98, 577

Silverman, J. M., Mazzali, P., Chornock, R., Filippenko, A. V., Clocchiatti, A., Phillips, M. M., Ganeshalingam, M., & Foley, R. J. 2009, PASP, 121, 689

Smartt, S. J. 2009, ARA&A, 47, 63

Smith, N., Foley, R. J., & Filippenko, A. V. 2008, ApJ, 680, 568

Smith, N., Silverman, J. M., Chornock, R., Filippenko, A. V., Wang, X., Li, W., Ganeshalingam, M., Foley, R. J., Rex, J., & Steele, T. N. 2009, ApJ, 695, 1334

Soderberg, A. 2006, The Astronomer's Telegram, 917, 1

Soderberg, A. M., Berger, E., Page, K. L., Schady, P., Parrent, J., Pooley, D., Wang, X., Ofek, E. O., Cucchiara, A., Rau, A., Waxman, E., Simon, J. D., Bock, D., Milne, P. A., Page, M. J., Barentine, J. C., Barthelmy, S. D., Beardmore, A. P., Bietenholz, M. F., Brown, P., Burrows, A., Burrows, D. N., Byrngelson, G., Cenko, S. B., Chandra, P., Cummings, J. R., Fox, D. B., Gal-Yam, A., Gehrels, N., Immler, S., Kasliwal, M., Kong, A. K. H., Krimm, H. A., Kulkarni, S. R., Maccarone, T. J., Mészáros, P., Nakar, E., O'Brien, P. T., Overzier, R. A., de Pasquale, M., Racusin, J., Rea, N., & York, D. G. 2008, Nature, 453, 469

Sollerman, J., Leibundgut, B., & Spyromilio, J. 1998, A&A, 337, 207

Stritzinger, M., Hamuy, M., Suntzeff, N. B., Smith, R. C., Phillips, M. M., Maza, J., Strolger, L., Antezana, R., González, L., Wischnjewsky, M., Candia, P., Espinoza, J., González, D., Stubbs, C., Becker, A. C., Rubenstein, E. P., & Galaz, G. 2002, AJ, 124, 2100

Stritzinger, M., Mazzali, P., Phillips, M. M., Immler, S., Soderberg, A., Sollerman, J., Boldt, L., Braithwaite, J., Brown, P., Burns, C. R., Contreras, C., Covarrubias, R., Folatelli, G., Freedman, W. L., González, S., Hamuy, M., Krzeminski, W., Madore, B. F., Milne, P., Morrell, N., Persson, S. E., Roth, M., Smith, M., & Suntzeff, N. B. 2009, ApJ, 696, 713

Suntzeff, N. B. & Bouchet, P. 1990, AJ, 99, 650

Tanaka, M., Maeda, K., Mazzali, P. A., & Nomoto, K. 2007, ApJ, 668, L19

Tanaka, M., Tominaga, N., Nomoto, K., Valenti, S., Sahu, D. K., Minezaki, T., Yoshii, Y., Yoshida, M., Anupama, G. C., Benetti, S., Chincarini, G., Della Valle, M., Mazzali, P. A., & Pian, E. 2009, ApJ, 692, 1131

Taubenberger, S., Pastorello, A., Mazzali, P. A., Valenti, S., Pignata, G., Sauer, D. N., Arbey, A., Bärnbantner, O., Benetti, S., Della Valle, A., Deng, J., Elias-Rosa, N., Filippenko, A. V., Foley, R. J., Goobar, A., Kotak, R., Li, W., Meikle, P., Mendez, J., Patat, F., Pian, E., Ries, C., Ruiz-Lapuente, P., Salvo, M., Stanishev, V., Turatto, M., & Hillebrandt, W. 2006, MNRAS, 371, 1459

Taubenberger, S., Valenti, S., Benetti, S., Cappellaro, E., Della Valle, M., Elias-Rosa, N., Hachinger, S., Hillebrandt, W., Maeda, K., Mazzali, P. A., Pastorello, A., Patat, F., Sim, S. A., & Turatto, M. 2009, MNRAS, 397, 677

Todini, P. & Ferrara, A. 2001, MNRAS, 325, 726

Tominaga, N., Limongi, M., Suzuki, T., Tanaka, M., Nomoto, K., Maeda, K., Chieffi, A., Tornambe, A., Minezaki, T., Yoshii, Y., Sakon, I., Wada, T., Ohyama, Y., Tanabé, T., Kaneda, H., Onaka, T., Nozawa, T., Kozasa, T., Kawabata, K. S., Anupama, G. C., Sahu, D. K., Gurugubelli, U. K., Prabhu, T. P., & Deng, J. 2008, ApJ, 687, 1208

Tomita, H., Deng, J., Maeda, K., Yoshii, Y., Nomoto, K., Mazzali, P. A., Suzuki, T., Kobayashi, Y., Minezaki, T., Aoki, T., Enya, K., & Suganuma, M. 2006, ApJ, 644, 400

Trimble, V. 1982, Reviews of Modern Physics, 54, 1183

—. 1983, Reviews of Modern Physics, 55, 511

Turatto, M., Benetti, S., & Cappellaro, E. 2003, in From Twilight to Highlight: The Physics of Supernovae, ed. W. Hillebrandt & B. Leibundgut, 200

Uomoto, A. & Kirshner, R. P. 1986, ApJ, 308, 685

Valenti, S., Benetti, S., Cappellaro, E., Patat, F., Mazzali, P., Turatto, M., Hurley, K., Maeda, K., Gal-Yam, A., Foley, R. J., Filippenko, A. V., Pastorello, A., Challis, P., Frontera, F., Harutyunyan, A., Iye, M., Kawabata, K., Kirshner, R. P., Li, W., Lipkin, Y. M., Matheson, T., Nomoto, K., Ofek, E. O., Ohyama, Y., Pian, E., Poznanski, D., Salvo, M., Sauer, D. N., Schmidt, B. P., Soderberg, A., & Zampieri, L. 2008, MNRAS, 383, 1485

Véron-Cetty, M., Joly, M., & Véron, P. 2004, A&A, 417, 515

Véron-Cetty, M., Joly, M., Véron, P., Boroson, T., Lipari, S., & Ogle, P. 2006, A&A, 451, 851

Vilchez, J. M. & Pagel, B. E. J. 1988, MNRAS, 231, 257

Weiler, K. W., van Dyk, S. D., Sramek, R. A., Panagia, N., Stockdale, C. J., & Montes, M. J. 2005, in Astronomical Society of the Pacific Conference Series, Vol. 342, 1604-2004: Supernovae as Cosmological Lighthouses, ed. M. Turatto, S. Benetti, L. Zampieri, & W. Shea, 290

Wheeler, J. C. & Harkness, R. P. 1986, in NATO ASIC Proc. 180: Galaxy Distances and Deviations from Universal Expansion, ed. B. F. Madore & R. B. Tully, 45–54

Wheeler, J. C. & Levreault, R. 1985, ApJ, 294, L17

Woosley, S. E. & Weaver, T. A. 1986, ARA&A, 24, 205

Zwicky, F., Herzog, E., & Wild, P. 1968, Catalogue of galaxies and of clusters of galaxies, ed. Zwicky, F., Herzog, E., & Wild, P.